

**DYNAMIC RESPONSE OF SHIP HULLS TO SLAMMING
LOADS IN IRREGULAR WAVES**

by

João Paulo Nunes Ramos do Ó

Thesis submitted for the Degree of Master of Science

Department of Naval Architecture and Ocean Engineering

University of Glasgow

October 1996

© João Ramos

ProQuest Number: 13815427

All rights reserved

INFORMATION TO ALL USERS

The quality of this reproduction is dependent upon the quality of the copy submitted.

In the unlikely event that the author did not send a complete manuscript and there are missing pages, these will be noted. Also, if material had to be removed, a note will indicate the deletion.



ProQuest 13815427

Published by ProQuest LLC (2018). Copyright of the Dissertation is held by the Author.

All rights reserved.

This work is protected against unauthorized copying under Title 17, United States Code
Microform Edition © ProQuest LLC.

ProQuest LLC.
789 East Eisenhower Parkway
P.O. Box 1346
Ann Arbor, MI 48106 – 1346

Thesis
10744
Copy 1



ABSTRACT

In this work the dynamic response of a ship to slamming loads in random seas was studied. This study focused only the vertical motions and loads. The motions were obtained using a linear strip method and the hydrodynamic coefficients were obtained by using the multipole expansion technique for circular shapes and a multiparametric conformal transformation which transforms a circle into an arbitrary form. Special attention was given to the common two dimensional methods to obtain the hydrodynamic coefficients and chapter 2 was dedicated to this study.

In this research it is assumed that the total vertical bending moment induced by waves is divided into two components: the first one is obtained by the linear theory and the second one is due to the slamming loads which induces whipping stresses. Several formulations for the determination of the slamming pressures and loads were compared in chapter 4.

The vibratory response of the ship is calculated by modelling it with two dimensional Timoshenko beam finite elements with a consistent mass formulation, which is used to determine the natural modes and frequencies. The response is obtained by modal superposition using direct integration methods.

Experiments to obtain the ship motions and sea loads were carried out in the Hydrodynamics Laboratory of the University of Glasgow with a segmented model of a container ship in the ballast condition. Comparisons between the measurements and the theoretical results were carried out for the vertical motions and bending moments, and satisfactory results were obtained for some of the theoretical methods.

Time domain simulations for the low and high frequency vertical bending moments were carried out for irregular seas. Some of the relevant statistical parameters involved in this process were compared in time and frequency domain. Based on the time domain simulations some statistical distributions were obtained for long term analysis for the slamming and total bending moments. The correlation between the several distributions were also analysed.

TABLE OF CONTENTS

Abstract	i
Contents	ii
Declaration	v
Dedication	vi
Acknowledgements	vii
List of figures	viii
Nomenclature	xv

CHAPTER 1

INTRODUCTION

1.1 - Historical Review	1
1.2 - Structure of the Thesis	5

CHAPTER 2

HYDRODYNAMIC FORCES

2.1 - Introduction	8
2.2 - Mapping Transformation	10
2.3 - Hydrodynamic Coefficients Using Multipole Expansion Technique ---	12
2.3.1 - Numerical Aspects	16
2.4 - Results	19
2.5 - Conclusions	32

CHAPTER 3

WAVE INDUCED MOTIONS AND LOADS

3.1 - Introduction	34
3.2 - Formulation of the Equations of Motion	35
3.3 - Solution of the Differential Equations	38
3.4 - Results	41
3.4.1 - Comparison of the Hydrodynamic Coefficients	43
3.4.2 - Vertical Motions	45
3.5 - Conclusions	49

CHAPTER 4
SLAMMING LOADS

4.1 - Introduction -----	50
4.2 - Maximum Slamming Pressure -----	52
4.3 - Slamming Vertical Force -----	57
4.3.1 - Time History of the Vertical Slamming Force -----	60
4.4 - Slamming Loads Considering Constant Impact Velocity -----	61
4.4.1 - Ochi and Motter Method -----	62
4.4.2 - Stavovy and Kawakami Methods -----	63
4.4.3 - Momentum Theory -----	64
4.4.4 - Wagner Solution Using the Korobkin Integral -----	64
4.5.5 - Comparison of Methods -----	64
4.5 - Slamming Loads for Regular Waves -----	70
4.5.1 - Travelling Velocity of Pressure in the Longitudinal Direction -	72
4.5.2 - Impulse Function Using the First Two Methods -----	73
4.5.3 - Wagner Solution for Regular Waves -----	73
4.5.4 - Momentum Theory Applied for Regular Waves -----	75
4.5.5 - Comparison of Methods -----	77
4.6 - Conclusions -----	80

CHAPTER 5
STRUCTURAL RESPONSE

5.1 - Introduction -----	82
5.2 - Problem Formulation -----	83
5.3 - Solution of the Differential Equations in the Time Domain -----	86
5.4 - Results -----	87

CHAPTER 6

VALIDATION OF METHODS WITH EXPERIMENTAL RESULTS

6.1 - Introduction	97
6.2 - Main Particulars of the Model	97
6.3 - Weight Distribution of the Model	99
6.4 - Structural Aspects of the Model	103
6.5 - Ship Motions and Wave Loads	110
6.6 - Combined Low Frequency and Whipping Bending Moments	115
6.6.1 - Bending Moments for $\lambda / L = 1.0$	116
6.6.1.1 - Linear Wave Induced VBM Combined with Empirical Methods for Slamming Loads	117
6.6.1.2 - Linear Wave Induced VBM Combined with the Momentum Term for Slamming Loads	120
6.7 - Conclusions	122

CHAPTER 7

SLAMMING IN IRREGULAR SEAS

7.1 - Representation of an Irregular Seaway	126
7.2 - Statistical Properties of Sea Surface Elevation	129
7.3 - Slamming Occurrence in Frequency and Time Domain	130
7.4 - Structural Response	135
7.5 - Slamming Combined with the Wave Induced Stresses	149
7.6 - Conclusions	155

CHAPTER 8

CONCLUSIONS

8.1 - General Conclusions	157
8.2 - Recommendations for Future Work	161
References	162

DECLARATION

Except where reference is made to the work of others
this thesis is believed to be original.

DEDICATION

To my parents, Alexandra and Beatriz.

ACKNOWLEDGEMENTS

The author would like to thank the following:

Professor D. Faulkner, former Head of the Department, and Professor Nigel Barltrop, present Head of the Department, for allowing him to carry out this study and for their continuous encouragement.

Professor C. Guedes Soares, for the strong encouragement of this research and for the continuous guidance and support.

Professor A. Incecik, former Superintendent of the Hydrodynamics Laboratory and present professor at the University of Newcastle, for his encouragement to carry out the experimental work and also for his support.

Professor P.T. Pettersen, Dr. J.J. Jensen and all the staff of the Department of Ocean Engineering of the Technical University of Denmark for their valuable suggestions in the first two months of this research.

Professor A. Korobkin, for the long hours spent discussing some aspects of this research and also for his contribution in some theoretical aspects of the slamming.

Dr. O. Yilmaz, for the valuable suggestions and his permanent assistance during the final part of the thesis.

Mr. Tao, for the use of the model prepared by him in the experimental work.

All the technicians at the Hydrodynamic Laboratory for their help during the experiments.

Financial support during the course of this work was provided by FUNDENAV - Fundo para o Desenvolvimento da Engenharia Naval, for which the author is very grateful.

LIST OF FIGURES

Chapter 1

<i>Figure 1.1 - Subjects studied in this research</i> _____	5
---	---

Chapter 2

<i>Figure 2.1 Circle transformation</i> _____	10
<i>Figure. 2.2 - Transverse ship lines resulting from the Lewis transformation, showing the input points for each section.</i> _____	12
<i>Figure. 2.3 - Transverse ship lines resulting from a 12 parameter transformation.</i> _____	13
<i>Figure 2.4 -Behaviour of function H for different values of x and k</i> _____	17
<i>Figure 2.5 - Midship section</i> _____	20
<i>Figure 2.6 - Bow sections</i> _____	20
<i>Figure 2.7 - Variation of the mean error with the number of coefficients for different midship sections</i> _____	21
<i>Figure 2.8 - Added mass deviations for the rectangular section (R00)</i> _____	21
<i>Figure 2.9 - Damping deviation for the rectangular section (R00)</i> _____	22
<i>Figure 2.10 - Variation of the added mass mean geometric error for the different midship sections</i> _____	22
<i>Figure 2.11 - Damping mean error for the different midship sections</i> _____	22
<i>Figure 2.12 - Comparison of the added mass from the three methods for the rectangular section(R00).</i> _____	23
<i>Figure 2.13 - Comparison of the damping coefficient from the three methods for the rectangular section (R00).</i> _____	23
<i>Figure 2.14 - Normalised added mass for section A</i> _____	24
<i>Figure 2.15 - Normalised damping for section A</i> _____	24
<i>Figure 2.16 - Normalised added mass for section B</i> _____	25
<i>Figure 2.17 - Normalised damping for section B</i> _____	25
<i>Figure 2.18 - Normalised added mass for section C</i> _____	25
<i>Figure 2.19 - Normalised damping for section C</i> _____	26
<i>Figure 2.20 - Added mass. Mean error</i> _____	26
<i>Figure 2.21 - Damping. Mean error</i> _____	27
<i>Figure 2.22 - Mean geometric error variation for the bow sections</i> _____	27
<i>Figure 2.23 - Added mass coefficient for section A</i> _____	28

<i>Figure 2.24 - Damping for section A</i>	28
<i>Figure 2.25 - Added mass for section B</i>	29
<i>Figure 2.26 - Damping for section B</i>	29
<i>Figure 2.27 - Added mass for section C</i>	29
<i>Figure 2.28 - Damping for section C</i>	30
<i>Figure 2.29 - Time consumption varying the number of coefficients (seconds)</i>	31
<i>Figure 2.30 - Correlation between the added mass deviations and the mean geometric error</i>	32
<i>Figure 2.31 - Correlation between the damping coefficient deviations and the mean geometric error</i>	32

Chapter 3

<i>Figure 3.1 - Body Plan</i>	42
<i>Figure 3.2 - Mass and section area distribution</i>	43
<i>Figure 3.3 - Coefficient a used in eqn. (3.2) for three different number of mapping coefficients used in the multipole expansion method.</i>	44
<i>Figure 3.4 - Coefficient b used in eqn. (3.2) for three different number of mapping coefficients used in the multipole expansion method.</i>	44
<i>Figure 3.5 - Coefficient A used in eqn. (3.3) for three different number of mapping coefficients used in the multipole expansion method.</i>	44
<i>Figure 3.6 - Coefficient B used in eqn. (3.3) for three different number of mapping coefficients used in the multipole expansion method.</i>	45
<i>Figure 3.7 - Heave transfer function</i>	46
<i>Figure 3.8 - Heave phase response</i>	46
<i>Figure 3.9 - Pitch transfer function</i>	47
<i>Figure 3.10 - Pitch phase response</i>	47
<i>Figure 3.11 - Relative motion for Station 61/2</i>	48
<i>Figure 3.12 - Relative motion for Station 71/2</i>	48
<i>Figure 3.13 - Relative motion for Station 91/2</i>	48
<i>Figure 3.14 - Longitudinal variation of the relative motion for $l/L = 1.0$</i>	49

Chapter 4

<i>Figure. 4.1-Probability of Occurrence of Slam for Various Loading Conditions and Course Angles, Ochi (1964).</i>	51
<i>Figure 4.2 - Form coefficient obtained using the Ochi's method for wedges with varying the deadrise angle</i>	52
<i>Figure 4.3 - Form coefficient as function of deadrise angle (Stavovy and Chuang, 1976)</i>	53

Figure 4.4 - <i>c</i> value for the Wagner approach	54
Figure 4.5 - Form coefficient for the Boundary element, Wagner and Asymptotic methods	56
Figure 4.6 - Comparison of the various methods	56
Figure 4.7 - Pressure distribution according to Ochi	57
Figure 4.8 - Wedge geometry and system coordinates for the Stavovy method	57
Figure 4.9 - Pressure distribution using the boundary element method	58
Figure 4.10 - Comparison of the different methods to calculate the vertical force	60
Figure 4.11 - Time history of the vertical slamming load proposed by Ochi and Motter (1971) and Kawakami et al (1977).	61
Figure 4.12 - Transverse lines of the chosen stations	65
Figure 4.13 - Impulse time function for the station 61/2, $V=4$ m/s	65
Figure 4.14 - Impulse time function for the station 61/2, $V=8$ m/s	66
Figure 4.15 - Impulse time function for the station 71/2, $V=4$ m/s	66
Figure 4.16 - Impulse time function for the station 71/2, $V=8$ m/s	66
Figure 4.17 - Impulse time function for station 91/2, and $V=4$ m/s	67
Figure 4.18 - Impulse time function for the station 91/2, $V=8$ m/s	67
Figure 4.19 - Line where the momentum theory and the method used by Belik and Price (1982) gave the same results for the impulse	68
Figure 4.20 - Relative motion amplitude longitudinal variation	70
Figure 4.21 - Phase angle	71
Figure 4.22 - Relative motion for the forward stations, $w = 0.55$ rad/s	71
Figure 4.23 - Longitudinal distribution of impact velocity	72
Figure 4.24 - Longitudinal travelling velocity of pressure	73
Figure 4.23 - Slamming contributions according to Wagner (eqn. 7.51)	74
Figure 4.24 - Contributions of some of the components of the slamming force	75
Figure 4.25 - Slamming impulse obtained from Wagner and momentum theories.	76
Figure 4.26 - Slamming impulse obtained from Wagner and momentum theories.	77
Figure 4.27 - Slamming impulse obtained from momentum theory assuming constant impact velocity and for regular waves, $A = 4m$.	78
Figure 4.28 - Slamming impulse obtained from momentum theory assuming constant impact velocity and for regular waves, $A = 4m$.	78
Figure 4.29 - Impulse calculated between 0 and 0.6 T for regular waves and constant velocity.	79
Figure 4.30 - Impulse calculated between 0 and 0.6 T for regular waves and constant velocity.	79

Chapter 5

<i>Figure 5.1 - Natural shape 1.mode</i>	89
<i>Figure 5.2 - Natural shape 2.mode</i>	89
<i>Figure 5.3 - Natural shape 3.mode</i>	90
<i>Figure 5.4 - Natural shape 4.mode</i>	90
<i>Figure 5.5 - Bending Moment, 1.mode</i>	91
<i>Figure 5.6 - Bending Moment, 2.mode</i>	91
<i>Figure 5.7 - Bending Moment, 3 mode</i>	92
<i>Figure 5.8 - Bending Moment, 4 mode</i>	92
<i>Figure 5.9 - Time function Kt1</i>	93
<i>Figure 5.10 - Time function Kt2</i>	93
<i>Figure 5.11 - Maximum force longitudinal distribution</i>	93
<i>Figure 5.12 - Midship displacement using Kt1</i>	94
<i>Figure 5.13 - Midship displacement using Kt2</i>	94
<i>Figure 5.14 - Midship BM using Kt1</i>	94
<i>Figure 5.15 - Midship BM using Kt2</i>	95
<i>Figure 5.16 - Maximum BM longitudinal distribution</i>	95
<i>Figure 5.17 Ratio between Sagging and Hogging</i>	96

Chapter 6

<i>Figure 6.1 - Logitudinal position of the strain gauges and diodes</i>	98
<i>Figure 6.2 Weight longitudinal distribution. curve I</i>	100
<i>Figure 6.3 Weight longitudinal distribution. Curve II</i>	100
<i>Figure 6.4 Vertical Bending Moment. Curve II</i>	100
<i>Figure 6.5 - Vertical bending moment induced by buoyancy</i>	101
<i>Figure 6.6 - Model mass distribution using the 8 coefficient polynomial</i>	102
<i>Figure 6.7 -Still water bending moments using the 8 coefficients polynomial</i>	103
<i>Figure 6.8 - Diagram of the equivalent system of the model</i>	103
<i>Figure 6.9 - Shape functions used in the finite element approximation</i>	104
<i>Figure 6.10 - Vertical Bending Moment for a free vibration test. Cut number 1</i>	106
<i>Figure 6.11 - Vertical Bending Moment for a free vibration test. Cut number 2</i>	106
<i>Figure 6.12 - Vertical Bending Moment for a free vibration test. Cut number 3</i>	106
<i>Figure 6.13 - VBM amplitude decay observed in the three strain gauges</i>	107

Figure 6.14 - Logarithmic decrement for the three strain gauges	108
Figure 6.15 - Natural shapes for the wet mode	109
Figure 6.16 - Still water structural displacement using direct and modal calculations	110
Figure 6.17 - Heave transfer function	111
Figure 6.18 - Pitch transfer function	111
Figure 6.19 - Heave Lag - Results comparison	112
Figure 6.20 - Pitch Lag - Results comparison	112
Figure 6.21 - Relative motion for $f=0.56$ Hz - Results comparison	113
Figure 6.22 - Relative motion for $f=0.64$ Hz - Results comparison	113
Figure 6.23 - Relative motion for $f=0.79$ Hz - Results comparison	113
Figure 6.24 - Vertical Bending Moment at Strain Gauge 1	114
Figure 6.25 - Vertical Bending Moment at Strain Gauge 2	114
Figure 6.26 - Vertical Bending Moment at Strain Gauge 3	115
Figure 6.27 - Longitudinal variation of the relative motion for $l/L = 1.0$	116
Figure 6.28 - Impact velocity for the two experiments	117
Figure 6.29 - Measured and predicted bending moments on SG 1 using empirical formulations for the whipping stresses $H/T=0.71$ $l/L=1.0$	118
Figure 6.30 - Measured and predicted bending moments on SG 1 using empirical formulations for the whipping stresses $H/T=0.87$ $l/L=1.0$	118
Figure 6.31 - Measured and predicted bending moments on SG 2 using empirical formulations for the whipping stresses $H/T=0.71$ $l/L=1.0$	118
Figure 6.32 - Measured and predicted bending moments on SG 2 using empirical formulations for the whipping stresses $H/T=0.87$ $l/L=1.0$	119
Figure 6.33 - Measured and predicted bending moments on SG 3 using empirical formulations for the whipping stresses $H/T=0.71$ $l/L=1.0$	119
Figure 6.34 - Measured and predicted bending moments on SG 3 using empirical formulations for the whipping stresses $H/T=0.87$ $l/L=1.0$	119
Figure 6.35 - Whipping stresses for the momentum method varying the hull domain of the slamming load $H/T=0.87$ $l/L=1.0$	120
Figure 6.36 - Whipping stresses for the momentum method varying the hull domain of the slamming load $H/T=0.87$ $l/L=1.0$	121
Figure 6.37 - Measured and predicted bending moments on SG 1 using the vertical derivative of added mass for the whipping stresses $H/T=0.87$ $l/L=1.0$	121
Figure 6.38 - Measured and predicted bending moments on SG 2 using the vertical derivative of added mass for the whipping stresses $H/T=0.87$ $l/L=1.0$	121
Figure 6.39 - Measured and predicted bending moments on SG 3 using the vertical derivative of added mass for the whipping stresses $H/T=0.87$ $l/L=1.0$	122
Figure 6.40 - Vertical bending moment assuming to be linear (obtained from the first experiment) and measured in the SG2, $H/T=0.71$ $l/L=1.0$	122

Figure 6.41 - Vertical bending moment assuming to be linear (obtained from the first experiment) and measured in the SG2, $H/T=0.87$ $l/L=1.0$	123
Figure 6.42 - Comparison of the coefficient K_s with the experiments and the several methods, SG1 $l/L=1.0$.	123
Figure 6.43 - Comparison of the coefficient K_s with the experiments and the several methods, SG2 $l/L=1.0$.	124
Figure 6.44 - Comparison of the coefficient K_s with the experiments and the several methods, SG2 $l/L=1.0$.	124

Chapter 7

Figure 7.1 - Pierson-Moskowitz spectrum for $H_s = 5$ m, $T_z = 8$ sec	127
Figure 7.2 - Surface elevation simulation of a sea state with $H_s = 5$ m $T_z = 8$ sec.	128
Figure 7.3 - Slamming probability $H_s=11$ m $T_z=10$ s	131
Figure 7.4 - Theoretical and observed probability distribution of the number of impacts in time period equal to 50 seconds .	132
Figure 7.5 - Probability of existence more than one impact during the period where the response is assumed important.	134
Figure 7.6 - Correction factors used for the simplified method	136
Figure 7.7 - Correction factors obtained for the container ship model	137
Figure 7.8 - Response using exact and approximate solutions for the 1. mode	137
Figure 7.9 - Response using exact and approximate solutions for the 2. mode	137
Figure 7.10 - Response using exact and approximate (without K_c correction) solutions for the 3. mode	137
Figure 7.11 - Response using exact and approximate solutions for the 4. mode	138
Figure 7.12 - Mean value of the whipping bending moment using one mode.	140
Figure 7.13 - Mean value of the whipping bending moment varying the number of modes used in eqn. 7.51.	140
Figure 7.14 - Whipping bending moment for three different travelling velocities of pressure $H_s = 7$ m and $T_z = 10$ sec.	141
Figure 7.15 - Spatial correlation of the impact velocities for the forward stations using a PM spectrum with $H_s = 7$ m and $T_z = 10$ sec.	142
Figure 7.16 - Impact velocities for $x/L = 0.9$	142
Figure 7.17 - Midship VBM First simulation	143
Figure 7.18 -Midship VBM. Second simulation.	144
Figure 7.19 - Mean value for maximum bending moment at the midship section.	144
Figure 7.20- Standard deviation for maximum bending moment at the midship section.	144
Figure 7.21 - Observed and theoretical curve fitting using the Gumbel distribution	146
Figure 7.22 - Density functions for the maximum sagging bending moment for several ship stations	147

<i>Figure 7.23 Maximum sagging bending moment prediction using Gamma function for $L/2$.</i>	147
<i>Figure 7.24 - Maximum sagging bending moment prediction using Gumbel function for $L/2$.</i>	148
<i>Figure 7.25 - Whipping bending moments. Probability of exceed for the midship position using the Gumbel distribution fitted by using 130 time simulations ($H_s=8$ m, $T_z=10$ s)</i>	148
<i>Figure 7.26 - Time simulation for the wave and combined bending moments</i>	149
<i>Figure 7.27 - Maximum values for the wave, whipping and combined VBM occurred for several time simulations</i>	149
<i>Figure 7.28 - Slamming contribution histogram ($H_s = 8$ m, $T_z = 8$ sec)</i>	150
<i>Figure 7.29 - Slamming contribution histogram ($H_s = 8$ m, $T_z = 10$ sec)</i>	151
<i>Figure 7.30 - Slamming contribution histogram ($H_s = 8$ m, $T_z = 13.2$ sec)</i>	151
<i>Figure 7.31 - Observed histograms and proposed distributions for K_s</i>	151
<i>Table 7.3 - Parameters proposed for the Beta function for the sagging condition</i>	152
<i>Figure 7.32 - Detail of the important region for the long term statistics of the observed histograms and proposed distribution for K_s</i>	152
<i>Figure 7.33 - Relation between the maximum whipping stresses and the slamming contribution factor</i>	153
<i>Figure 7.34 - Relation between the maximum whipping stresses and the maximum wave stresses</i>	153
<i>Figure 7.35 - Marginal functions for the slamming bending moment contribution</i>	154
<i>Figure 7.36 - Slamming component ($H_s = 8$ m, $T_z = 8$ s)</i>	155
<i>Figure 7.37 - Slamming component ($H_s = 8$ m, $T_z = 10$ s)</i>	155
<i>Figure 7.38 - Slamming component ($H_s = 8$ m, $T_z = 13$ s)</i>	155

NOMENCLATURE

- A - Sectional area.
- a - Ship added mass.
- A_n - Coefficients of the mapping transformation.
- a_n - Non-dimensional coefficients of the mapping transformation.
- b - Sectional breadth.
- B - Ship breadth.
- b - Ship damping coefficient.
- c - Ship restoring coefficient.
- COV - Coefficient of variation.
- Δt - Time step.
- E - Young modulus.
- F - Ship exciting vertical force.
- g - Acceleration of gravity.
- G - Shear modulus.
- g_k - Unit response function for the k mode.
- GM - Transversal metacentric height.
- h - Impulse response function for the vertical bending moment.
- H_θ - Pitch transfer function.
- H_r - Relative motion transfer function.
- H_z - Heave transfer function, significant wave height.
- I - Impulse, sectional inertia.
- I_r - Rotary inertia.
- k - Wave number, Form coefficient for the calculation of the slamming pressure.
- K_{kj} - Element of the stiffness matrix.
- K_v - Form coefficient for the calculation of the slamming force.
- L - Ship length.
- LCB - Longitudinal position of buoyancy centre.

- M - Ship exciting moment, vertical bending moment.
 M' - Non-dimensional vertical bending moment.
 m' - Sectional added mass.
 M_c - Combined bending moment.
 M_{kj} - Element of the mass matrix.
 m_n - N^{th} Spectral moment.
 M_s - Slamming bending moment.
 N' - Sectional damping coefficient.
 p - Pressure.
 P - Probability function.
 p_{max} - Maximum slamming pressure.
 S_r - Relative motion spectra.
 S_w - Sea spectra.
 T - Ship draft.
 T_c - Crest period.
 T_n - Natural period.
 T_z - Zero mean cross period.
 U - Ship forward speed.
 V - Shear force, variance.
VBM - Vertical Bending Moment.
 w_r - Modal shape function.
 z - Vertical position, heave motion.
 α - Deadrise angle.
 δ - Logarithmic decrement, Dirac delta function.
 Δ - Ship displacement.
 δ_{ij} - Kroneker delta coefficient.
 ε - Error function.
 ϕ - Velocity total potential.
 ϕ_{2m} - Multipole part of the velocity potential.
 ϕ_s - Source part of the velocity potential.
 η - Free surface shape, mass distribution per unit length.
 λ - Mean number of slamming occurrences in a period T .

- μ - Mean value.
- θ - Pitch motion.
- ρ - Water density, correlation coefficient.
- σ - Standard deviation
- ω - Wave frequency.
- ω' - Non-dimensional frequency.
- ω_e - Encounter frequency.
- Ψ_i - Shape function used in the finite element method.
- ψ - Stream function.
- ψ_{2m} - Multipole part of the stream function.
- ψ_s - Source part of the stream function.
- ζ - Wave amplitude, damping ratio.

CHAPTER 1

INTRODUCTION

1.1 - HISTORICAL REVIEW

The ship dynamics in waves is a problem which concerns several fields in engineering and the solution of this problem is of major importance for design purposes, ship owners, shipbuilders and classification societies.

The dynamics of ship hulls can be divided into two fields. The first one treats the ship motions for a certain seastate and by using some criteria related with the maximum acceleration and several other aspects, the ship operation conditions can be estimated (short term analysis) and long term predictions for the operation conditions can also be performed, which gives valuable information for shipping (voluntary and involuntary speed reductions, changes of course, etc.). The other field deals with the loads applied to the structure and corresponding shear forces and bending moments (primary stresses). These loads induce two different kinds of primary stresses named as low and high frequency stresses.

The low frequency stresses are obtained using a quasi-static analysis and the high frequency stresses are calculated using the hull vibration analysis. The high frequency stresses can be classified according to the nature of the loads and the more important ones for conventional ships are the whipping and springing stresses.

The whipping stresses are related with the slamming loads which occur when the ship sections emerge the water and, according to Ochi and Motter (1971), penetrates in water with some velocity greater than the threshold velocity. The springing stresses occur when the wave frequency is close to the structural natural frequencies of the ship hull.

For the structural design of conventional hulls, the whipping stresses are more important than the springing ones because these stresses will appear for extreme seas and for wave frequencies close to the values where the low frequency stresses reach the

maximum value and consequently the combination of these two stress components is also a very important task to study.

Ochi and Motter (1971) presented a complete description of the slamming problem. Due to the great amount of unknowns required for the determination of the whipping stresses they suggested some simple formulae for the calculation of the slamming loads, for practical purposes. These formulae were obtained based on experiments on frigates. Using the statistical framework they suggested that a threshold velocity must exist for the slamming occurrence and based on the Froude law scale they proposed an expression to evaluate that velocity. Based on the expressions for the short term statistics, they found the long term statistics for the pressures, loads and corresponding bending moments. They stressed the importance at the design stage of the combined effect of wave-induced and whipping stresses, i.e. the total bending moment induced by the waves. Using experimental data they found that the phase angle between the point where the maximum bending moment in hogging is reached and where the slamming starts is in the range of 20-70 degrees.

Based on an iterative scheme, Kaplan (1972) performed non-linear ship motion calculations in the time domain including the slamming loads. The basic approach used by Kaplan is the determination of the ship motions using linear theory and after that the effects of non-linear buoyancy and momentum are estimated and fed back to the time domain routine as corrections to the previous calculations. The slamming loads were evaluated using the momentum theory.

Using the linear strip theory to calculate the ship motions and the momentum theory to predict the slamming loads, Mansour and Oliveira (1975), presented a computational technique to evaluate the total bending moments for regular waves.

Kawakami et al. (1977), whose study was based on experimental work for a tanker, proposed an expression for the time history of the slamming loads. They found that the Ochi and Motter's (1971) formulation for the prediction of the maximum slamming pressure underpredicts the experimental measurements. Finally using long term statistics for the whipping stresses and for the wave bending moments obtained from the linear theory, they found that the return values of these two distributions have the same order of magnitude.

Belik et al. (1979) assumed that the bottom slamming can be divided into two different components named as impact and momentum slamming. Using this assumption they used the Ochi and Motter method for the determination of the maximum slamming pressure and the Kawakami et al expression for the determination of the time history of the slamming impact force. After that they carried out calculations for the vertical bending moments and shear forces in regular head seas.

Using the same approach for the calculation of the slamming loads, Belik and Price (1982) made comparisons for two different slamming theories using time simulation of ship responses in irregular seas. They found that the magnitudes of the responses after a slam depend very much on the mathematical model adopted in the calculation of the slamming loads.

Yamamoto et al. (1986) used non-linear ship motions based on the equations given by the linear theory but with time varying coefficients dependent of the instantaneous sectional draft. They also included the hydrodynamic impact component given by the rate of change of the sectional added mass, assuming that this force only acts on the vessel when the section is penetrating the water. Dynamic structural analysis was performed using the finite element method and considering Timoshenko's beam elements. After that they carried out experiments and calculations on a bulk carrier model for head seas. They found that the accuracy of the calculation of the hydrodynamic coefficients have a significant influence on the results of the slamming forces, and the computation with accurate coefficients result in better agreement with experiments. Guedes Soares (1989) used a similar method for the calculation of the slamming loads in regular waves with the Frank close fit method for the evaluation of the sectional added mass.

Three dimensional hydroelasticity theory was applied by Bishop et al. (1986) for a swath travelling in regular oblique sinusoidal waves. Using this theory they found that the magnitudes of the responses at a relative heading angle of 135° tend to be larger than those obtained for head seas, which contrasts with the usual predictions for monohulls.

Comparisons between the full scale measurements and theoretical predictions were carried out by Aksu et al. (1993) for a fast patrol boat travelling in rough seas. Due to

the uncertainty of the wave measurements in a real sea state, the experimental results of the vertical bending moments were compared with calculations for two different sea-states in a histogram form and satisfactory results were found.

In order to find out the effect of the forward speed effect on the slamming pressures, experiments were carried out by Radev and Beukelman (1993) using 3-D wedges with forward speed and they concluded that the forward speed has some influence in the slamming pressures and that the influence increases for wedges with larger trim angles.

For irregular seas, and considering the slamming process as a train of Poisson impulses of random intensity occurring in random time intervals with stationary intervals and assuming the structural response of the hull as linear, Mansour and Lozow (1982) developed a theory to determine the slamming bending moments statistics. Applying this theory in one example, they found that the ship speed has a great influence in the root mean square (RMS) of the vertical bending moment due to slamming loads.

Applying a similar theory but assuming that the slamming process can be described as a non stationary Poisson process, Chen (1980) determined the correlation between the RMS of the slamming bending moments and several factors, like the ship speed, significant wave height and peak frequency of the wave spectrum.

Ferro and Mansour (1985) stressed the fact that implementation of reliability analysis in the structural design depends to a large extent on the ability to combine the loads acting on the structure. Based on this statement the slamming statistics must be combined with the wave bending moments statistics. For that purpose they developed a theory which combines the bending moments in the frequency domain. In order to study the sensitivity of the results to several important input parameters such as the threshold velocity, the structural damping, pressure coefficient and significant wave height, they performed a sensitivity analysis on a cargo ship for the mean slamming induced stresses μ , standard deviation σ and the mean slamming rate λ . They found that the wave height has a larger influence in the μ , σ and λ , than other input parameters, and that the threshold velocity affects especially λ . They also found that the damping coefficient has some influence in the standard deviation σ , and that the pressure coefficient has a linear relation with the mean μ and σ . Finally they stressed that more research is needed in this field before using reliability analysis in the ship design. Some of the areas which

should be investigated are related with the statistical dependence of the wave and the slamming bending moments, so the assumption of random time intervals between successive impacts must be studied. The method used for the determination of the slamming loads and the spatial distribution and correlation of these loads must also be investigated.

1.2-STRUCTURE OF THE THESIS

The thesis is divided into eight chapters and the general structure of the research is represented in figure 1.1 with the different studied subjects and corresponding chapters. The first and last chapters (introduction and conclusions) and also chapter 6 which is the comparison of the theories with the experimental results are not represented in this figure.

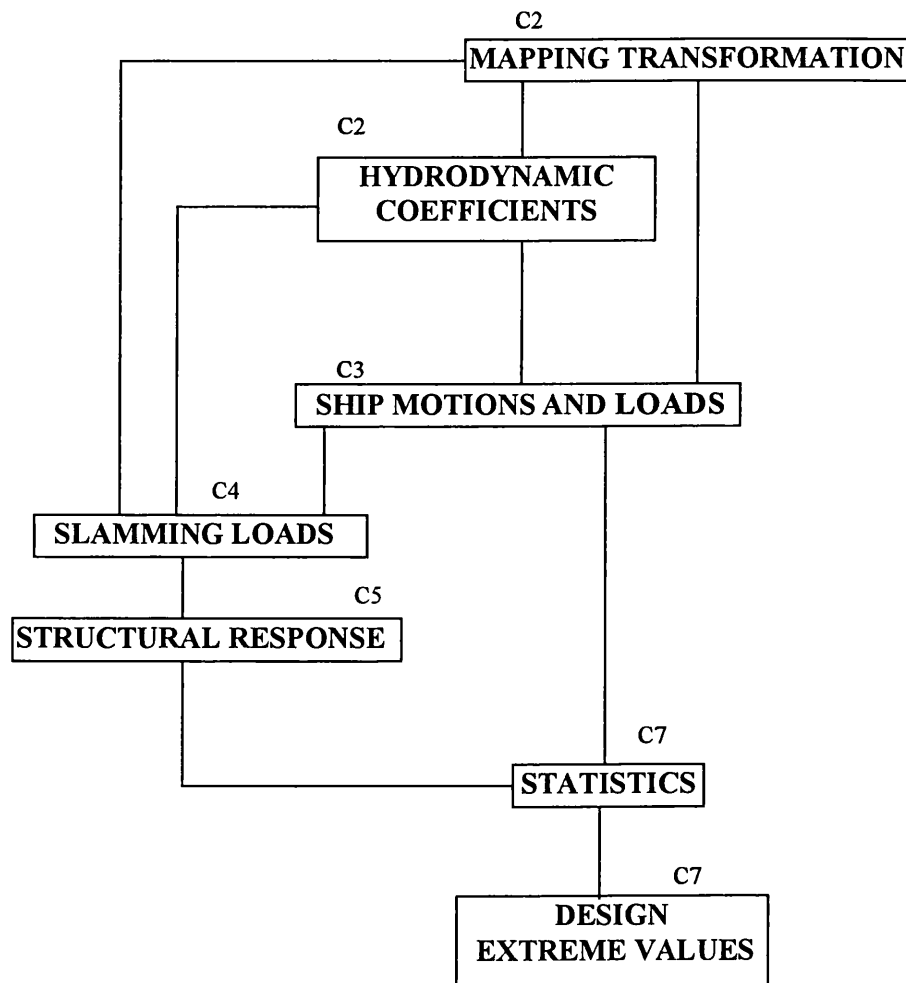


Figure 1.1 - Subjects studied in this research

Chapter 2 presents a review of the common two dimensional methods for the determination of the hydrodynamic forces and comparisons between the multipole expansion method combined with the multiparametric conformal and the Frank Close Fit method are performed for several sections. The accuracy of the conformal transformation and the corresponding hydrodynamic coefficients is also studied and the correlation between these two quantities is analysed.

In Chapter 3 the vertical motions and loads were obtained using a linear strip theory and the hydrodynamic coefficients were obtained by using the formulation explained in chapter 2. The results for the vertical motions were obtained for the container ship SL-175 (ITTC 1976) and compared with experimental results and with other linear strip theories.

In Chapter 4 several theories for the calculation of the maximum slamming pressure, and the slamming force for wedges with varying deadrise angle were compared. Two different empirical time history functions for the slamming forces are also compared and several methods were studied for some of the forward ship sections of the SL-175 container ship.

In Chapter 5 the finite element analysis using Timoshenko's beam formulation for the calculation of the stiffness matrix and consistent mass formulation for the evaluation of the mass matrix were used to describe the ship hull structure. The dynamic system is solved by using the modal decomposition and direct integration methods to perform the response in the time domain.

In Chapter 6 the ship motions and loads theory and the slamming theories were validated by comparison with experiments. The experiments were carried out on a segmented model of a container ship in the Hydrodynamics Laboratory of the University of Glasgow. In order to guarantee bottom emergence without green water effects the model was loaded in the ballast condition.

In Chapter 7 the whipping stresses and the combination of these stresses with the wave stresses were performed for irregular seas. In the first part of this chapter several important slamming statistics for the calculation of the whipping stresses were calculated and compared in time and frequency domain. After that, one of the slamming theories was chosen and, in order to use one method suitable to be studied in frequency

domain, the structural response was simplified by using the structural response to one impulse. Using this simplified theory the mean value and variance of the whipping stresses were obtained for the time and frequency domain. Based on time domain simulations the extreme distributions for the whipping bending moments were performed by fitting two theoretical distributions to the data. Using these distributions and the wave bending moment distribution, the combined or the total bending moment was obtained.

In Chapter 8 the general conclusions of the research are discussed and some recommendations for future work proposed.

CHAPTER 2

HYDRODYNAMIC FORCES

2.1 - INTRODUCTION

The calculation of the added mass and damping coefficients are very important for the determination of ship motions and sea loads and as a consequence several authors have dedicated special attention to it.

The accuracy in the determination of the hydrodynamic coefficients is also important in the determination of the slamming forces. In fact, Yamamoto et al. (1986) carried out experiments and calculations on a bulk carrier model for head seas and they found that the accuracy in the calculation of the hydrodynamic coefficients has a significant influence on the results of the slamming forces, and the computation with accurate coefficients results in better agreement with experiments.

Lewis (1929) using a two-parameter conformal mapping transformation, evaluated the added mass for infinite frequency, i.e., not taking into account the presence of the free surface. Landweber and Macagno (1957) extended this method to a more general N-parameter forms.

Ursell (1949) indicated a theoretical solution based on potential theory to evaluate the hydrodynamic coefficients of a cylinder in the presence of the free surface. Using this theory damping coefficients can be evaluated and the frequency dependence of the hydrodynamic coefficients is considered. Grim (1959) and Tasai (1959) extended Ursell's theory for the Lewis forms, and Porter (1960) and Tasai (1961), extended Ursell's method for an N-parameter family using a multiparametric transformation.

To perform the mapping transformation various methods were proposed. Landweber and Macagno (1967) adopted an approach based on the Bieberbach's method of inverse

transformation, De Jong (1973) proposed another method based on the orthogonality of the Fourier series and Von Kerzeck and Tuck (1969) proposed an iterative method based on the least square and the Newton-Rapson methods.

Frank (1970) proposed a different approach for the evaluation of the hydrodynamic coefficients. In this method the velocity potential is represented by a distribution of sources over the submerged cross section. Green functions, satisfying the Laplace equation, the conditions at infinity and the free surface boundary condition, are applied to represent the potential of the unit strength sources. The source density is an unknown function of the position along the contour, to be determined from the integral equations derived by applying the kinematic boundary condition on the submerged part of the cross section.

Experimental work has also been carried out on two dimensional sections and ship models. Porter (1960) measured the total vertical force and the pressure distribution on a heaving circular cylinder. Paulling and Richardson (1962) made experiments in four different sections and they measured the total force, pressure distribution, wave heights and phase angles. Vugts (1968) made experiments on five different sections for the heave, sway and roll motions and compared the experimental results with the theoretical method based on the multiparametric transformation. Vugts found good agreement in heave and sway motions. Frank (1970) also performed experimental work to validate his method.

Bishop et al (1978) compared the Lewis, Frank and the multiparametric conformal transformation methods for a variety of cross sections including a chine hull, a bulbous bow and other sectional shapes that cannot be adequately represented by a Lewis form fit. In this paper they concluded that the hydrodynamic coefficients evaluated by using the Lewis method are significantly different from the other methods in which the number of mapping coefficients is increased. They also stressed the presence of irregular frequencies in the Frank method and the high computation time to eliminate these irregularities by using interpolations schemes, particularly for the high frequency range, where there is increasing occurrence of these irregular frequencies.

To choose the best method for the evaluation of the hydrodynamic coefficients there are still some unanswered questions that must be clarified and if possible quantified, some of which are:

- The convergence of the multipole expansion method when the number of mapping coefficients used in the transformation is changed.
- The relation between the errors in the mapping transformation and in the hydrodynamic coefficients.
- The computation time used for the Frank method and for the multipole expansion.

So the objective of this chapter is to give a detailed comparison of the most common two dimensional methods used for the evaluation of the hydrodynamic coefficients. Special attention is given to the conformal transformation method, and the parameters that influence the accuracy of this method are studied. The results are compared with the ones of Frank close fit method, with respect to accuracy and the computation time involved. Finally the correlation between the geometric and hydrodynamic errors is examined and some relationships are proposed.

2.2- MAPPING TRANSFORMATION

An arbitrary section is described using the transformation to a circle in the complex form:

$$z = \sum_{n=1}^N C_n \zeta^{-n} \quad (2.1)$$

where z is a variable represented in the physical plane and ζ is represented in the reference plane, z and ζ being complex variables. The transformation is graphically represented in Fig. 2.1.

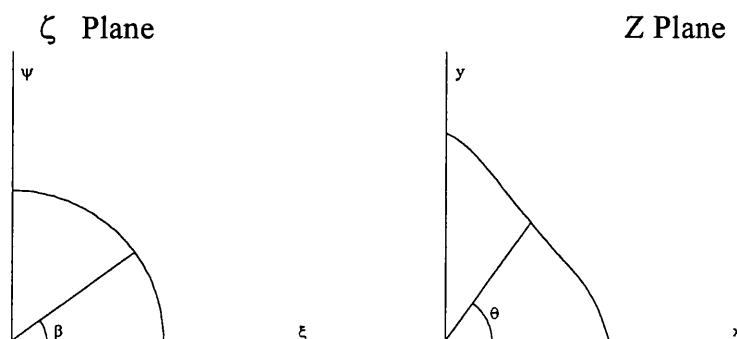


Figure 2.1 Circle transformation

For symmetric sections the conformal mapping transformation can be generally expressed by:

$$z_b = \sum_{n=1}^N A_n \zeta_b^{-(2n+1)} \quad (2.2)$$

Equation 2.2 can then be rewritten in parametric form by using:

$$x = \sum_{i=1}^N (-1)^n A_n \sin(2n+1) \gamma \quad (2.3)$$

$$y = \sum_{i=1}^N (-1)^{n+1} A_n \cos(2n+1) \gamma \quad (2.4)$$

The geometric problem is completely solved when the coefficients A_n of the conformal transformation are evaluated.

The method used in the present work to solve this problem was proposed by Von Kerzeck and Tuck (1969) who derived two different systems of equations based on the minimisation of two error functions.

The method starts with three mapping coefficients given by Lewis (1929), that are calculated recurrently using explicit expressions which use some geometric properties of the section. Using the first system of equations, which is non linear, the angles γ_i are calculated for the Lewis sections.

The number of unknown angles is equal to the number of the section offset points. For each offset point the corresponding angle is found by minimising the following expression:

$$\varepsilon = (x(\gamma) - x_i)^2 + (y(\gamma) - y_i)^2 \quad (2.5)$$

where x_i and y_i are the coordinates of the offset points and $x(\gamma)$, $y(\gamma)$ are given by (2.3) and (2.4).

Using these angles and the least square technique, a linear system of equations is solved. At each step the number of coefficients A_n is increased by one. After that the new angles can be evaluated by using the approach explained above. Consequently, this method is recursive and it stops when certain input parameters have been reached.

Figs. 2.3 and 2.4 show the precision of the mapping transformation in relation to the actual geometry for some of the transverse sections of a Series 60 ship.

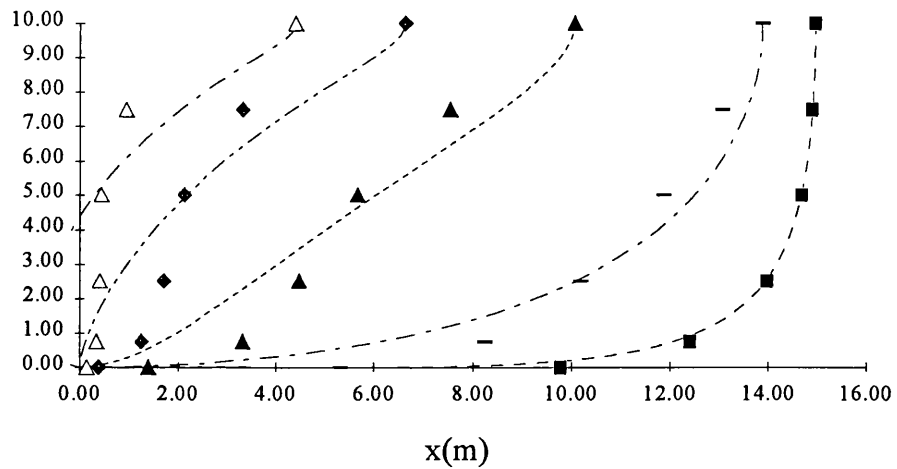


Figure. 2.2 - Transverse ship lines resulting from the Lewis transformation, showing the input points for each section.

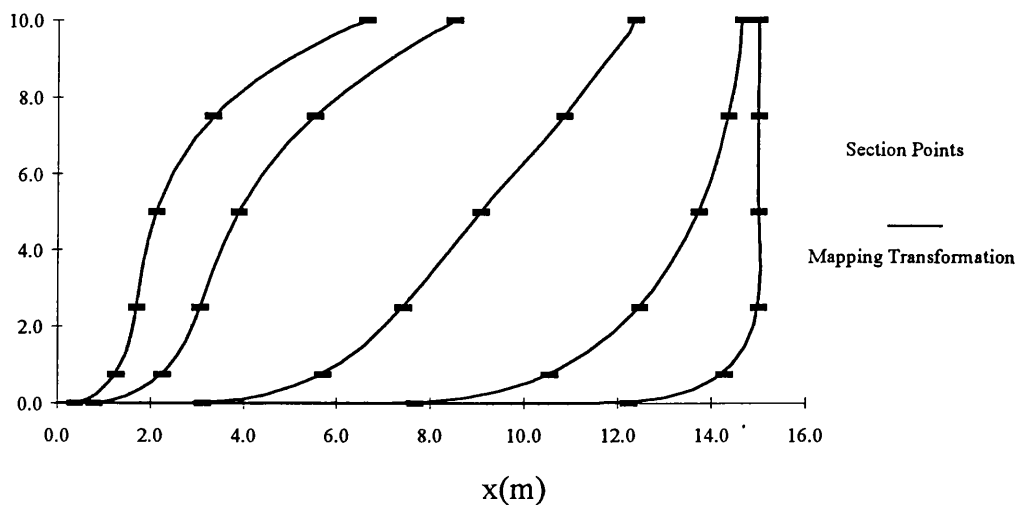


Figure. 2.3 - Transverse ship lines resulting from a 12 parameter transformation.

2.3- HYDRODYNAMIC COEFFICIENTS USING THE MULTIPOLE EXPANSION TECHNIQUE

In this section the formulation used in this work, which is basically the same as the one used by Vugts (1968), will be described. This method is a generalisation of the Ursell's (1949) method for arbitrary shaped cylinders. There are some differences between the expressions given in Vugts' report and the ones presented here.

The differences are related to the mapping transformation and the potential expressions employed in this study, which are slightly different from the ones used by Vugts. This is because he used non dimensional mapping coefficients and here dimensional mapping coefficients were used for the potential calculations, which simplifies these expressions.

Assuming

$$-dy = A_{-1} V(\gamma) d\gamma \quad (2.6)$$

and

$$dx = A_{-1} W(\gamma) d\gamma \quad (2.7)$$

where γ is the angular coordinate which is zero at the positive x axis and $\pi/2$ at the positive y axis. Substituting 2.6 and 2.7 in 2.3 and 2.4 gives the following expressions:

$$V(\gamma) = \sum_{i=-1}^N (-1)^{n+1} a_n (2n+1) \sin(2n+1)\gamma \quad (2.8)$$

$$W(\gamma) = \sum_{i=-1}^N (-1)^n a_n (2n+1) \cos(2n+1)\gamma \quad (2.9)$$

where

$$a_i = A_i / A_{-1} \quad i = -1, 0, 1, \dots, N \quad (2.10)$$

To evaluate the added mass and damping coefficient which result from radiation forces, the main assumption consists in considering the cylinder with a regular motion in a calm water, and performing the calculations of the radiation forces. The vertical motion of the cylinder can be expressed as follows:

$$y = y_a \cos(\omega t + \varepsilon) \quad (2.11)$$

where ω is the frequency of the motion and ε the phase angle.

Following Ursell's theory, the total potential for the heave motion is composed by a source potential at the origin and a sum of multipole potentials. For each one the strength is chosen in such a way that the boundary condition of the cylinder is satisfied. So the total potential can be written in the following form:

$$\phi = C_1 \operatorname{Re} \left| \left(\phi_s + \sum_{m=1}^{\infty} c_{2m} \phi_{2m} \right) e^{-i\omega t} \right| \quad (2.12)$$

where the constant C_1 ensures that the radiated waves at infinity will have the required amplitude.

$$C_1 = \frac{g \zeta_a}{\omega \pi} \quad (2.13)$$

The velocity potential on the section contour can be expressed as:

$$\phi_b = \phi(1, \gamma, t) = C_1 [M(\gamma) \sin(\omega t) + N(\gamma) \cos(\omega t)] \quad (2.14)$$

The functions M and N are obtained directly from the potential ϕ using the following relationships:

$$M(\gamma) = \phi_s + \sum_{m=1}^{\infty} q_{2m} \phi_{2m}(\gamma) \quad (2.15)$$

$$N(\gamma) = \phi_c + \sum_{m=1}^{\infty} p_{2m} \phi_{2m}(\gamma) \quad (2.16)$$

The pressure acting on a point on the cylinder can be obtained using the Bernoulli's equation,

$$p_b = p(1, \gamma, t) = -\rho \frac{\partial \phi_b}{\partial t} = \frac{-\rho g \zeta_a}{\pi} [M(\gamma) \cos(\omega t) - N(\gamma) \sin(\omega t)] \quad (2.17)$$

A stream function which satisfies the boundary condition on the section contour can be represented in a similar way:

$$\psi_b = \psi(1, \gamma, t) = C_1 [C(\gamma) \sin(\omega t) + D(\gamma) \cos(\omega t)] \quad (2.18)$$

where

$$C(\gamma) = \psi_s + \sum_{m=1}^{\infty} q_{2m} \psi_{2m}(\gamma) \quad (2.19)$$

$$D(\gamma) = \psi_c + \sum_{m=1}^{\infty} p_{2m} \psi_{2m}(\gamma) \quad (2.20)$$

The stream function and the velocity potential according to the potential theory are related by the Cauchy-Rieman equations, so the components of the stream function can be directly obtained if the velocity potential is known.

De Jong (1973) derived all the potential expressions for a generic multiparametric transformation and obtained the following expressions:

$$\phi_c(x, y) = \pi e^{-ky} \cos(kx) \quad (2.21)$$

$$\phi_s(x, y) = \pi e^{-ky} \sin(kx) + \int_0^\infty \frac{e^{-\beta x}}{k^2 + \beta^2} (k \sin(\beta y) - \beta \cos(\beta y)) d\beta \quad (2.22)$$

$$\phi_{2m}(\gamma) = \cos(2m\gamma) + k \left(\sum_{n=1}^N \frac{(-1)^n (2n+1) A_n \cos((2m+2n+1)\gamma)}{2m+2n+1} \right) \quad (2.23)$$

$$\psi_c(x, y) = \pi e^{-ky} \sin(kx) \quad (2.24)$$

$$\psi_s(x, y) = -\pi e^{-ky} \cos(kx) + \int_0^\infty \frac{e^{-\beta x}}{k^2 + \beta^2} (k \cos(\beta y) + \beta \sin(\beta y)) d\beta \quad (2.25)$$

$$\psi_{2m}(\gamma) = \sin(2m\gamma) + k \left(\sum_{n=1}^N \frac{(-1)^n (2n+1) A_n \sin((2m+2n+1)\gamma)}{2m+2n+1} \right) \quad (2.26)$$

Introducing the boundary conditions on the potential, De Jong shows that the stream function on the cylinder is determined by:

$$\psi_c(\gamma) - \frac{x(\gamma)}{b} \psi_c\left(\frac{\pi}{2}\right) = \sum_{m=1}^{\infty} p_{2m} f_{2m}(\gamma) \quad (2.27)$$

$$\psi_s(\gamma) - \frac{x(\gamma)}{b} \psi_s\left(\frac{\pi}{2}\right) = \sum_{m=1}^{\infty} q_{2m} f_{2m}(\gamma) \quad (2.28)$$

or putting in matrix form

$$\Psi_\gamma^c = F_{\gamma 2m} P_{2m} \quad \text{and} \quad \Psi_\gamma^s = F_{\gamma 2m} Q_{2m} \quad (2.29)$$

where

$$F_{\gamma 2m} = \frac{x(\gamma)}{b} \psi_{2m}\left(\frac{\pi}{2}\right) - \psi_{2m}(\gamma) \quad (2.30)$$

The only unknowns in these equations are q_{2m} and p_{2m} , their values can be computed by using a finite number of components. The number of chosen points must be at least equal to the number of coefficients.

If the number of points is equal to the number of coefficients then the equations can be solved by a linear system of equations, but in the other case p 's and q 's must be computed according to the least squares method.

Finally the added mass and damping coefficients are obtained using the following relations:

$$m' = 2\rho b^2 \frac{M_0 B + N_0 A}{A^2 + B^2} \quad (2.31)$$

$$N' = 2\rho b^2 \frac{M_0 A - N_0 B}{A^2 + B^2} \quad (2.32)$$

where

$$M_0 = \frac{1}{G} \int_0^{\frac{\pi}{2}} M(\gamma) W(\gamma) d\gamma \quad (2.33)$$

$$N_0 = \frac{1}{G} \int_0^{\frac{\pi}{2}} N(\gamma) W(\gamma) d\gamma \quad (2.34)$$

and A and B are related with the potentials parts C and D ,

$$A = D \left(\frac{\pi}{2} \right) \quad (2.35)$$

$$B = C \left(\frac{\pi}{2} \right) \quad (2.36)$$

and the constant G is a scale factor equal to:

$$G = \frac{b}{A_{,1}} \quad (2.37)$$

2.3.1 - Numerical Aspects

The main numerical problem of this method is how to perform the integrals ϕ_s (eqn. 2.22) and ψ_s (eqn. 2.25). This problem is related to the fact that the integral do not have an analytic solution, the upper limit of the integral is infinity and there are many variables involved in the expression.

However the integral always converges to a real value so it is possible to write them in the following form:

$$\int_0^{\infty} \frac{e^{-\beta x}}{k^2 + \beta^2} (k \sin(\beta y) - \beta \cos(\beta y)) d\beta \approx \int_0^{B_1} \frac{e^{-\beta x}}{k^2 + \beta^2} (k \sin(\beta y) - \beta \cos(\beta y)) d\beta \quad (2.38)$$

$$\int_0^{\infty} \frac{e^{-\beta x}}{k^2 + \beta^2} (k \cos(\beta y) + \beta \sin(\beta y)) d\beta \approx \int_0^{B_2} \frac{e^{-\beta x}}{k^2 + \beta^2} (k \cos(\beta y) + \beta \sin(\beta y)) d\beta \quad (2.39)$$

where B_1 and B_2 are significantly large real values.

To evaluate this integral the Romberg integration method was used, which divides the integral into 2^n equally spaced points and then the trapezoidal rule was used to perform the integration. Afterwards the integrated value is corrected by using some weighting factors given by this method. The method also estimates the error and if it is smaller than a certain input criteria then the method finds the integral value and if not n is increased by 1.

The main problem of this method, when trying to solve equations (2.38) and (2.39), is the value of upper limits B_1 and B_2 . If the limits are "too large" the Romberg integration method do not converge and if they are "too small" the integral value is not equal to the real value. Unfortunately the value of B_1 and B_2 are very dependent on the variables x and k , and they have some correlation with the variable y . Fig. 2.4 illustrates the different behaviour of the function for different values of k and x .

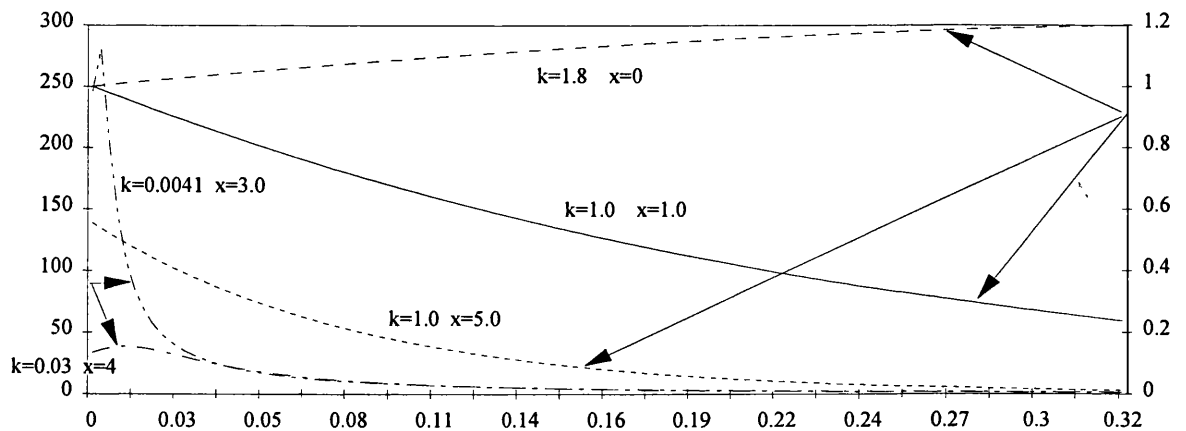


Figure 2.4 -Behaviour of function H for different values of x and k

Looking at equations (2.38) and (2.39) one can say that if the auxiliary integral,

$$H(x, k) = \int_0^B \frac{e^{-\beta x}}{k^2 + \beta^2} (k + \beta) d\beta \quad (2.40)$$

can be evaluated, it can be used to provide bounds to the integrals of interest:

$$-H(x, k) \leq \int_0^{B1} \frac{e^{-\beta x}}{k^2 + \beta^2} (k \sin(\beta y) - \beta \cos(\beta y)) d\beta \leq H(x, k) \quad (2.41)$$

$$-H(x, k) \leq \int_0^{B2} \frac{e^{-\beta x}}{k^2 + \beta^2} (k \cos(\beta y) + \beta \sin(\beta y)) d\beta \leq H(x, k) \quad (2.42)$$

So if for a certain value of B, the integral H(x,k) converges, then the integrals of eqns. 2.38 and 2.39 will also converge for the same upper limit. Let H' be equal to

$$H'(x, k, \beta) = \frac{e^{-\beta x}}{k^2 + \beta^2} (k + \beta) \quad (2.43)$$

The maximum value of H' occurs in almost all cases, when β is between 0 and 0.5. When $kx \geq 1$ the maximum will occur for $\beta=0$. The value of H' for $\beta=0$ is always very significant, so the limit of integration B of the first integral will be chosen such that:

$$\frac{H'(x, k, B)}{H'(x, k, 0)} = 10^{-4} \quad \text{or} \quad \frac{e^{-Bx}}{k^2 + B^2} (k + B) - \frac{10^{-4}}{k} = 0 \quad (2.44)$$

implying that, for values of B such that the integrand becomes much lower than $H'(x, k, 0)$, they can be neglected in the evaluation of the integral. By using this approach the first upper limit of the integral can be estimated. The roots of equation (2.44) are evaluated using the bisection method. Using this approach the values of B are evaluated and shown in table 2.1 for the five cases presented in the figure 2.4.

x	k	B
0.00	1.80	181.77
5.00	1.00	0.936
1.00	1.00	3.519
4.00	0.03	0.477
3.00	0.0041	0.221

Table 2.1 - Upper limits B for several values of x and k

The total integrals in equations (2.41) and (2.42) are evaluated by summing a series of integrals, where the limits of integration are given by eqn. (2.45):

$$\int_0^{\infty} \frac{e^{-\beta x}}{k^2 + \beta^2} (k \sin(\beta y) - \beta \cos(\beta y)) d\beta \approx \sum_{i=1}^N \int_{B_i}^{B_{i+1}} \frac{e^{-\beta x}}{k^2 + \beta^2} (k \sin(\beta y) - \beta \cos(\beta y)) d\beta$$

$$\int_0^{\infty} \frac{e^{-\beta x}}{k^2 + \beta^2} (k \cos(\beta y) + \beta \sin(\beta y)) d\beta \approx \sum_{i=1}^N \int_{B_i}^{B_{i+1}} \frac{e^{-\beta x}}{k^2 + \beta^2} (k \cos(\beta y) + \beta \sin(\beta y)) d\beta$$

where

$$B_1 = 0 \quad B_2 = B \quad B_{i+1} = B_i + i \frac{2\pi}{y} \quad i = 2, 3, \dots, N \quad (2.45)$$

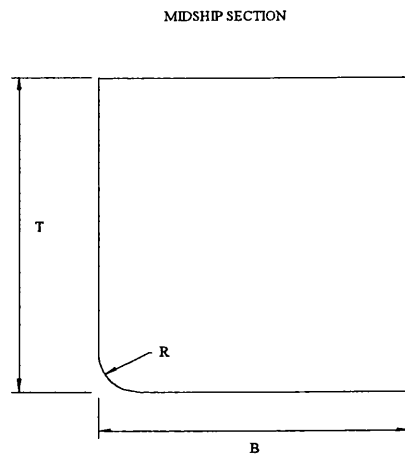
When the ratio of each integral by the sum of the previous ones is smaller than 10^{-4} , the summation is stopped.

2.4 - RESULTS

In this section the behaviour of the mapping transformation and the change of the hydrodynamic coefficients when the number of mapping coefficients is changed will be studied. The Frank close fit method is also used to evaluate the hydrodynamic coefficients and comparisons between these methods are carried out.

Another important aspect is the possible relation between the error produced by the mapping transformation and the deviations observed in the hydrodynamic coefficients, which will be studied here. Finally the computing time for the mapping transformation is evaluated for different numbers of coefficients and compared with the one obtained by using the Frank close fit method.

Eight different sections were chosen to perform this analysis. The first five represent typical midship sections for large conventional ships: rectangular section with a circular bilge whose radius varying from zero to 0.4 of the section draft. Fig. 2.5 represents one generic midship section. The other three sections have bow type shapes with different side steepness. The bow section labelled as A do not have a flare, and section C has a severe flare. The three sections are depicted in figure 2.6.



2.5 - Midship section

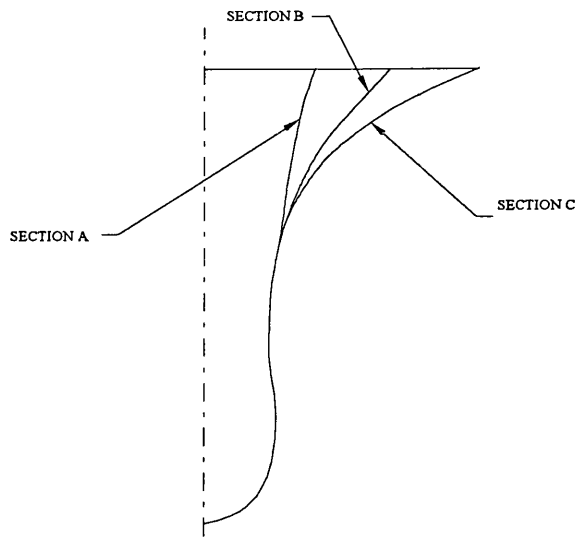


Figure 2.6 - Bow sections

The mean geometric error in defining the geometry with different number of mapping coefficients is obtained by using:

$$\epsilon_m = \frac{\epsilon_x + \epsilon_y}{2} \quad (2.51)$$

$$\epsilon_x = \frac{1}{N \cdot \sqrt{A}} \sum_{i=1}^N \text{abs}(x_i - x(\gamma_i)) \quad \epsilon_y = \frac{1}{N \cdot \sqrt{A}} \sum_{i=1}^N \text{abs}(y_i - y(\gamma_i))$$

where A represents the sectional area. Fig. 2.7 shows the dependence of the mean geometric error on the number of coefficients used in the transformation.

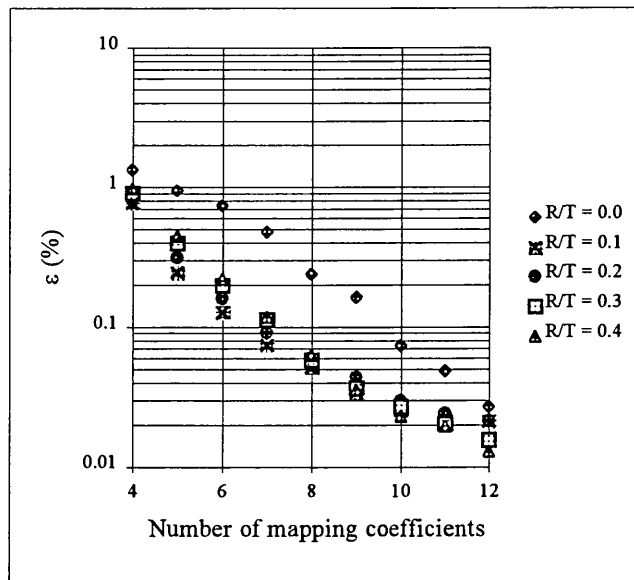


Figure 2.7 - Variation of the mean error with the number of coefficients for different midship sections

Figures 2.10 and 2.11 show the convergence of the hydrodynamic coefficients when the number of coefficients of the mapping transformation for the section with bilge keel with radius equal to zero (R00) is increased. For all midship sections the behaviour of the deviations in the hydrodynamic coefficients vs. frequency is also illustrated in figures 2.8 and 2.9. The hydrodynamic coefficients are non dimensionalised by the coefficients corresponding to a 12 conformal mapping transformation (M12 and N12). The frequency is non-dimensionalised using the following factor:

$$\omega' = \frac{\omega^2 B}{2g} \quad (2.54)$$

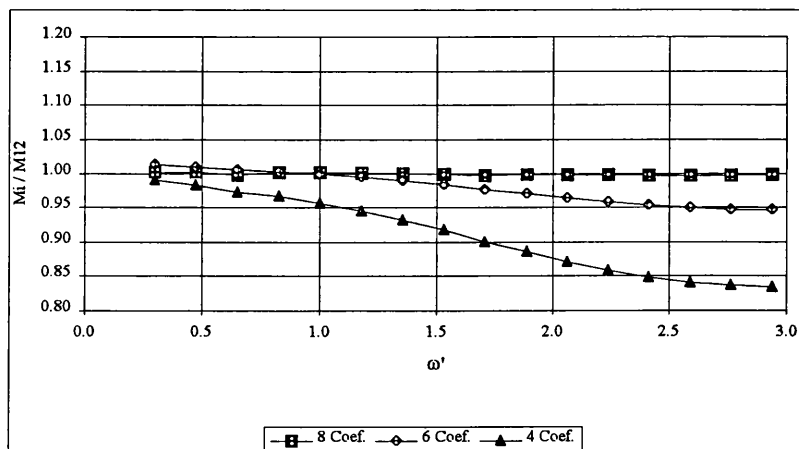


Figure 2.8 - Added mass deviations for the rectangular section (R00)

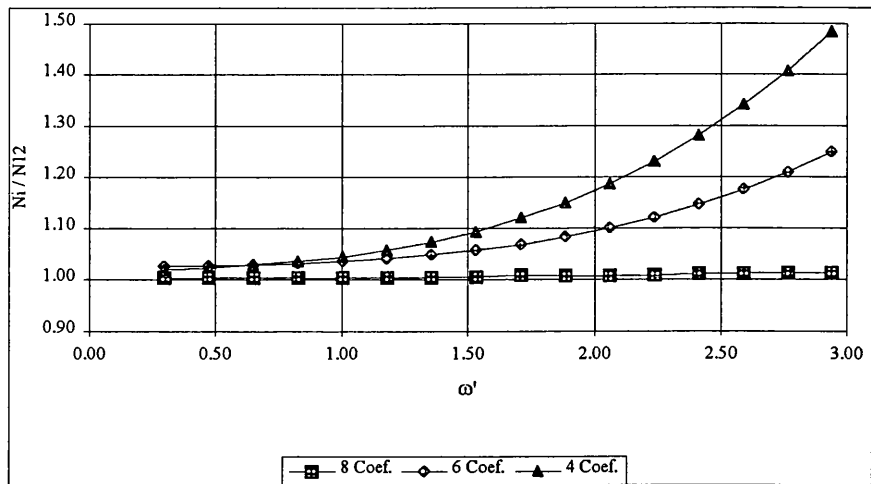


Figure 2.9 - Damping deviation for the rectangular section (R00)

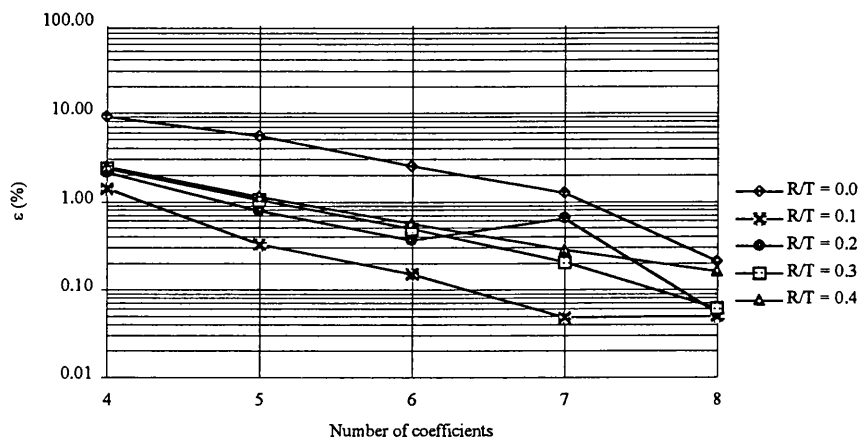


Figure 2.10 - Variation of the added mass mean geometric error for the different midship sections

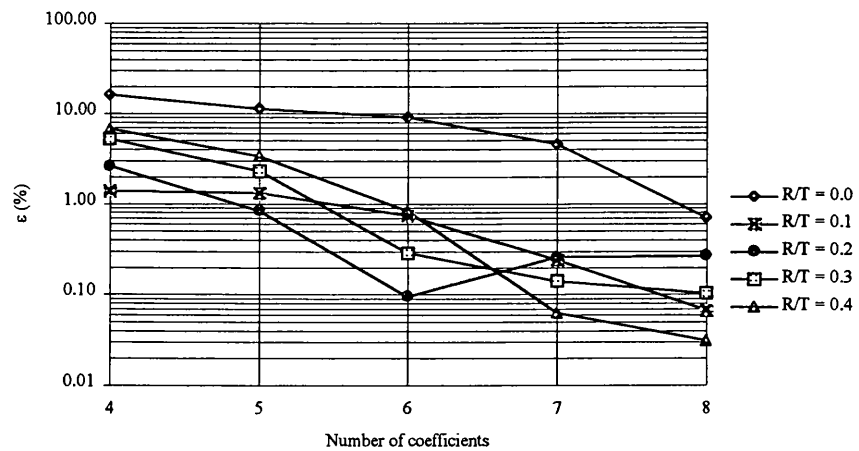


Figure 2.11 - Damping mean error for the different midship sections

Another important aspect is the comparison of more common methods used in the evaluation of the added mass and damping coefficient. Figs 2.12 and 2.13 show curves of added mass and damping coefficients versus frequency for the rectangular section.

Three curves for the comparison of added mass and damping coefficients are presented. The first one corresponds to the Lewis method which uses only the first three coefficients of the mapping transformation, the second curve represents the hydrodynamic coefficients for a 12 coefficient transformation and the last one is the Frank close fit method. The results are similar for the curves even for the rectangular section which is the section with greatest mean geometric and hydrodynamic errors. In conclusion, it was found that the Lewis method can predict reliable values for this type of sections.

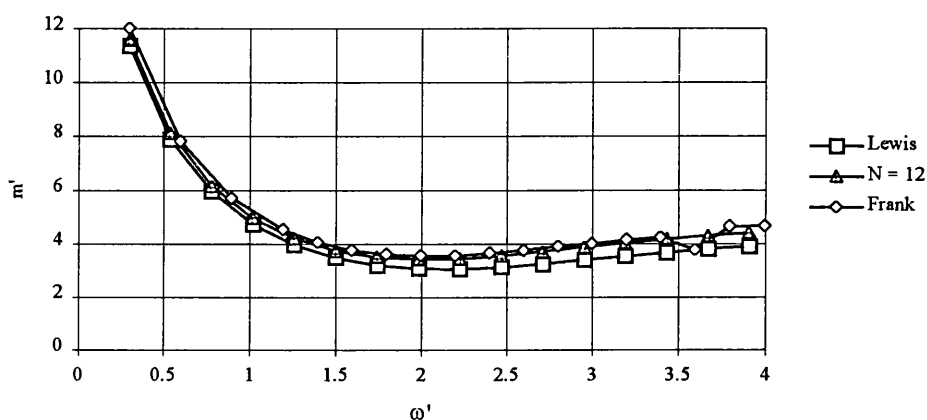


Figure 2.12 - Comparison of the added mass from the three methods for the rectangular section (R00).

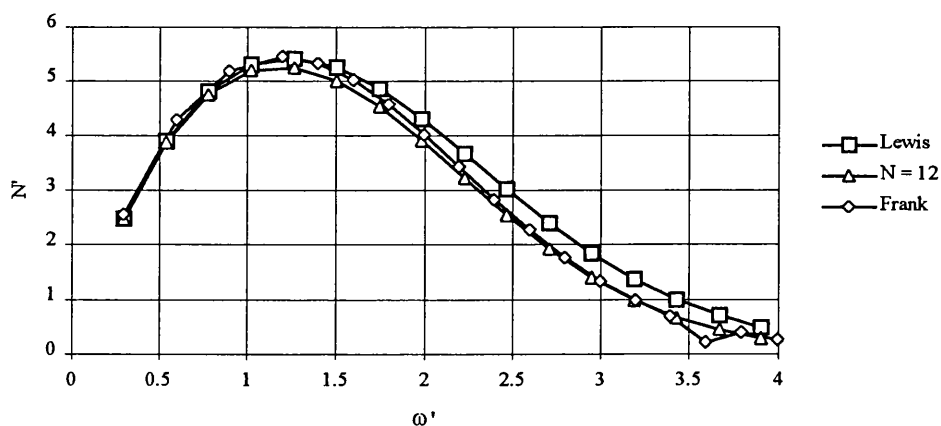


Figure 2.13 - Comparison of the damping coefficient from the three methods for the rectangular section (R00).

The methodology described above was used to study three non conventional bow sections. All sections have a bulbous bow and a flare at the upper part increasing from section A to C, as represented in fig. 2.6. This type of sections are chosen because it is shown in figure 2.2 that in this case the Lewis forms are very different from the real sections.

Figures 2.14 to 2.19 show the convergence of the hydrodynamic coefficients with the increase of the number of coefficients used in the mapping transformation for the three bow sections. The hydrodynamic coefficients are non dimensional by the same coefficients corresponding to 18 or 12 parameters of the conformal mapping transformation.

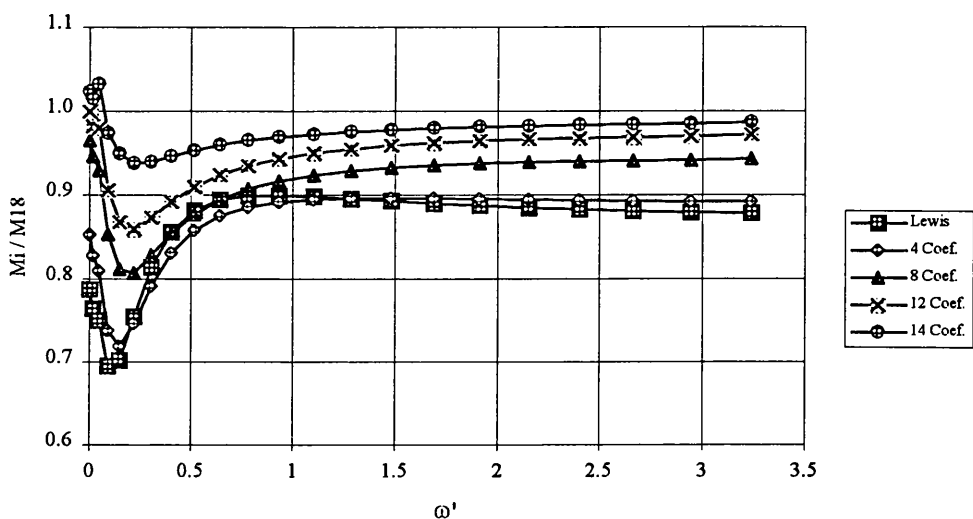


Figure 2.14 - Normalised added mass for section A

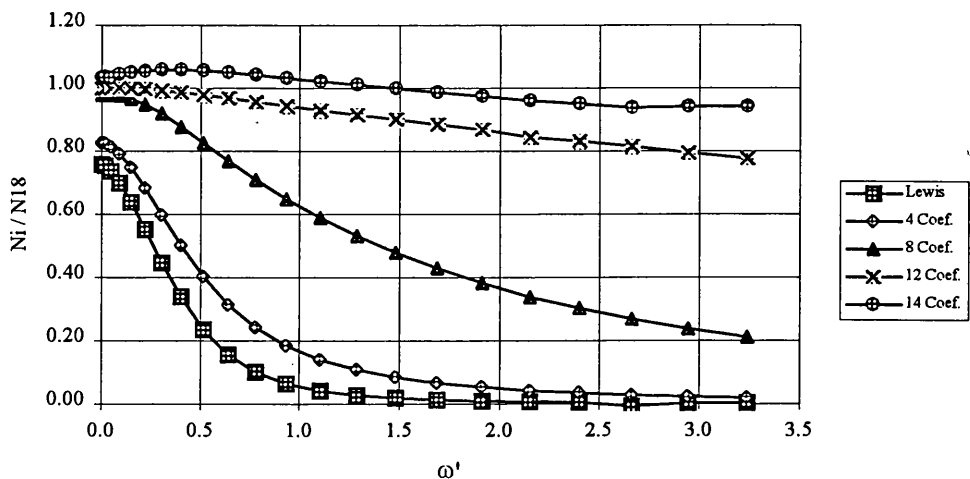


Figure 2.15 - Normalised damping for section A

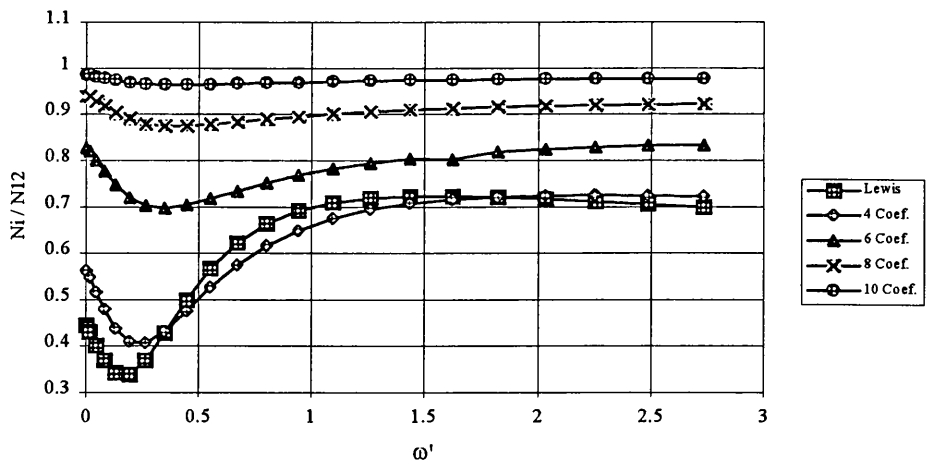


Figure 2.16 - Normalised added mass for section B

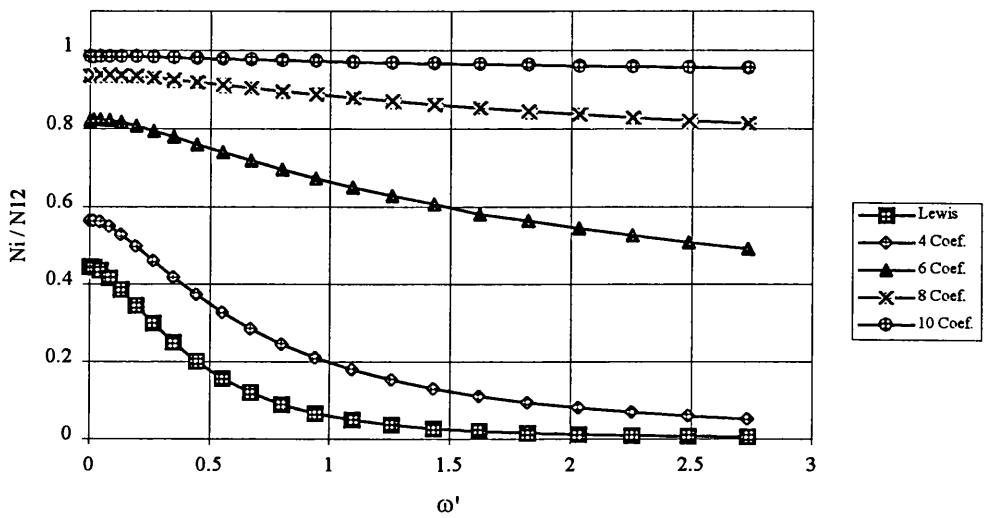


Figure 2.17 - Normalised damping for section B

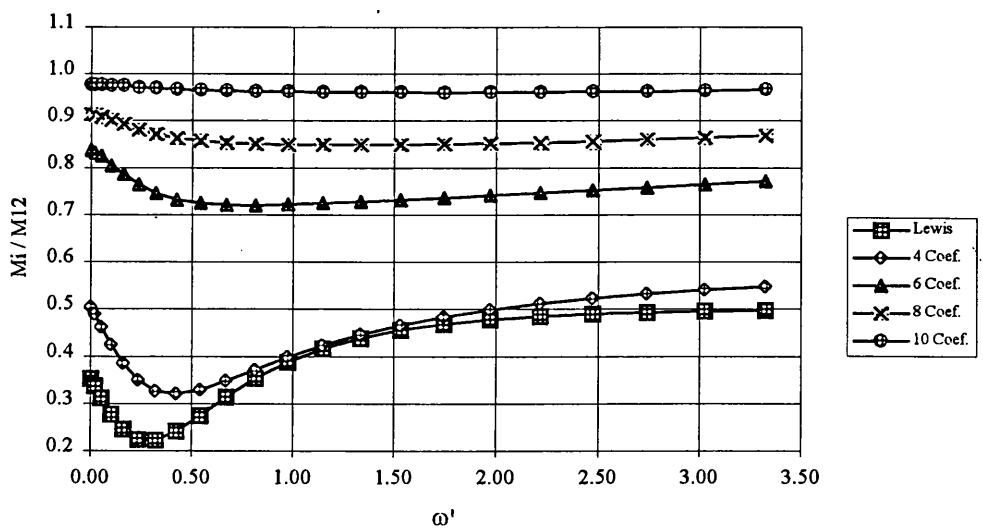


Figure 2.18 - Normalised added mass for section C

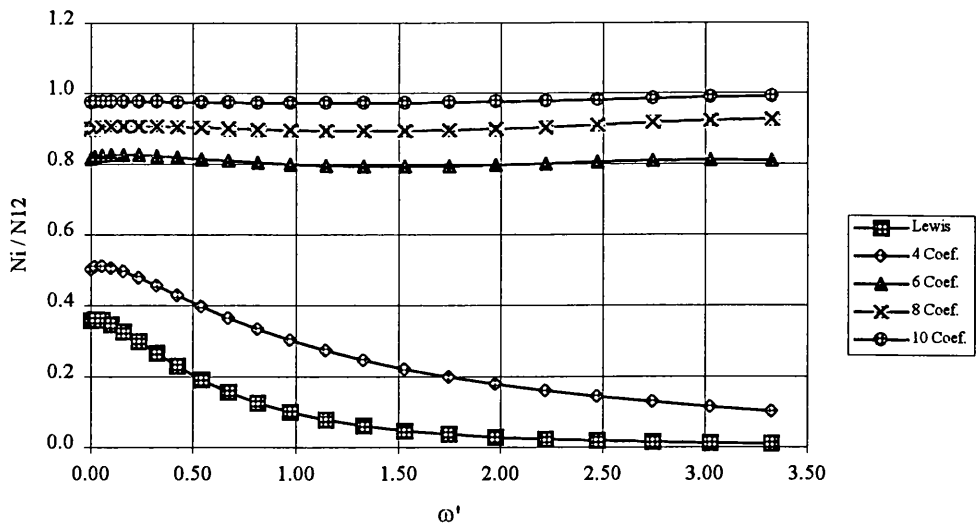


Figure 2.19 - Normalised damping for section C

Large deviations appear in the damping coefficient for the transformations with few coefficients. Two distinct error sources exist in the damping coefficient deviations, the first one is related to the absolute values i.e. the deviation of the maximum reached in damping and the variation of the damping coefficient with the frequency.

The first source is important for the total deviations, but the second contribution is the most important one. In the added mass deviations the behaviour is similar for all numbers of coefficients but the values have significant variations. The following figures represent the mean errors averaged over frequency for the added mass and damping coefficients with different number of coefficients used in the mapping transformation.

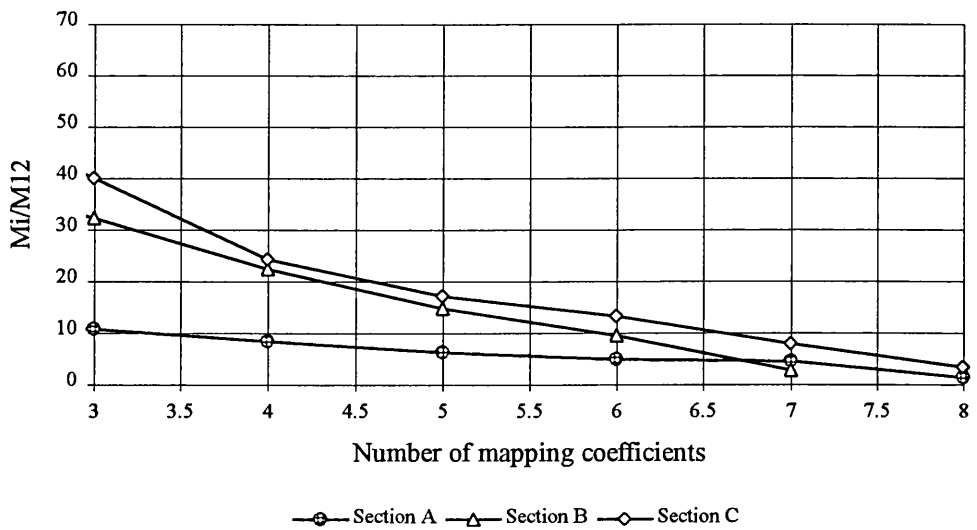


Figure 2.20 - Added mass. Mean error

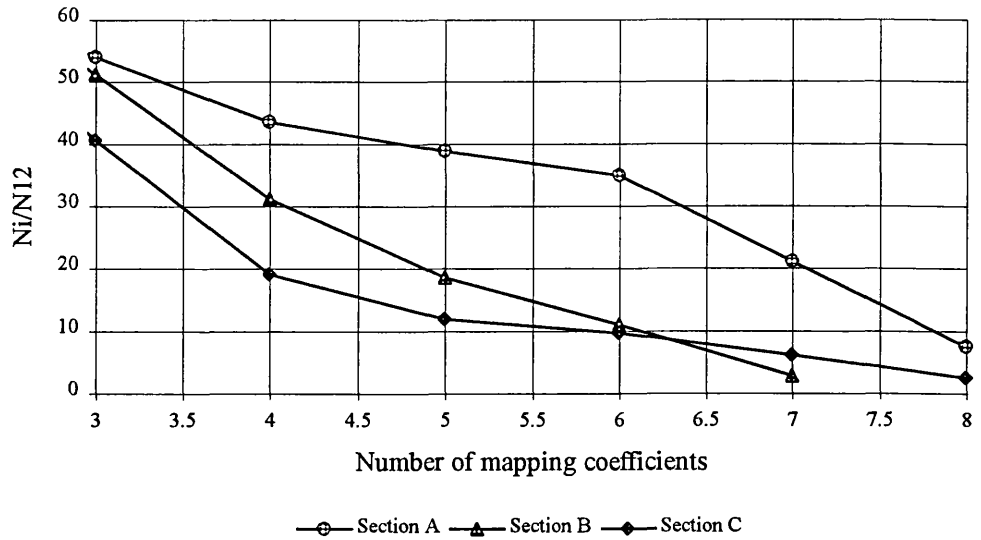


Figure 2.21 - Damping. Mean error

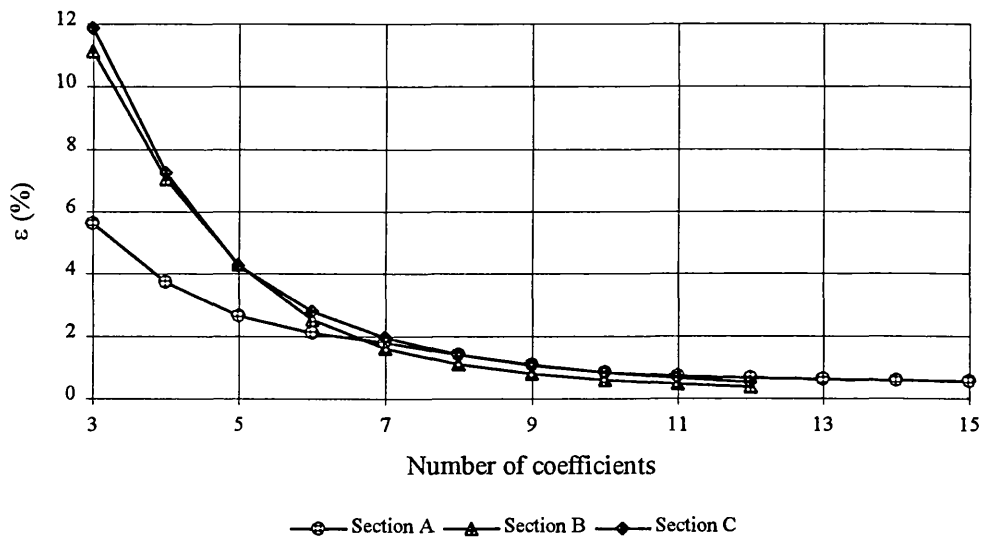


Figure 2.22 - Mean geometric error variation for the bow sections

Comparisons between the Frank close fit, Lewis methods and the transformation using 12 coefficients have been performed and figures 2.23 to 2.28 show the results. The Lewis method for this type of sections is a crude approximation when compared with the Frank close fit and the 12 parameter method. Good agreement was found between the Frank close fit method and the 12 parameter method specially for sections B and C. For high frequencies the Frank close fit method shows some irregularities.

Knowing that the Frank close fit method has irregular frequencies, its effect can be removed by calculating the hydrodynamic quantities for several frequencies, neglecting the irregular frequencies and interpolating. However, in this study the irregular results have not been removed.

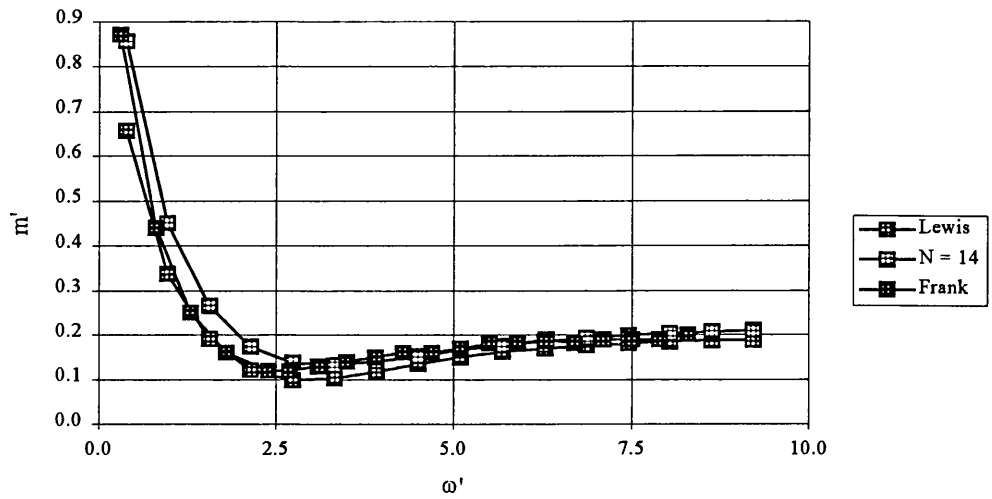


Figure 2.23 - Added mass coefficient for section A

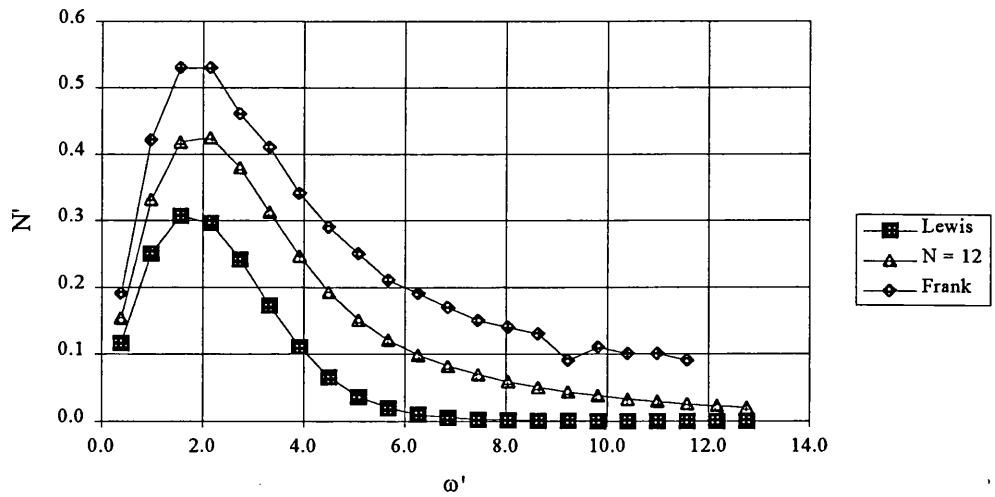


Figure 2.24 - Damping for section A

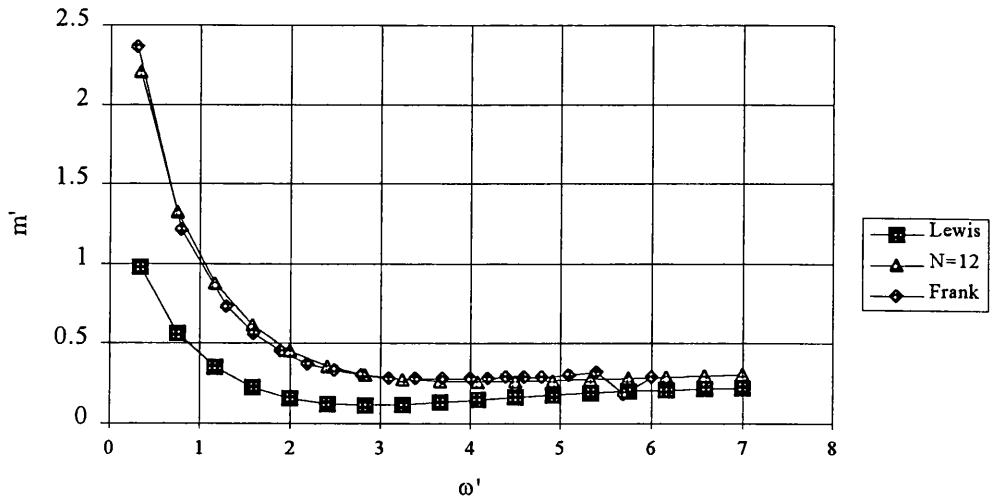


Figure 2.25 - Added mass for section B

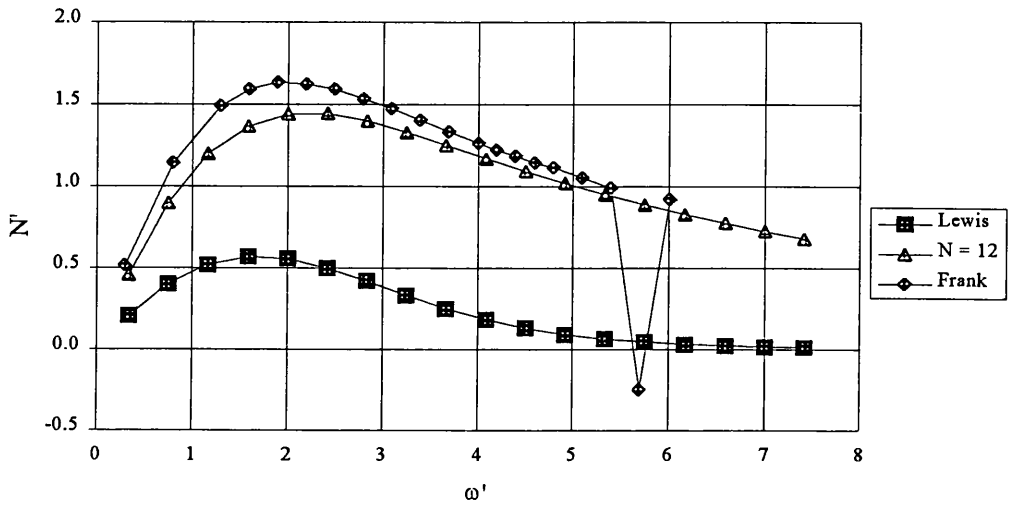


Figure 2.26 - Damping for section B

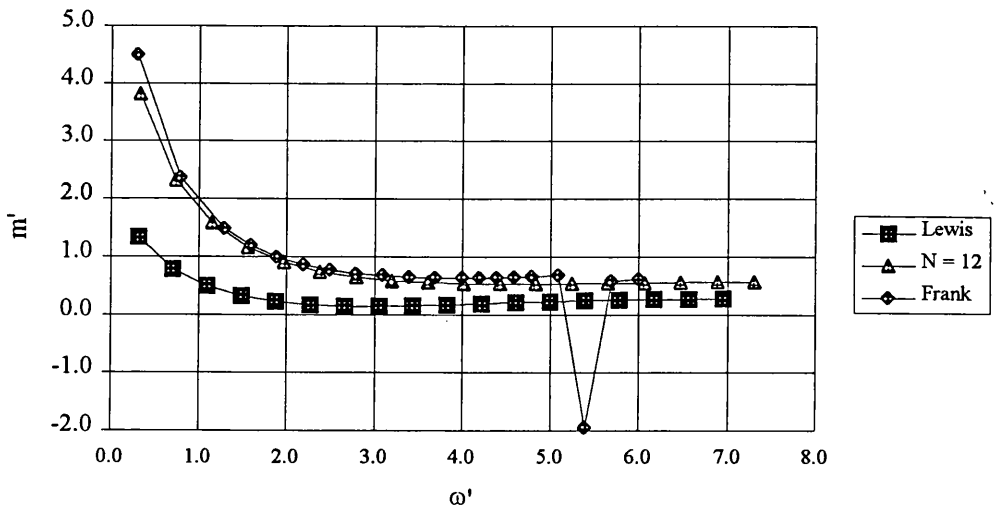


Figure 2.27 - Added mass for section C

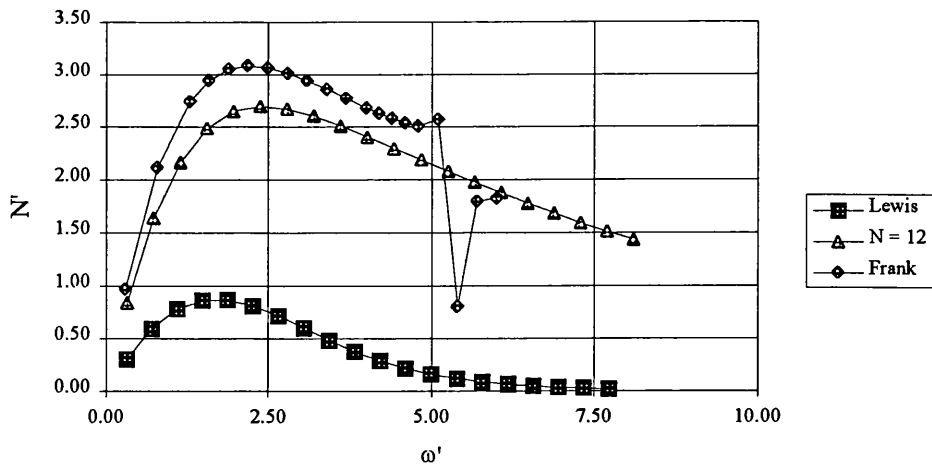


Figure 2.28 - Damping for section C

In order to define the “best method” it is important to consider not only the accuracy of the results but also the computation effort associated with each method. The computer which was used to perform all the computations is a personal computer 486/33. Two computer programs are used to perform the hydrodynamic coefficients using the mapping transformation. The first one evaluates the coefficients of the transformation and the second one calculates the hydrodynamic coefficients using the mapping coefficients. The time consumption for all sections and for the Lewis, Frank close fit and 12 parameter methods is illustrated in table 1. In the Frank method 14 segments were used to define the section geometry. The number of multipoles used in the multipole expansion is, as well, equal to 14. The mean value, variance and coefficient of variation (COV) are also calculated.

	Transformation		Hydrodynamic Coef.		Total		
	Lewis	12 Coef.	Lewis	12 Coef.	Lewis	12 Coef.	Frank
R00	0.91	11.26	6.26	9.71	7.17	20.97	100.8
R01	1.04	14.01	6.26	9.61	7.30	26.2	98.90
R02	1.10	14.05	6.27	9.67	7.37	27.2	92.7
R03	1.04	14.17	6.26	9.62	7.30	27.9	101.58
R04	1.10	14.17	6.26	9.63	7.36	28.0	104.12
Sec1	0.99	11.70	6.26	9.67	7.25	21.37	108.88
Sec2	0.95	11.90	6.24	9.66	7.19	21.56	120.56
Sec3	0.89	11.90	6.15	9.64	7.04	21.54	110.95
Mean	1.00	12.90	6.25	9.65	7.25	22.55	105.17
COV	0.081	0.101	0.006	0.003	0.015	0.057	0.079

Table 2.2 - Computation time (CPU) in seconds for the different sections

Based on the relatively small values obtained for the COV it can be assumed that the time consumed to calculate the hydrodynamic coefficients is independent of the section geometry.

Using this assumption Fig. 2.29 represents the mean value of the time spent in the transformation and in the calculation of the hydrodynamic coefficients and the total time consumed. The computation time for the Frank close fit method is about 4.8 times greater than the 12 parameter method and 14.5 times greater than the Lewis method.

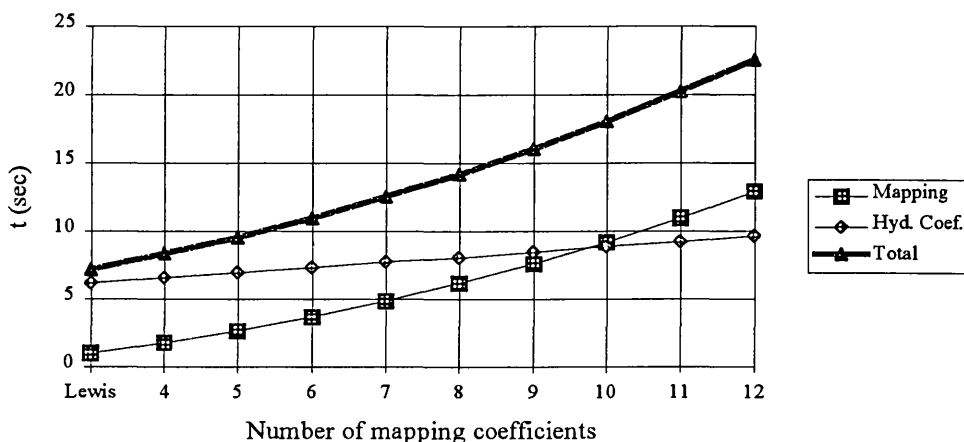


Figure 2.29 - Time consumption varying the number of coefficients (seconds)

Finally the next two figures show the relation between the errors in the definition of the geometry and in the hydrodynamic coefficients. The correlation between these two types of errors was evaluated based on the regression equation:

$$y = A x$$

where the coefficients are represented in table 2.

	Correlation coef. (ρ)	Coefficient A
Added mass	0.95	7.73
Damping coefficient	0.81	12.42

Table 2.3 - Correlation coefficient and slope coefficient

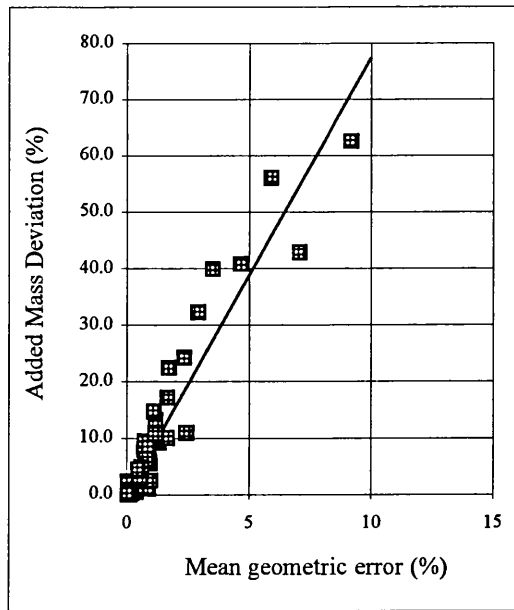


Figure 2.30 - Correlation between the added mass deviations and the mean geometric error

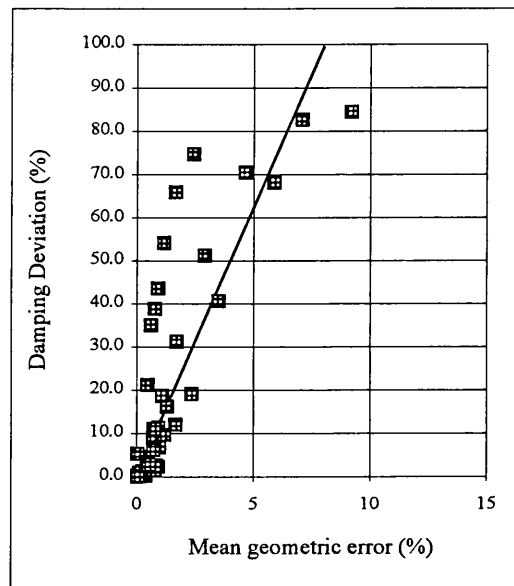


Figure 2.31 - Correlation between the damping coefficient deviations and the mean geometric error

2.5 - CONCLUSIONS

The important parameters that are involved in the determination of the added mass and damping coefficient are studied using the mapping transformation. These values are also compared with the results of the Frank close fit method.

For the midship sections, a small number of parameters is enough to obtain satisfactory results when compared with the Frank close fit method. For bow type sections with severe flare, great deviations occur between the Lewis and the Frank method.

The hydrodynamic coefficients obtained using the transformation method tend to approximate the Frank close fit method with the increase of the number of mapping parameters. The advantages of the transformation method when compared to the Frank method is the computation speed and the confidence in the results for high frequencies, but the disadvantage is that the mapping is impossible to be performed for some sections like close bulbs and completely submerged sections.

Some correlation between the geometric errors and the hydrodynamic errors was found, especially for the added mass and using those results the hydrodynamic errors can be estimated.

CHAPTER 3

WAVE INDUCED MOTIONS AND LOADS

3.1 - INTRODUCTION

In this chapter only the vertical ship motions and loads will be studied. This simplification is undertaken because for the purpose of this research, which is the calculation of the combined vertical shear forces and bending moments (due to waves and slamming), the only motions of interest are the vertical ones.

The prediction of ship motions and sea loads have been studied by several investigators since the end of the last century. Krilov (1896) calculated the vertical exciting forces acting on the ship hull, using the wave pressure distribution formulation ignoring the presence of the hull, i.e. he did not consider the radiation effects. Using this approach he formulated the equations for vertical motions using only the inertia and hydrostatic coefficients.

Weiblum and St. Denis (1950) stressed the importance of including the hydrodynamic forces in the equations of motion and they proposed simple formulae to estimate these quantities.

Korvin-Kroukovsky (1957) introduced a strip theory method with the objective of reducing the three dimensional problem to a series of two dimensional problems in several longitudinal strips with constant cross section. In order to obtain the global effect on the ship the strips contributions are integrated along the length. As a consequence of this approximation the assumption of slender body must be imposed, i.e. the beam and draft are much less than the ship length.

Based on the strip theory assumption and the relative motion concept Gerritsma and Beukelman (1967) extended this method, taking into account the ship forward speed.

To validate this method, Smith (1967) made comparisons with experiments for three different ships and he obtained quite satisfactory results for the vertical motions.

Salvesen, Tuck and Faltinsen (1970) derived the strip theory in a consistent way and they found some new terms that must be included in the original strip theory.

Newman (1978) gives a complete history of the development of theoretical methods to predict ship motions in regular waves.

3.2 - FORMULATION OF THE EQUATIONS OF MOTION

In determining the ship motions it was assumed that:

- The motion, velocity and acceleration of the ship have linear dependence on the wave amplitude
- The forward velocity of the ship is constant
- The ship has a slender form
- The ship can be considered as a rigid body

Using the slender body assumption, the real three-dimensional flow around the ship can be approximated by a series of two dimensional flows in transverse strips with constant cross section. The hydrodynamic coefficients of the sections are obtained by assuming that the ship do not have forward speed and the corrections related to the ship velocity are introduced in the coefficients of the differential equations.

It is considered that the ship is travelling in head seas and that the wave excitation forces and the resultant oscillatory motions are linear and harmonic at the frequency of encounter:

$$\omega_e = \omega + \frac{\omega^2}{g} U = \omega + k U \quad (3.1)$$

where ω is the wave frequency, U is the ship speed, g the acceleration due to gravity and k is the wave number. Using the linearity assumption and considering that, for the vertical motion the only coupling terms are between heave and pitch motions, then the equations of motion for these two motions can be written in the form of two coupled second-order differential equations with frequency-dependent coefficients.

In order to simplify the ship motion equations, the coordinate system is fixed to the body, with its origin situated at the free surface on a vertical line passing through the centre of gravity. So the equations of motion can be written in the following form:

$$(\Delta + a)\ddot{z} + b\dot{z} + cz + d\ddot{\theta} + e\dot{\theta} + g\theta = F \quad (3.2)$$

$$(I + A)\ddot{\theta} + B\dot{\theta} + C\theta + D\ddot{z} + E\dot{z} + Gz = M \quad (3.3)$$

where Δ is the ship displacement, I the inertia, z the heave motion, θ the pitch motion, F the vertical force, M the exciting moment and $a, b, c, d, e, g, A, B, C, D, E, G$ are coefficients of the differential equations obtained from the ship hydrostatic and hydrodynamic properties.

The coefficients on the left hand side of the equations (3.2) and (3.3) are evaluated using the method proposed by Salvesen, Tuck and Faltinsen (1970).

$$a = \int_L a' dx - \frac{U}{\omega_e^2} N^{IA} \quad (3.4)$$

$$b = \int_L N' dx + U a^{IA} \quad (3.5)$$

$$d = -\int_L x a' dx - \frac{U}{\omega_e^2} b + \frac{U}{\omega_e^2} x_A N^{IA} - \frac{U^2}{\omega_e^2} a^{IA} \quad (3.6)$$

$$e = -\int_L x N' dx + U a - U x_A a^{IA} - \frac{U^2}{\omega_e^2} N^{IA} \quad (3.7)$$

$$A = \int_L x^2 a_{33} dx + \frac{U^2}{\omega_e^2} a - \frac{U}{\omega_e^2} x_A N^{IA} + \frac{U^2}{\omega_e^2} x_A a^{IA} \quad (3.8)$$

$$B = \int_L x^2 b_{33} dx + \frac{U^2}{\omega_e^2} b + U x_A a^{IA} + \frac{U^2}{\omega_e^2} x_A N^{IA} \quad (3.9)$$

$$D = -\int_L x a' dx + \frac{U}{\omega_e^2} b + \frac{U}{\omega_e^2} x_A N^{IA} \quad (3.10)$$

$$E = -\int_L x N' dx - U a - U x_A a^{IA} \quad (3.11)$$

$$c = \rho g \int_L b dx \quad (3.12)$$

$$g = G = -\rho g \int_L x b dx \quad (3.13)$$

$$C = -\rho g \int_L x^2 b dx \quad (3.14)$$

where a' and N' represent the sectional added mass and damping coefficient for the vertical motion, the superscript A denotes the aftermost cross-section of the ship, b the section beam, x the longitudinal position, L the ship length and ρ the water density.

The formulation for the excitation forces is different from Salvesen et al. and is obtained using the method proposed by Korvin-Kroukovsky and Jacobs (1958). The difference between these two methods is related to the following empirical assumption used by Korvin-Kroukovsky:

$$\int_c e^{kz} dl = e^{-kT^*} \quad T^* = \frac{A}{b} \quad (3.15)$$

where A represents the sectional area.

Using this approximation the expressions for the exciting forces are simplified and they can be expressed in terms of the added mass and damping coefficient. Gerritsma and Beukelman (1967) used this method for the calculation of the exciting forces and they concluded that this method requires less computation time than the Salvesen et al. one and produces similar results for conventional ship forms. The amplitudes of the exciting force and moment for the two methods are obtained using the equations (3.16) and (3.17).

$$F_0 = \rho \zeta \int (f_z + h_z) dx + \rho \zeta \frac{U}{i\omega_e} h_z^A \quad (3.16)$$

$$M_0 = -\rho \zeta \int \left[x (f_z + h_z) + \frac{U}{i\omega_e} h_z \right] dx - \rho \zeta \frac{U}{i\omega_e} x_A h_z^A \quad (3.17)$$

The difference between these two methods is in the simplification of the functions f_z and h_z . For head seas the functions f_z and h_z obtained by the two methods are for the Salvesen et al.'s method

$$h_z = i\omega e^{ikx} \int_c N_z \psi_z e^{kz} ds \quad (3.18)$$

$$f_z = g e^{ikx} \int_c N_z e^{kz} ds \quad (3.19)$$

and for the Korvin-Kroukovsky's method they are:

$$h_z = -\frac{1}{\rho \omega_e} e^{ikx} e^{-kT^*} (\omega_e^2 a' - i\omega_e N') \quad (3.20)$$

$$f_z = g e^{ikx} e^{-kT^*} b \quad (3.21)$$

where ω represents the wave frequency and ζ the wave amplitude.

The added mass and damping coefficients are obtained using the method proposed in the previous chapter.

3.3 - SOLUTION OF THE DIFERENTIAL EQUATIONS

In order to solve the system of equations, the forces are written in the following complex form:

$$F = F_0 e^{i\omega_e t} \quad (3.22)$$

$$M = M_0 e^{i\omega_e t} \quad (3.23)$$

Where F_0 and M_0 are complex numbers given by,

$$F_0 = F_R + i F_I \quad (3.24)$$

$$M_0 = M_R + i M_I \quad (3.25)$$

In the linear theory, the harmonic responses of the vessel will be proportional to the amplitude of the exciting forces with the same frequency, but with a phase shift. Consequently the ship motions will have the form:

$$z = z_0 e^{i\omega_e t} \quad (3.26a)$$

$$\theta = \theta_0 e^{i\omega_e t} \quad (3.26b)$$

where z represents the heave motion and θ the pitch motion.

The velocity and the acceleration of the motion are obtained taking the time derivatives

$$\dot{z} = i z_0 \omega_e e^{i\omega_e t} \quad (3.27a)$$

$$\ddot{z} = -z_0 \omega_e^2 e^{i\omega_e t} \quad (3.27b)$$

$$\dot{\theta} = i \theta_0 \omega_e e^{i\omega_e t} \quad (3.28a)$$

$$\ddot{\theta} = -\theta_0 \omega_e^2 e^{i\omega_e t} \quad (3.28b)$$

Substituting equations (3.26), (3.27) and (3.28) into (3.2) and (3.3) one obtains:

$$\left\{ -(\Delta + a) \omega_e^2 + b i \omega_e + c \right\} z_0 + (-d \omega_e^2 + e i \omega_e + g) \theta_0 = F_0 \quad (3.29)$$

$$\left\{ -(I + A) \omega_e^2 + B i \omega_e + C \right\} \theta_0 + (-D \omega_e^2 + E i \omega_e + G) z_0 = M_0 \quad (3.30)$$

The system can be easily solved in an explicit way. If one define the frequency-dependent constants P, Q, R, S as:

$$P = -(\Delta + a) \omega_e^2 + b i \omega_e + c \quad (3.31)$$

$$Q = -d \omega_e^2 + e i \omega_e + g \quad (3.32)$$

$$R = -(I + A) \omega_e^2 + B i \omega_e + C \quad (3.33)$$

$$S = -D \omega_e^2 + E i \omega_e + G \quad (3.34)$$

Then the motion complex variables are obtained using the following relations:

$$z_0 = \frac{FS - MQ}{PS - QR} \quad (3.35)$$

$$\theta_0 = \frac{MP - FR}{PS - QR} \quad (3.36)$$

In order to obtain the equations of heave and pitch motion in a regular wave, equations (3.26a), (3.26b) obtained in a complex form have to be changed to the real form, using the relation:

$$|z_0| = \sqrt{z_r^2 + z_i^2} \quad (3.37)$$

$$\varepsilon_z = \tan^{-1} \left(\frac{z_i}{z_r} \right) \quad (3.38)$$

The transfer function for the heave motion represents, for a certain frequency, the ratio between the heave and wave amplitudes and for the pitch motion it quantifies the amplitude of the pitch angle divided by the wave slope.

$$\text{TRF}_z(\omega_0) = \frac{z(\omega_0)}{\zeta} \quad (3.39)$$

$$\text{TRF}_\theta(\omega_0) = \frac{\theta(\omega_0)}{k\zeta} \quad (3.40)$$

The response amplitude operators for heave and pitch motions are obtained using the following relations

$$|H_z|^2 = \text{TRF}_z^2 \quad (3.41)$$

$$|H_\theta|^2 = (\text{TRF}_\theta k)^2 \quad (3.42)$$

These functions are very important in the calculation of the ship response in irregular seas, because if an irregular seastate can be represented by sea spectra, then according to the linear theory of motions the response spectra for that sea is obtained by using the following equations:

$$S_z = |H_z|^2 S_w \quad (3.43)$$

$$S_\theta = |H_\theta|^2 S_w \quad (3.44)$$

The response amplitude operator (RAO) for the relative motion at an arbitrary section is obtained using the RAO for heave and pitch and the phase between the wave and the corresponding motions

$$|H_r|^2 = 1 + |H_v|^2 - 2 |H_v| \cos (kx - \varepsilon_x) \quad (3.45)$$

where H_v represents the RAO for the vertical motion of the ship for a given longitudinal position x and ε_x the phase between the vertical motion in the x position and the wave at the centre of gravity. These two values are obtained using:

$$|H_r|^2 = |H_z|^2 + x^2 |H_\theta|^2 - 2x |H_z| |H_\theta| \cos (\varepsilon_\theta - \varepsilon_z) \quad (3.46)$$

$$\varepsilon_x = \tan^{-1} \left(\frac{|H_z| \sin(\varepsilon_z) + x |H_\theta| \sin(\varepsilon_\theta)}{|H_z| \cos(\varepsilon_z) + x |H_\theta| \cos(\varepsilon_\theta)} \right) \quad (3.47)$$

As it is done in the heave and pitch motions, the relative motion spectra of the ship $S_r(\omega, x)$ is obtained by multiplying the response amplitude operator of the ship by the sea spectra.

$$S_r(\omega, x) = |H_r(\omega, x)|^2 S_w(\omega) \quad (3.48)$$

When the ship velocity is non-zero and the transfer functions are dependent on the wave frequency, the relative motion spectra has to be transformed in terms of the encounter frequency using the following relation:

$$S_r(\omega, x) d\omega = S_r(\omega_e, x) d\omega_e \quad (3.49)$$

Substituting (3.1) into (3.49) one obtains:

$$S_r(\omega_e, x) = \frac{S_r(\omega, x)}{1 + 2U \frac{\omega}{g}} \quad (3.50)$$

The relative velocity spectrum is obtained using

$$S_{\dot{x}}(\omega_e, x) = \omega_e^2 S_r(\omega_e, x) \quad (3.51)$$

The formulation to obtain the shear forces and bending moments is given by:

$$Q(x) = \int_x^{FP} \{m_s(\ddot{z} - \xi\ddot{\theta}) - F'\} d\xi \quad (3.52)$$

$$M(x) = \int_x^{FP} \{m_s(\ddot{z} - \xi\ddot{\theta}) - F'\}(x - \xi) d\xi \quad (3.53)$$

where m_s is the longitudinal mass distribution. F' can be divided into three components

$$F' = F'_1 + F'_2 + F'_3 \quad (3.54)$$

with

$$F'_1 = -m' \ddot{z} - \left(N' - V \frac{dm'}{dx}\right) \dot{z} - \rho g b z \quad (3.55)$$

$$F'_2 = m' x \ddot{\theta} + \left(N' x - 2m' V - x V \frac{dm'}{dx}\right) \dot{\theta} + \left(\rho g b x - V N' + V^2 \frac{dm'}{dx}\right) \theta \quad (3.56)$$

$$F'_3 = \pm \zeta e^{-kT} \left\{ \rho g b \frac{\cos kx}{\sin kx} \mp \omega \left(N' - V \frac{dm'}{dx} \right) \frac{\sin kx}{\cos kx} - \omega^2 m' \frac{\cos kx}{\sin kx} \right\} \omega_e t \quad (3.57)$$

3.4 - RESULTS

Using the formulation given in this chapter, the hydrodynamic coefficients and the transfer functions for the heave and pitch motions were obtained for a container ship named as S-175. This ship was proposed by the seakeeping committee of the ITTC and extensively studied during the period of 1976-1978, and some experiments have also been made on this ship. The results of the experiments and the various ship motion

theories were published in the Proceedings of the 15th ITTC (1978). The offset data is available in one of the ITTC reports (1978). Table 3.1 gives the ship principal particulars.

Ship	S-175
L_{pp} (m)	175.0
B (m)	25.4
T (m)	9.5
Δ (t)	24 742
LCB (%L)	1.417
C_b	0.572
C_M	0.970
GM (m)	1.0
K_{yy}/L_{pp}	0.24
K_{xx}/B	0.328

Table 3.1 - Ship main particulars

The body plan of the container ship is shown in figure 3.1.

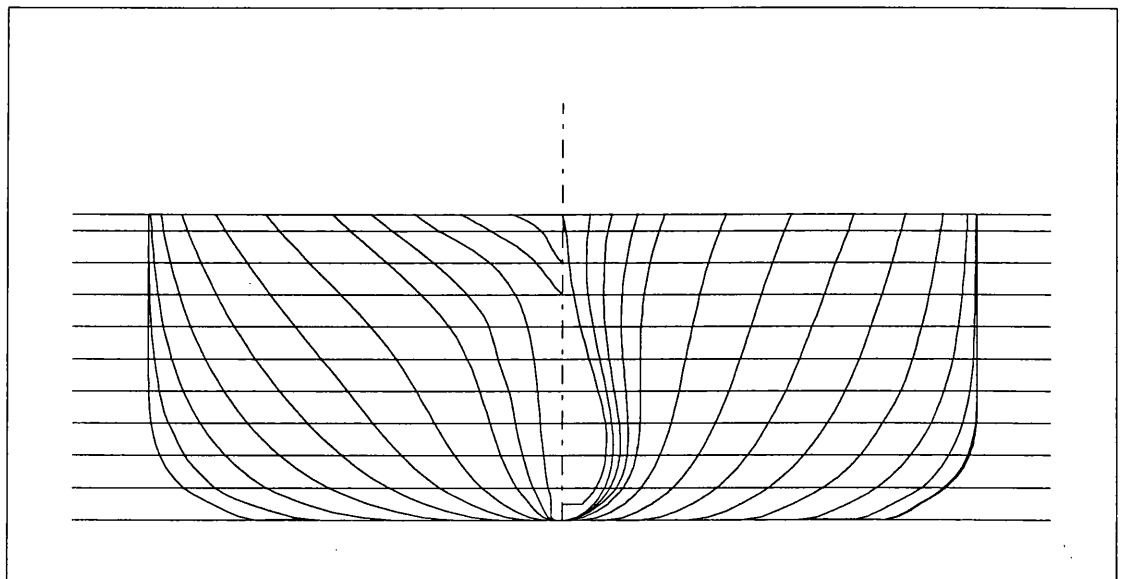


Figure 3.1 - Body Plan

The ITTC committee also gave the ship mass distribution which is illustrated together with the section area distribution in figure 3.2.

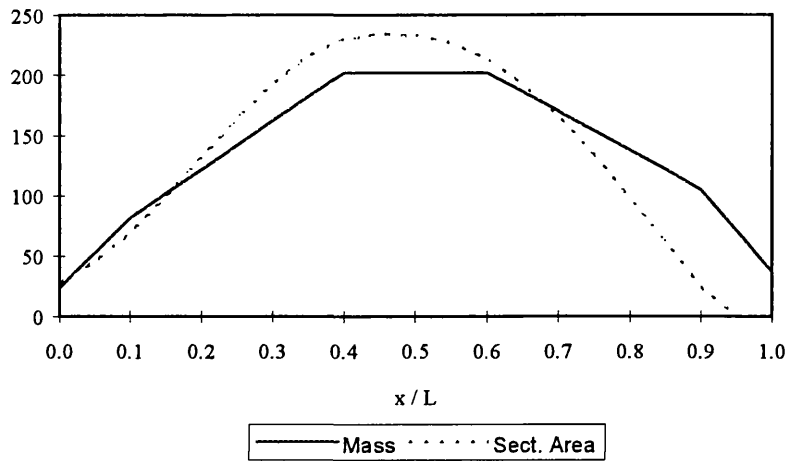


Figure 3.2 - Mass and section area distribution

The hydrodynamic coefficients were evaluated using mapping transformations with 4, 8 and 12 coefficients. It is assumed that the ship is travelling in head seas with a Froude number equal to 0.275. The results for the heave and pitch motions were compared with several results obtained from some of the partners involved in the ITTC project. The organizations and the programs used are listed in table 3.2.

Organization	Program
Helsinki University of Technology	Honkanen (1976)
Hamburg Ship Model Basin (HSVA)	Grim (1960)
Delft Shipbuilding Laboratory (Delft)	Delft (1975)
Netherlands Ship Model Basin	NSMB

Table 3.2 - Ship motion programs used for the ITTC comparison

The heave and pitch transfer functions were also compared with the experimental results carried out by the Ship Research Centre of Japan.

3.4.1 - Comparison of the Hydrodynamic Coefficients

In the first part of this section some coefficients of the equations (3.2) and (3.3) are compared for different numbers of mapping coefficients against the Lewis method,. Figs. 3.3 and 3.4 illustrate this.

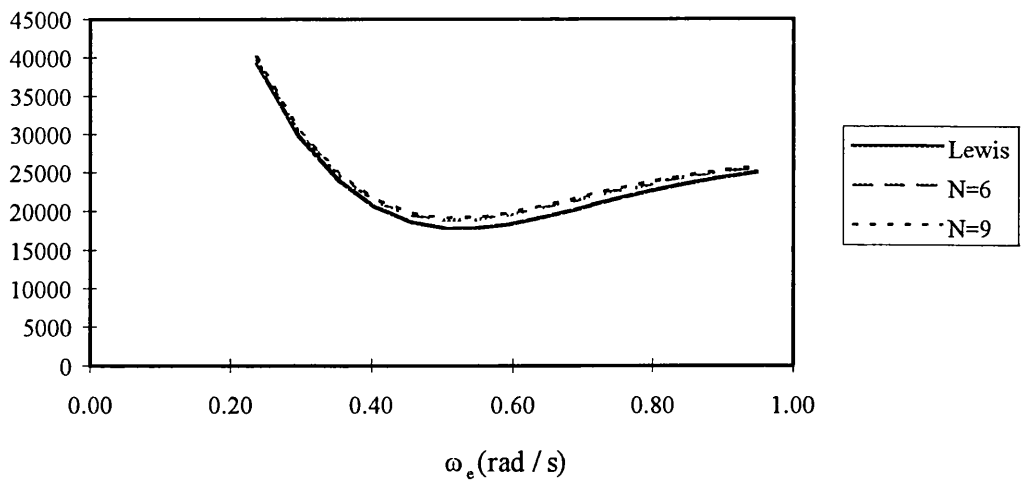


Figure 3.3 - Coefficient a used in eqn. (3.2) for three different number of mapping coefficients used in the multipole expansion method.

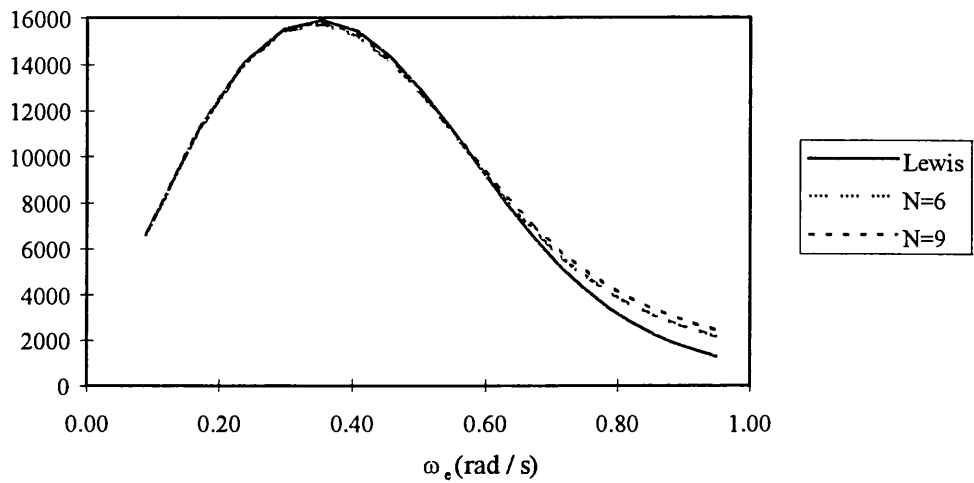


Figure 3.4 - Coefficient b used in eqn. (3.2) for three different number of mapping coefficients used in the multipole expansion method.

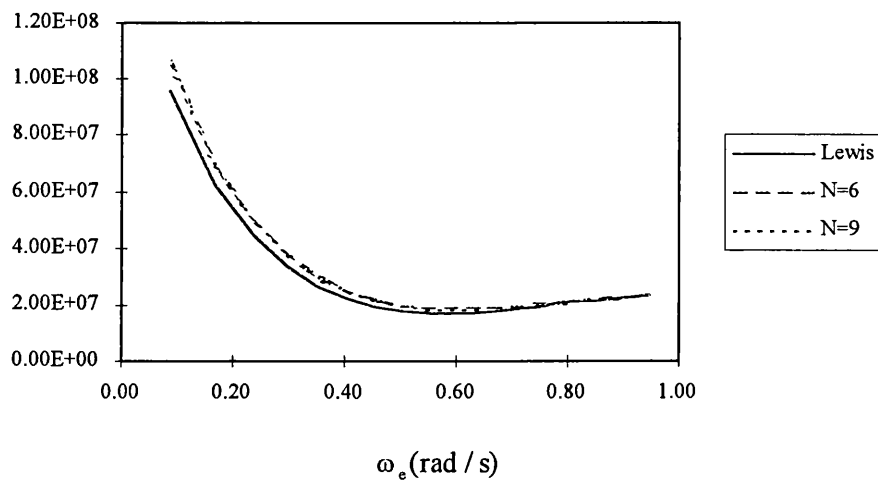


Figure 3.5 - Coefficient A used in eqn. (3.3) for three different number of mapping coefficients used in the multipole expansion method.

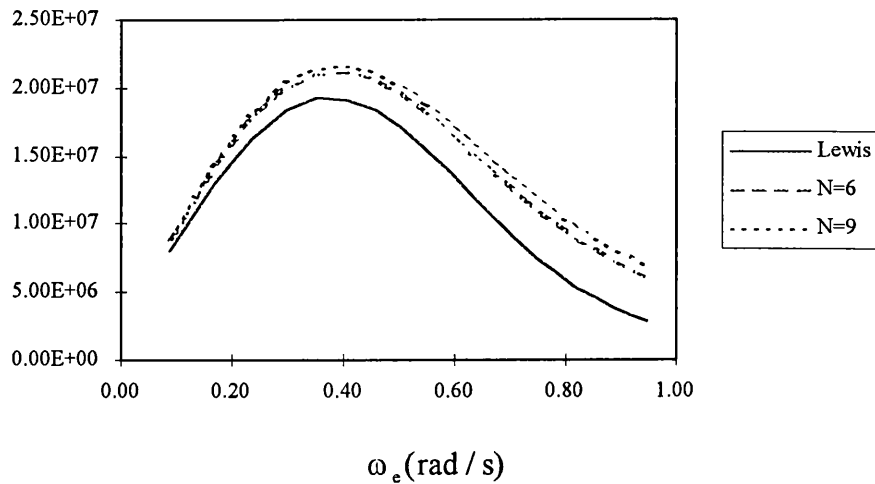


Figure 3.6 - Coefficient B used in eqn. (3.3) for three different number of mapping coefficients used in the multipole expansion method.

From figures 3.3 to 3.6 it can be concluded that for this ship the number of coefficients used in the mapping transformation will not produce significant deviations in the hydrodynamic coefficients.

As with the analysis done in chapter 2, the major deviations occur in the damping coefficient in the extreme sections, which can be seen by comparing figure 3.4 with figure 3.6.

3.4.2 - Vertical Motions

For the evaluation of the heave and pitch motions several formulations are compared with the proposed one and with the experimental results. The theoretical methods and the experiments produced quite similar results. The variation of the number of mapping coefficients in the transformation do not produce significant deviations in the transfer functions, and for the heave motion this deviation is in practice irrelevant.

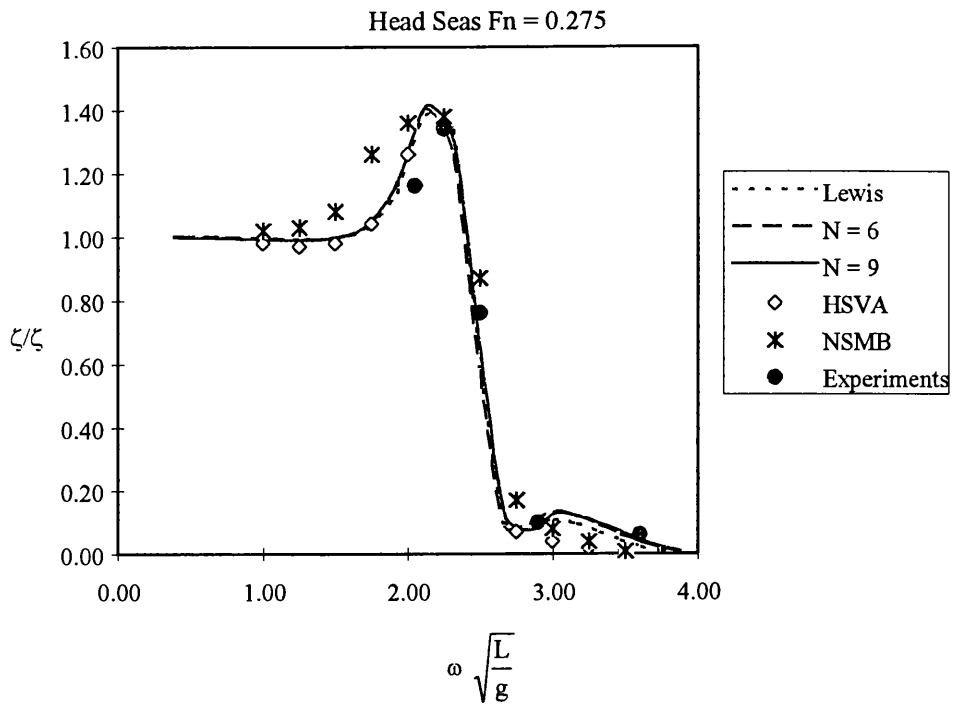


Figure 3.7 - Heave transfer function

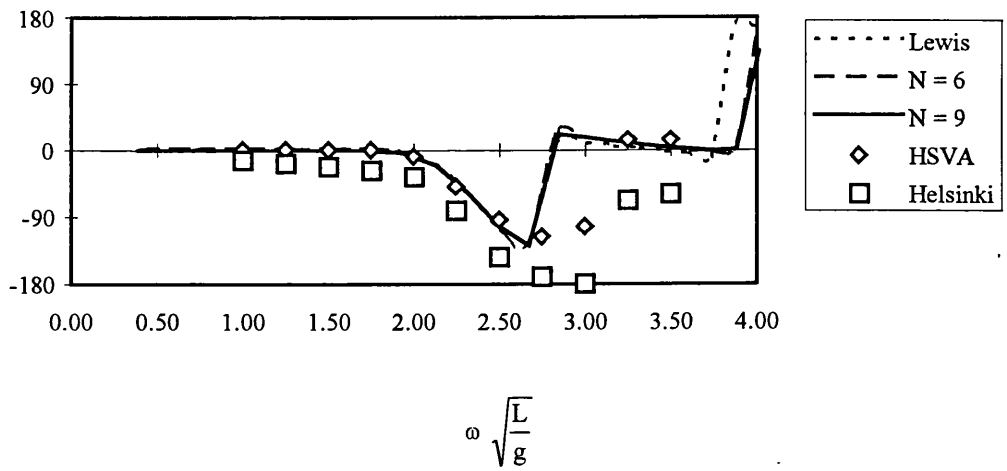


Figure 3.8 - Heave phase response

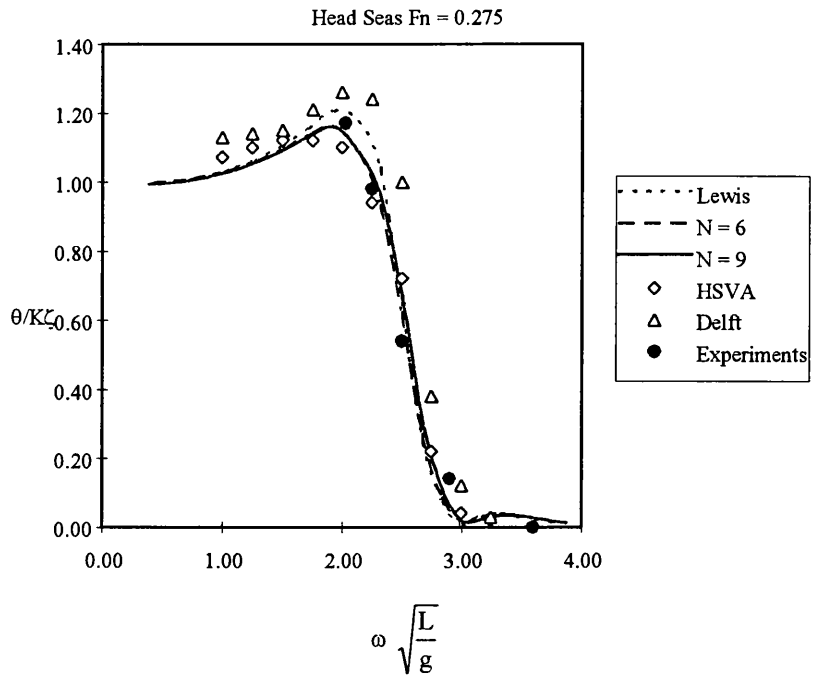


Figure 3.9 - Pitch transfer function

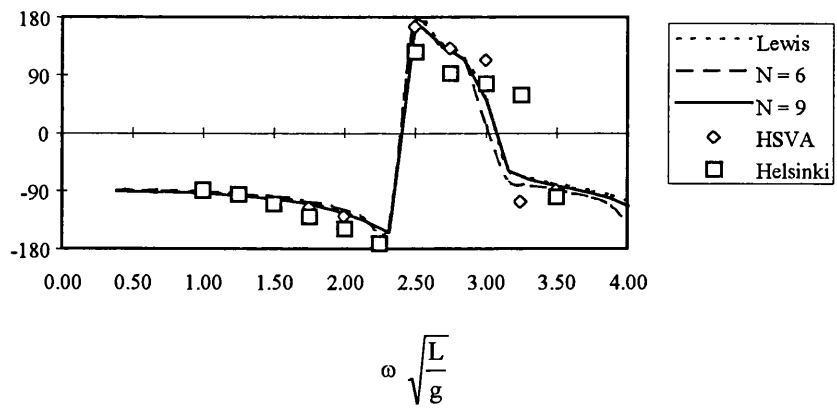


Figure 3.10 - Pitch phase response

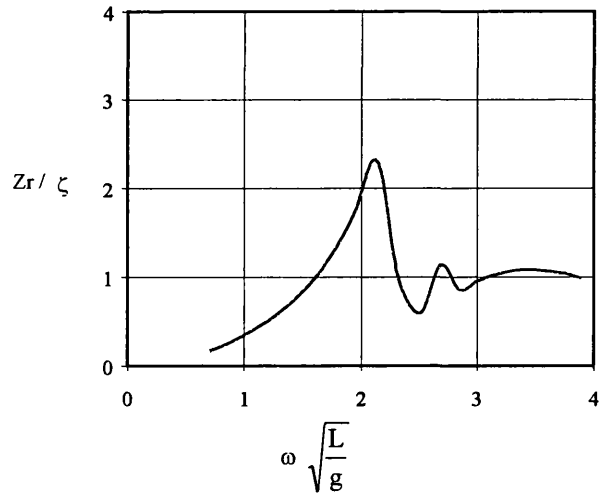


Figure 3.11 - Relative motion for Station 61/2

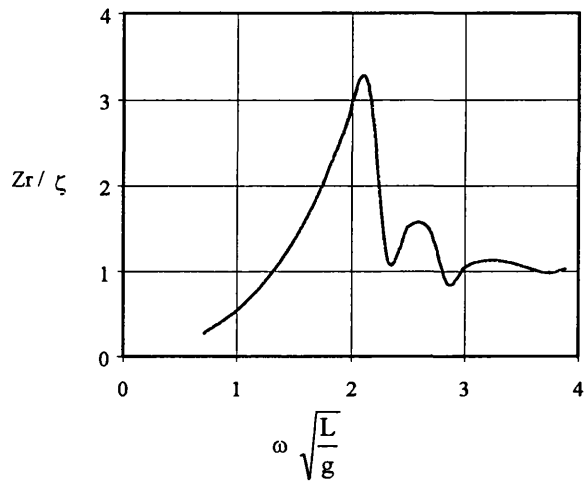


Figure 3.12 - Relative motion for Station 71/2

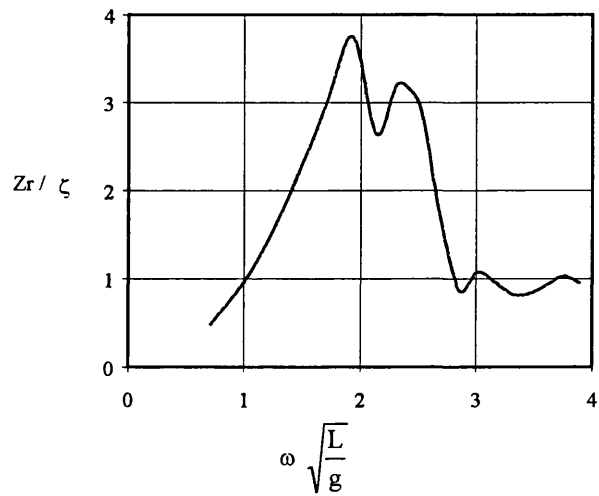


Figure 3.13 - Relative motion for Station 91/2

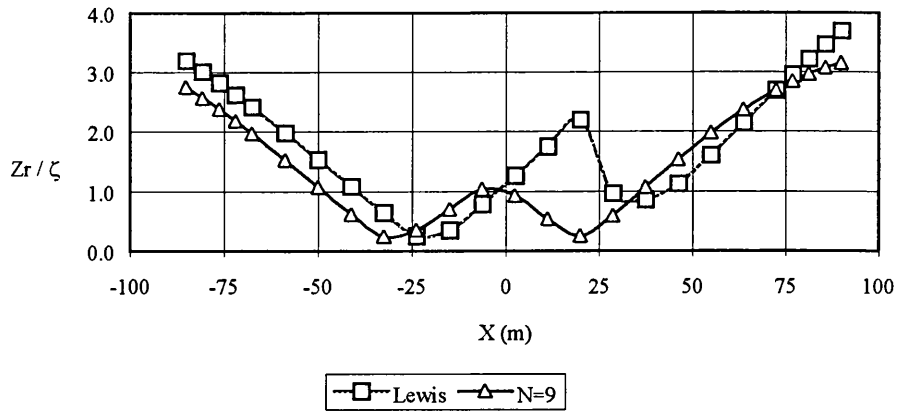


Figure 3.14 - Longitudinal variation of the relative motion for $\lambda / L = 1.0$

3.5 - CONCLUSIONS

For the heave and pitch motions, the predicted results are quite accurate when compared with experimental results. The variation in the number of mapping coefficients does not produce significant deviations in the transfer functions especially for the heave motion.

The comparison of the relative motion with the experimental results was not carried out because no experimental data for the motion phases was available, but these values are close to the theoretical values given by the organisations involved in the ITTC project.

However, significant deviations were observed in the relative motion between the Lewis method, the one that uses 9 parameters in the mapping transformation. This means that the relative motion transfer function is more sensitive to small variations in the hydrodynamic coefficients than the heave and pitch transfer functions, because to evaluate this function the phase between the motions and the wave were taken into account.

CHAPTER 4

SLAMMING LOADS

4.1 INTRODUCTION

The impact loads induced by waves on ships are, as a rule, concentrated at their forward sections. These slamming loads can consist of bottom impacts or of the development of sudden forces at bow-flared sections. The interest on slamming has often been raised from the point of view of the structural strength of the hull and from the ship and from of the ship operational standpoint.

From the structural side, slamming is looked upon as a possible cause of structural damage and also as a significant component of the primary stresses that the hull is subjected to.

As a consequence of the impact loads, structural damage like breaking of masts, excessive flexure of the shell plating, panels, fractures in the hull, piping, etc can occur. These damages cause extra costs to the ship owners. Studies in the early 1960s have shown that in 390 US general cargo vessels, 199 experienced damage. In that study 229 damages were found with average costs equal to \$28,700 Aertssen (1968).

The slamming pressures increase with the ship forward speed, so for the new kind of fast container ships this problem is very important. The usual way to prevent the severe slamming is to reduce the speed or change the course.

Aertssen (1968) found that in the North Atlantic, high speed vessels had to reduce their speed as a percentage of the total time at sea something like 4% for ships with length above 260 m and 15% for ships under 125 m.

Slamming occurs during extreme ship motions and impact forces are generated when the forward bottom of a ship emerges from the water and re-enters with a certain velocity greater than the threshold velocity Ochi and Motter (1971).

Experimental investigations were carried out to determine the impact pressures for plates, scale models of ship bottoms with various deadrise angles and real ship sections. Chuang (1967) performed various drop tests for three dimensional models and in rigid wedge shaped bodies for different deadrise angles.

Impact tests for ship models were also carried out by various researchers. Ochi (1958) performed extensive work in this area.

For the reasons explained above it is very important to know the loads generated by slamming. In order to evaluate these loads certain factors must be known; the most important ones are: the maximum slamming pressure and its distribution along the section and the time variation of the loads.

Another important aspect is the probability of slamming for a given loading condition and heading angle. Ochi (1964) produced figures for the probability distributions of slamming occurrence for several vessels, one of them is shown in Fig. 4.1.

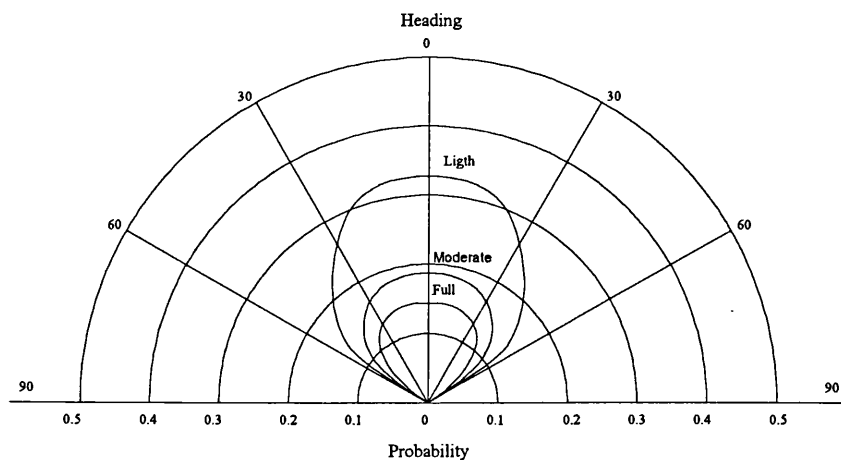


Figure. 4.1-Probability of Occurence of Slam for Various Loading Conditions and Course Angles (0° = Head seas), Ochi (1964).

4.2 - MAXIMUM SLAMMING PRESSURE

The first problem is related to the determination of the maximum slamming pressure. There are several methodologies to evaluate the maximum slam pressure and the objective of this section is to compare them. All the methods assume that the maximum slamming pressure is given by the following relation:

$$p_{\max} = \frac{1}{2} \rho k v^2 \quad (4.1)$$

where v is the impact velocity and k is a form coefficient that depends on the section geometry and its orientation to the water surface. So the problem reduces to the determination of the k factor.

The first method studied in this section was developed by Ochi and Motter (1973). In their work 15 sections are analysed and regression analysis was used to establish the following relation:

$$k = e^{(1.377 + 2.419 a_1 - 0.873 a_2 + 9.624 a_3)} \quad (4.2)$$

where a_1 , a_2 and a_3 are non-dimensional coefficients of the mapping transformation.

The mapping is performed for any conventional hull shape between the baseline and $1/10^{\text{th}}$ of the design draft. Using Ochi's method, the mapping transformation was performed for wedges with deadrise angles varying from 0 to 45 degrees and the k values are plotted in the following figure.

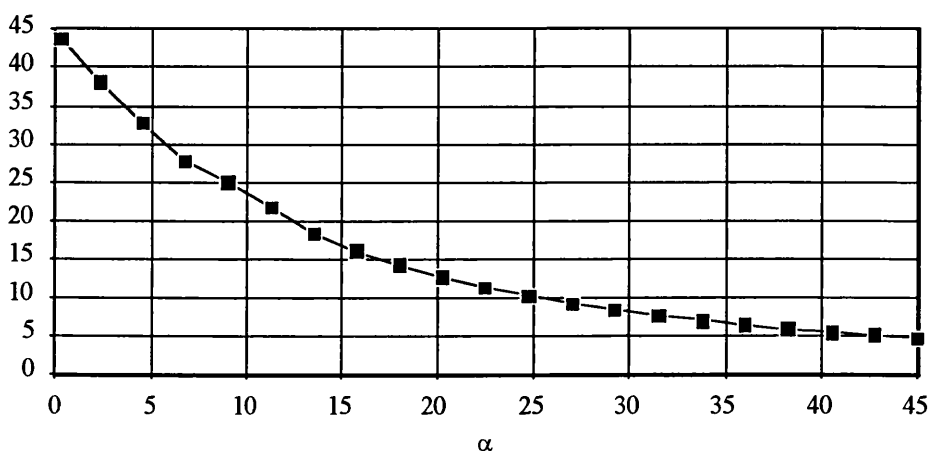


Figure 4.2 - Form coefficient obtained using Ochi's method for wedges by varying the deadrise angle

The second method was proposed by Stavovy and Chuang (1976) and according to them "the method can predict the maximum slamming pressures on all types of ships including advanced vehicles that may travel at speeds up to 100 knots and even higher speeds". The method gives the k value for any given angle. The maximum pressure along the ship section is evaluated using the local deadrise angle. The k value is obtained using a series of polynomials that fit experimental values and given as follows:

1. For $0 \leq \alpha \leq 2.2$ deg

$$k_1 = \frac{0.37 \alpha}{2.2} + 0.5 \quad (4.3)$$

2. For $2.2 \leq \alpha \leq 11$ deg

$$k_1 = 2.182094 - 0.9451815 \alpha + 0.2037541 \alpha^2 - 0.0233896 \alpha^3 + 0.0013578 \alpha^4 - 0.00003132 \alpha^5 \quad (4.4)$$

3. For $11 \leq \alpha \leq 20$ deg

$$k_1 = 4.748742 - 1.3450284 \alpha + 0.1576516 \alpha^2 - 0.0092976 \alpha^3 + 0.0002735 \alpha^4 - 0.00000319864 \alpha^5 \quad (4.5)$$

4. For $\alpha \geq 20$ deg

$$k_1 = 0.768546471 \frac{(1 + 2.4674 \tan^2 \alpha)}{288} \quad (4.6)$$

The relation between k and k_1 is given by

$$k = 288 \frac{k_1}{\cos^4 \alpha} \quad (4.7)$$

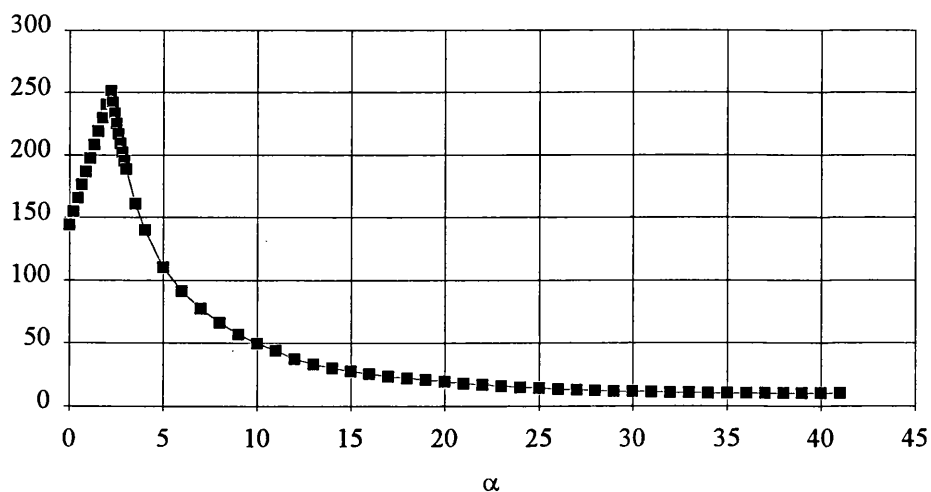


Figure 4.3 - Form coefficient as function of deadrise angle (Stavovy and Chuang, 1976)

The methods presented above are empirical and based on experiments, however some theoretical work for the determination of the slamming pressures has also been made. The following method was originally proposed by Wagner (1932) and was later extended by several investigators.

In the Wagner approach the fluid is considered ideal, so the potential theory can be applicable. Assuming that the flow is two dimensional, the boundary value problem for the velocity potential is given by,

$$\Delta\phi = 0 \quad (y < 0) \quad (4.8)$$

$$\phi = 0 \quad (y = 0, |x| > c(t)) \quad (4.9)$$

$$\frac{\partial\phi}{\partial y} = \frac{\partial y_b}{\partial t}(x, t) \quad (y = 0, |x| \leq c(t)) \quad (4.10)$$

$$\phi \rightarrow 0 \quad (x^2 + y^2 \rightarrow \infty) \quad (4.11)$$

where eqn. (4.8) is the Laplace equation, $c(t)$ is an unknown function (figure. 4.4) and $y_b(x, t)$ represents the wetted part of the body:

$$y_b(x, t) = f(x) - s(t) \quad (4.12)$$

where $f(x)$ describes the body shape and $s(t)$ the penetration depth of the body. For constant penetration velocity, equation (4.12) is rewritten as:

$$y_b(x, t) = f(x) - Vt \quad (4.13)$$

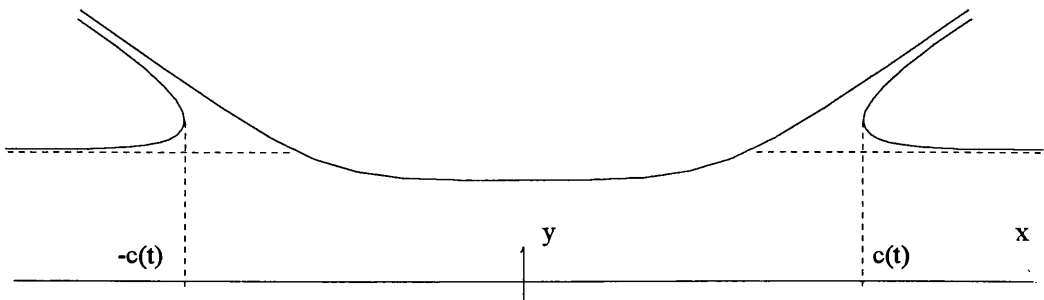


Figure 4.4 - c value for the Wagner approach

The solution to the problem given by eqns. (4.8)-(4.11) can be found for arbitrary functions of y_b and $c(t)$. The shape of the free surface $|x| > c(t)$ is given by the equation $y = \eta(x, t)$ where

$$\eta(x, t) = \int_0^t \frac{\partial\phi}{\partial y}(x, 0, \tau) d\tau \quad (4.14)$$

In the Wagner approach it is assumed (figure 4.4) that the spray jets are very thin compared to the dimension of the wetted area and they can be approximately disregarded to determine the flow and the pressure in the main liquid region. The elevation of the free surface at the contact point $c(t)$ must be equal to the body position,

$$\eta(c(t), t) = y_b[c(t), t] \quad (4.15)$$

Korobkin (1995) showed that eqn. (4.15) can be transformed to:

$$\int_0^{\pi} y_b[c(t) \sin \theta, t] d\theta = 0 \quad (4.16)$$

The pressure distribution along the body is given by the following equation:

$$p(x, 0, t) = \rho \left[\frac{c \dot{c} \dot{s}}{\sqrt{c^2 - x^2}} + \ddot{s} \sqrt{c^2 - x^2} \right] \quad (4.17)$$

For wedges and considering constant impact velocity, the maximum slamming pressure occurs at the end of the jet region and is given by:

$$p_{\max} = \frac{\pi^2}{8} \rho \cotan^2(\alpha) v^2 \quad (4.18)$$

Based on the analytical formulation by Dobrovol'skaya (1969), Zhao and Faltinsen (1993) present a numerical method to solve the slamming problem based on the non-linear boundary method. This method is different from the Wagner solution because the jet is taken into account. Using this method the slamming forces can be evaluated for deadrise angles larger than 2-3°. After that they performed calculations using this method for wedges with deadrise angles varying from 4° to 40° and compared with two different methods:

- 1) Similarity solution for wedges.
- 2) Asymptotic Solution based on the Wagner (1932) work.

The form coefficient values obtained for the three methods are represented in the table 4.1 and plotted in figure 4.5.

α	Simil.	Wagner	BE
4.0	503.03	504.61	521.40
7.5	140.59	142.36	148.30
10	77.85	79.36	80.20
15	33.27	34.37	32.80
20	17.77	18.63	18.20
25	10.96	11.35	10.90
30	6.93	7.40	6.94
40	3.27	3.50	3.26

Table 4.1 - k values according to Zhao and Faltinsen and using eqn. 4.18.

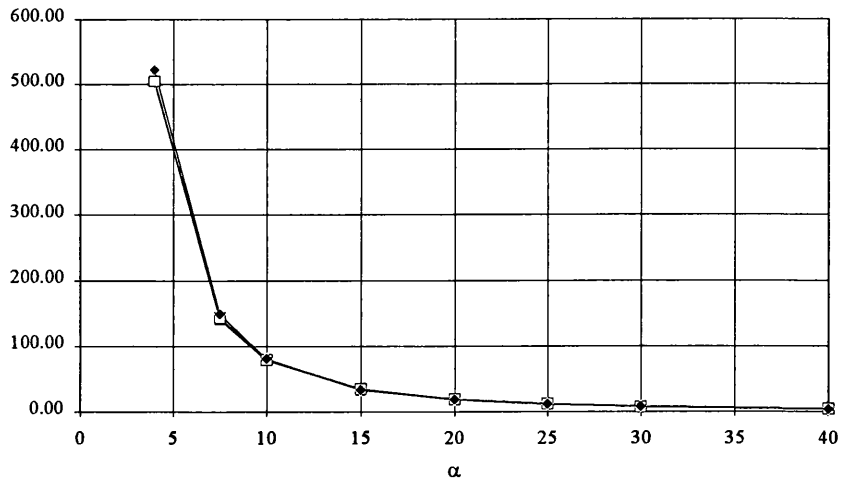


Figure 4.5 - Form coefficient for the Boundary Element, Wagner and Asymptotic methods

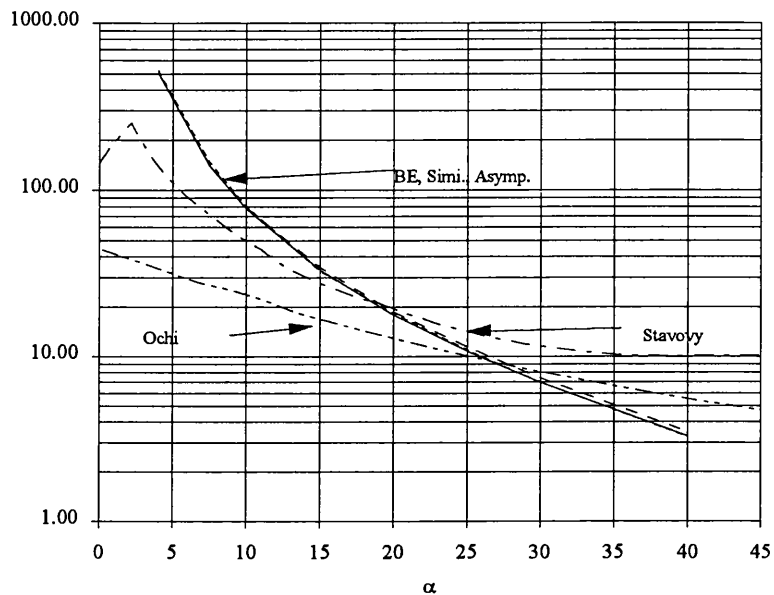


Figure 4.6 - Comparison of the various methods

Figure 4.6 represents the results of the several methods previously presented in figs. 4.2, 4.3 and 4.5. By looking at this figure one can conclude that large deviations exist between the methods and the pressures given by the Wagner theory and by the other theoretical methods are much greater than those given by the formulation of Ochi and Motter and by the Stavovy and Chuang's method which is based on experimental results. Hagiwara and Yuhara (1974) carried out tests for wedges with small deadrise angles and they measured pressure peaks under the water impact, that are close to the values obtained by the Wagner theory with a short duration in time, as predicted by the Wagner method.

4.3 - SLAMMING VERTICAL FORCE

Ochi and Motter (1973) and Kawakami et al. (1977) assumed that the slamming pressure has a linear distribution vertically with the maximum value at the bottom and the zero value at one tenth of the design draft. Fig. 4.7 illustrates the pressure distribution using this approximation for a general cross section.

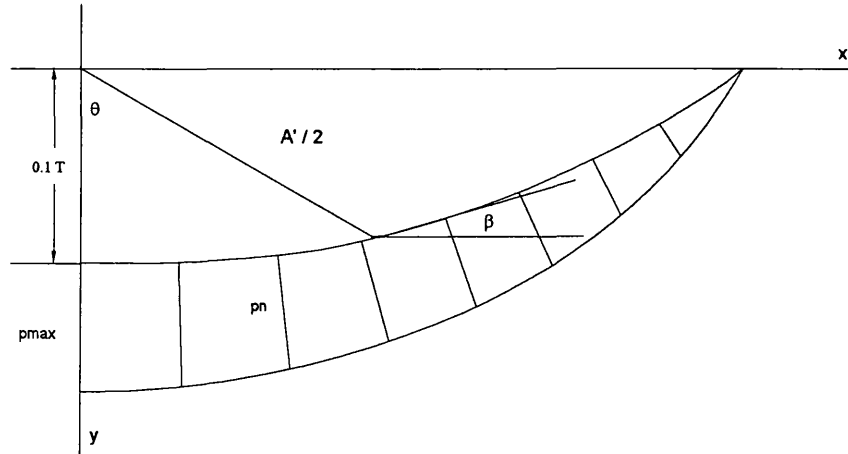


Figure 4.7 - Pressure distribution according to Ochi

Assuming the pressure distribution linear vertically, the pressure at any point is given by

$$p_n = p_{\max} \frac{y(\theta)}{d} \quad d = 0.1 T \quad (4.19)$$

The total vertical force is obtained by integration:

$$F = 2 p_{\max} \int_0^{\pi/2} \frac{y(\theta)}{d} \cos \alpha(\theta) d\theta = p_{\max} \frac{A'}{d} \quad (4.20)$$

or substituting the maximum pressure in equation (4.1)

$$F = \frac{A'}{2d} \rho k v^2 \quad (4.21)$$

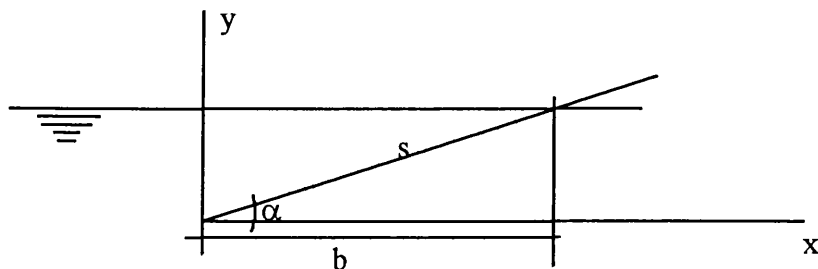


Figure 4.8 wedge geometry and system coordinates for the Stavovy method

Using the formulation given by Stavovy and Chuang, the pressure in an entering wedge is assumed constant and so the vertical force is obtained as:

$$F = p_{\max} s \cos\alpha = p_{\max} b = \frac{b}{2} \rho k v^2 \quad (4.22)$$

where b represents the breadth of the wedge.

The pressure distribution obtained by Zhao and Faltinsen (1993) has the form depicted in figure 4.9 with a sharply increased value in a z position, according to the asymptotic theory, equal to $(0.5\pi - 1) z'$.

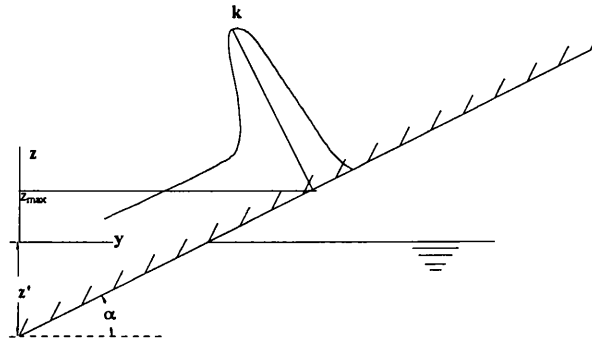


Figure 4.9 - Pressure distribution using the boundary element method

Korobkin (1995) has shown that the force for an arbitrary body can be calculated by using the following equation which is based on the Wagner theory,

$$F(t) = -2 c \dot{c} \int_0^{\pi} \frac{\partial y_b}{\partial t} [c(t) \sin \theta, t] - \frac{\partial^2 y_b}{\partial t^2} [c(t) \sin \theta, t] \cos^2 \theta d\theta \quad (4.23)$$

For constant impact velocity, the second part of equation (4.23) is zero, therefore:

$$F(t) = -2 c \dot{c} \int_0^{\pi} y_{bt} [c(t) \sin \theta, t] d\theta \quad (4.24)$$

The vertical force calculation in the other two methods compared by Zhao and Faltinsen is based on the direct integration of the pressure. In these studies the total vertical force were non-dimensionalized by using:

$$F_{AD} = \frac{F}{\rho v^2 z'} \quad (4.25)$$

with

$$z' = vt$$

The non-dimensional forces using the three methods are given in the table 4.2.

α	Simil.	Wagner	BE
4	1503.64	1540.51	1491.80
7.5	399.82	423.74	417.90
10	213.98	213.97	220.80
15	85.52	96.88	85.50
20	42.49	50.64	43.00
25	23.66	29.77	23.70
30	14.14	18.75	13.90
40	5.48	8.32	5.31

Table 4.2 - Non-dimensional vertical force F_{AD}

Another method to calculate the slamming force is based on the added mass theory (momentum theory). This method was proposed by Leibowitz (1963) and many authors used this method with some corrections. Belik and Price (1982) suggested that the total slamming force is equal to the momentum contribution plus the impact slamming, using this approach they made comparisons between the impact forces obtained by the Ochi method and the Stavovy method. Guedes Soares (1989) used the Leibowitz formulation and the Frank close fit method to perform time domain calculations in regular waves. In the Leibowitz method the section force can be obtained by using:

$$F = \frac{D}{Dt} (m_h \dot{z}) \quad (4.26)$$

Using the assumptions that the vertical velocity during the slamming process is constant and the wedge longitudinal velocity is equal to zero (drop test), the vertical slamming load expression is reduced to the following expression:

$$F = \frac{dm_h}{dz} \dot{z}^2 = \frac{dm_h}{dz} v^2 \quad (4.27)$$

The added mass is computed assuming that the free surface is undisturbed and that it can be evaluated using Landweber's (1967) method,

$$m_h = \frac{A_{-1}}{2} \left((1 + 2a_0 + \sum_{i=1}^N (2i-1) a_i^2) \right) \quad (4.28)$$

Figure 4.10 represents the methods non-dimensionalized vertical force on wedges with varying deadrise angle obtained by the several using eqn. (4.25).

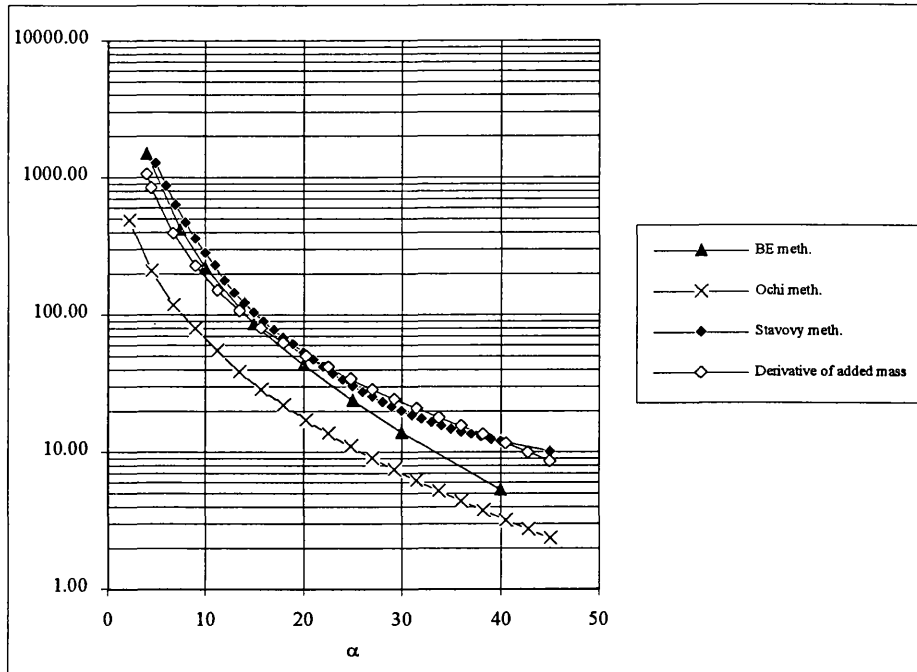


Figure 4.10 - Comparison of the different methods to calculate the vertical force

The problem of the Wagner theory and the momentum theory is that the force will be equal to infinity when the deadrise angle is zero. But in this case the time duration of the high pressures tends to zero, and the impulse exerted by the water on a unit length of the body is equal to the added mass for the equivalent horizontal plate times the impact velocity:

$$I = \frac{\pi}{2} \rho c^2 v \quad (4.29)$$

where c is equal to half breadth of the equivalent plate.

4.3.1 - Time History of the Vertical Slamming Force.

In order to evaluate the time history of the vertical slamming force, Ochi and Motter (1973) assumed that the force has a triangular shape varying from zero to F_{\max} and zero again during a period T_d . He proposed that the time period T_d , can be evaluated using the Froude scale law. Using experimental results he found the following relation between the period and the ship length:

$$T_d = 0.00794 \sqrt{L} \quad (\text{for SI units}) \quad (4.30)$$

Based on this approximation and in experimental observations, Kawakami et al. (1977) proposed another expression for the vertical slamming force as function of time, (see Fig. 4.11).

$$F(t) = F \frac{e^{-t/T_0}}{T_0} \quad (4.31)$$

where F represents the vertical force evaluated for $1/10^{\text{th}}$ of the design draft, T_0 is given:

$$T_0 = 0.00088 \sqrt{L} \quad (4.32)$$

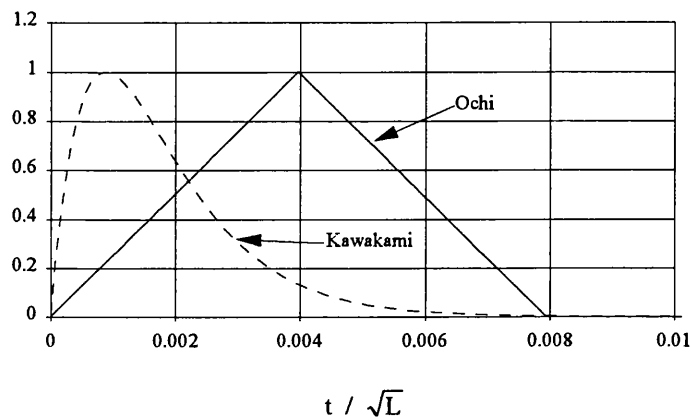


Figure 4.11 - Time history of the vertical slamming load proposed by Ochi and Motter (1973) and Kawakami et al (1977).

4.4 - SLAMMING LOADS CONSIDERING CONSTANT IMPACT VELOCITY

Three different stations and two different impact velocities of the S7-175 container ship were chosen to perform comparisons between the several methods. Considering the nature of these forces which act on the ship for a short period compared with the structural natural periods, it is suggested to compare the impulses instead of the forces. The impulse is defined as:

$$I = \int_0^t F(t) dt \quad (4.33)$$

The methods that will be compared are

1. *Ochi and Motter method for the maximum slamming pressure and time history.*
2. *Stavovy and Chuang method for the pressure and Kawakami et al method for the time duration.*
3. *Method based on the derivative of the added mass.*
4. *Wagner solution using the Korobkin equation for the wetted area.*

4.4.1 - Ochi and Motter Method

The three coefficients of the mapping transformation, the sectional area and the k value were performed for the forward stations of the container ship and given in the table 4.4.

Station	a1	a2	a3	A'	k
7	0.7652	-0.0186	0.0101	13.75	56.70
7 ^{1/2}	0.7170	-0.0154	0.0129	10.61	51.60
8	0.6460	-0.0086	0.0158	7.67	44.23
8 ^{1/2}	0.5428	-0.0009	0.0174	5.30	34.53
9	0.4176	0.0095	0.0158	3.63	24.79
9 ^{1/4}	0.3079	0.0228	0.0126	2.67	18.26
9 ^{1/2}	0.2515	0.0339	0.0122	2.28	15.76
9 ^{3/4}	0.1943	0.0287	0.0118	2.06	13.71
10	0.1315	0.0219	0.0125	1.85	11.91

table 4.4 - Ochi parameters for the determination of the k value

According to Ochi and Motter, the time duration for the slamming force for this vessel is equal to

$$T_d = 0.105 \text{ s}$$

The maximum slamming force can be written as

$$F = \rho K_v v_r^2 \quad (4.34)$$

where K_v for the Ochi and Motter method is given by

$$K_v = \frac{A'}{2 d} k \quad (4.35)$$

Substituting values given in table 4.4 in the equation (4.35) the coefficient K_v can be obtained.

Station	K_v
7	409.46
7 ^{1/2}	287.55
8	178.19
8 ^{1/2}	96.01
9	47.28
9 ^{1/4}	25.61
9 ^{1/2}	18.89
9 ^{3/4}	14.85
10	11.60

Table 4.5 - K_v values according to Ochi and Motter.

The impulse function for this method is equal to:

$$\begin{cases} I(t) = \frac{K_v v^2}{2T} t^2 & 0 < t < T_d \\ I(t) = \left[-\frac{1}{2T} t^2 + 2t + T \right] K_v v^2 & T_d < t < 2 T_d \\ I(t) = T K_v v^2 & t > 2 T_d \end{cases} \quad (4.36)$$

4.4.2 - Combining the Method of Stavovy and Chuang and of Kawakami et al. Method

In this method, the pressure distribution is obtained using the equations (4.3) to (4.7). To evaluate the k value for an arbitrary point in the section, the local deadrise angle must be computed which can be computed using the conformal mapping of the section:

$$\alpha = \tan^{-1} \left(\frac{dy}{dx} \right) \quad (4.37)$$

$$\alpha = \tan^{-1} \left(\frac{\sum_{i=1}^N A_i (2n+1) \cos(2n+1)\theta}{\sum_{i=1}^N A_i (2n+1) \sin(2n+1)\theta} \right) \quad (4.38)$$

where α represents the deadrise angle.

In this method eight parameters are used in the transformation to guarantee that the deadrise angles will be close to the real values. The maximum vertical force is obtained using the direct pressure integration limits proposed by Ochi. In table 4.5 the K_v values for the different stations are shown.

Station	K_v
7	1041.5
7 _{1/2}	757.4
8	494.2
8 _{1/2}	309.9
9	179.6
9 _{1/4}	95.5
9 _{1/2}	68.1
9 _{3/4}	52.2
10	41.0

table 4.5 - K_v values according to Stavovy and Chuang

According to Kawakami et al the value T_0 given by eqn. (4.32) for this vessel is equal to:

$$T_0 = 0.0116 \text{ s}$$

Finally, the impulse function can be easily obtained by integrated eqn. (4.31):

$$I(t) = \left[-e^{-\frac{t-T_0}{T_0}} (t+T_0) + T_0 e \right] K_v v^2 \quad (4.39)$$

4.4.3 - Momentum Theory

In this method the added mass was computed for several waterlines between the base line and the design draft and its vertical derivative was obtained. Using the multipole expansion method for the determination of the added mass, the mapping must be performed for each waterline position.

If the station has a flat bottom, equation (4.28) is used to evaluate the added mass for the flat bottom part. The added mass was calculated in twenty vertical positions. The impulse function for this method is equal to:

$$I(t) = m(z) \dot{z} = m(z)v \quad (4.40)$$

4.4.4 - Wagner Solution Using the Korobkin Integral

In this method the impact force is also infinite for the flat bottom. This numerical problem can easily be solved if one is interested in the impulse function. For flat bottoms in order to evaluate the forces, it is sufficient to carry out the calculations for deadrises which are close to zero. For example, if one considered the deadrise angle equal to 0.01° the final result for the impulse function will be practically the same.

4.4.5 - Comparison of Methods

Three stations chosen for the methods comparison are illustrated in figure 4.12. These three stations were chosen in order to study the slamming in typical forward stations: the first one without flat bottom and the local deadrise angle will be equal to 0 degrees near the bottom, the second one with small flat bottom and the last with significant flat bottom and small deadrise angles between 0 and $1/10^{\text{th}}$ of the design draft.

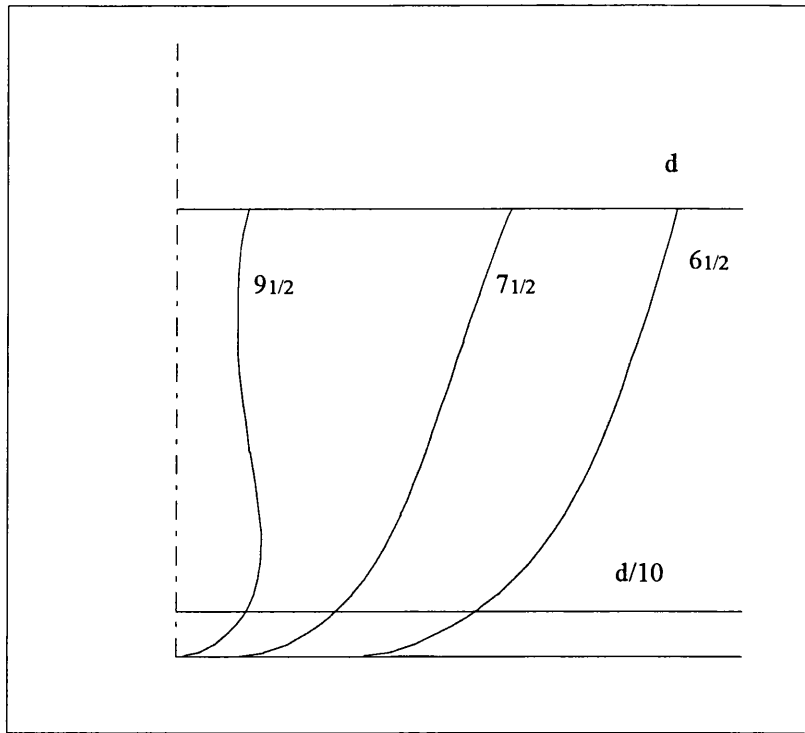


Figure 4.12 - Transverse lines of the chosen stations

The resulting impulse time functions obtained by four different methods and for two different velocities on the three stations are shown in figures 4.13 to 4.18.

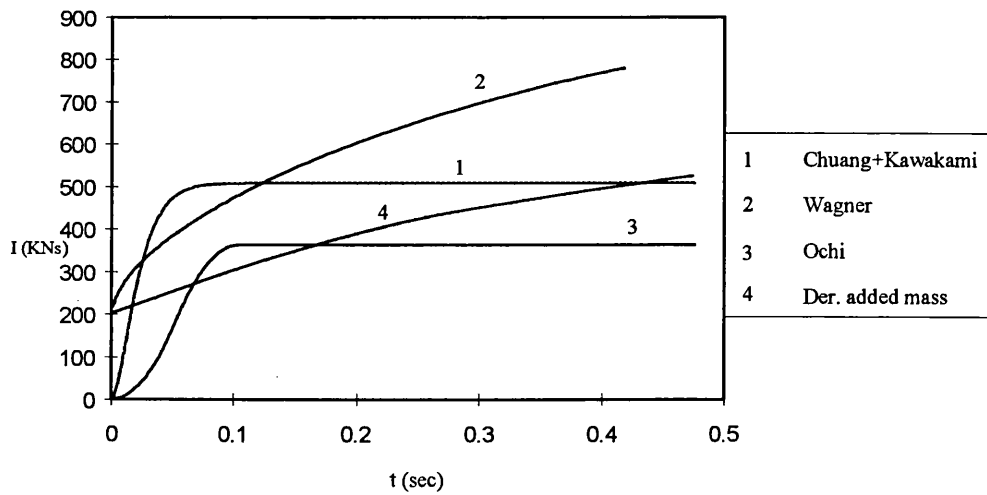


Figure 4.13 - Impulse time function for the station $6^{1/2}$, $V=4$ m/s

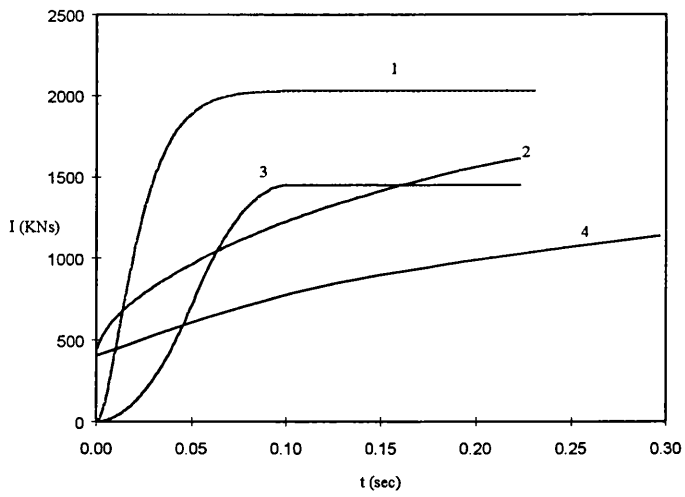


Figure 4.14 - Impulse time function for the station $6^{1/2}$, $V=8$ m/s

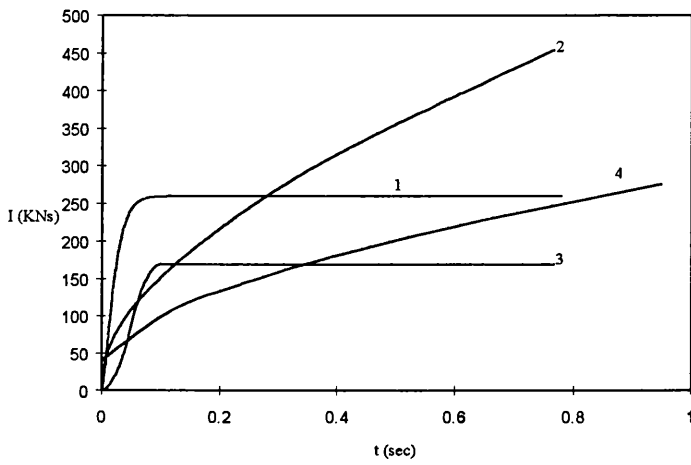


Figure 4.15 - Impulse time function for the station $7^{1/2}$, $V=4$ m/s

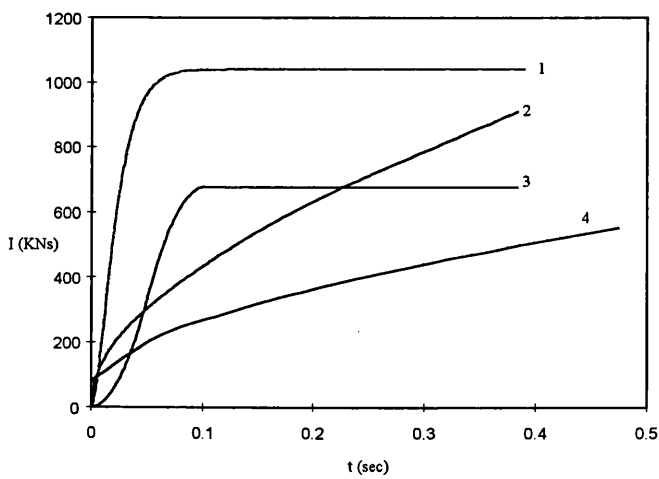


Figure 4.16 - Impulse time function for the station $7^{1/2}$, $V=8$ m/s

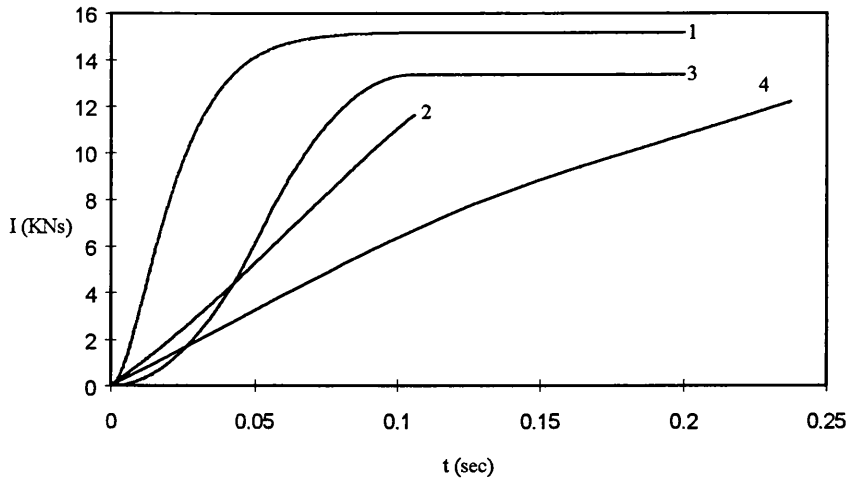


Figure 4.17 - Impulse time function for station $9^{1/2}$, and $V=4$ m/s

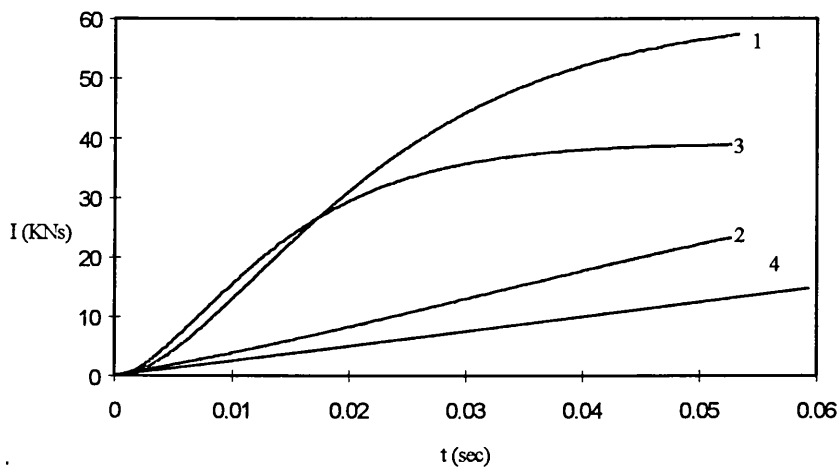


Figure 4.18 - Impulse time function for the station $9^{1/2}$, $V=8$ m/s

Belik and Price (1982) suggested that the slamming force is the summation of an impulsive force associated with a pressure peak with the sudden force calculated with the momentum theory. For impulsive force they compared the Ochi and Motter method with the Stavovy and Chuang method for the calculation of the maximum slamming force combined with the Kawakami formula to describe the time history of the impact force. In the Stavovy method, the evaluation of the maximum slamming pressure it is assumed that this value is obtained taking into account only the flat bottom or near the keel.

This method can be compared in the initial stage with the impulse method which gives the impulse by using the momentum theory for flat plates:

$$I_0 = \frac{\pi}{2} \rho c^2 v$$

The impulse obtained using the method of Stavovy and Chuang and the Belik and Price approximation is given by:

$$I' = T_0 e K_v v^2 \tag{4.41}$$

For a flat bottom and using the Stavovy and Chuang method K_v is equal to

$$K_v = \frac{k(0^\circ)}{2} \rho 2 c \cos(0^\circ) = 144 \rho c \tag{4.42}$$

Comparing the two expressions for the impulse one gets the following expression for T_0

$$144 T_0 \rho c v^2 = \frac{\pi}{2} \rho c^2 v \Leftrightarrow T_0 = 0.01091 \frac{c}{v} \tag{4.43}$$

So, according to the momentum theory and if one uses the Kawakami method for the time dependence of the slamming force, the parameter T_0 will not depend on the Froude number but is dependent of the impact velocity and the section shape. This last result seems more reasonable than the Ochi and Kawakami's approximation in which T_0 depends on the Froude number. Fig. 4.19 shows the curve where both methods will give the same impulse values.

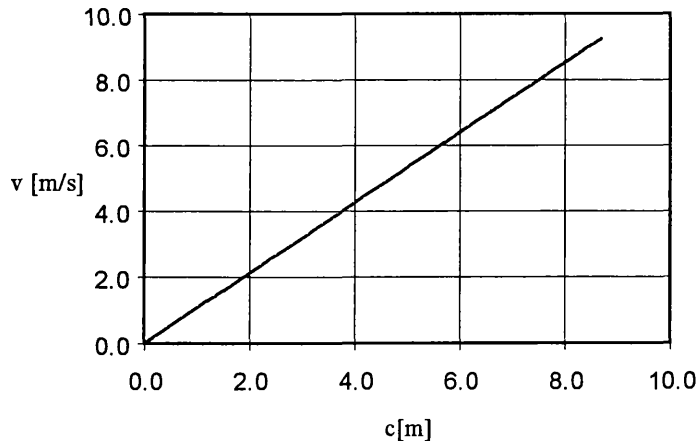


Figure 4.19 - Line where the momentum theory and the method used by Belik and Price (1982) gave the same results for the impulse

Figure 4.19 shows that for flat plates the impulse given by the method of Stavovy and Chuang combined with the one of Kawakami et al when compared with the one based on the momentum theory gives results c (half breadth) within the dimensions of the container vessel for the expected impact velocities. So one can say that the line represented on figure 4.19 is inside the physical region for this vessel.

The problem arises when T_0 goes outside this line, the impulse can be different from the results obtained using the Wagner method and the momentum method. The figures for the same station but for different impact velocities shows that the impulse can be quite different for one impact velocity and for another similar see for example figures 4.13 and 4.14.

Analogous results are obtained using the Ochi method and the only difference is that the values for the impulse are smaller.

The behaviour of the impulse functions obtained by the Wagner solution and the momentum theory is similar but the results obtained by Wagner are higher than the momentum theory. This difference can be explained by the fact that the momentum theory does not take into account the free surface elevation which is very important for the first phase of the slamming process when the deadrise angle is small.

On the other hand the Wagner theory is based on the assumption that the wetted part of the section can be approximated by a plate and it is only valid for the initial stage of the slamming process where, for the usual ship sections, the relation between the breadth and the draft is large.

So the more reasonable solution can be obtained by a hybrid method which uses the Wagner theory for the initial stage and the momentum theory for the penetration. So the first stage of the phenomena can be classified as impact and the second one as penetration. The problem with this assumption is to find the boundary between the two stages.

4.5 - SLAMMING LOADS IN REGULAR WAVES

In the previous section the impact velocity was considered constant. This approximation can be made without significant errors if the time duration of the impact loads is small when compared with the frequency of encounter. For the Ochi and Kawakami formulations this assumption can be used but for the Wagner and momentum theory this assumption should not be used.

Taking this into account, comparisons for slamming forces when the ship is advancing in regular waves will be treated in this section.

For a sinusoidal wave it is possible to perform analytical calculations for the relative motion and velocity, and thus, to compare the slamming loads it is useful to carry out the calculations for a single wave system. The comparison will be made for two different wave frequencies with a single wave amplitude which is chosen to guarantee the occurrence of slamming. The wave amplitude was considered to be 4 m and the wave frequencies are equal to 0.45 and 0.55 rad/s. The vessel is travelling in head seas with a Froude number equal to 0.275.

Figure 4.20 shows the longitudinal variation of the amplitude of the relative motions for the two wave systems. The horizontal line represents the ship draft and relative motion amplitudes larger than the draft means the emergence of the bow at those stations. The longitudinal phase angles ϵ_x for the relative motion are represented in fig. 4.21. Figure 4.22 illustrates the time simulation of the relative motion for the foremost stations and for the wave frequency equal to 0.55 rad/s.

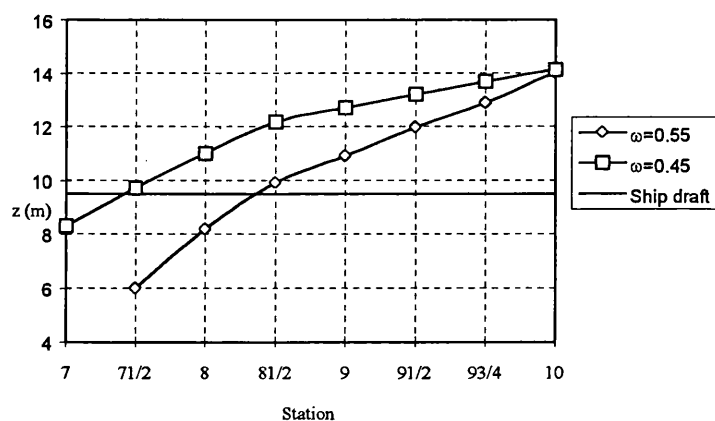


Figure 4.20 - Relative motion amplitude longitudinal variation

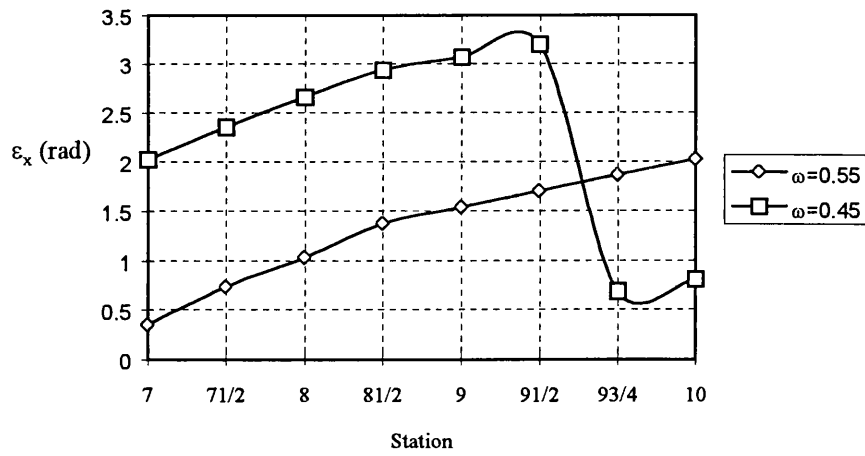


Figure 4.21 - Phase angle

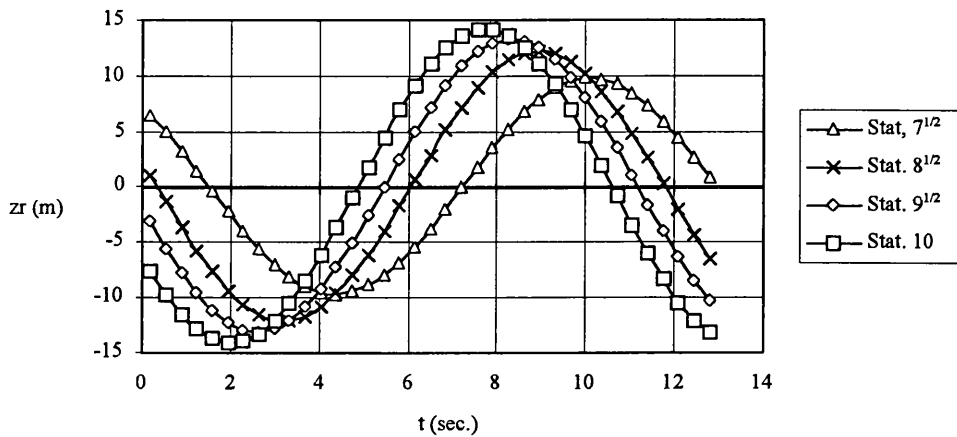


Figure 4.22 - Relative motion for the forward stations, $\omega = 0.55$ rad/s

The time instant when the section hits the water τ is evaluated using the following relation:

$$\tau = \frac{1}{\omega_e} \left[\cos^{-1} \left(\frac{T}{z_r} \right) - \varepsilon_x \right] \quad (4.44)$$

Table 4.6 shows the time instant, for the different stations and waves, when the sections reenter the water.

	Station						
ω_e	55.21	63.96	72.71	77.09	81.46	85.84	90.21
0.45	1.458	1.481	1.285	1.165	1.038	0.930	0.870
0.55	-	-	2.286	2.352	2.327	2.243	2.159

Table 4.6 - Time instant when the section reenters the water

The vertical velocity of the relative motion for the impact instant is obtained using eqn. (4.45) and illustrated in figure 4.23.

$$\dot{z}_r = z_r \omega_e \cos(\omega_e \tau + \varepsilon_x) \quad (4.45)$$

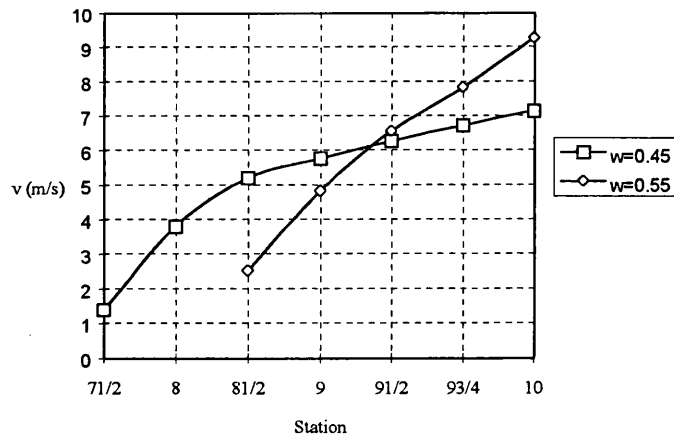


Figure 4.23 - Longitudinal distribution of impact velocity

4.5.1 - Travelling Velocity of Pressure in the Longitudinal Direction.

One important aspect of the slamming process is the travelling velocity of the impact pressure in the longitudinal direction. This is important for studying slamming in irregular waves, where usually for simplification purposes the travelling velocity of pressure v_t in the longitudinal direction is assumed to be constant, or equal to infinity i.e. all the stations hit the water at the same time e.g. Kawakami (1977).

Ochi and Motter made experiments in a Mariner ship and obtained values between 260 and 520 fps for a 520 ft vessel. From the structural point of view they concluded that the worst impact occurs for the slowest travelling velocity. Based on these conclusions they proposed one expression using the Froude's law,

$$v_t = 6.30 \sqrt{L} \quad (4.46)$$

Figure 4.24 shows the pressure travelling velocity obtained for the container ship and the line represents the travelling velocity computed using expression 4.46.

In this particular case the mean of the computed travelling velocity of the water pressure is close to the value obtained by using the Ochi and Motter expression:

Ochi and Motter method $V = 83.4 \text{ m/s}$

Mean (Computed) $V = 94.2 \text{ m/s}$

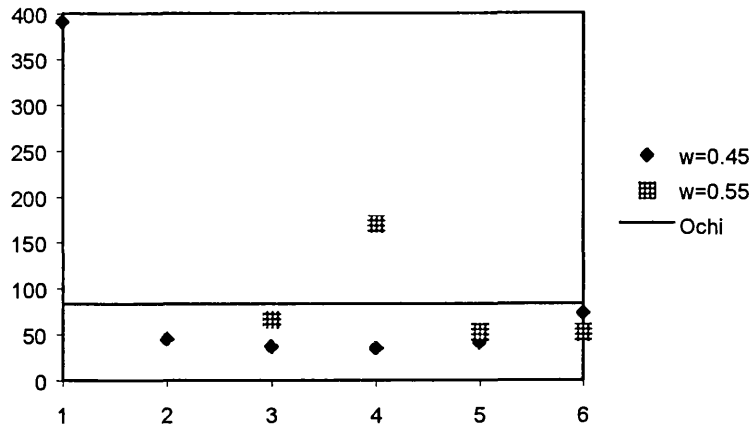


Figure 4.24 - Longitudinal travelling velocity of the pressure

4.5.2 - Impulse Using the First Two Methods (1-Ochi and Motter 2-Stavovy et al + Kawakami et al)

The impulse shape for these two methods is similar if constant velocity of impact is assumed. This can be easily proved if one compares the period after which the impulse force becomes zero or negligible with the encounter period:

Ochi and Motter method	$T_0 = 0.105 \text{ s}$
Kawakami et al. method	$T_0 = 0.079 \text{ s}$
Encounter period (minimum)	$T_e = 10 \text{ s}$

4.5.3 - Wagner Solution for Regular Waves

For regular seas the impact velocity cannot be considered constant and the Wagner method becomes more complicated. The wetted part of the section for regular waves is given by:

$$y_b(x, t) = f(x) - A_r \cos[\omega_e(t + \tau) + \beta] \quad (4.47)$$

Substituting (4.47) in (4.16) the following equation can be easily obtained,

$$\int_0^{\pi} f(c(t)\cos(\theta)) - A_r \cos[\omega_e(t + \tau) + \beta] d\theta = 0 \quad (4.48)$$

$$\int_0^{\pi} f(c(t)\cos(\theta)) d\theta = \frac{\pi}{2} [A_r \cos(\omega_e(t + \tau) + \beta)] \quad (4.49)$$

This integral equation can be solved in a non-formal way. If $c(t)$ is assumed equal to C , which is an arbitrary value between 0 and the half breadth, then the instant t can be obtained by:

$$t = \frac{1}{\omega_e} \left[\cos^{-1} \left(\frac{2 \int_0^{\frac{\pi}{2}} f(C \cos(\theta)) d\theta}{\pi A_r} \right) - \beta \right] - \tau \quad (4.50)$$

The force is obtained by substituting (4.50) in (4.23)

$$F(t) = \rho \frac{\pi}{2} A_r \omega_e \left[\sin(\omega_e(t + \tau) + \beta) \dot{c}^2 + c^2 \omega_e \cos(\omega_e(t + \tau) + \beta) \right] \quad (4.51)$$

There are two different contributions in the total slamming force given by eqn.(4.51). The first one is related to the impact velocity and the second one to the acceleration of the body during the impact. From the second contribution it can be seen that the Wagner solution assumed that the penetrated body is considered a flat plate with half breadth equal to c . Figure 4.23 quantifies these two contributions during the impact period of the station and demonstrates that at the initial stage the first contribution is the greater one.

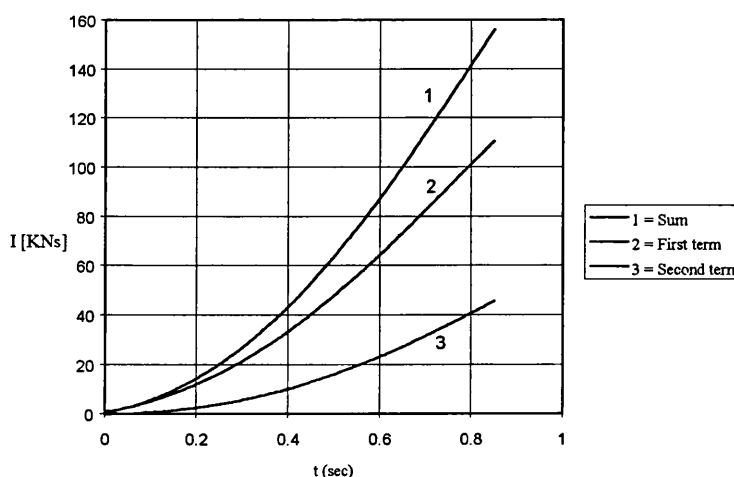


Figure 4.23 - Slamming contributions according to Wagner (eqn. 4.51)

4.5.4 - Momentum Theory Applied to Regular Waves

For the ship advancing in head seas in regular waves, the vertical force given by this method is as follows,

$$F = \frac{D}{Dt}(m' v) = \frac{dm'}{dt}v + m' \dot{v} - U \frac{dm'}{dx}v - U(\theta + k\zeta) m' \quad (4.52)$$

The first two terms of equation (4.52) are similar to the ones given in the Wagner theory. Eqn. (4.52) can be rewritten as:

$$F = F_1 + F_2 + F_3 + F_4 \quad (4.53)$$

where

$$F_1 = \frac{dm'}{dz} A_r^2 \omega_e^2 \sin^2(\omega_e(t + \tau) + \beta) \quad (4.54)$$

$$F_2 = -m' A_r \omega_e^2 \cos(\omega_e(t + \tau) + \beta) \quad (4.55)$$

$$F_3 = U \frac{dm'}{dx} A_r \omega_e \sin(\omega_e(t + \tau) + \beta) \quad (4.56)$$

$$F_4 = -Um'(A_p \cos(\omega_e(t + \tau) + \theta_p) + \zeta k \cos(kx + \omega_e(t + \tau))) \quad (4.57)$$

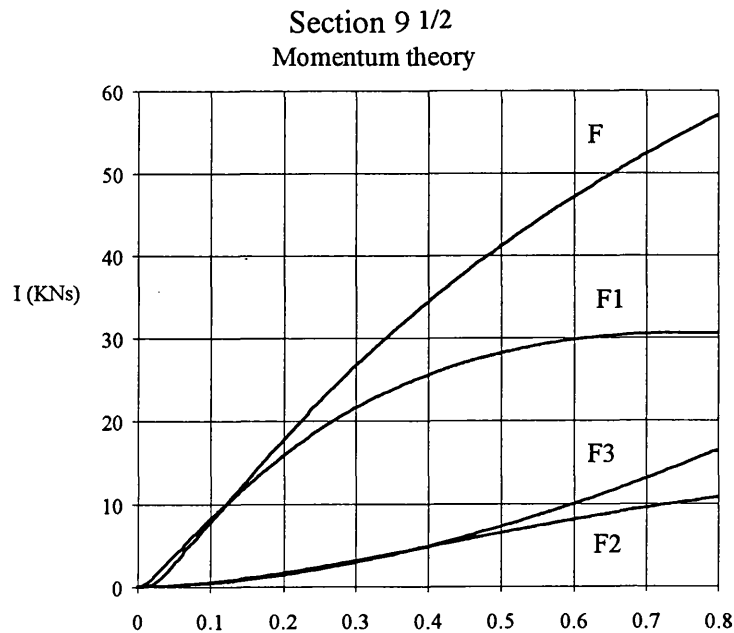


Figure 4.24 - Contributions of some of the components of the slamming force

The problem with this method when combined with the linear theory for the prediction of the ship motions and the wave bending moments is that the last three terms of equation 4.53 are already included in the linear theory but with constant values for the coefficients. From figure 4.24 it can be seen that the last three terms have a small contribution in the initial stage of the slamming process. For the time 0.3 s which for this case corresponds to a draft equal to 1.9 m (0.2 T), this contribution is equal to 25% and for the time equal to 0.7 s (immersion equal to 0.63 T) the contribution is equal to 65% but for this immersion the linear theory will produce similar results for the last three contributions.

Figure 4.24 represents the slamming forces for a foremost station. For these stations where there is no flat bottom, the contribution of F_1 is smaller than the other components. The same calculations were performed for other stations and for station 8 the first component contribution was equal to 84% for 0.2 T. So it seems appropriate not to include these three components in the slamming forces and to use as for the constant velocity, only the first term of equation 4.52.

The same approximation will be made for the Wagner solution to determine the slamming bending stresses. For these two methods, only terms related with the vertical variation of the added mass will be included, knowing that this assumption is not theoretically correct but for the calculation of the whipping stresses small deviations are expected.

Further investigations will be made in this area and the results of the structural bending moments including these terms will be calculated and compared in chapter 6.

4.5.5 - Comparison of Methods

In this section, comparisons between the Wagner and the momentum methods will be performed for two stations and two different waves. Comparisons will also be made between the calculated impulse for regular waves and the one that assumes constant velocity during the slamming process.

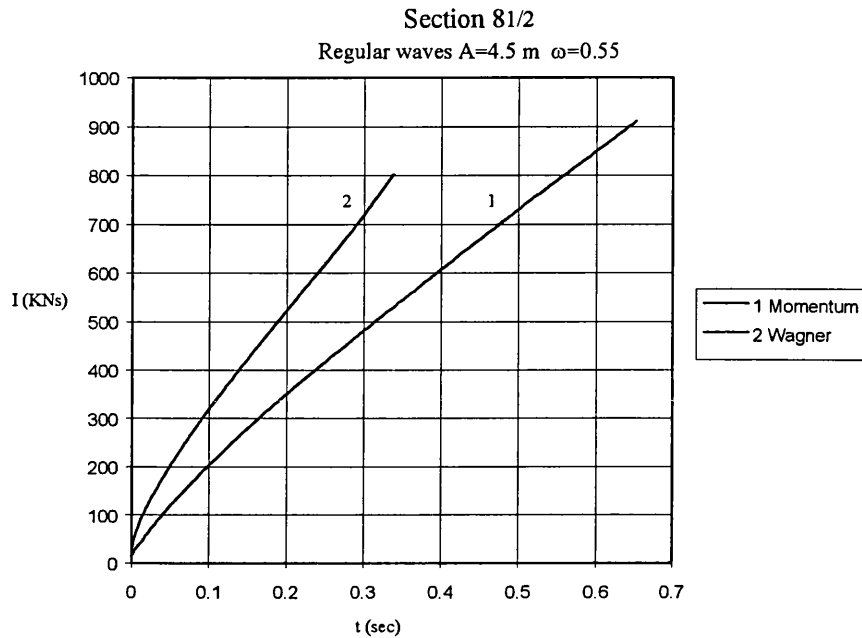


Figure 4.25 - Slamming impulse obtained from Wagner and momentum theories.

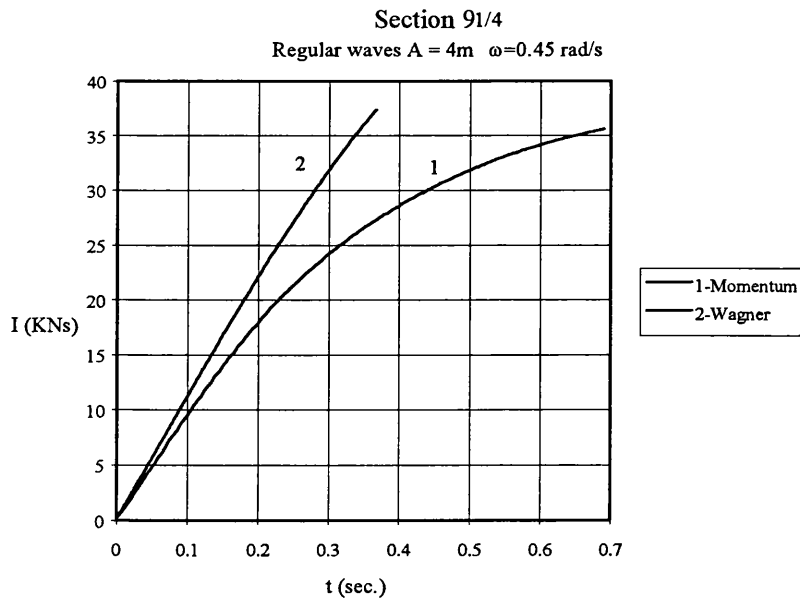


Figure 4.26 - Slamming impulse obtained from Wagner and momentum theories.

The behaviour of these two methods for regular waves is the same as mentioned in the previous section. Another comparison for simplification purposes is between the impulse obtained from the regular waves and the one that assumes constant impact velocity.

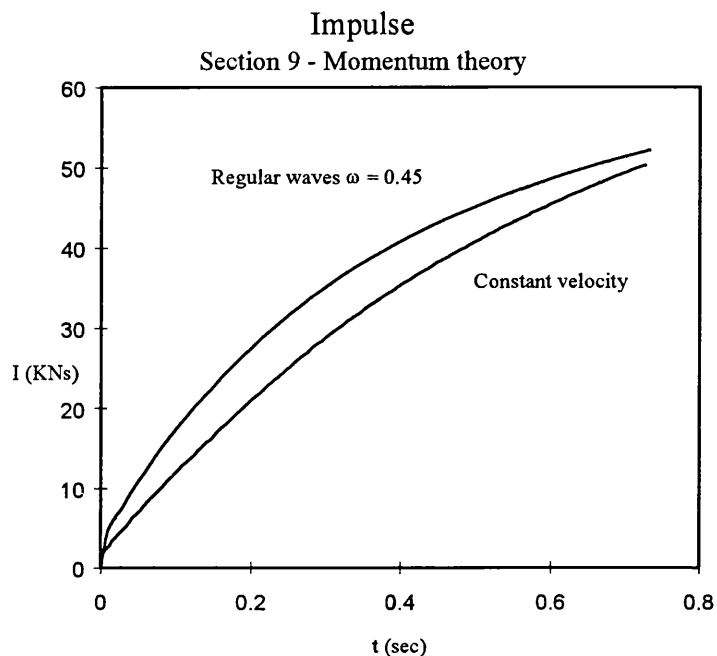


Figure 4.25 - Slamming impulse obtained from momentum theory assuming constant impact velocity and for regular waves, $A = 4m$.

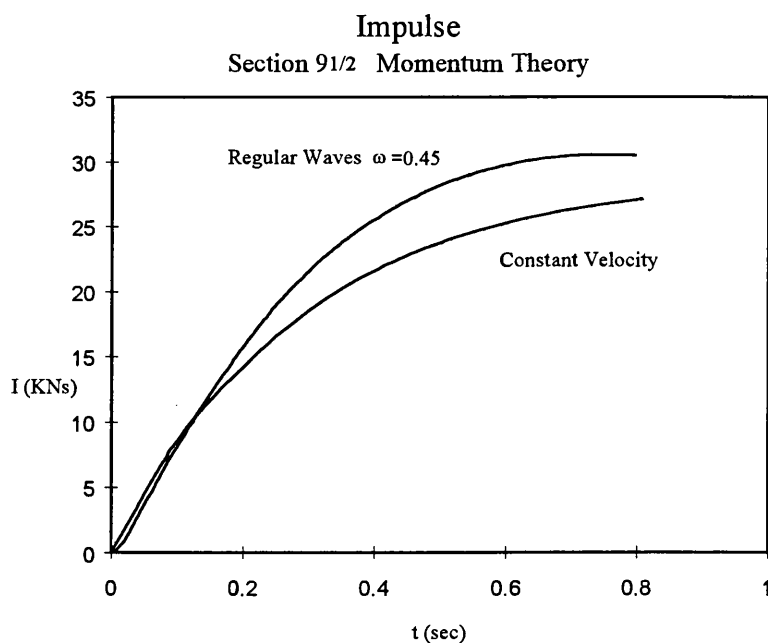


Figure 4.26 - Slamming impulse obtained from momentum theory assuming constant impact velocity and for regular waves, $A = 4m$.

From Figs. 4.25 and 4.26 one can say that the impulse for regular waves is higher when compared with the impulse when constant impact velocity is considered. This means that the absolute value of the velocity increases during the section penetration.

No general conclusion can be made about the increase of the impulse for regular waves because this value depends on the phase of the velocity in the impact instant and the amplitude of the velocity.

Figures 4.27 and 4.28 shows two curves representing the impulse calculated between the baseline and 0.6 of the design draft. The first one is obtained for regular waves and the second one assuming constant velocity.

From these figures it can be concluded that the difference between the impulse for regular waves and the one which considered constant impact velocity, decreases with the increase of the wave amplitude and consequently with the velocity.

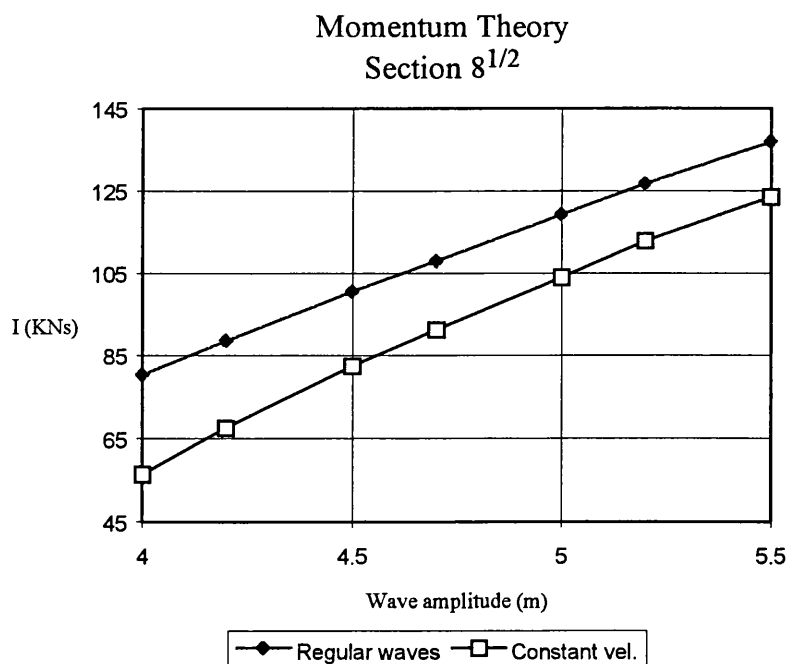


Figure 4.27 - Impulse calculated between 0 and 0.6 T for regular waves and assuming constant velocity.

Momentum Theory
Section 91/2

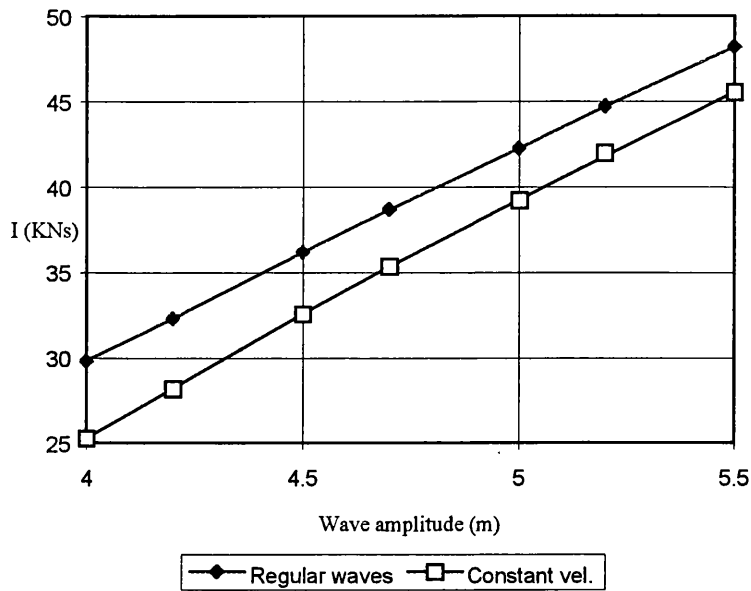


Figure 4.28 - Impulse calculated between 0 and 0.6 T for regular waves and assuming constant velocity.

4.6 - CONCLUSIONS

In this chapter, important parameters related to the slamming pressures and loads were studied and the several formulations to predict them were compared.

In the first section, the maximum slamming pressure represented by the form coefficient was compared for the several methods using a wedge geometry with varying the deadrise angle. Two of the methods are empirical and based on experiments and the rest of the methods are analytical. Large deviations exist between the results of the methods and the higher results obtained for the analytical methods, particularly for small deadrise angles. The Ochi and Motter method gives the lower results for the maximum slamming pressure for all deadrise angles.

Similar behaviour were obtained for the several methods used in the calculation of the maximum slamming forces but with smaller deviations. For the calculation of the maximum slamming force another method based on the momentum theory was compared and similar results were obtained for the Stavovy, momentum and Wagner methods. Ochi's method, as for the maximum slamming pressure, produces the smaller results.

For the evaluation of the whipping stresses it is necessary to obtain the time history of the maximum slamming force. Knowing that these loads act on the ship in small periods, when compared with the natural period of the structure, it is more reasonable to compare the impulse than the loads. So the impulses obtained by using the several methods were compared in three sections assuming constant impact velocity and in regular waves.

Two different constant impact velocities were chosen for the first study, and different behaviour was observed between the empirical and the analytical methods. The first group of methods assumed that the time history of the impact force depends on the Froude number and second one that the time history of the impact loads is dependent on the impact velocity and section shape.

The impulse function for regular waves tends to give higher results than that which assumes constant impact velocity.

CHAPTER 5

STRUCTURAL RESPONSE

5.1 - INTRODUCTION

To assess the ship's structural response due to vertical slamming loads, the ship is modelled using the finite element method (FEM) with Timoshenko's beam elements. For typical hull sections, Timoshenko's beam theory produces better results than the conventional Euler one, because the ratio between the sectional inertia and area is relatively high and consequently the shear deformations cannot be neglected. Bishop and Price (1979) studied the difference in the natural frequencies obtained with these two theories and concluded that significant deviations can appear in the natural frequencies for the higher modes.

The reason to model the ship structure as a beam instead of using real plate elements is related to the fact that, for the prediction of natural frequencies, vibration modes and structural response, a lot of computer time is required if the ship is modelled with the plate elements. Also, the errors associated in the prediction of the natural modes will increase with the size of the system. Another reason to adopt this simplification is that for conventional ships the beam theory gives good results for the calculation of the longitudinal stresses, displacements, rotations, forces and moments, if the ship is properly divided.

5.2 - PROBLEM FORMULATION

The damped transverse elastic response of the non-uniform beam is governed by the following system of partial differential equations:

$$\mu(x) \frac{\partial^2 y}{\partial t^2} + c'(x) \frac{\partial y}{\partial t} + \frac{\partial V(x,t)}{\partial x} = F(x,t) \quad (5.1)$$

$$\frac{\partial M(x,t)}{\partial x} = V(x,t) + I_r(x) \frac{\partial^2 \gamma}{\partial t^2} \quad (5.2)$$

where μ represents the mass distribution per unit length, I_r is the rotary inertia, c' is the structural damping distribution, V the shear force, M the vertical bending moment, and γ bending slope.

Bishop and Price (1979) demonstrated that the rotary inertia term do not have a great influence on the resulting natural frequencies and mode shapes.

$$M(x, t) = EI \frac{\partial \gamma(x, t)}{\partial x} \quad (5.3a)$$

$$\frac{\partial y}{\partial x} = -\frac{V(x, t)}{K_s AG} + \gamma(x, t) \quad (5.3b)$$

The finite element method is a numerical procedure which uses integral formulations to generate a system of equations in the following form:

$$M_{ij} \ddot{u}_j + C_{ij} \dot{u}_j + K_{ij} u_j = F_i \quad (5.4)$$

The matrices M and K represent the mass and stiffness for the system i.e. in this particular case for the whole ship beam. To evaluate these matrices, several steps must be undertaken and, in a simple way, the scheme for the evaluation of these two matrices can be described as follows:

- The beam is discretized using several nodes points.
- The function that describes the displacements and rotations (degrees of freedom in the nodes) between the nodes is assumed to be linear, so the functions are completely defined using two known values, i.e. the local elements can be defined by using only two nodes.
- The potential energy formulation is written in terms of the nodal displacements. It is then minimised giving one equation for each of the unknown displacements. Using this process the local element matrix can be obtained in an analytic form.
- Using the local element matrices, the boundary conditions and compatible node displacements, the local matrices are assembled into a so called global matrix, as represented in eqn. (5.4).

If the damping matrix do not have some properties, see Bishop and Price (1979), the system (5.4) is difficult to solve and the existence of normal modes is not guaranteed. In

real structures, damping forces are often small when compared with the inertial and stiffness forces and for that reason the natural frequencies will not be significantly affected by damping.

So the calculation of the natural frequencies and natural mode shapes can be done by assuming that damping does not exist, and the damping contribution will be included in the equations of motion for the calculation of the structural response. Using that statement the non-damped system is:

$$M_{kj} \ddot{u}_j + K_{kj} u_j = 0 \quad (5.5)$$

The displacement $u(x,t)$ can be written in the following way

$$u(x,t) = \text{Re} \left[e^{i\omega t} w(x) \right] \quad (5.6)$$

where Re represents the real part of the complex function.

The eigenvalue problem is formulated as

$$(-\omega^2 M_{kj} + K_{kj}) w_j = 0 \quad (5.7)$$

The solution of this system gives n values of ω_j and eigenvectors w_j . The eigenvectors are orthogonal to each other and if they are properly normalised the following relations must be preserved

$$w_k M_{kj} w_j = \delta_{kj} \quad (5.8)$$

and

$$w_k K_{kj} w_j = \delta_{kj} \omega_j^2 \quad (5.9)$$

where the terms of the matrix are the Kronecker δ_{kj} .

Defining the transformation Φ_{ij} obtained using the matrix columns equal to the eigenvectors of the system, expression (5.4) can be written in the following form:

$$\Phi^T M \Phi \ddot{p} + \Phi^T K \Phi p = \Phi^T F \quad (5.10)$$

or

$$\delta_{kj} \ddot{p}_j + \Omega_{kj} p_j = q_k \quad (5.11)$$

where

$$\Omega = \begin{bmatrix} \omega_1^2 & 0 & \dots & 0 \\ 0 & \omega_2^2 & \dots & 0 \\ \dots & \dots & \dots & \dots \\ 0 & \dots & 0 & \omega_n^2 \end{bmatrix}$$

For the ship hull and considering the nature of the exciting forces, several authors e.g. Bishop and Price (1979) have shown that the response for modes higher than the fifth mode is negligible.

The displacement and bending moment are obtained using the following equations:

$$w(x, t) = \sum_{r=1}^N p_r(t) w_r(x) \quad (5.12)$$

$$M(x, t) = \sum_{r=1}^N p_r(t) M_r(x) \quad (5.13)$$

For the simplification of the equations of motion, the cross-coefficients of the transformed damping matrix (eqn. 5.17) are assumed to be equal to zero. Bishop and Price (1979) compared five formulations for the evaluation of the damping coefficients and they stressed that none of the formulations can be generalised for all ships, because they don't predict aspects like cargo damping, welding quality and many other aspects.

The damping coefficients in this work are estimated using the formulation given by Kumai (1958). According to his work the logarithmic decrement can be obtained using the following relations:

$$\delta_1 = 0.0024 \omega_1 \quad \text{and} \quad \delta_n = 0.0068 \omega_n^{0.7} \quad n > 1 \quad (5.14)$$

Using this assumption, the response for each mode in the principal coordinates are obtained using the following equation:

$$m_r \ddot{p}_r + c_r \dot{p}_r + k_r p_r = q_r \quad (5.15)$$

The coefficients of the differential equation are obtained using the following relations

$$m_r = \int_L \mu w_r^2 dx \quad (5.16)$$

$$c_r = \int_L c' w_r^2 dx \quad (5.17)$$

$$k_r = m_r \omega_r^2 \quad (5.18)$$

5.3 - SOLUTION OF THE DIFFERENTIAL EQUATIONS IN THE TIME DOMAIN

The equations given by (5.15) are solved using the central difference method. This method is obtained from Taylor's expansion. According to Taylor's series expansion, the solution for a step $i+1$ and $i-1$ can be obtained by using the following expressions

$$x_{i-1} = x_i + h \dot{x}_i + \frac{h^2}{2} \ddot{x}_i + \frac{h^3}{6} \dddot{x}_i + \dots \quad (5.19)$$

$$x_{i+1} = x_i - h \dot{x}_i + \frac{h^2}{2} \ddot{x}_i - \frac{h^3}{6} \dddot{x}_i + \dots \quad (5.20)$$

Taking constant time steps, using the first three terms of the series expansion and rearranging the equations, the velocity and acceleration can be obtained from the displacements:

$$\dot{x}_{i+1} = \frac{1}{2h}(x_{i+1} - x_{i-1}) \quad (5.21)$$

$$\ddot{x}_{i+1} = \frac{1}{h^2}(x_{i+1} - 2x_i + x_{i-1}) \quad (5.22)$$

Replacing the derivatives obtained in the damped second order differential equation, and putting h equal to Δt , the solution for the displacement at the time instant $i+1$ is

$$x_{i+1} = \left\{ \frac{1}{\frac{m}{\Delta t^2} + \frac{c}{2\Delta t}} \right\} \left[\left\{ \frac{2m}{\Delta t^2} - k \right\} x_i + \left\{ \frac{c}{2\Delta t} - \frac{m}{\Delta t^2} \right\} x_{i-1} + q_i \right] \quad (5.23)$$

This is a recurrent expression and the method requires some initial conditions. The initial velocity and displacement are sufficient to start the solution because the acceleration can be obtained using the equilibrium equation:

$$\ddot{x}_0 = \frac{1}{m}[q_0 - c\dot{x}_0 - kx_0] \quad (5.24)$$

If the time step Δt is smaller than the critical time step, then the method is conditionally stable. For this method the critical time step is equal to:

$$\Delta t_{\text{cri}} = \frac{T_n}{2\pi}$$

where T_n is the minimum natural period of the system.

5.4 - RESULTS

To find the errors associated with the numerical approximation used in this chapter, a beam is represented by the Bernoulli formulation with uniform distribution of weight and inertia. This choice is made, because for this formulation it is possible to find the theoretical solution and to compare it with the finite element results. To study the sensitivity of the system to the variation of the number of elements, the beam was modelled with 10, 20 and 25 elements. For the Bernoulli beam formulation the relation between the shear force and bending moment and the vertical displacement is

$$M_r(x) = EI \frac{\partial^2 w_r(x)}{\partial x^2} \quad (5.25)$$

$$V_r(x) = EI \frac{\partial^3 w_r(x)}{\partial x^3} \quad (5.26)$$

The beam properties of this example are the same as the properties given by Bishop and Price (1979).

$$L = 100 \text{ m}$$

$$I = 3.092 \text{ m}^4$$

$$E = 207 \text{ GPa}$$

$$\mu = 20000 \text{ Kg/m}$$

The natural frequencies for a free-free Bernoulli beam are obtained using the following expression:

$$\omega_r = \frac{\alpha_r^2}{L^2} \sqrt{\frac{EI}{\mu}} \quad (5.27)$$

For this particular beam one has:

$$\omega_r = 0.5657 \alpha_r^2$$

whose α_r is the root of the characteristic function,

$$\cos \alpha_r \cosh \alpha_r - 1 = 0 \quad (5.28)$$

The values ω_r are calculated by using the finite element method which is compared with the analytical natural frequencies as described in table 5.1.

r	α_r	ω_r	FEM 10	FEM 20	FEM 25
1	4.7243	12.63	12.65	12.69	12.72
2	7.8532	34.89	35.09	34.89	34.89
3	10.9954	68.39	68.43	68.39	68.39
4	14.1371	113.1	113.25	112.98	112.98

Table 5.1 Natural frequencies (rad/s) of a beam predicted by an analytical expression and the finite element method with 10, 20 and 25 elements.

For the natural frequency calculations, the finite element method shows good agreement with the theoretical values. For the first four modes, the number of the elements chosen for the discretization of the beam do not have a significant effect on the accuracy of the results.

The vibration modes for a free-free Bernoulli beam can be obtained with an explicit formula. Bishop and Price show that for a free-free beam using as conditions $w_r=1$ for the beam at $x=0$ and $x=L$, the vibration modes can be expressed as follows,

$$w_r(x) = \frac{1}{2} \left(\cosh\left(\alpha_r \frac{x}{L}\right) + \cos\left(\alpha_r \frac{x}{L}\right) - \sigma_r \left(\sinh\left(\alpha_r \frac{x}{L}\right) + \sin\left(\alpha_r \frac{x}{L}\right) \right) \right) \quad (5.29)$$

where σ_r is a function independent of the spatial variable x :

$$\sigma_r = \frac{\cosh \alpha_r - \cos \alpha_r}{\sinh \alpha_r - \sin \alpha_r} \quad (5.30)$$

The mean error obtained for the natural modes is defined as,

$$\varepsilon_w = \frac{100}{N} \sum_{i=1}^N \text{ABS} \left(\frac{w_{ri}^e - w_r(x_i)}{w_r(x_i)} \right) \quad (5.31)$$

where ABS represents the absolute value and N the number of nodes.

N	10 Elem.	20 Elem.	25 Elem.
1	1.41	0.81	0.96
2	0.09	0.09	0.07
3	0.04	0.09	0.10
4	0.11	0.05	0.06

Table 5.2 - Mean errors (%) for the natural shapes using eqn. (5.31)

Table 5.2 contains the mean errors evaluated by using eqn. (5.31). As in the case of the calculation of the natural frequencies, the errors are quite small, even if the number of elements used to model the beam is small, and it is also difficult to draw conclusions about the behaviour of the error when the number of the elements is changed.

A possible explanation for these results is that, with an increase in the number of elements, the accuracy of the finite element model will increase, but the errors associated with the evaluation of the natural values and shapes will also increase.

To see the fitting of the numerical models to the theoretical curves given by (5.27), the values for all the models and the theoretical curves are plotted for the first four natural frequencies.

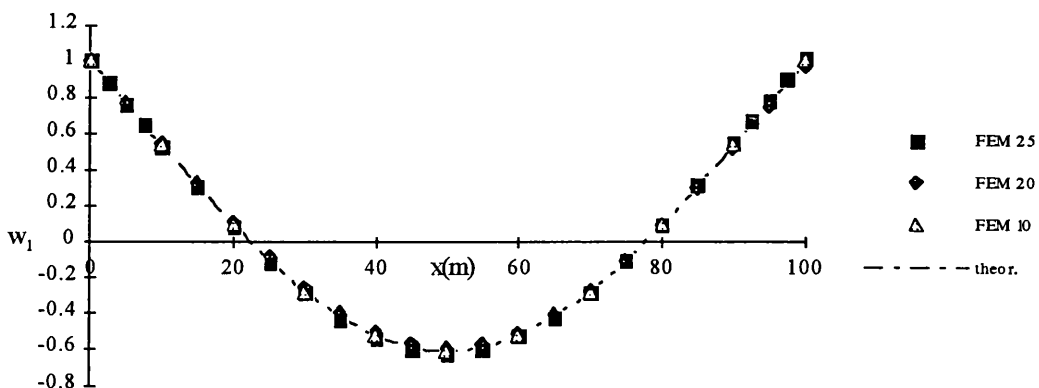


Figure 5.1 - Natural shape 1st mode

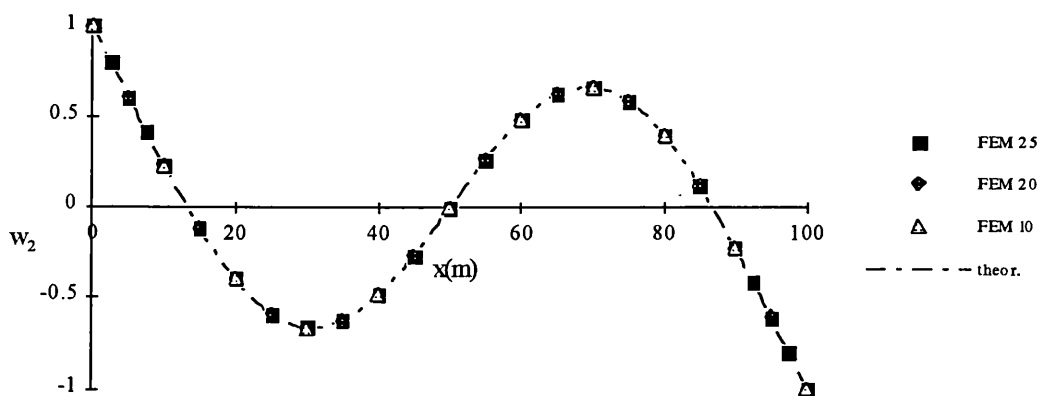


Figure 5.2 - Natural shape 2nd mode

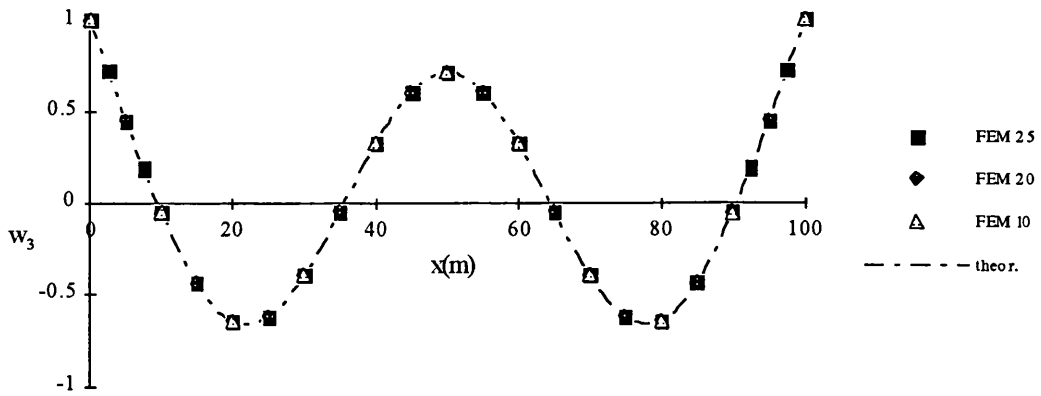


Figure 5.3 - Natural shape 3rd mode

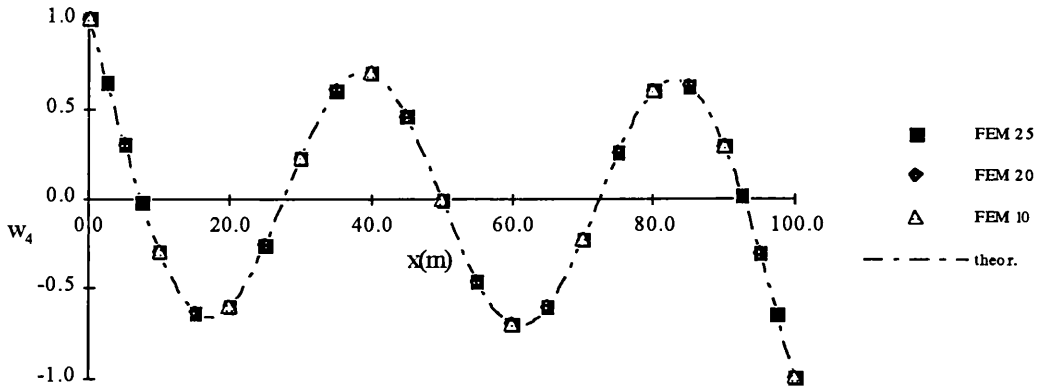


Figure 5.4 - Natural shape 4rd mode

In the finite element method the final output is w_r and θ_r for the nodes. So the shear forces and bending moments are evaluated assuming that the natural shape between two nodes can be represented by a third order polynomial, with the conditions that the displacements and rotations in the nodes must be the same:

$$w_r^{ei}(x) = A x^3 + B x^2 + C x + D \quad x \in D_{ei} \quad (5.32)$$

The shear forces and vertical bending moments are obtained using the Bernoulli formulation and eqn. (5.31):

$$M_r^{ei}(x) = EI (6A x + B) \quad x \in D_{ei} \quad (5.33)$$

$$V_r^{ei}(x) = EI (6A) \quad x \in D_{ei} \quad (5.34)$$

Observing the equation for the shear force and the approximation outlined above, the values are constant for the elements, so the error associated with it will increase as the number of elements used in the model decreases.

For the bending moment the behaviour of the error is the same as the shear force, and as shown in the following figures the error increases with the mode.

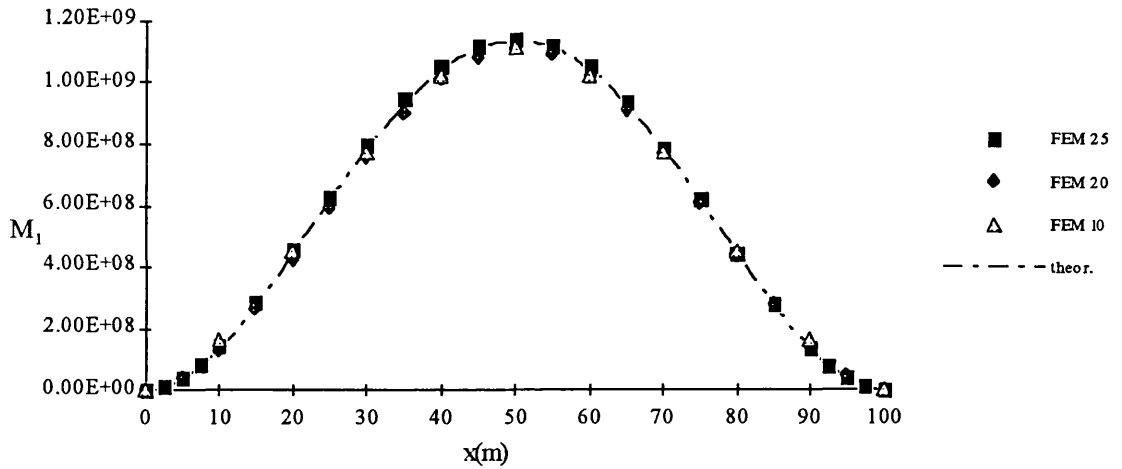


Figure 5.5 - Bending Moment, 1st mode

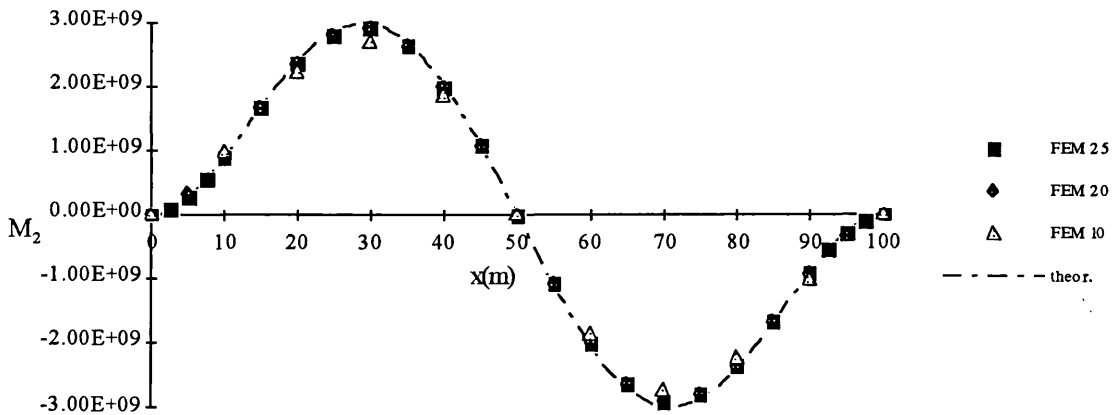


Figure 5.6 - Bending Moment, 2nd mode

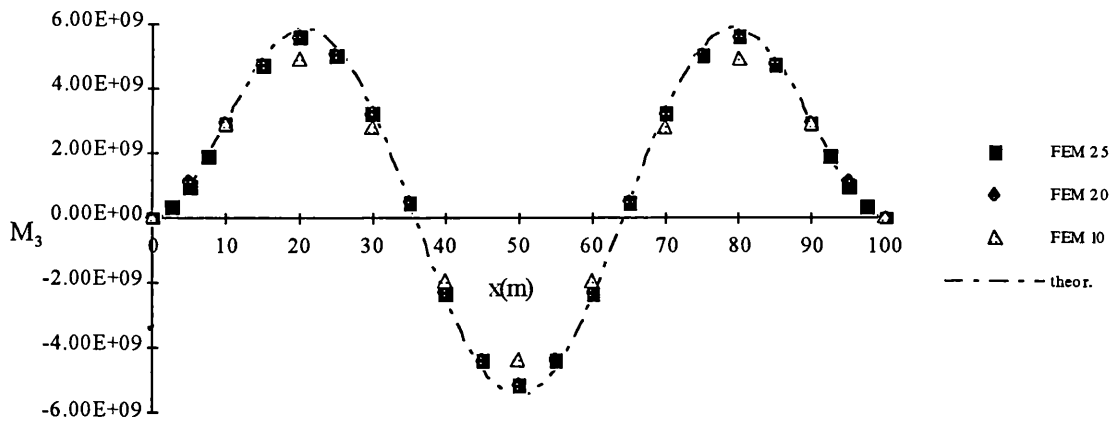


Figure 5.7 - Bending Moment, 3rd mode

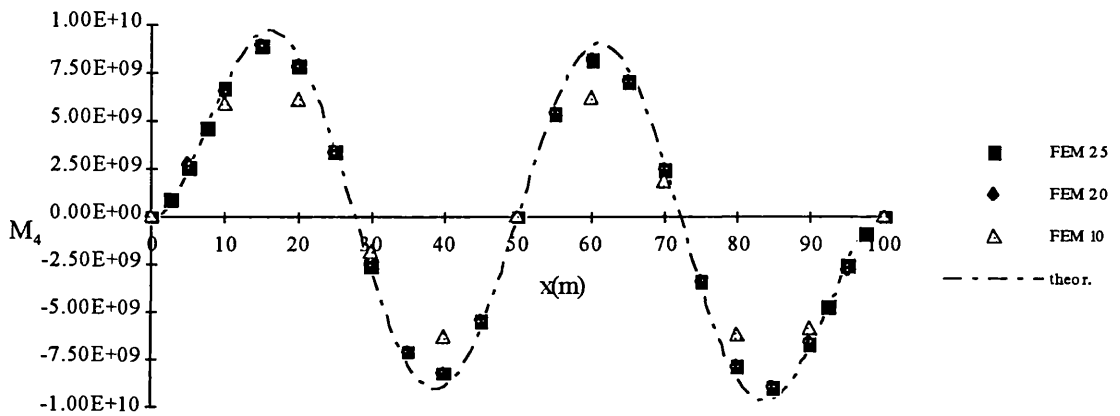


Figure 5.8 - Bending Moment, 4th mode

Table 5.3 shows the vertical bending moment mean error for the three models and for the first four modes.

N	FEM 10	FEM 20	FEM 25
1	3.41	2.18	1.58
2	5.80	3.09	1.72
3	11.80	3.63	2.03
4	20.10	6.69	2.31

Table 5.3 - Mean error (%) for the vertical bending moment

So in conclusion, one can say that the precision of this method depends on the number of elements used in the beam model, and for that kind of analysis normally only the first four modes are required to have a good approximation. If the number of elements used

is greater than twenty, then the expected results for the beam modal analysis will be quite accurate. The apparent large deviations in the last mode will not produce large errors in the final result, because for that mode the responses in the principal coordinates will be very small for the usual ship excitations. For this example the beam in vacuo is loaded with two different loads:

$$F_1(x, t) = F_x(x) K_{t1}$$

$$F_2(x, t) = F_x(x) K_{t2}$$

where F_x , K_{t1} and K_{t2} are represented in the figures 5.9 and 5.10.

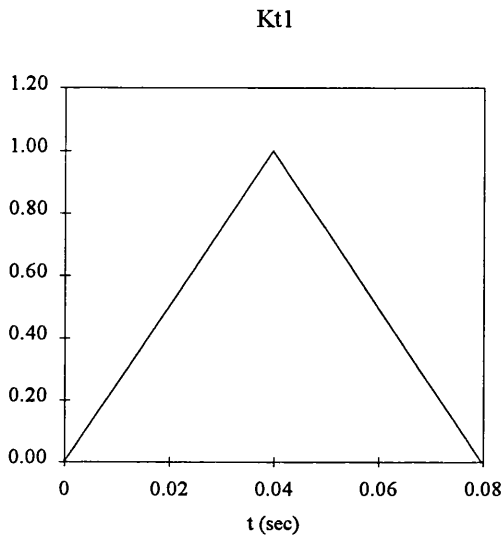


Figure 5.9 - Time function K_{t1}

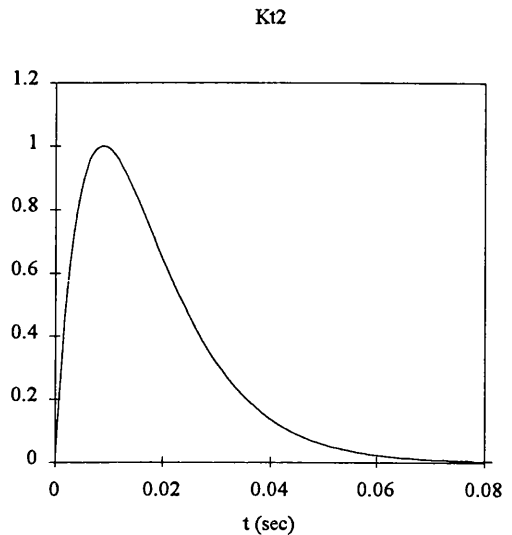


Figure 5.10 - Time function K_{t2}

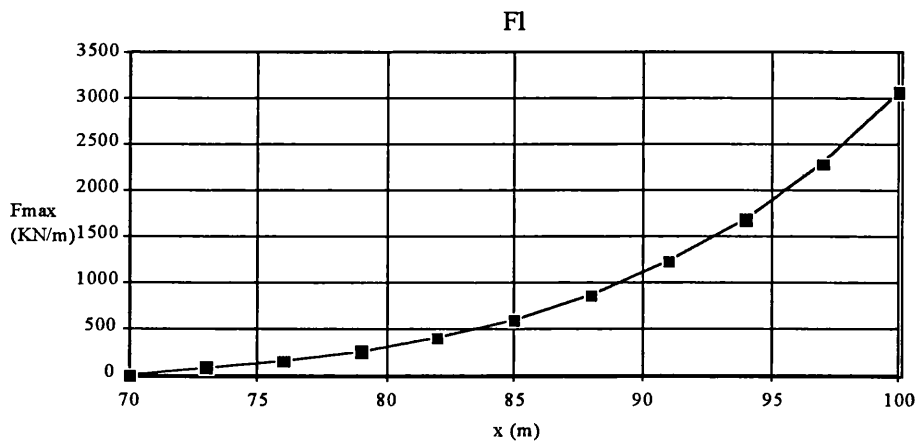


Figure 5.11 - Maximum force longitudinal distribution

The time step for this particular beam is equal to

$$\Delta t = \frac{T_N}{2\pi} = \frac{1}{\omega_n} = \frac{1}{113.1} = 0.00884$$

The response for the two loads and for the first four modes are plotted in figures 5.12 to 5.15.

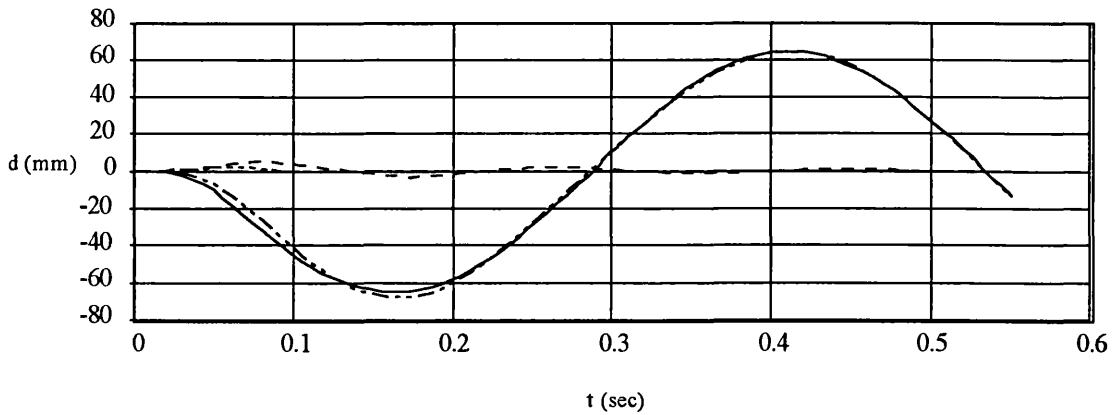


Figure 5.12 - Midship displacement using K_{t1}

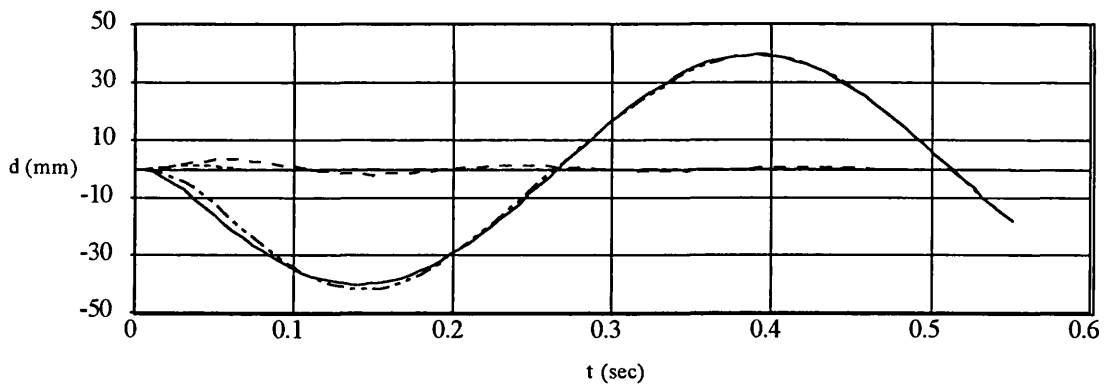


Figure 5.13 - Midship displacement using K_{t2}

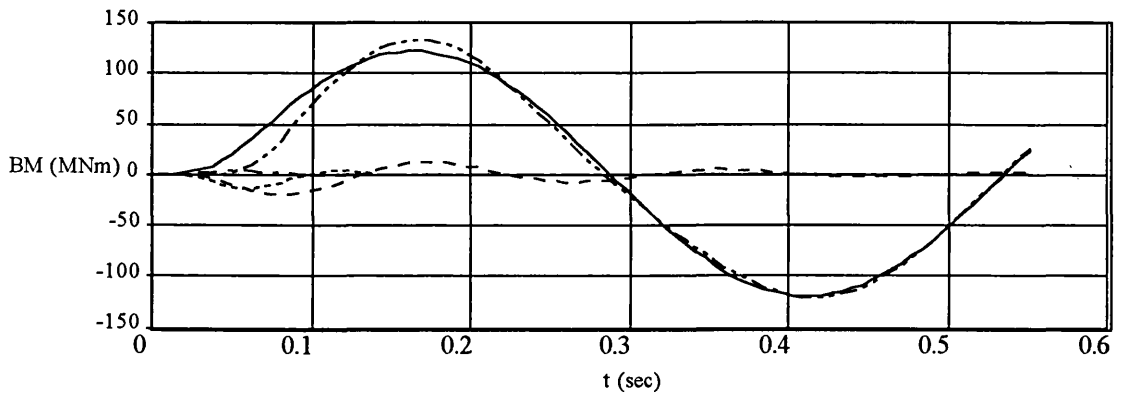


Figure 5.14 - Midship BM using K_{t1}

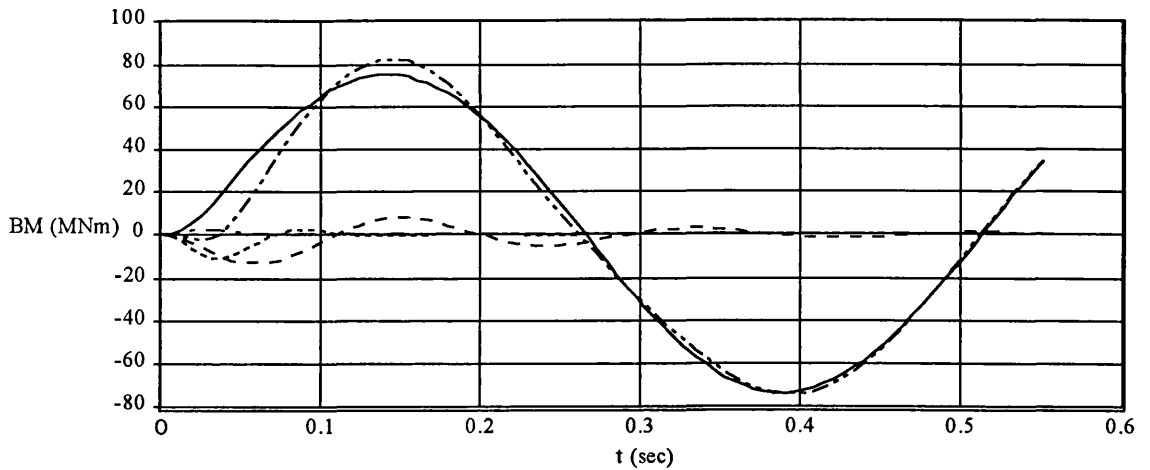


Figure 5.15 - Midship BM using K_{t2}

Other important figure is the longitudinal variation of the maximum bending moment in sagging and hogging obtained for the two methods.

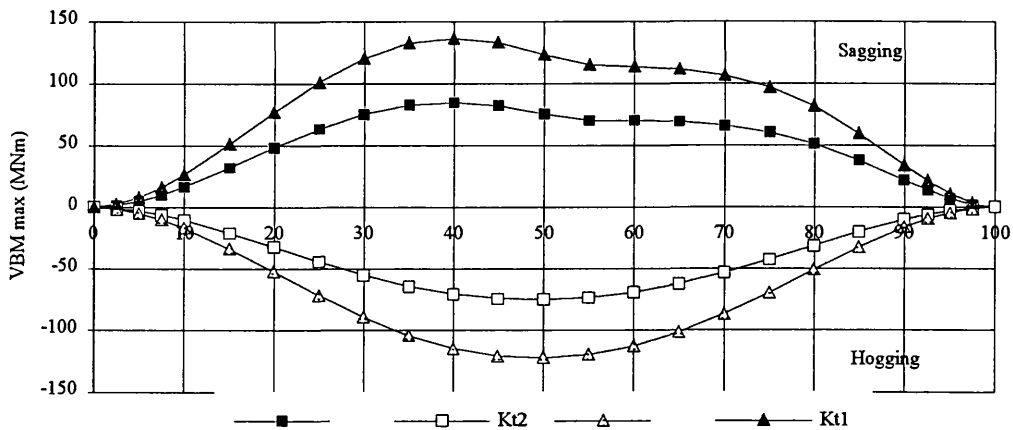


Figure 5.16 - Maximum BM longitudinal distribution

Looking at the bending moments curves i.e. figures 5.14 and 5.15, the values for the 3rd and 4th modes are very small when compared with the first mode, and for the first mode second half cycle the bending moments for the higher modes can be neglected. So in conclusion, the higher modes only have some influence in the total response for a very short period (less than one half cycle in the first mode). Figure 5.17 shows the longitudinal variation of the sagging and hogging ratio for the maximum bending moments.

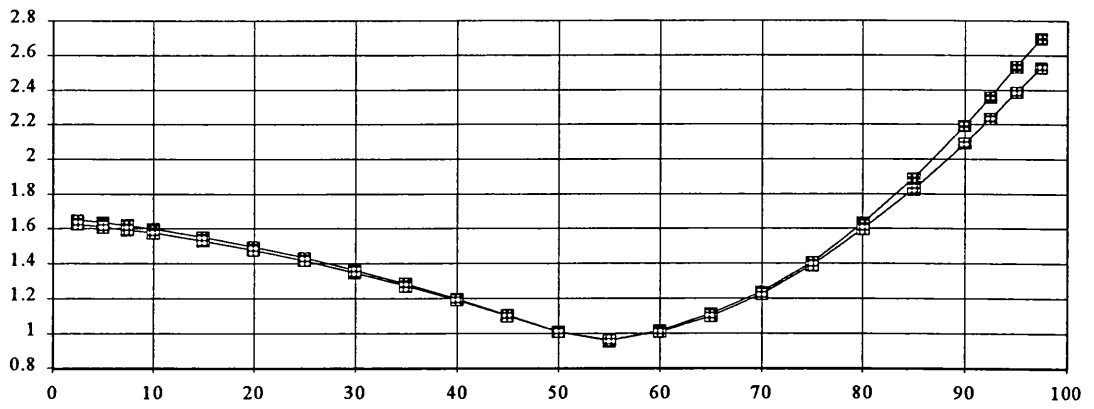


Figure 5.17 Ratio between sagging and hogging bending moments

Even for two different values of vertical bending moments the longitudinal ratio between the sagging and hogging bending moment is approximately the same and the maximum values are, as expected, in the forward stations.

CHAPTER 6

VALIDATION OF METHODS WITH EXPERIMENTAL RESULTS

6.1 - INTRODUCTION

Experiments to measure ship motions and wave induced loads for head seas, were carried out in the towing tank of the University of Glasgow, which is 77 m long, 4.6 m wide and 2.7. deep, with an X-carriage that can travel at a maximum speed of 6.4 m/s. One end of the tank contains a wave maker which can generate regular and irregular waves and at the other end there is a wave absorbing beach. The wave maker is driven by an hydraulic pump controlled electronically by a micro-computer which contains a suitable software to generate the desired sea conditions.

6.2 - MAIN PARTICULARS OF THE MODEL

The model used to validate the motions and loads was the S-175 container ship whose main particulars are given in chapter 3. The scale ratio of the model is 1/70 and the experiments were carried out in the ballast condition. This choice was made in order to attain the bottom emergence without green water effects. Table 6.1 shows the model main particulars for the ballast condition.

L _{pp} (m)	2.50
B (m)	0.363
T (m)	0.10
Δ (Kg)	48.8
C _b	0.54
LCG (aft of midship)	0.8% L _{pp}
Pitch radius of gyration	0.61

Table 6.1 - Model's main particulars

In order to measure the vertical shear forces and bending moments, the model was cut in three longitudinal positions and the segments were connected using flexible bars. In each bar three strain gauges were mounted, two of which were used to measure the normal stresses, i.e. bending moments and the last one to measure the shear forces. Near the forward and aft perpendiculars, two light emitting diodes were mounted on the model. The signals emitted by these diodes were received by two cameras fixed on the main carriage. Using these signals and the positions of the LED's in the model, the heave and pitch motions can be easily obtained.

To measure the incident wave height, one wave probe was fixed in the main carriage near the model forward perpendicular. This probe induced an electrical signal whose intensity depends on its wetted height. All these signals (12 channels) were amplified and sent to a data collection system and recorded in a micro-computer which presents the experimental results in a graphical form. Figure 6.1 shows the longitudinal positions of the strain gauges and the diodes.

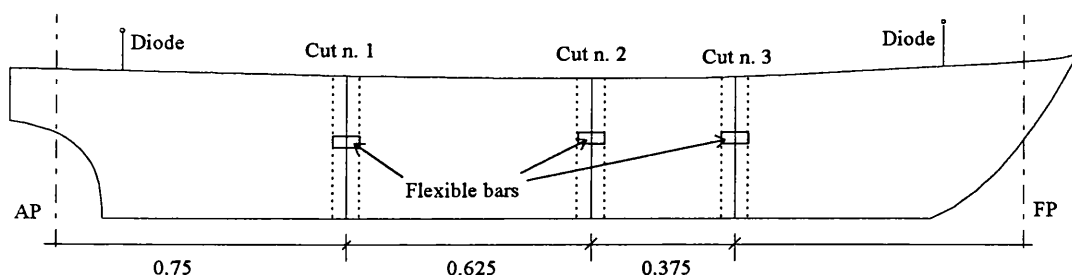


Figure 6.1 - Logitudinal position of the strain gauges and diodes

Channel	Description
1	Strain Gauge for measuring VBM cut n.1 (bottom of the bar)
2	Strain Gauge for measuring VBM cut n.1 (top of the bar)
3	Strain Gauge for measuring Shear Force cut n.1
4	Strain Gauge for measuring VBM cut n.2 (bottom of the bar)
5	Strain Gauge for measuring VBM cut n.2 (top of the bar)
6	Strain Gauge for measuring Shear Force cut n.2
7	Strain Gauge for measuring VBM cut n.3 (bottom of the bar)
8	Strain Gauge for measuring VBM cut n.3 (top of the bar)
9	Strain Gauge for measuring Shear Force cut n.3
10	Forward Diode
11	Aft Diode
12	Wave Probe

Table 6.2 - Channels description used in the experimental measurements

6.3 - WEIGHT DISTRIBUTION OF THE MODEL

The weight distribution of the S-175 container model is unknown because there was not available data about the longitudinal distribution of the model hull weight.

So the longitudinal weight distribution must be approximated and it is assumed that it can be described by an N order polynomial function with N+1 unknown coefficients,

$$w(x) = \sum_{n=0}^N C_n x^n \quad (6.1)$$

The coefficients are determined using some properties obtained from measurements on the hull model such as the hull weight, the longitudinal centre of gravity, the gyration radius and the still water bending moments in three longitudinal positions. The weight distribution of the model was assumed such that it was zero at the extremes. Since the number of measurement quantities is eight, this is also the maximum number of coefficients that can be in the polynomial.

To obtain the deviations of this approximation from the real weight distribution, two different weight distributions were considered and for each one four different polynomial curves were determined using the following number of coefficients and conditions.

Conditions for curve 1 - Zero weight at the extremes, specified displacement and position of LCG, leading with 4 coefficients in the polynomial.

Conditions for curve 2 - Zero weight at the extremes, specified displacement, position of LCG and radius of gyration, leading with 5 coefficients in the polynomial.

Conditions for curve 3 - Zero weight at the extremes, specified displacement, position of LCG, radius of gyration and vertical bending moment in three longitudinal positions, leading with 8 coefficients in the polynomial.

Conditions for curve 4 - Zero weight at the extremes, specified displacement, position of LCG, radius of gyration, vertical bending moment and shear force in three longitudinal positions, leading with 11 coefficients in the polynomial.

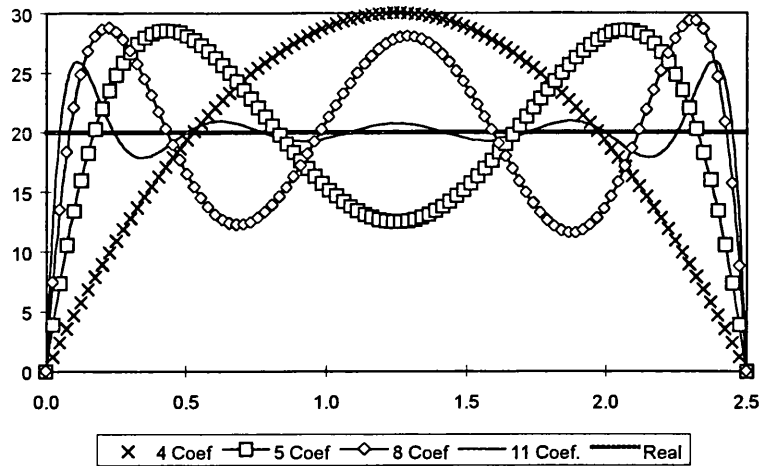


Figure 6.2 Weight longitudinal distribution. curve I

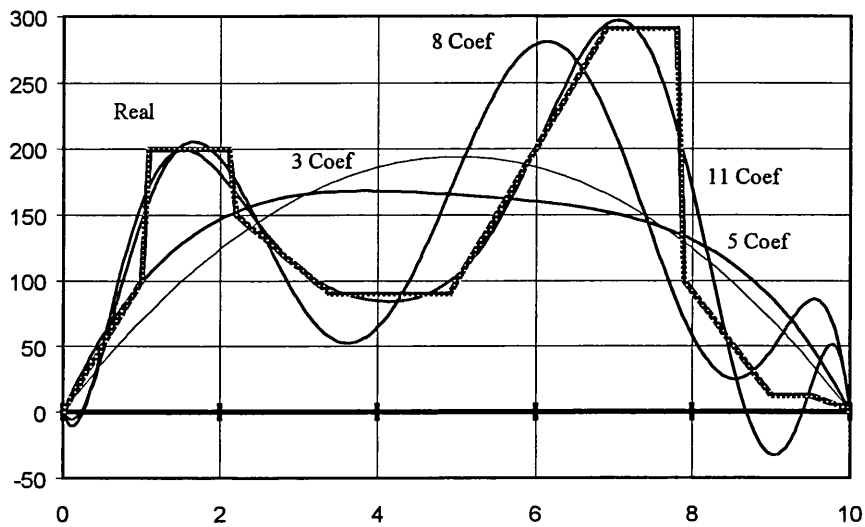


Figure 6.3 Weight longitudinal distribution. Curve II

From figures 6.2 and 6.3 it can be concluded that the polynomial that use 8 and 11 coefficients fit the real curve well from a practical point of view. The problem with the curve in Fig. 6.3, is that some values are negative and this is physically impossible. However, if we obtain the bending moment curve from the weight distribution, this approximation gives very similar results to the real curve, as can be seen from figure 6.4.

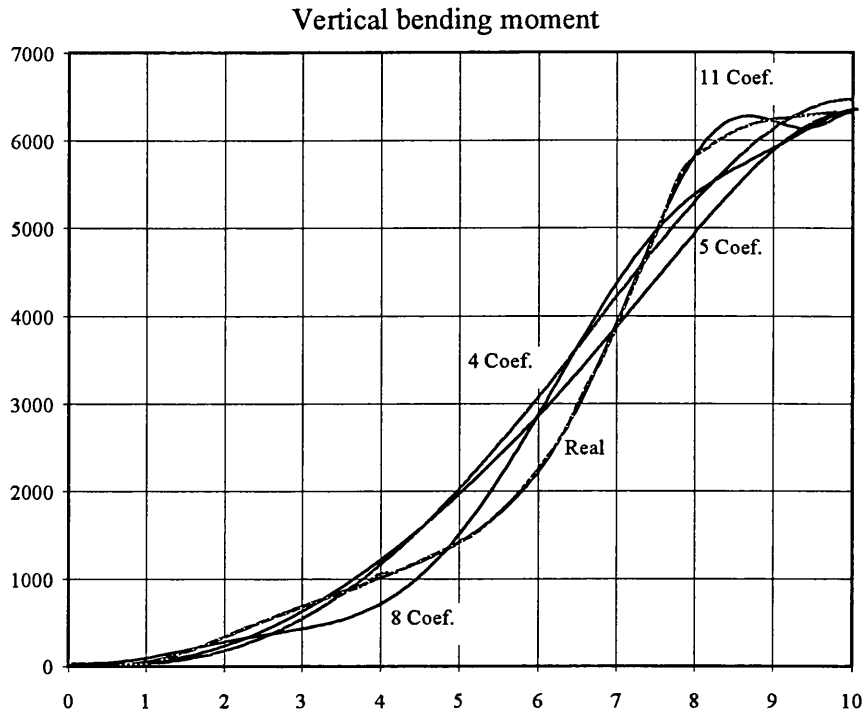


Figure 6.4 Vertical Bending Moment calculated for curve II

The static bending moments of the model were measured and the values are shown in table 6.3.

	M (Kgm)
Strain gauge 1	1.45
Strain gauge 2	4.75
Strain gauge 3	2.40

Table 6.3 Measured bending moments

The static bending moments presented in table 6.2 can be calculated using the following relation,

$$M(x) = \int_0^x V_m(x) - V_b(x) dx \quad (6.2)$$

where V_m is the shear force due to the mass distribution and V_b due to the buoyancy. For calculation of the vertical bending moments due to the mass distribution equation (6.2) can be rewritten for the strain locations using the following set of equations,

$$\int_0^{0.75} V_m dx = M_b(0.75) + 1.45$$

$$\int_0^{1.375} V_m dx = M_b(1.375) + 4.75$$

$$\int_0^{1.75} V_m dx = M_b(1.75) + 2.4$$

Figure 6.5 represents the vertical bending moment induced by buoyancy.

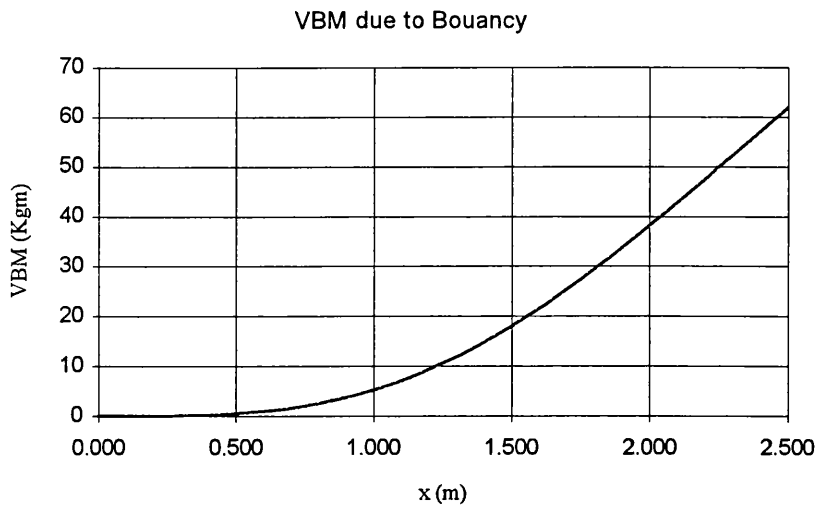


Figure 6.5 - Vertical bending moment induced by buoyancy

The bending moment induced by the mass distribution for the three points, can be obtained,

$$\int_0^{0.75} \dot{V}_m dx = 3.35 \text{ Kgm}$$

$$\int_0^{1.35} \dot{V}_m dx = 18.83 \text{ Kgm}$$

$$\int_0^{1.75} \dot{V}_m dx = 29.63 \text{ Kgm}$$

Using the information about the displacement, radius of gyration, longitudinal position of the gravity centre, the weight distribution at the ship extremes and the bending moments in three longitudinal positions, one polynomial with 8 coefficients to represent the mass distribution was found and its curve is shown in figure 6.6.

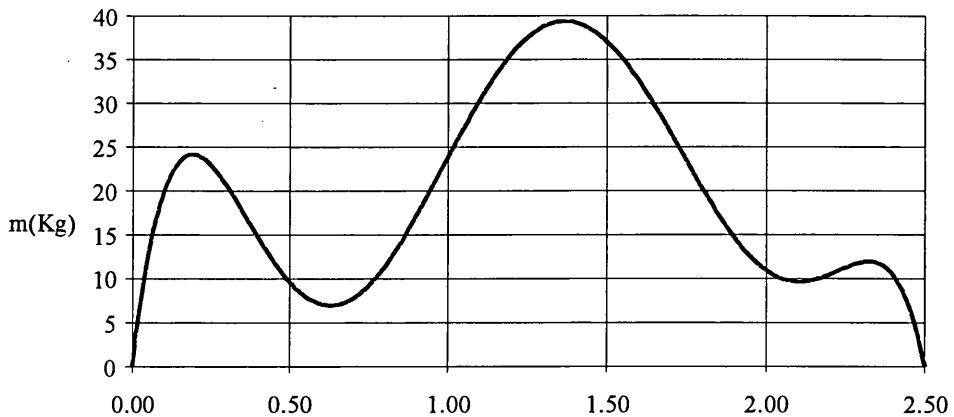


Figure 6.6 - Model mass distribution using the 8 coefficient polynomial

The still water bending moment distribution for this condition is illustrated in figure 6.7.

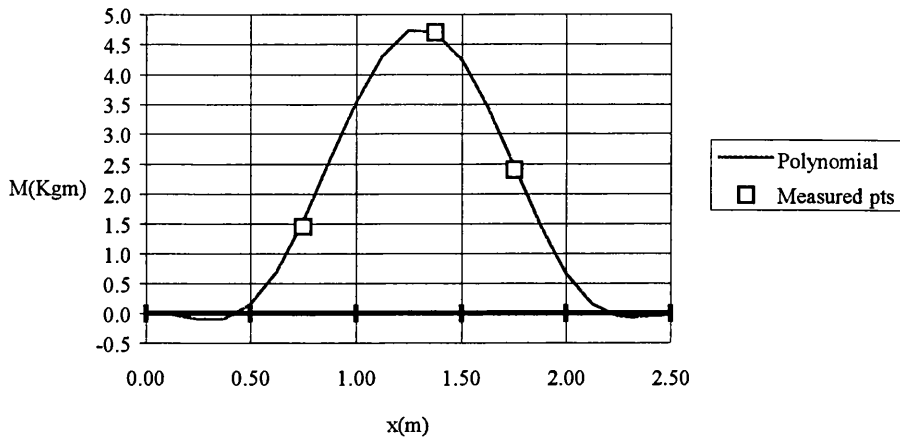


Figure 6.7 -Still water bending moments using the 8 coefficients polynomial

6.4 - STRUCTURAL ASPECTS OF THE MODEL

In order to measure the vertical bending moment and shear forces, the model was segmented into three parts. From a structural point of view the model can be considered as three nodes with rotational stiffness and four rigid segments that are linked to the nodes. Figure 6.8 shows this in diagrammatic form.



Figure 6.8 - Diagram of the equivalent system of the model

In this system the unknown variables are the rotations. For practical purposes it is better to transform the rotations into vertical translations and to find the equivalent system for the stiffness and mass matrices. For the evaluation of the mass matrix and the force vector, the finite element approximation can be used. Assuming that each element has only two degrees of freedom, the shape functions can be considered as linear.

$$\Psi_1 = 1 - \frac{x}{L} \quad (6.3)$$

$$\Psi_2 = \frac{x}{L} \quad (6.4)$$

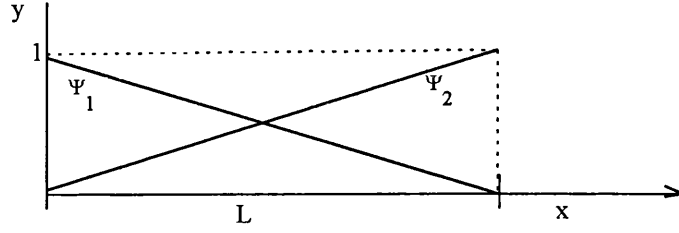


Figure 6.9 - Shape functions used in the finite element approximation

Applying the definition that a unit acceleration at node 1 will create a force in node 2 and by using the principle of virtual displacement, the element mass matrix can be obtained using the following expression,

$$m_{ij} = \int_0^L m(x) \Psi_i \Psi_j dx \quad (6.5)$$

where $m(x)$ is the total mass distribution i.e. including the added mass contribution. The applied force vector can be evaluated in a similar form,

$$F_i(x, t) = \int_0^L q(x, t) \Psi_i dx \quad (6.6)$$

The expression for the stiffness matrix is more complicated because it requires the transformation of the rotational stiffness into translation stiffness. Using the unit displacement method combined with static equilibrium for the forces and moments, the global stiffness matrix was derived as follows

$$\begin{aligned} K_{11} &= \frac{K_2}{L_a^2} & K_{21} &= -\frac{K_2}{L_a} \left(\frac{1}{L_a} + \frac{1}{L_b} \right) & K_{31} &= \frac{K_2}{L_a L_b} & K_{41} &= 0 & K_{51} &= 0 \\ K_{22} &= \frac{K_3}{L_b^2} + K_2 \left(\frac{1}{L_a} + \frac{1}{L_b} \right)^2 & K_{32} &= -\frac{K_3}{L_b} \left(\frac{1}{L_b} + \frac{1}{L_c} \right) - \frac{K_2}{L_b} \left(\frac{1}{L_c} + \frac{1}{L_d} \right) \\ K_{42} &= \frac{K_3}{L_b L_c} & K_{52} &= 0 \\ K_{43} &= -\frac{K_4}{L_c} \left(\frac{1}{L_c} + \frac{1}{L_d} \right) - \frac{K_3}{L_c} \left(\frac{1}{L_c} + \frac{1}{L_b} \right) & K_{53} &= \frac{K_4}{L_c L_d} & K_{33} &= -K_{13} - K_{23} - K_{43} - K_{53} \\ K_{54} &= -\frac{K_4}{L_d} \left(\frac{1}{L_c} + \frac{1}{L_d} \right) & K_{44} &= -K_{24} - K_{34} - K_{54} \\ K_{55} &= \frac{K_4}{L_d^2} \end{aligned}$$

Since the stiffness matrix is symmetric the other elements of the matrix were obtained using this property.

For the evaluation of the natural frequencies and mode shapes of the structural model in water, some amount of water mass must be added to the mass distribution of the model. This quantity can be determined using the Landweber or the Lewis method for determination of the added mass for infinite frequencies, and then the value is corrected using a “J” value or a reduction factor to allow for the three dimensional effects.

Some work has been done on the determination of the J value, Lewis (1929) obtained an expression for ratio of the kinetic energy of the fluid surrounding a vibrating ellipsoid, the axis of which is deformed into the arc of a parabola as it deflects while vibrating and the same kinetic energy for a non deformable ellipse using the common two dimensional approach. Based on this type of analysis and using Euler’s beams formulation, Daidola (1984) deduced the J values for several cylinders varying the ratio L/B. Some more complex three dimensional work based on a finite element approach to derive the added mass of a vibrating ship hull was made by Armand and Orsero (1979). Full scale experiments conducted by Ohtaka (1966) have shown that Lewis forms with the Lewis three dimensional correction factor showed good results for the first vibrating modes. Based on experimental results on ellipsoids and ship models, Townsin (1969) proposed a very simple formula for the J coefficient and for the first three modes of vertical flexural vibration of ships,

$$J_n = 1.02 - 3 \frac{B}{L} \left(1.2 - \frac{1}{n} \right) \quad (6.7)$$

Considering the simplicity of this formulation, the fact that all of the above methods will produce similar results for the first natural frequencies as shown by Townsin (1969), eqn. (6.7) will be used for the calculation of the natural frequencies and shapes. The problem of the equivalent model illustrated in figure 6.8 is to find the equivalent values of the rotational stiffener springs K and the associated structural damping. For this purpose three different free vibration experimental tests were conducted. Figs 6.10-6.12 show the measured vertical bending moments (VBM) for the three strain gauges.

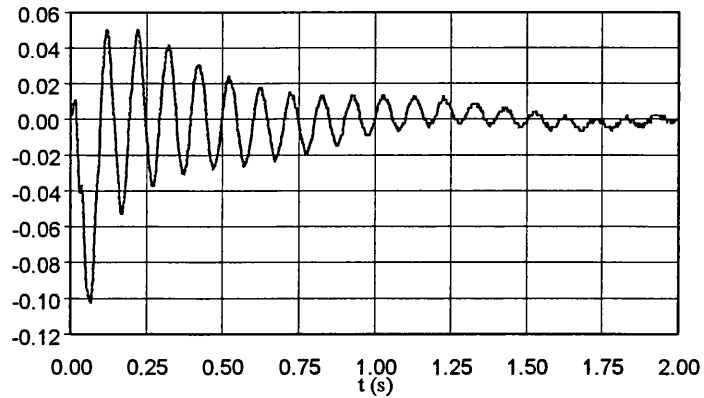


Figure 6.10 - Vertical Bending Moment for a free vibration test. Cut number 1

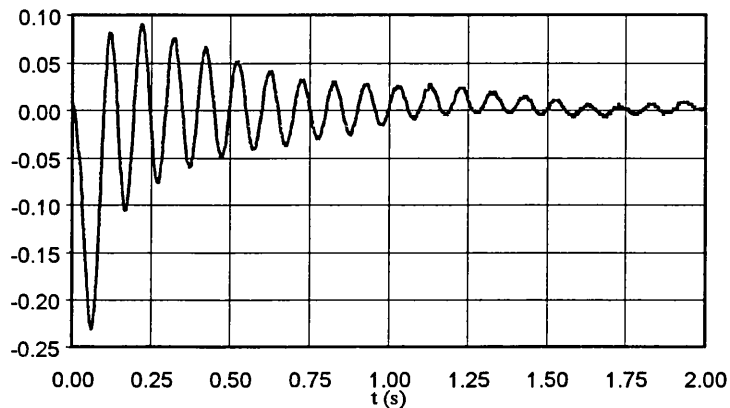


Figure 6.11 - Vertical Bending Moment for a free vibration test. Cut number 2

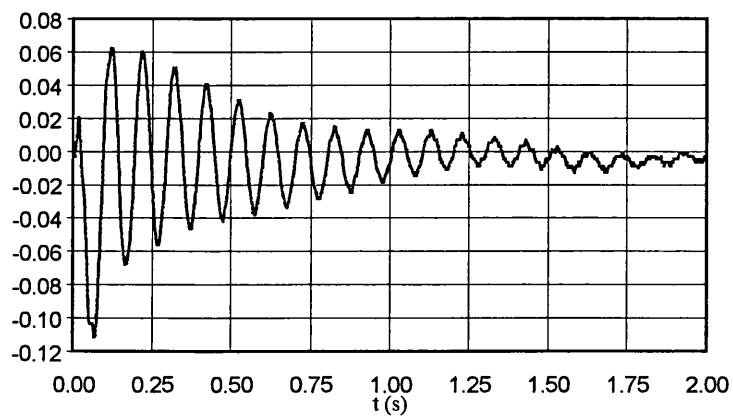


Figure 6.12 - Vertical Bending Moment for a free vibration test. Cut number 3

Using the information contained in figures 10-12, the first natural frequency of the structure can easily be obtained and table 6.4 shows the mean first natural frequency obtained using the data from the three experimental tests.

	Natural Frequency (rad/s)
Strain gauge 1	61.37
Strain gauge 2	61.48
Strain gauge 3	61.29
Mean	61.38

Table 6.4 - First natural frequency of the model structure

The higher frequencies of the structural model cannot be seen and obtained because the measured data is filtered, using one analogic filter, for frequencies higher than 50 Hz. The logarithmic decrement of the dynamic system can be obtained using the following expression:

$$\delta = \frac{1}{n} \ln \frac{u_1}{u_{n+1}} \quad (6.8)$$

where n is the number of positive or negative peaks and u_1 is the first positive or negative peak and u_{n+1} the $n+1$ peak. This approximation is valid if the bending moments are oscillating about the zero value. Looking at figures 6.10-6.12 it can be seen that there is a small oscillation in the mean position so it is desirable to use an equivalent amplitude in equation 6.8, which is given by,

$$\bar{u} = \frac{u_{\max} - u_{\min}}{2} \quad (6.9)$$

where u_{\max} is the maximum peak of the cycle n and u_{\min} the minimum for the same cycle. Figure 6.13 shows the amplitude decay for the three strain gauges.

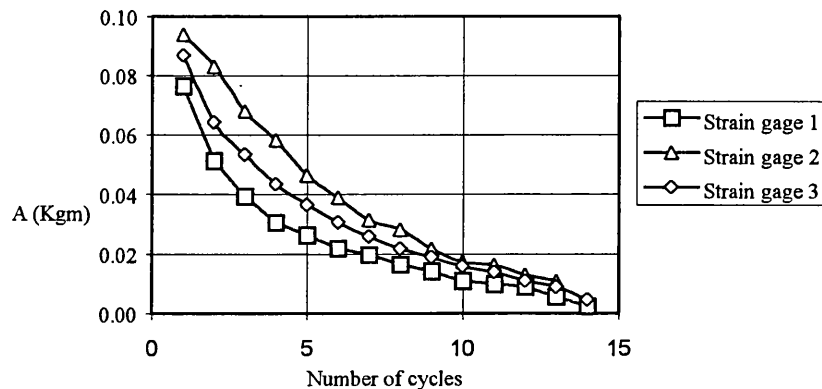


Figure 6.13 - VBM amplitude decay observed in the three strain gauges

Using the information contained in Fig. 6.13 and eqn. (6.8) the logarithmic decrement was calculated in the three sections during 10 cycles and is shown in Fig. 6.14.

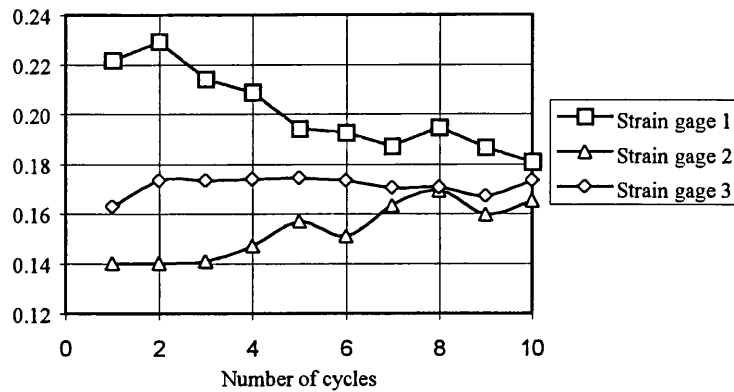


Figure 6.14 - Logarithmic decrement for the three strain gauges

From figure 6.14 one important conclusion can be drawn: the logarithmic decrement for the three strain gauges converge for the same value. This means that the coupled terms of the damping matrix can be neglected.

The mean value obtained for the logarithmic decrement is equal to:

$$\delta_1 = 0.174$$

Based on the small value obtained for the logarithmic decrement, the damping ratio can be obtained using the following linear relation,

$$\zeta_1 = \frac{\delta}{2\pi} = 2.77\%$$

This value is within the region in which the natural frequency can be considered equal to the natural frequency of damped vibration, which implies that the classical modal analysis can be performed with some confidence.

Using this assumption and the value obtained for the first natural frequency, the rotational stiffness of the springs was found to be:

$$K = 9.44 \text{ KN}$$

Using this value, the three first natural frequencies and the natural shapes were obtained and these values are represented in table 6.5 and figure 6.15.

	Natural Frequency (rad/s)
Mode 1	61.4
Mode 2	165.9
Mode 3	338.5

Table 6.5 - Natural frequencies for the wet mode

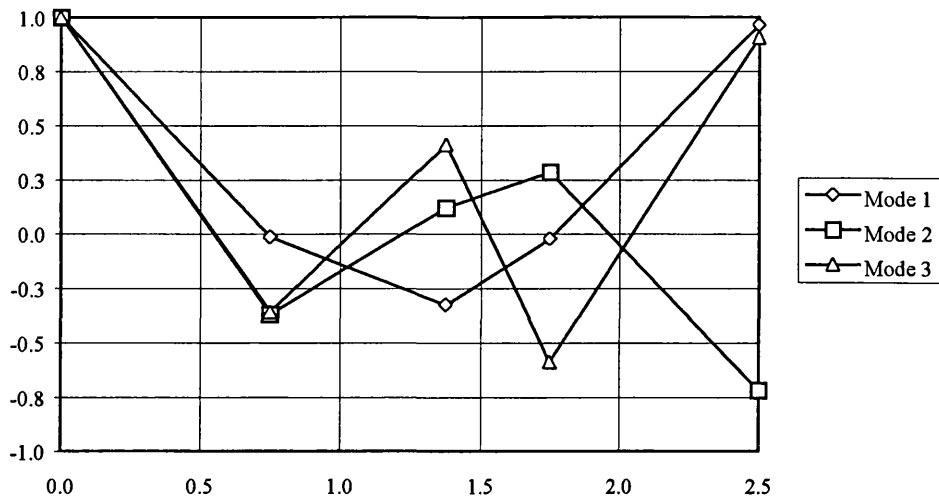


Figure 6.15 - Natural shapes for the wet mode

Kumai (1958) suggests a formula to evaluate the logarithmic decrement for the higher frequencies

$$\delta_N = \delta_1 \left(\frac{\omega_N}{\omega_1} \right)^{0.75} \quad (6.10)$$

Using the formulation explained in chapter 5, the mass and stiffness coefficients were obtained for the first three modes and the values are presented in table 6.6.

Mode	Mass	Damping	Stiffness
1	7.76	26.56	3.04E4
2	2.86	55.49	7.87E4
3	9.14	616.91	1.04E6

Table 6.6 - Coefficients of the decoupled dynamic system

In order to check the derivation of the stiffness matrix, the node displacements were evaluated for the still water condition and afterwards the total rotations of the nodes were also calculated. Using these values the bending moments were obtained using the following relation

$$M_i = K_i \theta_i \quad (6.11)$$

Using this approximation table 6.7 shows the bending moment results

	Real	Calculated	Dif. (%)
Spring 1	1.450	1.377	-5.006
Spring 2	4.850	4.895	0.936
Spring 3	2.400	2.599	8.312

Table 6.7 - Comparison of the still water bending moments

So it can be concluded that this approximation gave reasonable results despite the small number of elements used in the model. Also in order to check the modal analysis mentioned in chapter 5, the structural nodal displacements were evaluated and compared with the ones obtained using a static analysis. Figure 6.16 shows the results for the two approximations indicating a good agreement.

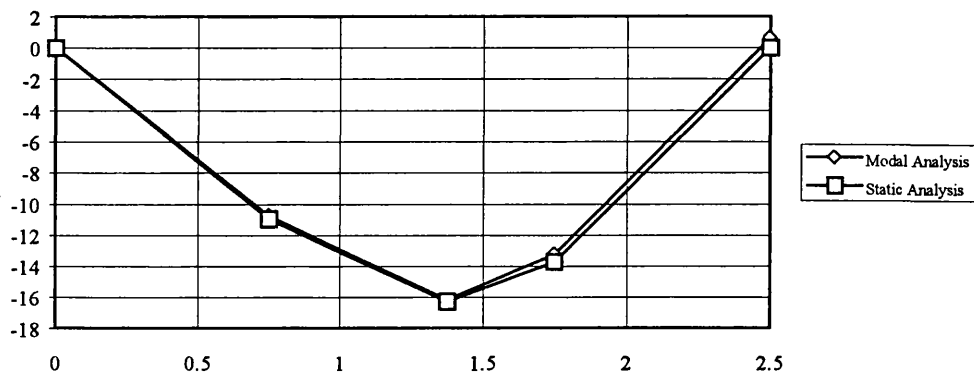


Figure 6.16 - Still water structural displacement using direct and modal calculations

6.5 - SHIP MOTIONS AND WAVE LOADS

The heave and pitch transfer functions were calculated using the formulation given in chapter 3 and the results were compared with the experimental measurements.

Twelve different runs were carried out with a Froude number equal to 0.2. Table 6.8 represents the main particulars of the tests.

Run	Speed (m/s)	Wave freq. (Hz)	Wave Amp (cm)
1	0.989	0.48	1.71
2	0.989	0.56	1.84
3	0.999	0.64	1.77
4	0.985	0.79	1.58
5	0.990	0.96	1.31
6	0.992	1.11	1.40
7	0.992	0.56	3.62
8	0.991	0.64	3.51
9	0.996	0.79	3.56
10	0.988	0.56	5.37
11	0.993	0.64	5.40
12	0.994	0.79	4.35

Table 6.8 - Model speed and Wave data for the different runs

Figures 6.17 and 6.18 show the experimental and theoretical results using the linear strip theory for the model with a Froude number of 0.2. From these figures it can be concluded that the linear theory can predict quite well the heave and pitch ship motions even for severe seas.

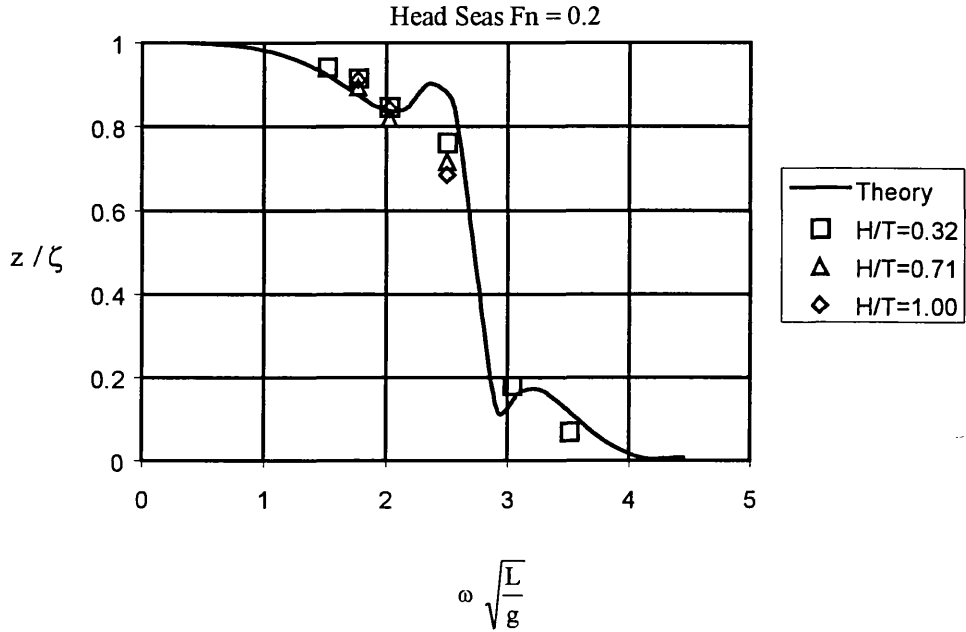


Figure 6.17 - Heave transfer function

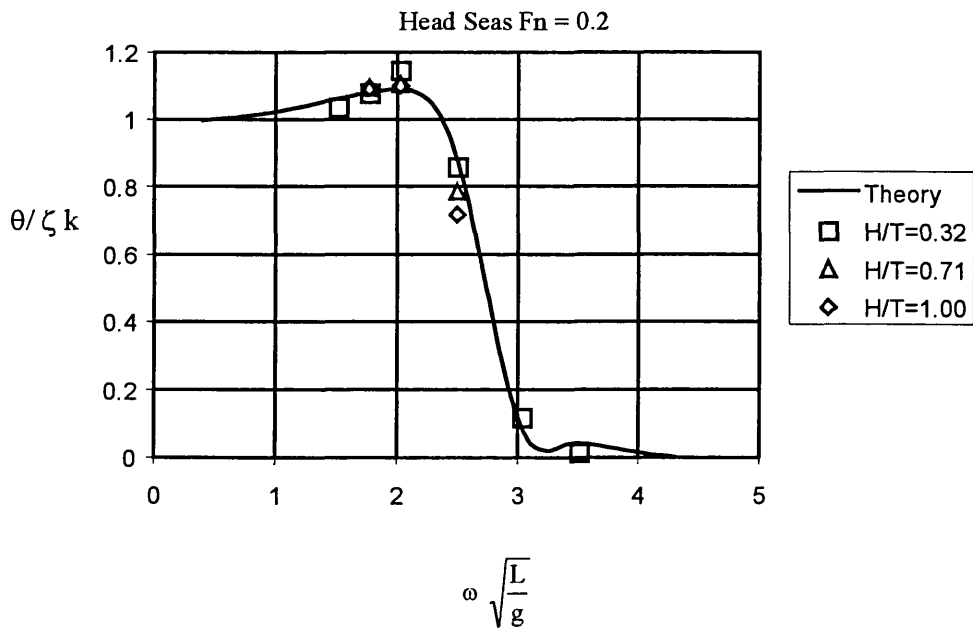


Figure 6.18 - Pitch transfer function

The lag between the wave and the heave and pitch motions can be evaluated using the signals of the wave probe that was mounted on the forward perpendicular.

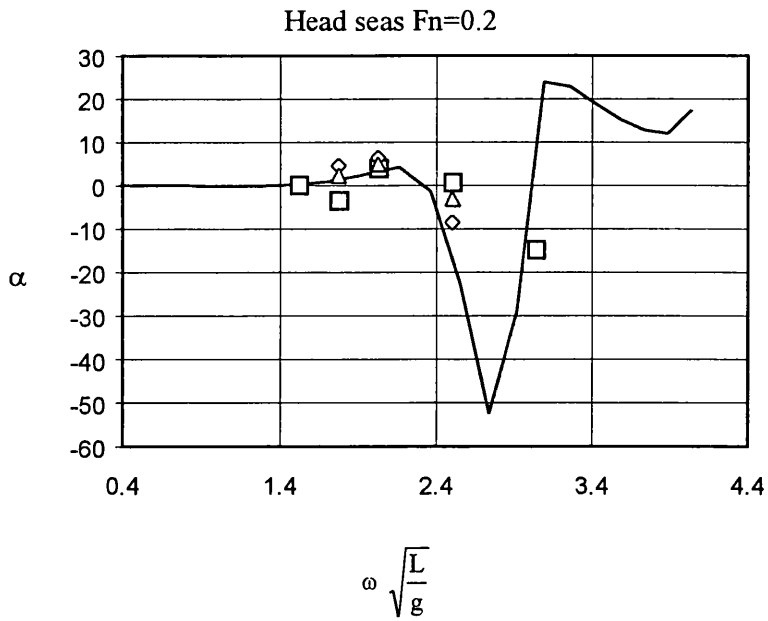


Figure 6.19 - Heave Lag - Results comparison

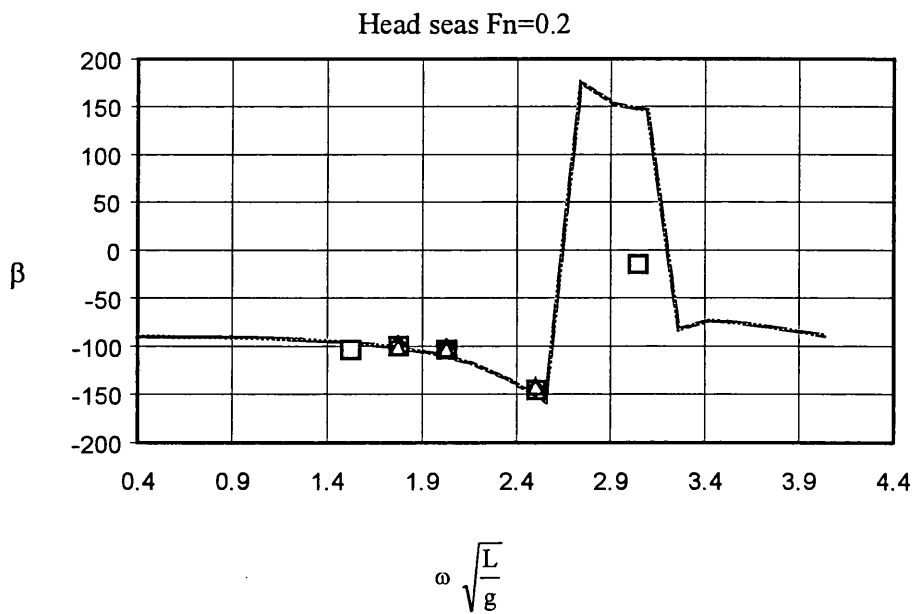


Figure 6.20 - Pitch Lag - Results comparison

Using the experimental data from the heave and pitch transfer functions and phase angles, the relative motion transfer functions for any longitudinal position can be obtained. Figures 6.21 to 6.23 shows the comparison between the experiments and the theory.

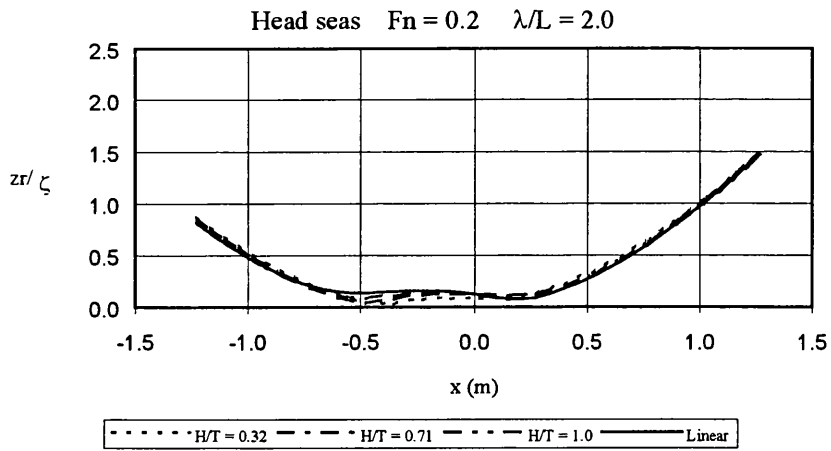


Figure 6.21 - Measured and calculated relative motion for $f=0.56$ Hz

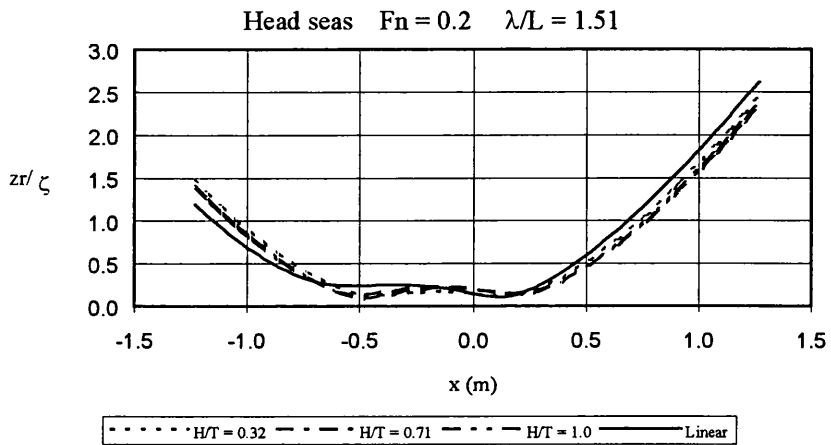


Figure 6.22 - Measured and calculated relative motion for $f=0.64$ Hz

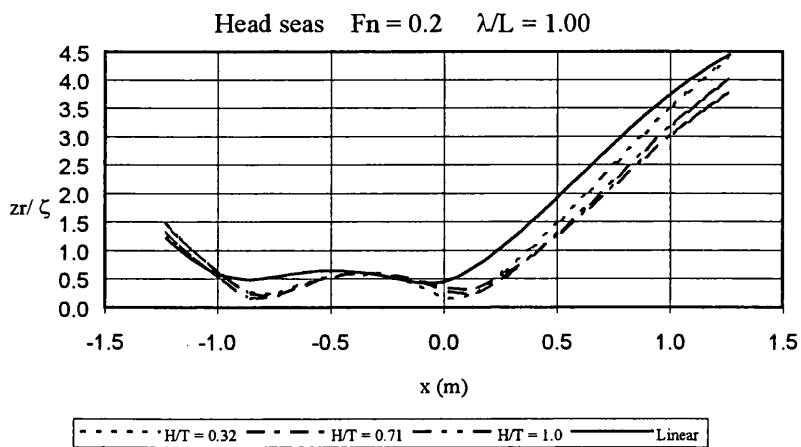


Figure 6.23 - Measured and calculated relative motion for $f=0.79$ Hz - Results comparison

From the figures of the relative motions it can be concluded that linear theory gives satisfactory results for the vertical motions and even for large waves this theory can be applied with some confidence. However for the frequencies which produce the larger

relative motion amplitudes the linear theory shows some deviations from the experimental results. For larger wave amplitudes linear theory produces, like for the pitch transfer function, higher relative motion amplitudes.

Using the formulation described in chapter 3, the vertical bending moments were calculated and compared with measurements for the first six runs in which the wave amplitude is small compared with the ship length. The vertical bending moments were non-dimensionalized using the following relation:

$$M' = \frac{M}{\rho g L^2 B} \quad (6.12)$$

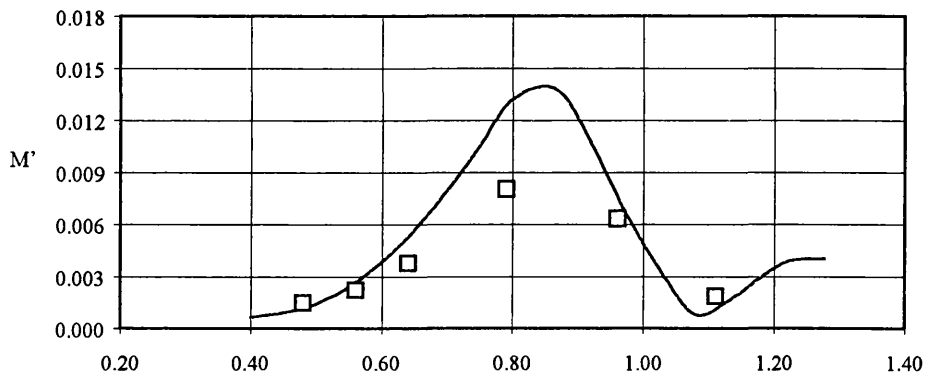


Figure 6.24 - Vertical Bending Moment at Strain Gauge 1

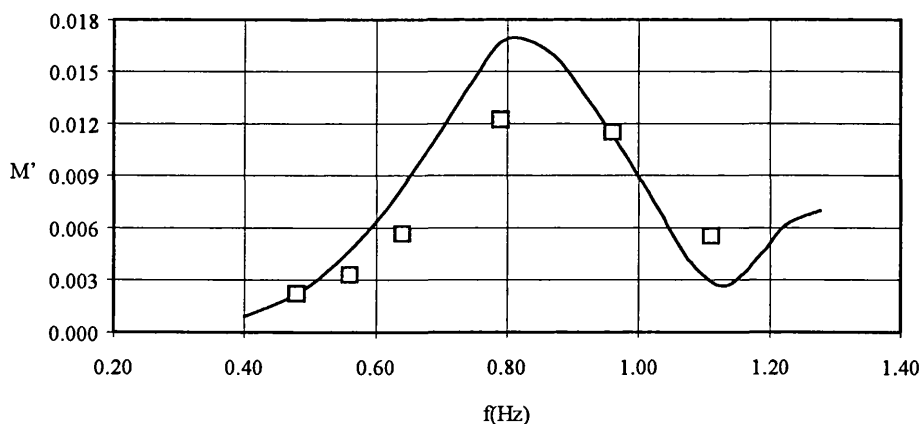


Figure 6.25 - Vertical Bending Moment at Strain Gauge 2

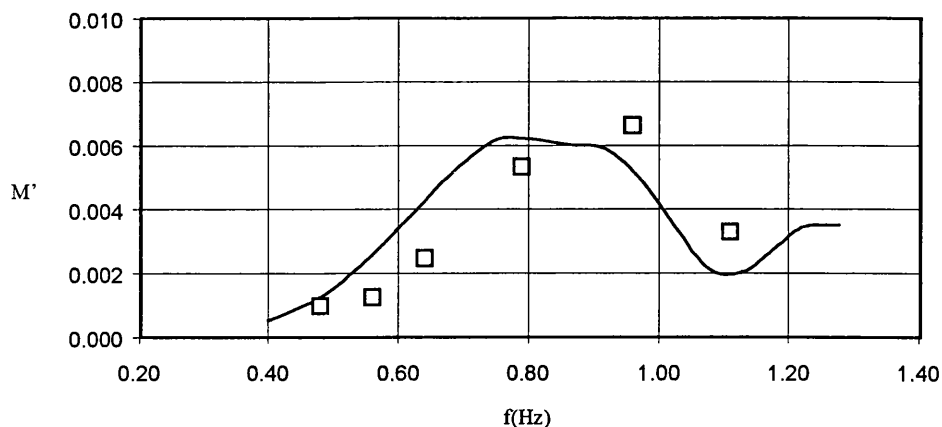


Figure 6.26 - Vertical Bending Moment at Strain Gauge 3

From figures 6.24-6.26 it can be concluded that, considering all the possible error sources due to the unknown weight distribution and the calibration of the experimental equipment, satisfactory agreement between measured and predicted values for the wave bending moments were found.

6.6 - COMBINED LOW FREQUENCY AND WHIPPING BENDING MOMENTS

In this section comparisons between the experimental results and some of the methods described in chapter 4 are reported. Due to the large number of methods considered these were divided into two distinct groups.

The first one uses the linear theory for the calculation of the wave bending moments and the empirical formulations for the calculation of the whipping stresses. Two different methods are compared in this group, one using the formulation proposed by Ochi and Motter and the other one is the combination of the Stavovy and Chuang method for calculation of the maximum slamming force and the Kawakami et al formula for evaluation of the time history of the slamming force.

The second group uses the linear theory in association with the vertical derivative of the added mass for evaluation of the slamming bending moments.

Before starting the comparison of the methods, some conclusions can be drawn from the theoretical and experimental results:

- More severe slamming occurs when the relative motion attains the maximum values and this occurs for tests 9 and 12 for $\lambda/L = 1.0$ ($f = 0.79$ Hz).
- For $\lambda/L = 1.5$ ($f = 0.64$ Hz) only a mild slamming occurs for the highest wave amplitude which corresponds to test number 11.
- For $\lambda/L = 2.0$ ($f = 0.56$ Hz) no slamming occurs.

6.6.1 - Bending Moments for $\lambda/L = 1.0$

Three experiments were made for $\lambda/L=1.0$ with different wave amplitudes. In order to check the validity of the linear theory for the ship motions and wave loads, the first test was made with small amplitudes. In the last two tests, the wave amplitude was chosen such that slamming occurs.

Figure 6.26 shows the longitudinal variation of the relative motion amplitude divided by the ship draft, obtained from the last two tests. It is understood from the figure that when this value is greater than one the bottom will emerge. From the information contained in this figure it can be seen that for the second test the slamming extension is about 20% of the ship length and for the last one it is equal to 25%. These are typical values that can be considered to represent severe slamming, Ochi and Motter (1973).

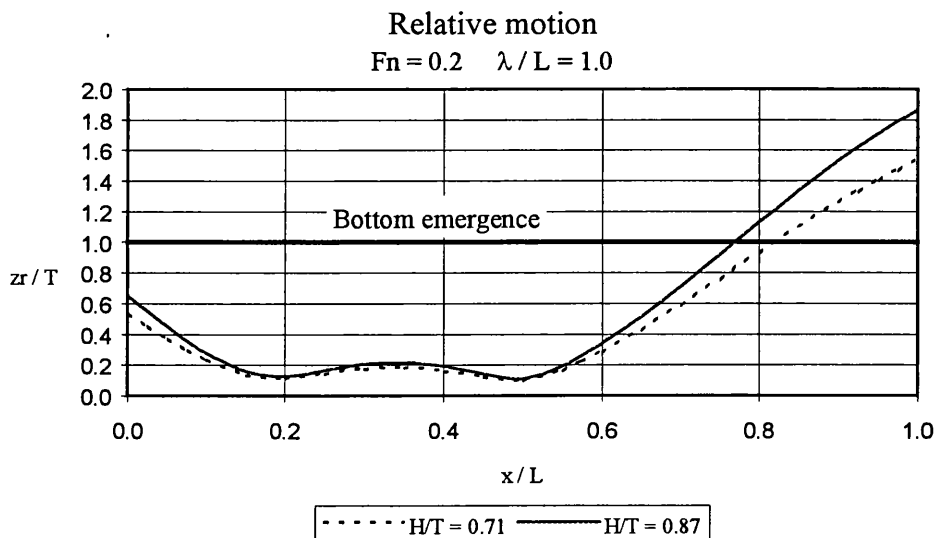


Figure 6.27 - Longitudinal variation of the relative motion for $\lambda/L = 1.0$

The calculated impact velocities for the last two runs are shown in the next figure. The velocities increased, as expected, in the forward direction and with the increase in wave amplitudes.

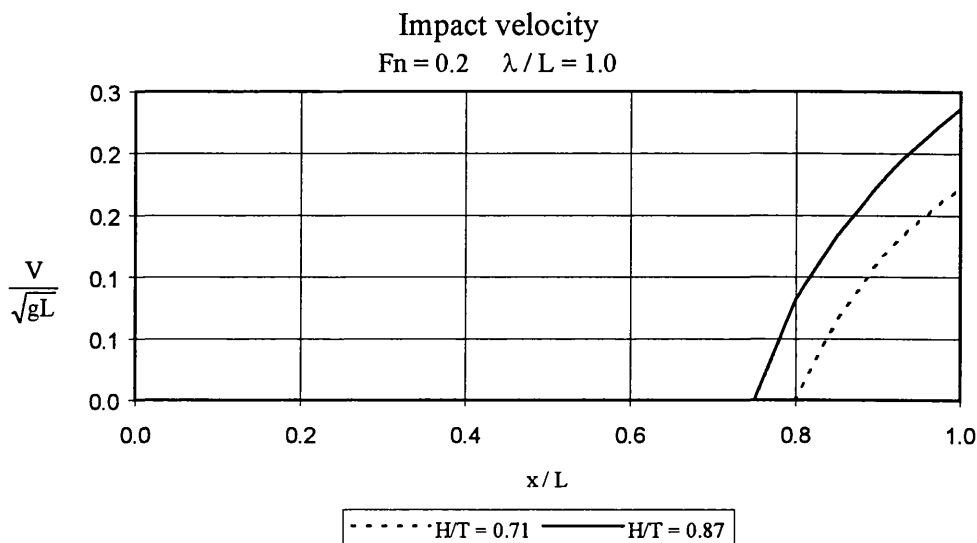


Figure 6.28 - Impact velocity for the two experiments

6.6.1.1 Linear Wave Induced VBM Combined with Empirical Methods for Slamming Loads

In this section the experimental measurements will be compared with two theoretical methods using different approaches. The first one uses the linear theory combined with the slamming methods proposed by Ochi and Motter, and the second one combines the linear theory with the slamming methods of Stavovy and Chuang and Kawakami et al.

The bending moments will be compared in the three longitudinal positions shown in Fig. 6.1. From table 6.2 it can be seen that two strain gauges were used at each section, so the bending moments represented in the next figures, denominated as strain gauges, are in fact the mean of the two strain gauges at each position as shown in table 6.8.

Denomination	Cut number (fig 6.1)	Channels
Strain gauge 1	1	1 and 2
Strain gauge 2	2	4 and 5
Strain gauge 3	3	7 and 8

Table 6.8 - Equivalent strain gauges used in the comparisons

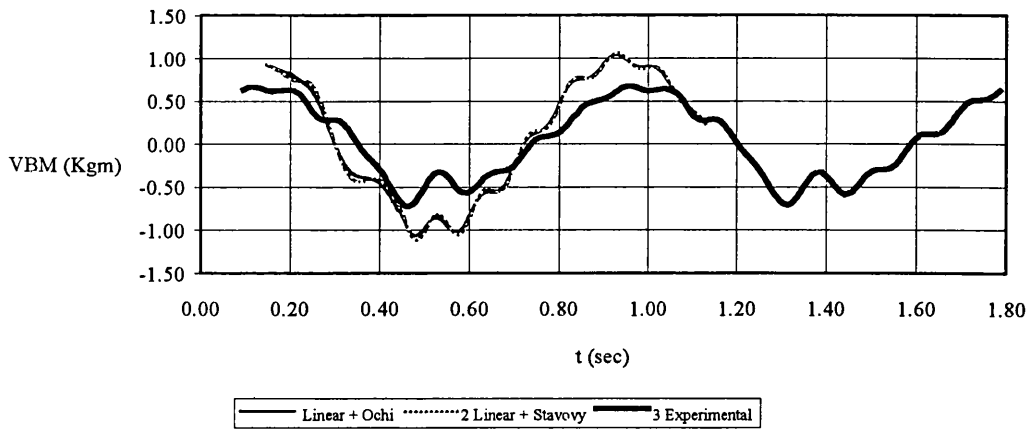


Figure 6.29 - Measured and predicted bending moments on SG 1 using empirical formulations for the whipping stresses $H/T=0.71$ $\lambda/L=1.0$

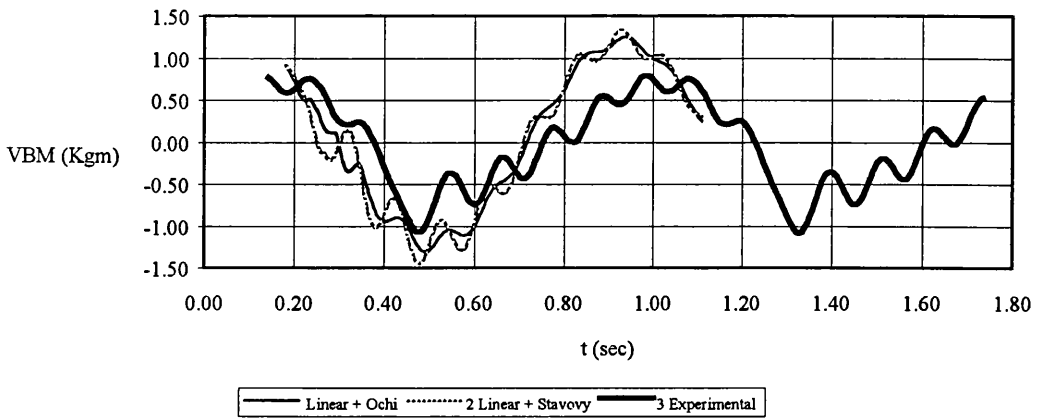


Figure 6.30 - Measured and predicted bending moments on SG 1 using empirical formulations for the whipping stresses $H/T=0.87$ $\lambda/L=1.0$

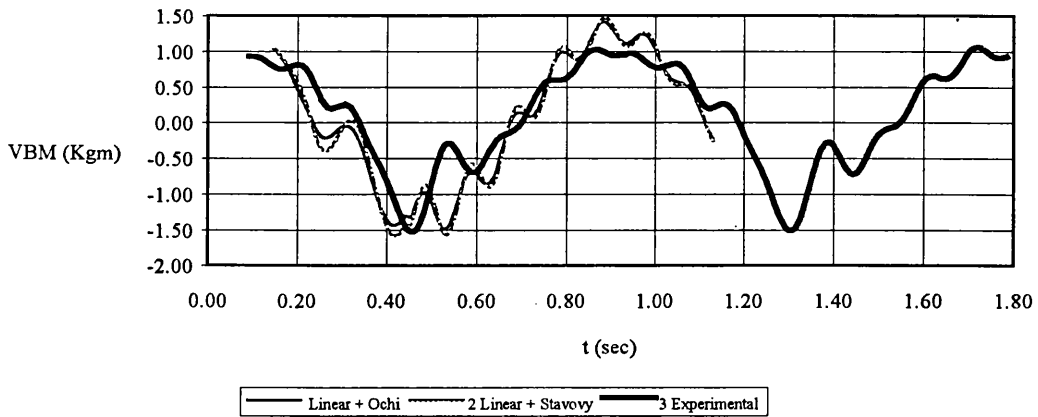


Figure 6.31 - Measured and predicted bending moments on SG 2 using empirical formulations for the whipping stresses $H/T=0.71$ $\lambda/L=1.0$

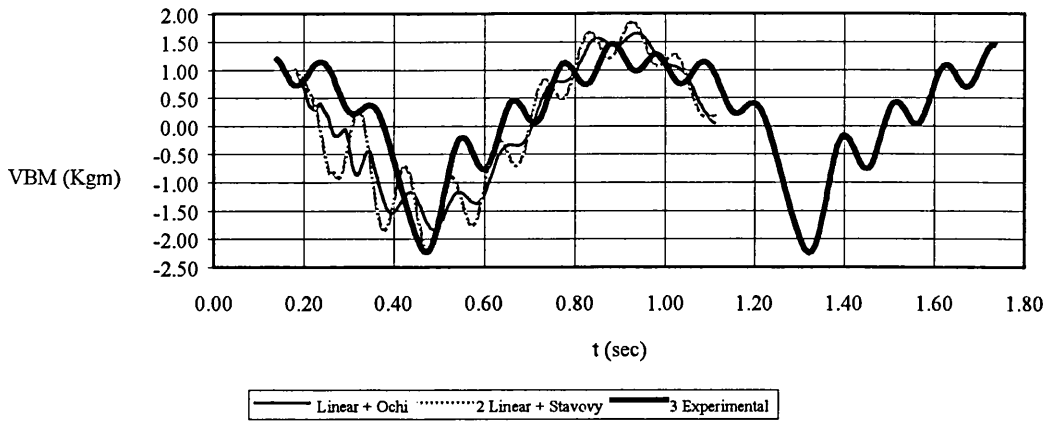


Figure 6.32 - Measured and predicted bending moments on SG 2 using empirical formulations for the whipping stresses $H/T=0.87$ $\lambda/L=1.0$

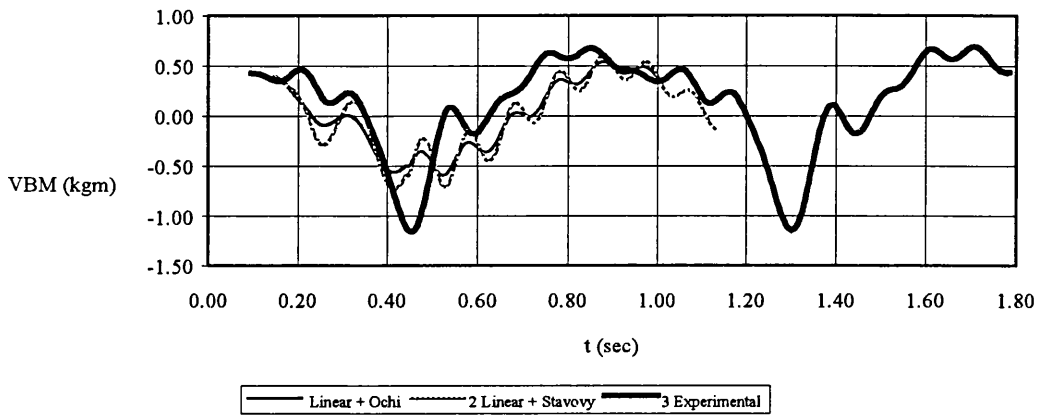


Figure 6.33 - Measured and predicted bending moments on SG 3 using empirical formulations for the whipping stresses $H/T=0.71$ $\lambda/L=1.0$

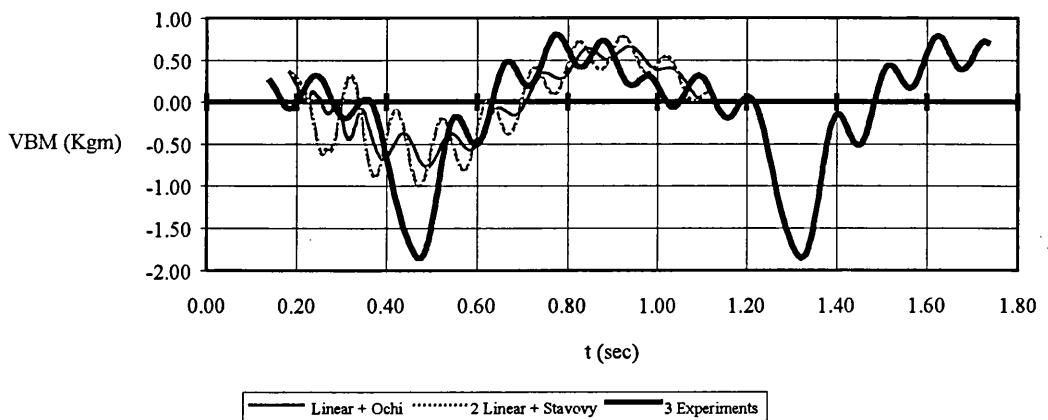


Figure 6.34 - Measured and predicted bending moments on SG 3 using empirical formulations for the whipping stresses $H/T=0.87$ $\lambda/L=1.0$

6.6.1.2 Linear Wave Induced VBM Combined with Momentum term for Slamming Loads

In chapter 4, when the slamming loads were compared, some questions related to possible simplifications of the method were kept for investigation in connection with the structural bending moment results. The first one is related to the extent of the hull domain where the impact force produces significant whipping stresses i.e. resorting to equation 4.27,

$$F(t) = \frac{dm(t)}{dt} \dot{z}_r^2$$

Knowing that this force will have a great value in the beginning of the impact and that the force will sharply decrease afterwards, the question is, how long and what is the vertical hull position where these forces will not have influence the whipping stresses. This question has a difficult answer which depends on several factors like, the impact velocities, the longitudinal extension of the bottom emergence and the natural frequencies of the ship hull. From figure 6.35 it can be found that if the slamming loads are evaluated between 0 and 0.3 T the stresses are closed to the ones if the loads are performed between 0 and 0.6 T.

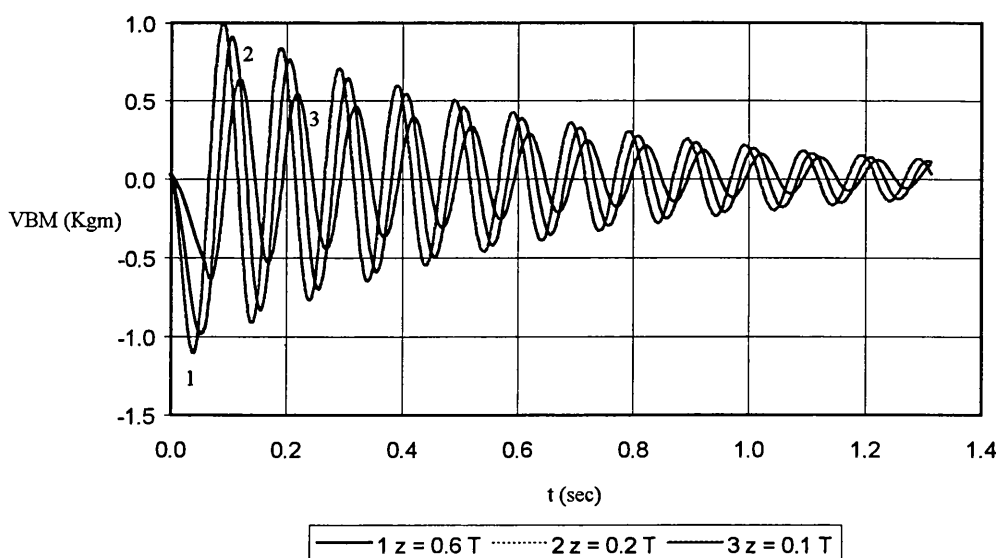


Figure 6.35 - Whipping stresses for the momentum method varying the maximum draft in which the slamming loads are taken into account $H/T=0.87$ $\lambda/L=1.0$

The other important aspect is the contribution of the whipping stresses compared with the other force components described in eqn 4.52. Figure 6.36 represents the whipping stresses calculated using only the momentum term and the other one using all the components of eqn. 4.53. From this figure one can conclude that the other components of the force will not have significant influence in determination of the whipping stresses. So the next calculations will be made using only eqn.4.27 for the determination of the slamming loads.

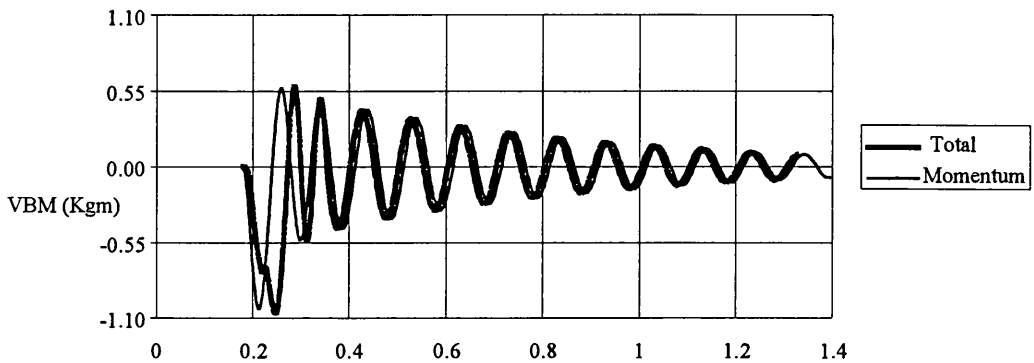


Figure 6.36 - Whipping stresses for the momentum method varying the hull domain of the slamming load $H/T=0.87$ $\lambda L=1.0$

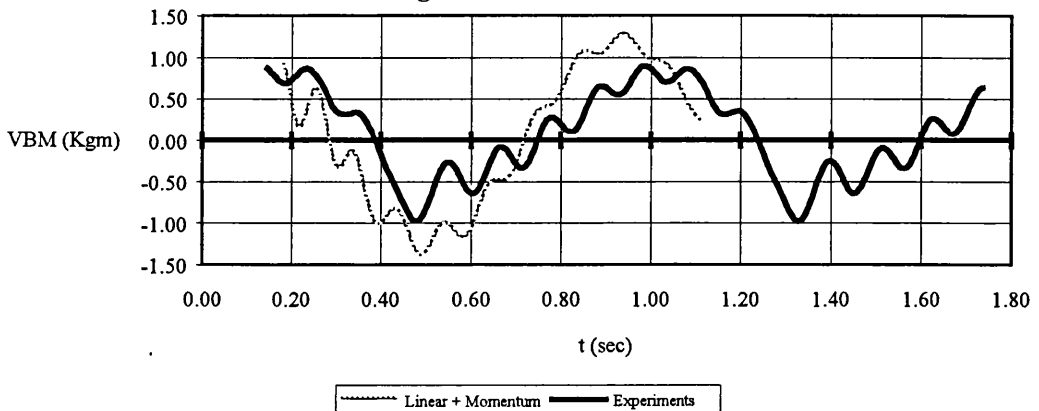


Figure 6.37 - Measured and predicted bending moments on SG 1 using the vertical derivative of added mass for the whipping stresses $H/T=0.87$ $\lambda L=1.0$

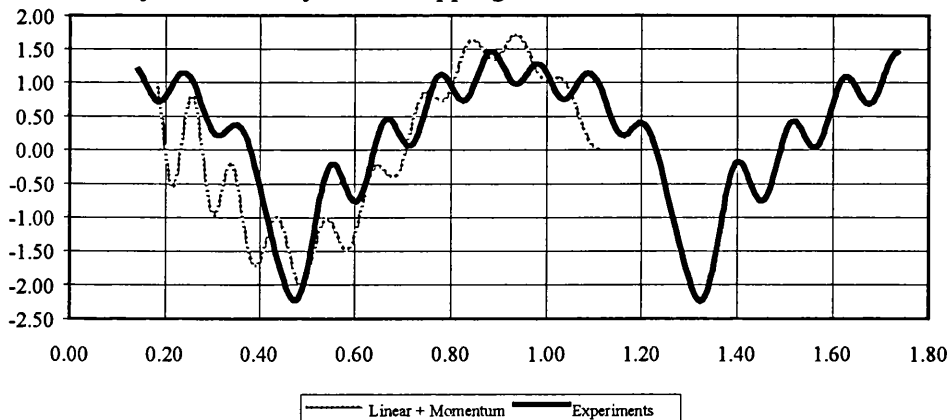


Figure 6.38 - Measured and predicted bending moments on SG 2 using the vertical derivative of added mass for the whipping stresses $H/T=0.87$ $\lambda L=1.0$

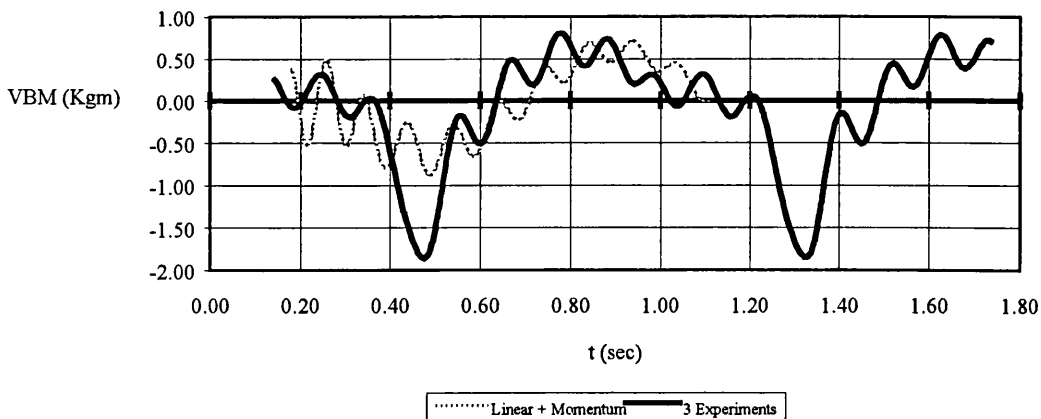


Figure 6.39 - Measured and predicted bending moments on SG 3 using the vertical derivative of added mass for the whipping stresses $H/T=0.87$ $\lambda L=1.0$

6.7 - CONCLUSIONS

One of the main assumptions of this work is that the total bending moment acting on the ship can be divided into linear low frequency and whipping components. In other words, linear strip theory is used for the calculation of the low frequency stresses and the whipping stresses are added when slamming occurs. Figs. 6.40 and 6.41 compare the measured vertical bending moments for two different wave heights, and the higher one causes non-linear bending moments. From these figures one can conclude that the strong non-linearity is related to the structural vibration, due to the slamming loads and corresponding bending moments. So this approximation from the practical point of view seems to be reasonable.

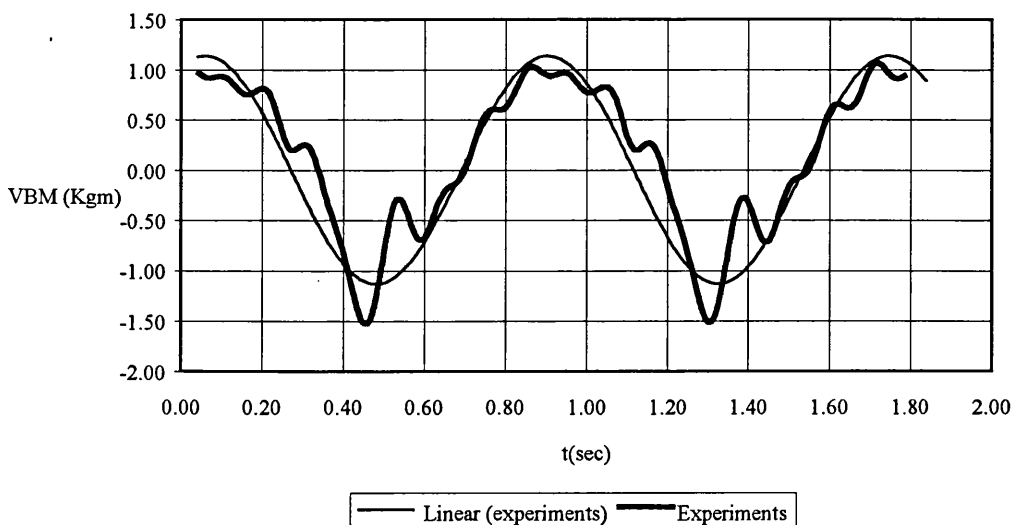


Figure 6.40 - Vertical bending moment assuming to be linear (obtained from the first experiment) and measured in the SG2, $H/T=0.71$ $\lambda L=1.0$

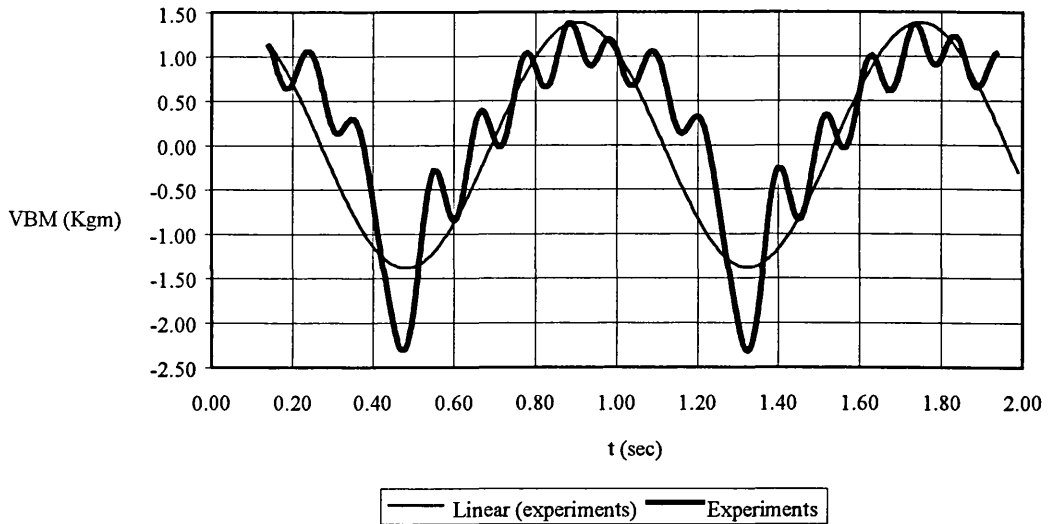


Figure 6.41 - Vertical bending moment assuming to be linear (obtained from the first experiment) and measured in the SG2, $H/T=0.87$ $\lambda L=1.0$

Figs. 6.42-6.43 show the slamming contribution K_s obtained from the experiments and the three methods. The coefficient K_s is obtained by using the following relation:

$$K_s = \frac{\text{Max}(M(t)) - \text{Min}(M(t))}{2 M_a} \quad (6.13)$$

where $M(t)$ is the bending moment time history and M_a is the amplitude of the vertical bending moment obtained using the linear theory.

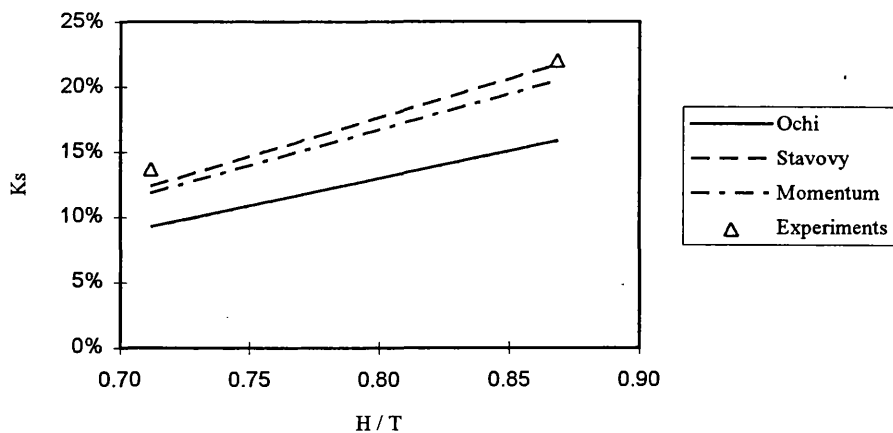


Figure 6.42 - Comparison of the coefficient K_s with the experiments and the several methods, SG1 $\lambda L=1.0$

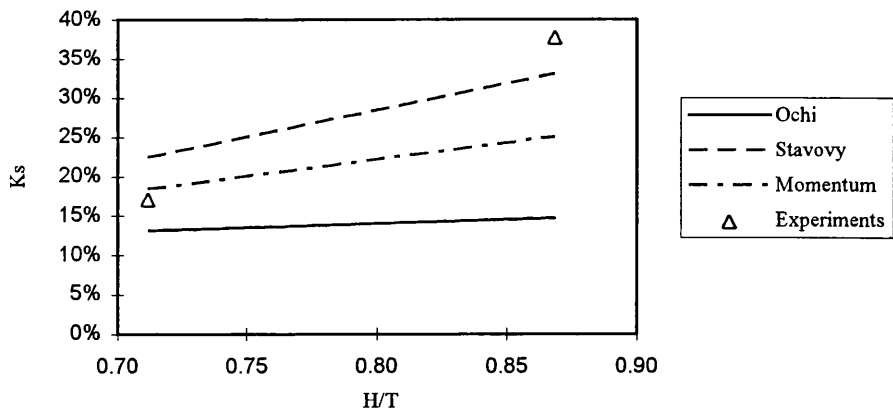


Figure 6.43 - Comparison of the coefficient K_s with the experiments and the several methods, $SG2 \lambda L=1.0$

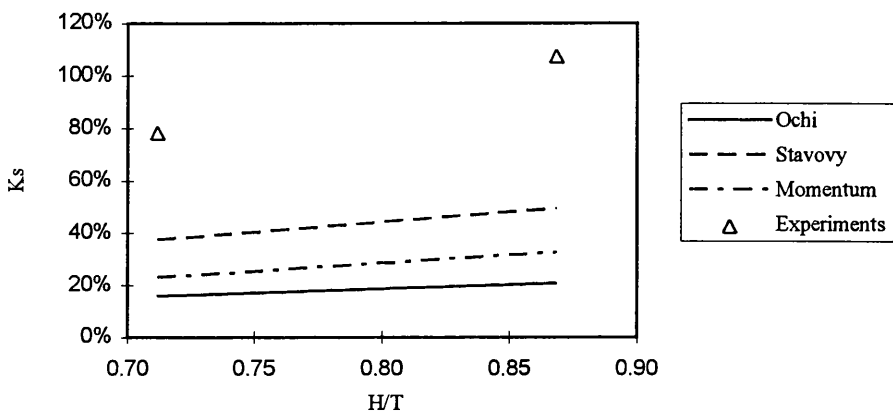


Figure 6.44 - Comparison of the coefficient K_s with the experiments and the several methods, $SG3 \lambda L=1.0$.

Good agreement was found between experiments, the Stavovy and Chuang and the momentum theory for coefficient K_s for the first two strain gauges, but the Ochi and Motter method tends to produce lower values for the coefficient. For the last strain gauge large deviations were observed between the experiments and the theories. Several factors, which are not related to the slamming loads, can produce these deviations:

- 1 - The structural model.
- 2 - The structural damping was assumed constant.
- 3 - Errors in the measurements (Strain gauges).
- 4 - Interaction between the bars used in the forward part of the model which can induce extra loads and localised the bending moments in this strain gauge due to the structural vibration of the model.

Knowing all these error sources and the relative simplicity of the theoretical model, satisfactory and encouraging results were obtained for the momentum theory and Stavovy and Chuang method combined with the Kawakami et al method for the prediction of the time history of the slamming force.

CHAPTER 7

SLAMMING IN IRREGULAR SEAS

7.1-REPRESENTATION OF AN IRREGULAR SEAWAY

The mathematical models of wave spectra are governed by one or more parameters like the significant wave height, mean period and shape factors. The most common spectra used for engineering purposes are the Pierson-Moskowitz (1964) and the Jonswap (1965) spectrum. Very often the ISSC (1964) and the ITTC (1966) parameterization of the Pierson-Moskowitz spectrum are used. Ochi and Hubble (1976) presented a more complicated spectrum with six parameters. This spectrum describes two peaks in order to account for the combined existence of swell and wind sea. Guedes Soares (1984) proposed a simpler model with only two parameters which is also able to describe two-peaked spectra. Furthermore it was shown that the additional spectral parameters are independent of H_s , Guedes Soares (1991) but some dependency exists on the mean period (Guedes Soares and Nolasco, 1992).

Most of the mathematical models of the wave spectra have the following general form:

$$S(\omega) = B \omega^{-p} e^{-C\omega^{-q}} \quad (7.1)$$

The spectral parameters change with time (eg. Guedes Soares and Ferreira 1995, 1996) and so the spectrum represents the real wave environment only for periods of 20 to 30 minutes although they are taken as representative of periods of 3 hours. The wave energy spectrum $S(\omega)$ used in this work is the Pierson Moskowitz which is defined by two characteristic parameters, the significant wave height H_s and the mean zero crossing period T_z . This spectrum fits the experimental measurements quite well for deep water and developed seas. Fig. 7.1 represents a Pierson-Moskowitz spectrum with the parametrization proposed by the ISSC, for a significant wave height of 5 m and a zero crossing period of 8 seconds.

The expression for the Pierson-Moskowitz spectrum with the proposed ISSC parametrization is:

$$S(\omega) = \frac{1}{4} H_s^2 B \omega^{-5} e^{-B \omega^{-4}} \quad (7.2)$$

$$B = 0.44 \pi^4 T_z^4 \quad (7.3)$$

where H_s represents the significant height and T_z the mean zero crossing period. These quantities are obtained using:

$$H_s = 4\sqrt{m_0} \quad (7.4)$$

$$T_z = 2\pi \sqrt{\frac{m_0}{m_2}} \quad (7.5)$$

where m_n represents the n^{th} spectral moment.

$$m_n = \int_0^{\infty} \omega^n S(\omega) d\omega \quad (7.6)$$

The zeroth moment can be obtained easily from the expression of the spectrum:

$$m_0 = 0.0625 H_s^2 e^{\frac{1}{\pi}(T_z \omega)^4} \Big|_0^{\infty} = 0.0625 H_s^2$$

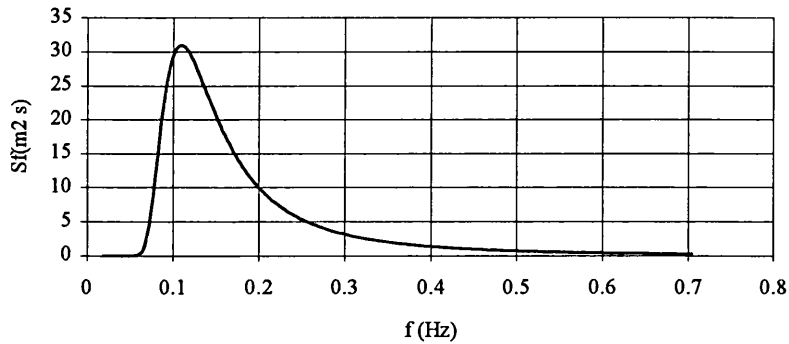


Figure 7.1 - Pierson-Moskowitz spectrum for $H_s = 5 \text{ m}$, $T_z = 8 \text{ sec}$

The wave elevation for an irregular sea state can be represented by a Fourier series using the following expression:

$$\eta(\xi, t) = \sum_{i=1}^N a_i \omega_i \cos(\omega_i t + k_i \xi + \phi_i) \quad (7.7)$$

$$k_i = \frac{2\pi}{\lambda_i} = \frac{\omega_i^2}{g} \quad (7.8)$$

where k represents the wave number and ϕ is the phase angle which is a random variable uniformly distributed in the range $(0, 2\pi)$.

In order to obtain the amplitude of each wave component the sea spectrum is divided into equally distributed intervals $\Delta\omega$ and the relation between the amplitudes of the wave components and the ordinates of the sea spectrum is:

$$a_i = \sqrt{2 S(\omega_i) \Delta\omega} \quad (7.9)$$

The vertical surface velocity and acceleration is obtained by using the following equations:

$$\frac{\partial\eta}{\partial t} = -\sum_{i=1}^N a_i \omega_i \sin(\omega_i t + k_i \xi + \phi_i) \quad (7.10)$$

$$\frac{\partial^2\eta}{\partial t^2} = -\sum_{i=1}^N a_i \omega_i^2 \cos(\omega_i t + k_i \xi + \phi_i) \quad (7.11)$$

A typical wave elevation simulation obtained for the Pierson-Moskowitz spectrum shown in Fig. 7.1 is illustrated in Fig. 7.2.

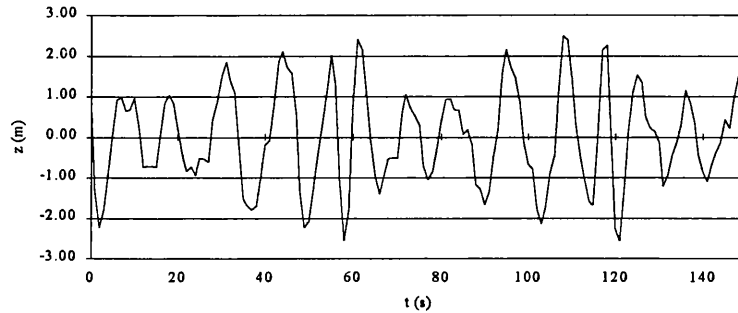


Figure 7.2 - Surface elevation simulation of a sea state with $H_s = 5$ m $T_z = 8$ sec.

The spectral width parameter ϵ is a measure of the width of the wave energy density spectrum, and its value ranges from 0 to 1. If ϵ is close to 0 the spectrum is a narrow banded and the energy is concentrated in a narrow frequency range and for values close to 1 the spectrum tends to a white noise. The spectral width is given by:

$$\epsilon^2 = 1 - \frac{m_2^2}{m_0 m_4} \quad (7.12)$$

where m_i are the moments of the spectrum.

The spectrum is considered reasonably narrow banded if the spectral width parameter is lower than 0.6. In the time domain this parameter can be obtained using the following equation:

$$\epsilon^2 = 1 - \left(\frac{T_c}{T_z}\right)^2 \quad (7.13)$$

where T_c is the crest period.

7.2 - STATISTICAL PROPERTIES OF THE SEA SURFACE ELEVATION

Consider the random variable Y_i which represents a single wave as

$$Y_i = a_i \cos(\phi_i) \quad (7.14)$$

where ϕ_i is a random variable with a uniform distribution. The probability density function of the random variable Y_i can be easily obtained:

$$\begin{cases} f(y_i) = \frac{1}{\pi \sqrt{a_i^2 - y_i^2}} & y_i^2 < a_i^2 \\ 0 & y_i^2 \geq a_i^2 \end{cases} \quad (7.15)$$

The mean value and variance for the random variable Y_i are equal to:

$$\begin{aligned} E[Y_i] &= \int_{-a}^a \frac{y_i}{\sqrt{a_i^2 - y_i^2}} dy = 0 \\ V[Y_i] &= E[Y_i^2] = \int_{-a}^a \frac{y_i^2}{\sqrt{a_i^2 - y_i^2}} dy = \frac{a_i^2}{2} \end{aligned}$$

Considering now the random variable Y as,

$$Y = \sum_{i=1}^N Y_i \quad (7.16)$$

The mean value and variance of this random variable can be obtained from the previous results

$$\begin{aligned} E[Y] &= E\left[\sum_{i=1}^N Y_i\right] = \sum_{i=1}^N E[Y_i] = 0 \\ V[Y] &= V\left[\sum_{i=1}^N Y_i\right] = E\left[\sum_{i=1}^N Y_i^2\right] = \sum_{i=1}^N E[Y_i^2] = \sum_{i=1}^N \frac{a_i^2}{2} \end{aligned}$$

Replacing the result obtained for the variance of the Y process in equation (7.9) the following equation is obtained:

$$V[Y] = \int S d\omega \quad (7.17)$$

So the variance of the wave process can be calculated directly from the wave spectrum. For the wave velocity and acceleration the same scheme can be done and similar relations between the variance of the process and the spectrum are obtained.

If \dot{Y} is the random variable that represents the wave velocity, the variance for this process is:

$$V[\dot{Y}] = V\left[\sum_{i=1}^N \dot{Y}_i\right] = E\left[\sum_{i=1}^N \dot{Y}_i^2\right] = \sum_{i=1}^N E[\dot{Y}_i^2] = \sum_{i=1}^N \frac{(\omega_i a_i)^2}{2} = \int_0^{\infty} S \omega^2 d\omega \quad (7.18)$$

Another important relation, especially for this work is the correlation between the wave elevation and the wave velocity which is obtained using the following relation,

$$\text{COV}[Y \dot{Y}] = E[Y \dot{Y}] - E[Y] E[\dot{Y}] = E[Y \dot{Y}] \quad (7.19)$$

$$\text{COV}[Y \dot{Y}] = \sum_{i=1}^N \int_{-a_i}^{a_i} \int_{-\omega_i a_i}^{\omega_i a_i} \frac{y_i}{\pi \sqrt{a_i^2 - y_i^2}} \frac{\dot{y}_i}{\pi \sqrt{(\omega_i a_i)^2 - \dot{y}_i^2}} dy_i d\dot{y}_i = 0$$

So the wave elevation and velocity are not correlated and may be considered as statistically independent. Finally using the central limit theorem: If Y_1, Y_2, \dots, Y_N are random independent variables with mean $E[Y_i] = \mu_i$ and $V[Y_i] = \sigma_i^2$ with $i = 1, 2, \dots, N$, the random variable given by $Y = Y_1 + Y_2 + \dots + Y_N$ have a Gaussian distribution with the following parameters:

$$\mu = \sum_{i=1}^N \mu_i \quad \text{and} \quad \sigma = \sqrt{\sum_{i=1}^N \sigma_i^2}$$

So the wave elevation and velocity can be considered as a Gaussian distributions.

7.3 - SLAMMING OCCURRENCE IN THE FREQUENCY AND TIME DOMAINS

For a certain sea state, and if the transfer functions for the relative motion are known, it is possible to simulate the relative motion in the time domain for an arbitrary station, to identify when slamming occurs and to calculate the impact velocity. Using this information it is also possible to evaluate the slamming impact force, and consequently the bending moments, structural displacements and shear forces. After that, short and long term statistics can be calculated if a certain number of simulations are undertaken. This approach has a big disadvantage resulting from the large CPU required time to perform all these calculations. Ochi and Motter's research, based on experimental work, concluded that slamming produces significant stresses only if the impact velocity is greater than a certain magnitude that he named as threshold velocity. He established the following expression based in the Froude scale law:

$$\dot{y}_i = 0.29 \sqrt{L} \quad (7.20)$$

Using this assumption and considering that the relative displacement and velocity are independent, Ochi and Motter proposed that the conditions for slamming occurrence are the relative motion amplitude greater than the ship draft and the relative velocity amplitude greater in absolute value than the threshold velocity.

Using these assumptions and the Rayleigh distribution to describe the amplitudes of the relative motion y , the probability of the combined event is calculated by using the following expression:

$$P(y > T, |\dot{y}| > \dot{y}_t) = P((y > T) P(|\dot{y}| > \dot{y}_t)) = e^{-\left(\frac{T^2}{2\sigma_y^2} + \frac{\dot{y}_t^2}{2\sigma_{\dot{y}}^2}\right)} \quad (7.21)$$

with

$$\sigma_y^2 = \int_0^\infty S_y d\omega \quad \sigma_{\dot{y}}^2 = \int_0^\infty \omega^2 S_y d\omega$$

where S_y is the spectrum for the relative motion. It should be noted that, according to the convention used at the previous chapters, the velocity in the impact instant is always negative.

Figure 7.3 represents the slamming probability for the Folkstra (1974) container ship and for a Pierson-Moskowitz spectrum with a significant wave height of 11m and a mean period of 10s. The solid line represents the slamming probability using eqn. (7.21) and the points were obtained for five different time simulations with a time duration of 25 min each.

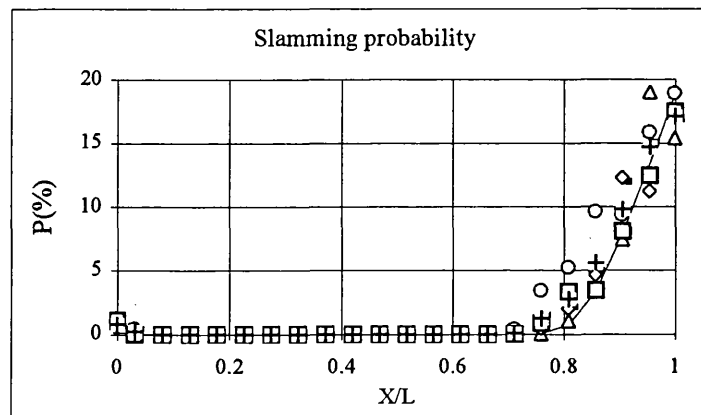


Figure 7.3 - Slamming probability(%) for $H_s=11m$ $T_z=10s$

Good agreement was observed between these two methods, and it seems that the Rayleigh distribution and the independence between the relative motion and velocity are realistic assumptions.

The next aspect is the time interval between successive impacts. Ochi's (1964) research based on full scale observations, concluded that the probability of the number impacts in a specific time period can be obtained by using the properties of the Poisson process.

$$P(X = n) = \frac{\lambda^n}{n!} e^{-\lambda} \quad (7.22)$$

where λ represents the mean number of occurrences in a period T.

This quantity is easily obtained dividing the slamming probability by the mean period of the relative motion and multiplying the time duration t_0 .

$$\lambda = \frac{t_0}{2\pi} \frac{\sigma_f}{\sigma_r} P(y > T) P(\dot{y} < \dot{y}_t) \quad (7.23)$$

Figure 7.4 shows the probability of the number of slamming impacts for the forward station and for a series of 30 simulations with a period equal to 50 seconds. The sea spectrum is the same as the one used for the calculation of the slamming probability. Good correlation is obtained between the theoretical probabilities and the ones obtained using time domain simulation.

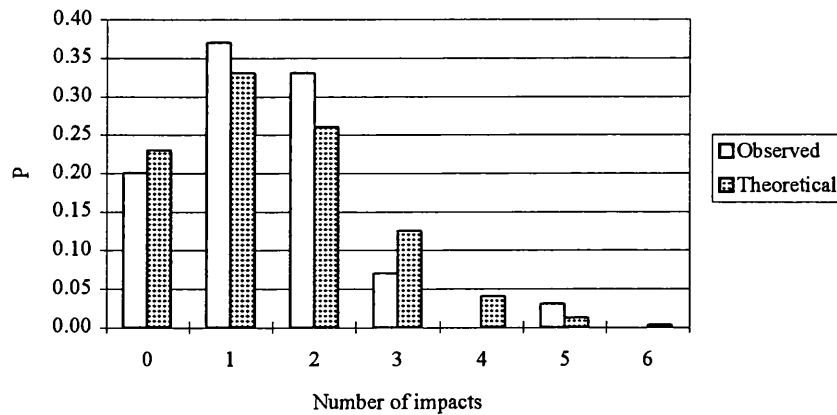


Figure 7.4 - Theoretical and observed (from time domain simulations) probability distribution of the number of impacts in time period equal to 50 seconds .

Assuming that the maximum slamming pressure is given as a function of the square of the relative velocity, the density distribution for the slamming pressure can easily be obtained if the relative velocity density distribution is known. Ochi (1973) proposed that the relative velocity has a Rayleigh distribution, so he derived the following expression for the probability distribution:

$$f(p) = \lambda_p e^{-\lambda_p(p-p_0)} \quad (7.24)$$

where p is the slamming pressure and p_0 is the threshold pressure.

The parameter λ_p is given by:

$$\lambda_p = \frac{1}{\rho k \sigma_f^2} \quad (7.25)$$

Ferro and Mansour (1985) suggested that the relative velocity does not follow the Rayleigh distribution but instead the Gaussian distribution and, consequently the slamming pressure density distribution can be described by a Chi-square distribution, with one degree of freedom:

$$\left\{ \begin{array}{ll} f(p) = \frac{1}{\sigma_y^2 \sqrt{4\pi\rho k p} \Phi\left(\frac{\dot{y}_t}{2\sigma_y}\right)} e^{-\frac{p}{\rho k \sigma_y^2}} & p \geq p_0 \\ 0 & p < p_0 \end{array} \right. \quad (7.26)$$

where Φ represents the standard normal distribution.

They also compared these two distributions with experimental measurements using an histogram, and found that for the relatively high values of pressure the differences between them are not significant when compared with the deviations obtained from the experimental data.

Using this information for the evaluation of extreme values of pressure, the exponential distribution proposed by Ochi and Motter can be used. So the extreme value in n finite number of impacts can be written using the following expression:

$$f(p_n) = n \lambda_p e^{-\lambda_p(p_n-p_0)} \left\{ 1 - e^{-\lambda_p(p_n-p_0)} \right\}^{n-1} \quad p_0 \leq p_n < \infty \quad (7.27)$$

where n must be a large number.

This expression can be rearranged in order to express the maximum predicted pressure whose probability of exceedance is lower than a certain probability value α :

$$p_n(\alpha) = p_0 - \frac{1}{\lambda_p} \ln\left\{ 1 - (1-\alpha)^{1/n} \right\} \quad (7.28)$$

After the evaluation of the maximum slamming pressure, the slamming force can also be obtained. Considering that the travelling velocity of the slamming force is equal to infinity, i.e. all stations impact the water at the same time, the whipping stresses can be evaluated for the given probability of exceedance.

The formulation proposed by Ochi and Motter is consistent if the superposition of the bending moments caused by slamming impacts can be neglected. After one impact, the time duration which the vertical bending moment can be considered to be significant depends on the structural damping. After the slamming force extinction the structural response is governed by the following equation for the free vibration of a beam:

$$x(t) = A e^{-\zeta\omega_n t} \sin(\omega_d t - \beta) \quad (7.29)$$

For practical purposes, the response can be considered as extinct if

$$e^{-\zeta_1\omega_{n1}T} = 10^{-2} \quad \text{or} \quad T = -\frac{\ln 10^{-2}}{\zeta_1\omega_{n1}} = \frac{4.605}{\zeta_1\omega_{n1}} \quad (7.30)$$

For the Flokstra container ship the period of response extinction was found to be 61s.

Using this period, the mean rate of occurrence of slamming λ can be evaluated and the probability of the number of impacts greater than one can also be calculated,

$$P(X > 1) = 1 - P(X = 1) - P(X = 0) \quad (7.31)$$

where $P(X)$ is given by eqn. (7.22).

If the value of this probability is greater than a certain criteria, than the Ochi and Motter model for the prediction of slamming stresses can not be used. Fig. 7.5 illustrates the longitudinal distribution of the probability for three different significant wave heights and for a mean period of 10 seconds.

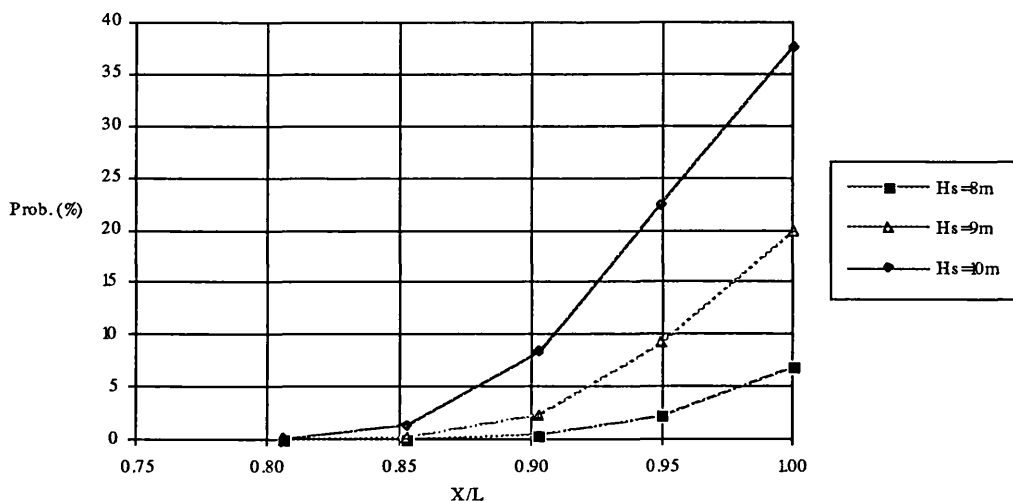


Figure 7.5 - Probability of existence more than one impact during the period where the response is assumed important.

7.4 - STRUCTURAL RESPONSE

In the previous chapter the structural response of the ship hull to slamming in regular waves was calculated using direct integration methods because the principal objective was to compare the effect of the various formulations for calculating the slamming forces. Direct integration methods are usually more time consuming when compared with convolution methods, especially if it is possible to find an analytical solution, in the CPU time to perform the response.

In this chapter the method that will be used for the evaluation of the slamming forces is the combination of the Stavovy and Chuang method for the evaluation of the maximum slamming force, with Kawakami et al method for the time history. The force developed at each impact and for each mode, can be expressed by using the equation suggested by Kawakami et al:

$$f_k(t) = F_k \frac{e^{-t/T_0}}{T_0} \quad (7.33)$$

The dynamic response of the system for the k^{th} mode can be obtained using the convolution integral given by:

$$x_k(t) = \int_0^t f_k(\tau) g_k(t-\tau) d\tau \quad (7.34)$$

where g_k is the response function to a unit impact and is given by:

$$g_k(t) \begin{cases} \frac{1}{m_k \omega_{dk}} e^{-\zeta_k \omega_{nk} t} \sin \omega_{dk} t & t \geq 0 \\ 0 & t < 0 \end{cases} \quad (7.35)$$

After solving the convolution integral, the following expression for the response is obtained:

$$x_k(t) = \frac{F_k}{m_k \omega_{dk}} \left\{ \Phi_1 \left[\frac{\Phi_2 K_1 + \Phi_3 K_2 + K_3}{K_4} \right] + \frac{\Phi_4 \Phi_5}{K_4^2} \right\} \quad (7.36)$$

where

$$\Phi_1 = 2T_0 e^{1-\zeta \omega_{nk} t} \quad \Phi_2 = \tan^2 \left(\frac{1}{2} \omega_{dk} t \right)$$

$$\Phi_3 = \tan \left(\frac{1}{2} \omega_{dk} t \right) \quad \Phi_4 = e^{1-\frac{t}{T_0}}$$

$$\Phi_5 = \zeta^2 \omega_{nk}^2 T_0^2 - 2\zeta \omega_{nk} T_0 t - 2T_0^2 \zeta \omega_{nk} + T_0 \omega_{nk}^2 t + 2T_0$$

$$K_1 = -T_0^2 \omega_{dk} \zeta \omega_{nk} + T_0 \omega_{dk}$$

$$K_2 = -\omega_{dk}^2 T_0^2 + \zeta^2 \omega_{nk}^2 T_0^2 - 2\zeta \omega_{nk} T_0 + 1$$

$$K_3 = -\omega_{dk} T_0 + \zeta \omega_{nk} T_0^2 \omega_{dk}$$

$$K_4 = \omega_{dk}^2 T_0^2 + \zeta^2 \omega_{nk}^2 T_0^2 - 2\zeta \omega_{nk} T_0 + 1$$

The expression for the response to a unit impact seems rather complicated, but the computer time required to calculate the response is approximately 1/27 the CPU time used by the direct integration method using five modes.

If the time duration of the impact forces that acts on the vessel is small when compared with the natural periods of vibration, the force time history can be reduced to an equivalent impulse. Using this simplification, the response for each mode given by this method is obtained by using the following relation:

$$x_k(t) = K_c I_0 g_k \quad (7.37)$$

where K_c is a correction factor that depends on the ratio between T_0 and the natural period T_n of the structure and I_0 is the total impulse obtained recurring to eqn. (7.33).

$$I_0 = F e T_0 \quad (7.38)$$

The coefficient K_c was obtained, for several relations of T_0/T_n , by calculating the ratio between the peak values obtained from equation (7.36) which is the exact solution and (7.37) that gives the approximate solution. The results are presented in Figure 7.6.

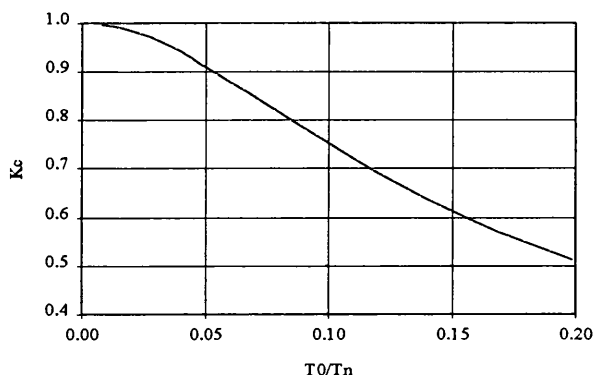


Figure 7.6 - Correction factor used for the simplified method

To determine the deviations produced by the simplified method when compared with the one that uses the exact solution, the response calculation was performed for the first three natural modes under an arbitrary force F applied the container model described in chapter 6. The coefficients used in the differential equation are the ones indicated in table 6.6. The ratio between T_0 and T_n and the corresponding correction factor is shown in table 7.1 and in figure 7.7.

T_0 / T_n	K_c
0.014	0.993
0.037	0.949
0.075	0.883

Table 7.1 - Coefficients used in the equation 7.37.

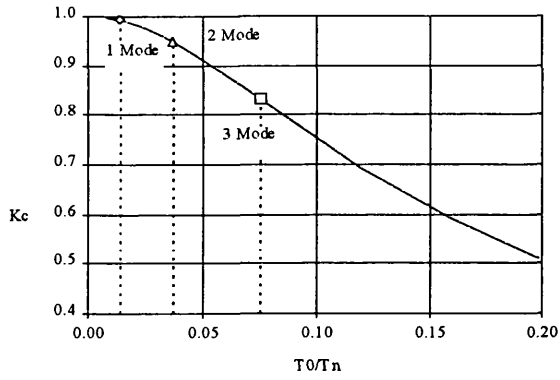


Figure 7.7 - Correction factors obtained for the container ship model

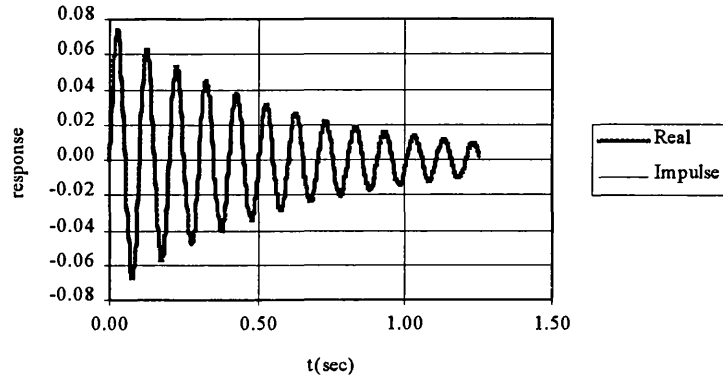


Figure 7.8 - Response using exact and approximate solutions for the 1st mode

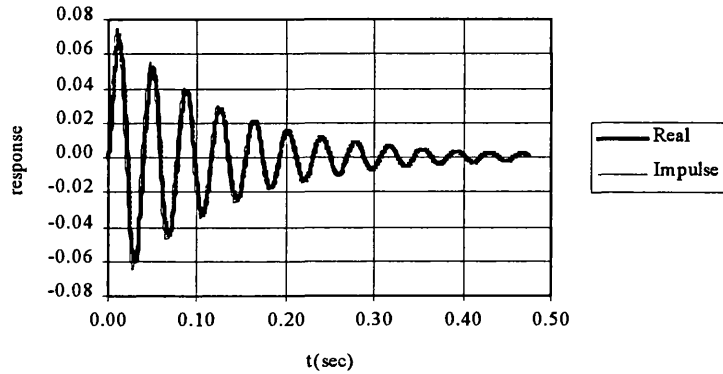


Figure 7.9 - Response using exact and approximate solutions for the 2nd mode

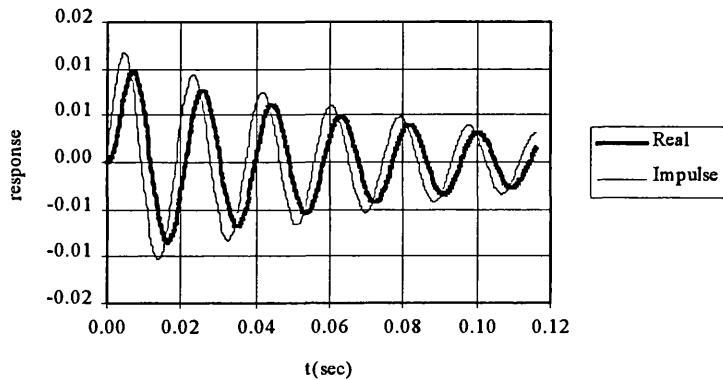


Figure 7.10 - Response using exact and approximate (without K_c correction) solutions for the 3rd mode

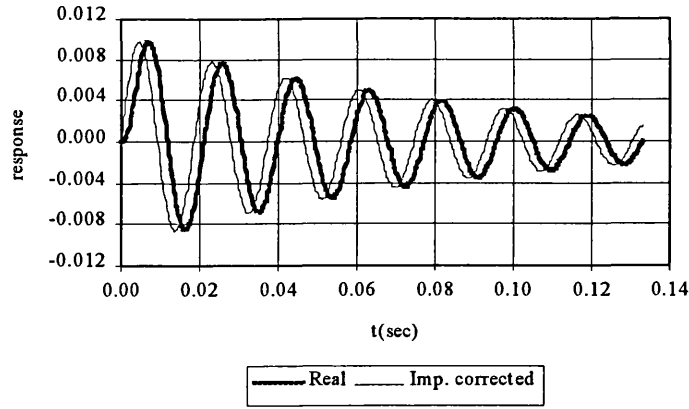


Figure 7.11 - Response using exact and approximate solutions for the 4th mode

In view of the significant reduction of computation time when the approximate method is used, and having verified that the deviations of this method as compared with the exact one are very small, it seems appropriate to use it in the time domain calculations for irregular seas. This simplification is also convenient for the statistical analysis in the frequency domain.

Using this approximation the impulse process can be written as a sequence of independent random variables I_n , according to Mansour and Lozow (1982):

$$Z(\xi, t) = \sum_{n=1}^{N(\xi, t)} I_n(\xi) \delta(t - \tau_n) \quad (7.39)$$

where ξ is the longitudinal coordinate at which the impulse load is applied. The vertical bending moment induced by these impulses is given by:

$$M(x, \xi, t) = \sum_{n=1}^{N(\xi, t)} I_n(\xi) h(x, \xi, t - \tau_n) \quad (7.40)$$

where $h(x, \xi, t)$ is the impulse response function for the vertical bending moment:

$$h(x, \xi, t) = \sum_{k=1}^{\infty} g_k(t) M_k(x) w_k(\xi) \quad (7.41)$$

where w_k and M_k are the natural shapes and natural bending moments described in chapter 5. M_k can also be obtained directly from the natural modes and frequencies:

$$M_k(x) = \omega_k^2 \int_{-L}^x (x - \xi) m(\xi) w(\xi) d\xi \quad (7.42)$$

From eqns. (7.39) and (7.41) and using the equivalent method given in eqn. (7.37), eqn. (7.40) is rewritten in the following way:

$$M(x, \xi, t) = \sum_{n=1}^{N(\xi, t)} \sum_{k=1}^{\infty} I_{nk}(\xi) g_k(t) M_k(x) w_k(\xi) \quad (7.43)$$

The equivalent impulse given by eqn. (7.37) gives an additional complexity to equation (7.43). However taking into account that the values for the correction coefficients K_c

and for the first natural frequencies are very close to one, then eqn. (7.39) can be used for describing the loading process. Using this approximation the mean value and covariance for the bending moment response process and for an arbitrary longitudinal position can be expressed, according to Lin (1967), in the general form as:

$$E[M(x, t)] = \sum_{k=1}^{\infty} M_k(x) \int_0^t g_k(t - \tau) \int_L w_k(\xi) E[Z(\xi, \tau)] d\xi d\tau \quad (7.44)$$

$$\begin{aligned} \text{COV}_{MM}(t_1, t_2, x_1, x_2) = & \sum_{j=1}^{\infty} \sum_{k=1}^{\infty} M_j(x_1) M_k(x_2) \int_{t_0}^{t_1} \int_{t_0}^{t_2} \int_L \int_L w_j(\xi_1) w_k(\xi_2) \\ & g_j(t_1 - \tau_1) g_k(t_2 - \tau_2) \rho_{ZZ}(\xi_1, \xi_2, \tau_1, \tau_2) d\xi_1 d\xi_2 d\tau_1 d\tau_2 \end{aligned} \quad (7.45)$$

The problem in these two expressions is related with the cumulant functions of the loading process. Considering a stationary number of increments $N(t)$ in eqn. (7.39), the mean value for $Z(x, t)$ is given by:

$$E[Z(\xi, t)] = \lambda(\xi) E[I(\xi)] \quad (7.46)$$

where $\lambda(\xi)$ is the number of slams per unit time for an arbitrary station which, according to Ochi (1964), can be calculated by using:

$$\lambda(\xi) = \frac{1}{2\pi} \left(\frac{\sigma_y}{\sigma_{\dot{y}}} \right) e^{-\left(\frac{T^2}{2\sigma_y^2} + \frac{\dot{y}_1^2}{2\sigma_{\dot{y}}^2} \right)} \quad (7.47)$$

According to Mansour and Lozow (1982), the mean of the process I can be obtained by using:

$$E[I(\xi)] = K_g E[P(\xi)] K_{\xi} \quad (7.48)$$

where $P(\xi)$ is given by eqns. (7.24) or (7.26) and K_g for the proposed method is given by:

$$K_g = eT_0 \quad (7.50)$$

The constant K_{ξ} represents the ratio between the maximum force and the maximum pressure for the ξ station. Replacing (7.48) in (7.46) and substituting in (7.44), the expression for the mean value of the slamming bending moment response can be written in the final form:

$$E[M(x)] = K_g \sum_{k=1}^{\infty} M_k(x) G_k \int_L w_k(\xi) \lambda(\xi) E[P(\xi)] K_{\xi} d\xi \quad (7.51)$$

where

$$G_k = \int_0^{\infty} \frac{1}{m_k \omega_{dk}} e^{-\zeta_k \omega_{dk} \tau} \sin \omega_{dk} \tau d\tau = \frac{1}{m_k \omega_{nk}} \quad (7.52)$$

Figure 7.12 shows the longitudinal distribution of the mean value of the vertical bending moment induced by slamming obtained using eqn. (7.51) and calculated directly from the time domain calculations. The calculations were made using only the first mode.

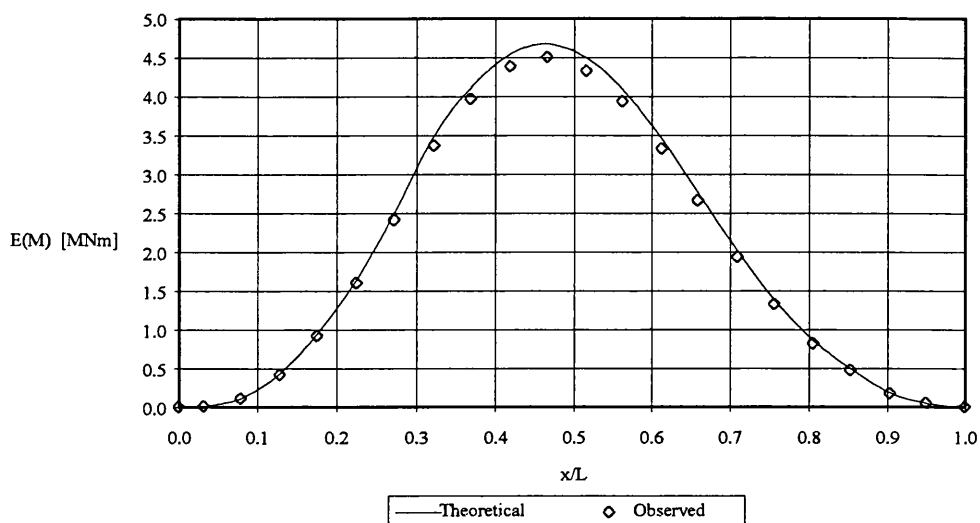


Figure 7.12 - Mean value of the whipping bending moment using one mode.

Eqn. (7.51) is also useful to find the number of modes that have significant contribution for the calculation of the whipping stresses. Fig. 7.13 shows the mean value of the vertical bending moment when varying the number of modes. From this figure it can be concluded that the contribution of the modes higher than the third one becomes small for the Flokstra container ship.

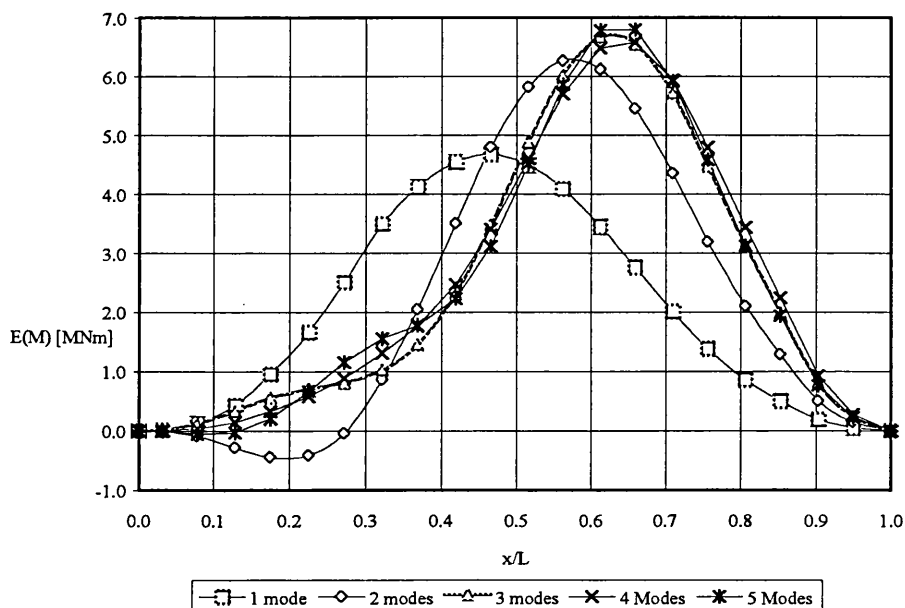


Figure 7.13 - Mean value of the whipping bending moment varying the number of modes used in eqn. 7.51.

Assuming that the slamming process is stationary and highly correlated in time and space and the natural frequencies of the structure are well separated and with light damping, than eqn. (7.45) can be simplified and the variance of the bending moment is obtained by using:

$$\sigma_{MM}^2(x) = \sum_{k=1}^{\infty} M_k^2(x) G_{2k} \left(\left[\int_L w_k(\xi) \sigma_{ZZ}(\xi) d\xi \right]^2 + \left[\int_L w_k(\xi) E [Z(\xi)] d\xi \right]^2 \right) \quad (7.53)$$

where

$$G_{2k} = \int_0^{\infty} \left(\frac{1}{m_k \omega_{dk}} e^{-\zeta_k \omega_{nk} \tau} \sin \omega_{dk} \tau \right)^2 d\tau = \frac{1}{m_k^2 \zeta_k \omega_{nk}^2} \quad (7.54)$$

Two of the main assumptions used to obtain (7.53) are related with the time and space correlation in the slamming pulse process. Kawakami et al. (1977) computed the time history for the whipping stresses using three different longitudinal travelling velocities and they found similar behaviour for the response, suggesting that the correlation in time will not generate significant deviations in the variance of the response. Fig. 7.14 shows the vertical bending moment obtained for the Flokstra container ship using three different longitudinal travelling velocities.

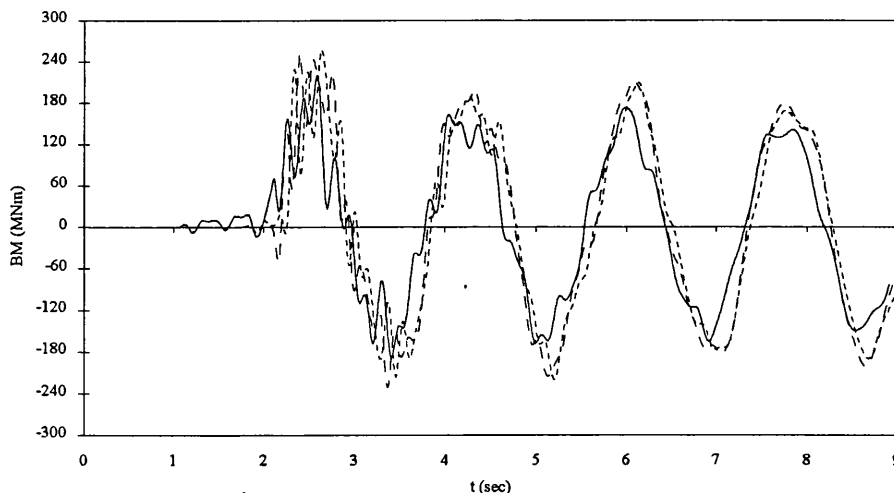


Figure 7.14 - Whipping bending moment for three different travelling velocities of pressure $H_s = 7$ m and $T_z = 10$ sec.

In order to find the spatial correlation of the impulse loads, time domain simulations for the relative motion were carried out and the impact velocities and the correlation between them were obtained. Fig.(7.15) represents the correlation between the impact velocities using a Pierson-Moskowitz spectrum with $H_s = 7$ m and $T_z = 10$ sec. Using the information contained in this figure one can say that eqn. (7.53) tends to over predict the variance of the bending moment response.

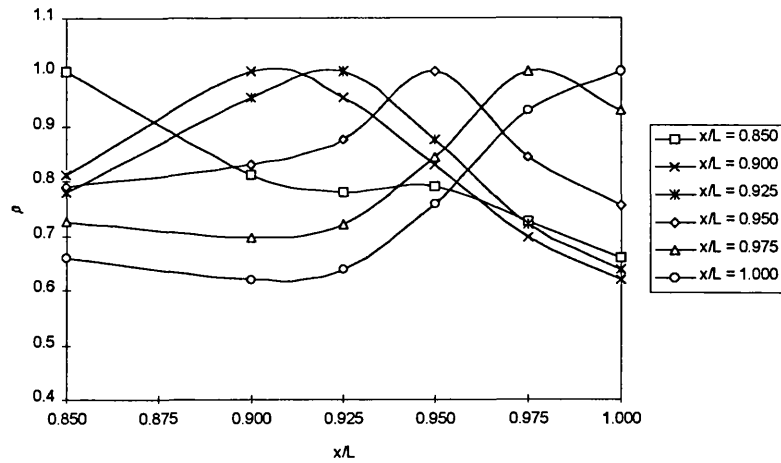


Figure 7.15 - Spatial correlation of the impact velocities for the forward stations using a Pierson-Moskowitz spectrum with $H_s = 7$ m and $T_z = 10$ sec.

Using the convolution method the structural response for the container ship was performed for head seas and for a Pierson-Moskowitz spectrum with a significant height of 8 m and a mean period of 10 s. The time duration of the simulation was equal to 25 minutes. The next figure illustrates the impact velocities obtained from one time simulation for one forward station localised at $x/L = 0.9$. Figures 7.17 and 7.18 shows the midship bending moment for two different simulations.

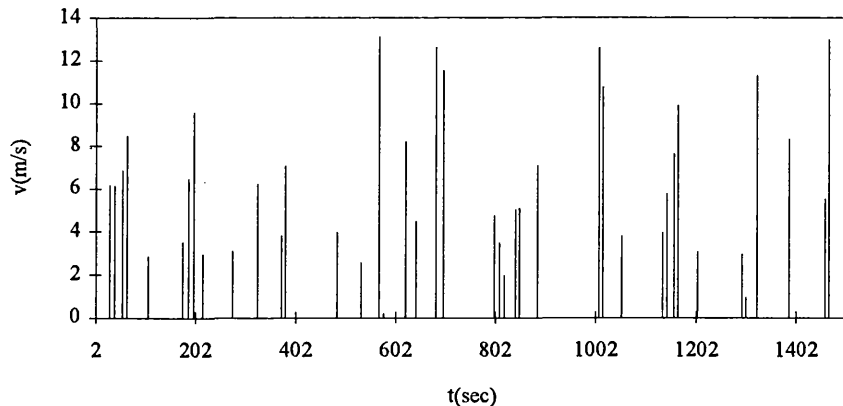


Figure 7.16 - Impact velocities for $x/L = 0.9$ using one time domain simulation.

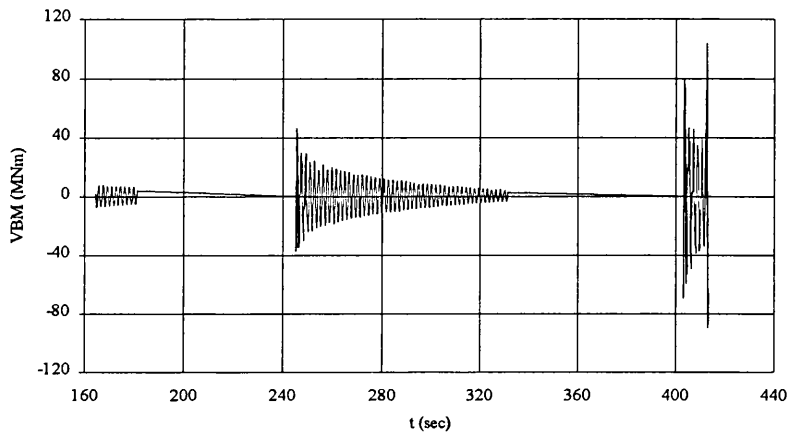
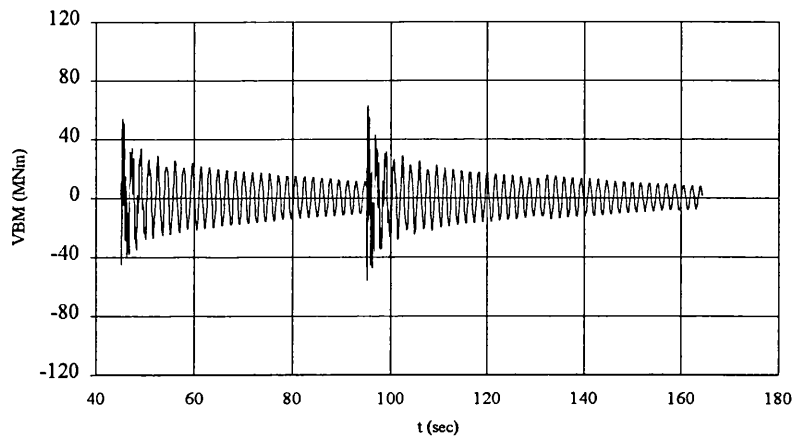
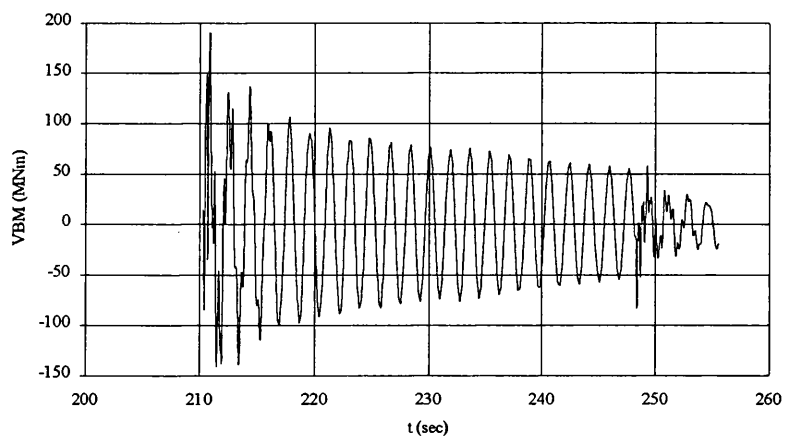


Figure 7.17 - Midship VBM. First simulation



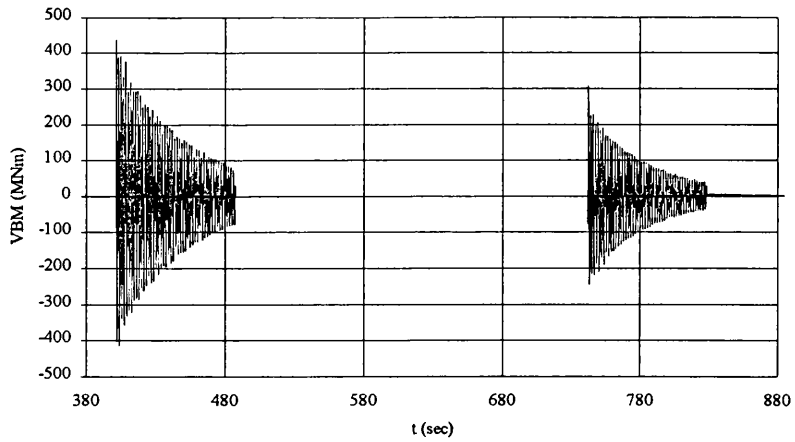


Figure 7.18 -Midship VBM. Second simulation.

If one compares the results of the two simulations it can be concluded that the maximum bending moment reached for each simulation is quite different i.e. 115 MNm for the first simulation and 435 MNm for the second one. This observation is important for the prediction of extremes. Figs 7.19 and 7.20 represent the mean value and standard deviation of the midship maximum bending moment. The convergence is slower for the standard deviation and for the first 20 simulations the oscillations for the mean value are quite significant.

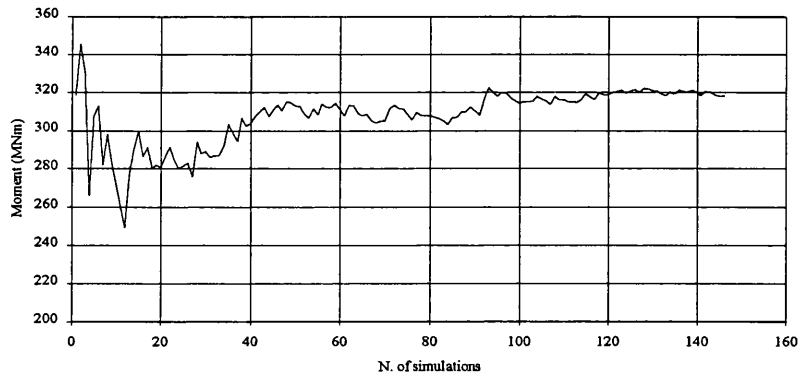


Figure 7.19 - Mean value for maximum bending moment at the midship section.

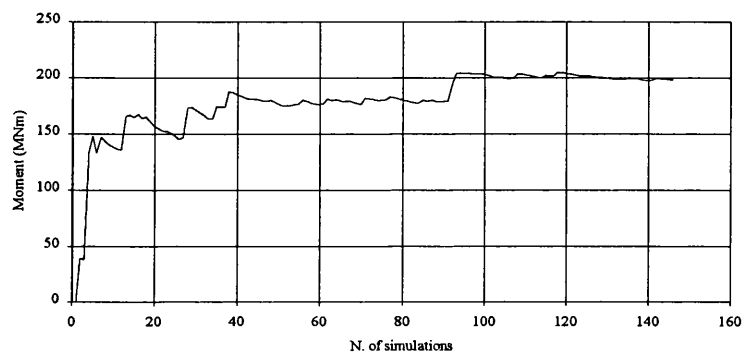


Figure 7.20- Standard deviation for maximum bending moment at the midship section.

Two different distributions will be studied for the description of the maximum bending moment. The first one is the gamma distribution and the density distribution is given by following equation:

$$f_1(x) = \frac{\alpha}{\Gamma(x)} (\alpha x)^{r-1} e^{-\alpha x} \quad (7.55)$$

where Γ is the gamma function. The r and α parameters are estimated using the mean and the variance of the sample,

$$\hat{\alpha} = \frac{E(X)}{V(X)} \quad (7.56)$$

$$\hat{r} = \frac{E^2(X)}{V(X)} \quad (7.57)$$

The gamma distribution was chosen only because the simplicity of the expressions to obtain the distribution parameters and also it is a non-symmetric distribution.

The second distribution the Gumbel which is given by following equation:

$$f_2(x) = \frac{1}{\delta} e^{-\frac{x-\lambda}{\delta}} e^{-e^{-\frac{x-\lambda}{\delta}}} \quad (7.58)$$

The parameters δ and λ are estimated using

$$\hat{\lambda} = -\hat{\delta} \log\left(\frac{1}{N} \sum_{i=1}^N e^{-\frac{x_i}{\hat{\delta}}}\right) \quad (7.59)$$

$$\hat{\delta} = E[X] - \frac{\sum_{i=1}^N x_i e^{-\frac{x_i}{\hat{\delta}}}}{\sum_{i=1}^N e^{-\frac{x_i}{\hat{\delta}}}} \quad (7.60)$$

The second equation is easily solved using the Newton-Raphson method with few iterations. Once $\hat{\delta}$ is known, $\hat{\lambda}$ is immediately computed.

The seed to start the Newton-Raphson method δ^* can be obtained using the following expression:

$$\delta^* = \sqrt{\frac{6 V[X]}{\pi^2}} \quad (7.61)$$

The observed data were sorted and compared with the theoretical distribution using the reduced variate given by:

$$\gamma' = -\ln[-\ln P] \tag{7.62}$$

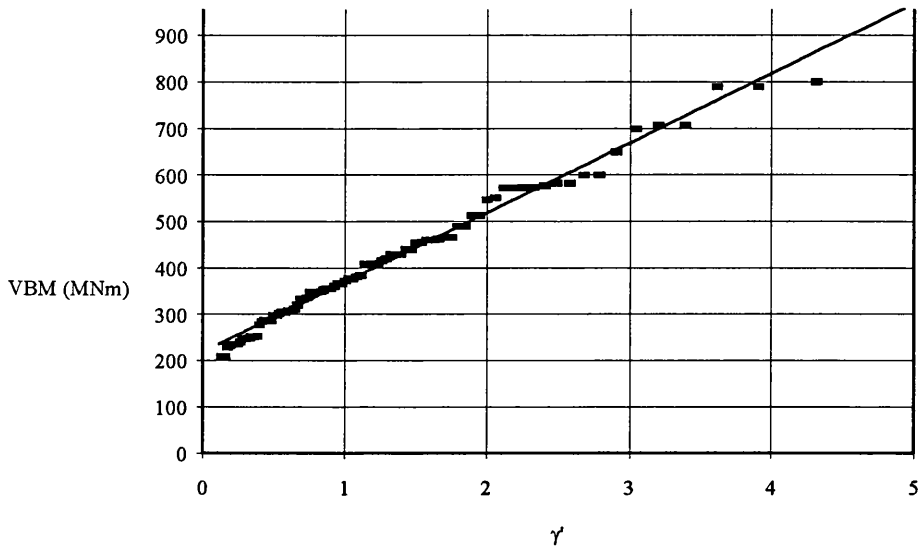
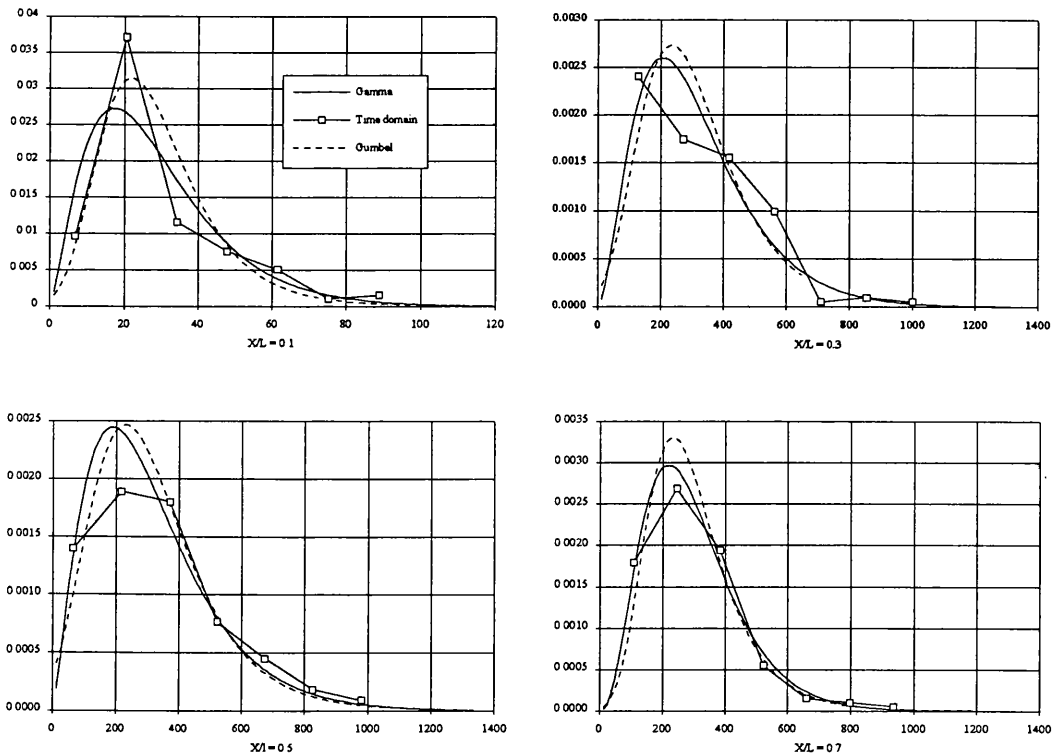


Figure 7.21 - Observed and theoretical curve fitting using the Gumbel distribution

The following figures show the histograms obtained for several ship stations and the two density distributions using 150 time simulations.



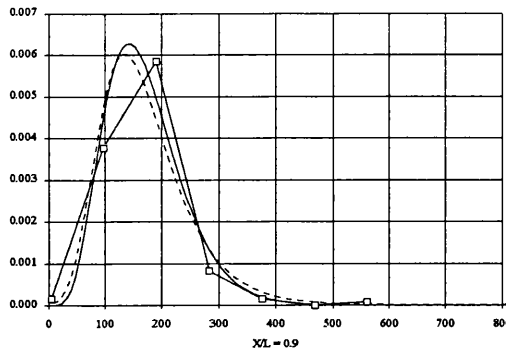


Figure 7.22 - Density functions for the maximum sagging bending moment for several ship stations

The two distributions fit the numerical results satisfactorily in all stations. Another important aspect is the convergence of the distributions with the increasing number of simulations. In practice the best distribution is the one that needs fewer time simulations to predict with a small deviation, the maximum bending moment for a certain probability.

So the density functions are obtained using 30, 60, 100 and 150 simulations and the maximum bending moment was compared with the one obtained from 150 time domain simulations. The following figures show the longitudinal variation of the maximum bending moment for the two distributions.

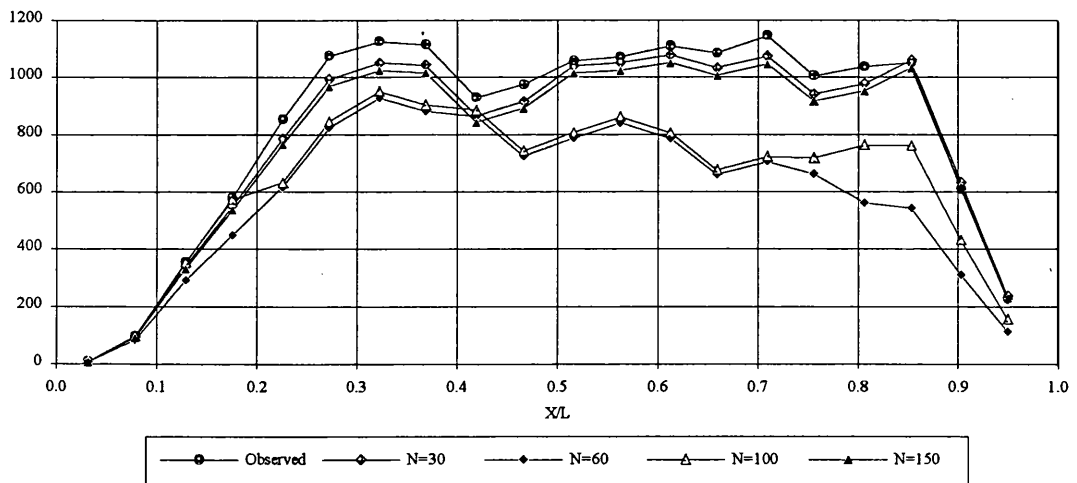


Figure 7.23 Midship maximum sagging bending moment prediction using Gamma function.

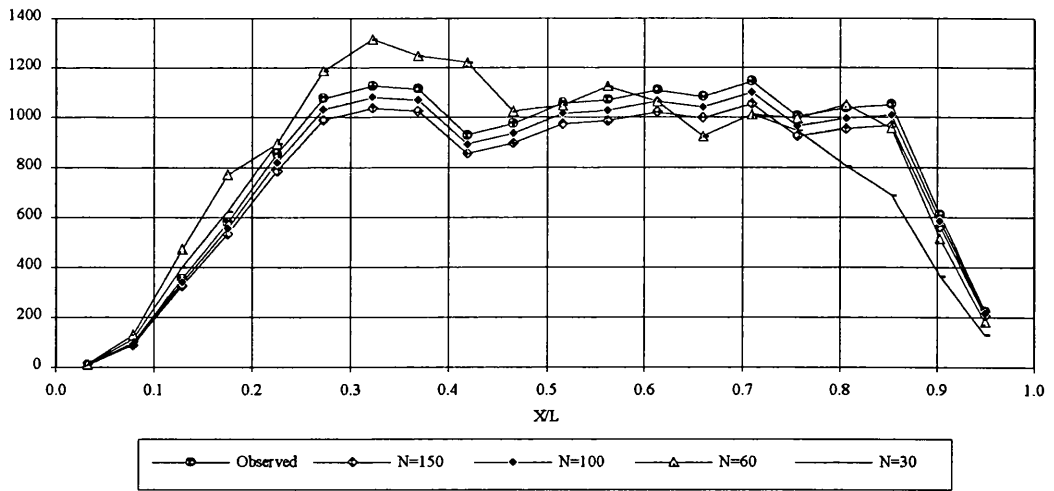


Figure 7.24 - Midship maximum sagging bending moment prediction using Gumbel function.

Looking at the Figs. 7.23 and 7.24, it can be concluded that the Gumbel distribution requires less time domain simulations to predict, with some confidence level, the observed probability. The Gumbel function is also more stable than the Gamma distribution and the convergence is faster.

Figure 7.25 represents the long term distribution of the whipping stresses for the midship position using the Gumbel distribution.

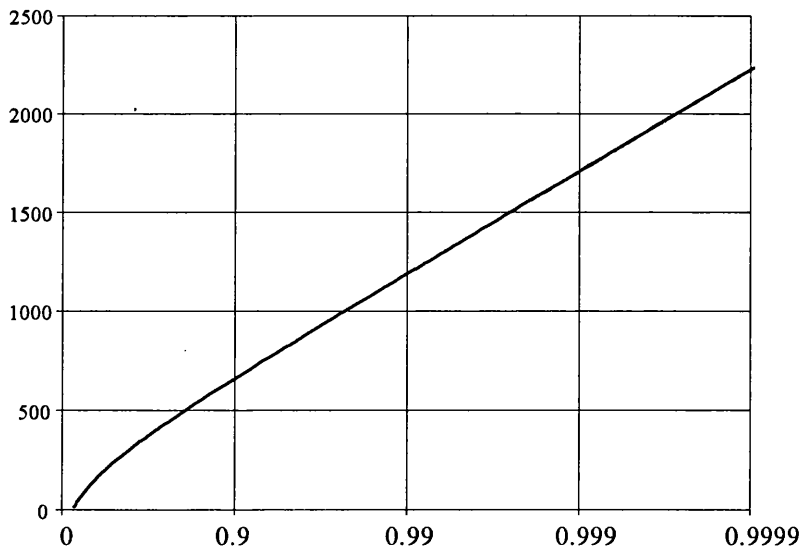


Figure 7.25 - Whipping bending moments. Probability of exceed for the midship position using the Gumbel distribution fitted by using 130 time simulations ($H_s=8$ m, $T_z=10$ s)

7.5 - SLAMMING COMBINED WITH THE WAVE INDUCED STRESSES

For the structural design it is important to know the total stresses i.e. the slamming stresses combined with the wave induced ones. The wave bending moments for the container ship adopted by Flokstra (1974) were obtained using the formulation given in chapter 3. Using the inverse Fourier transform, time domain simulations for the linear bending moment are obtained for irregular seas, and the combined loads are also evaluated. The following figures show some typical results obtained for irregular seas with $H_s = 8$ m and $T_z = 10$ s and for the container ship.

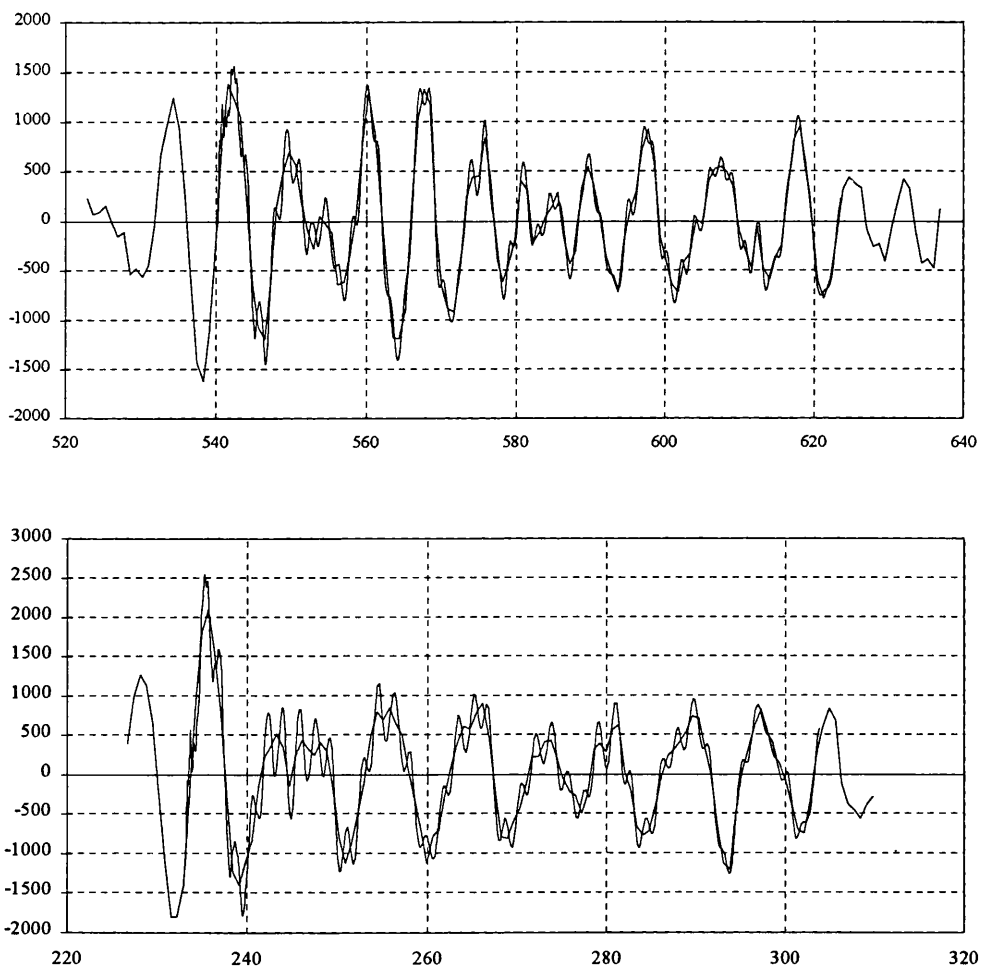


Figure 7.26 - Time simulations for the wave and combined bending moments amidships.

Performing several time simulations, the maximum wave bending moment, the whipping bending moment and the combined moment were calculated and the results were tabulated in table 7.2. Fig. 7.27 shows the results for the sagging bending moment.

Wave	Sagging		Wave	Hogging	
	Slamming	Combined		Slamming	Combined
1828	170	1821	1409	136	1465
1567	78	1578	1233	67	1241
1767	153	1813	1673	113	1744
1529	532	1567	1748	364	1786
2017	255	2050	1620	159	1602
1612	174	1603	1886	121	1933
2098	324	2167	2244	175	2301
1911	513	2211	1804	403	1730
1800	153	1843	1648	122	1658
2052	188	2121	2111	144	2183
2110	747	2553	2021	624	2058
1497	192	1584	1526	152	1574
1610	320	1737	1352	297	1564
1717	492	2070	1643	433	1729
1683	280	1710	1689	149	1713
2145	460	2187	1835	371	1964
1905	162	1898	1652	131	1733
1774	420	2081	1456	333	1648
1722	433	1733	1723	324	1719
1712	225	1776	1893	213	2000
1632	118	1652	1369	94	1376
1796	124	1791	1888	109	1924
1622	549	1943	1948	466	2011
1738	182	1753	2011	109	1993
1825	196	1830	1580	200	1550
1729	213	1802	1770	153	1771

Table 7.2 - Maximum values for the wave, whipping and combined VBM occurred for several time simulations amidships.

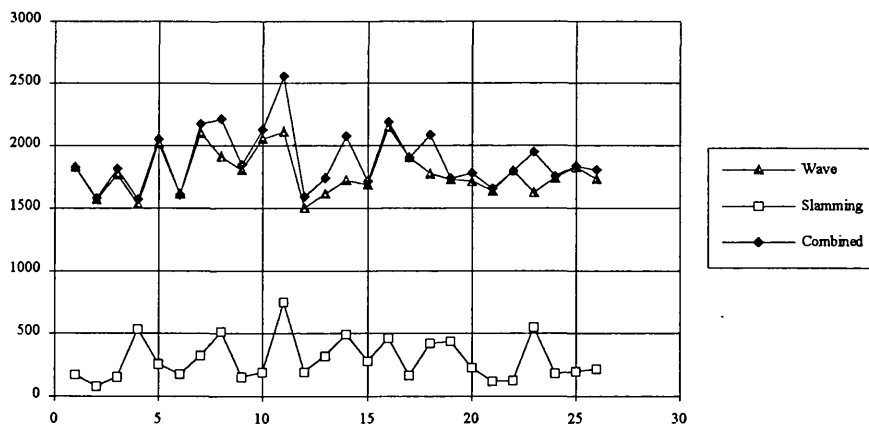


Figure 7.27 - Maximum values for the wave, whipping and combined VBM occurred for several time simulations

The maximum combined bending moment can be written in the following form:

$$M_c = M_w + K M_s \quad (7.63)$$

where M_w is the wave component M_s the slamming component and K the slamming contribution that can be varied in the range [-1,1].

All of the right term quantities are random variables. To assess the appearance of the distribution of K three histograms are obtained from the time domain results. The histograms are evaluated for three different seastates. Figures 7.28-7.30 represents the histograms obtained using 100 time domain simulations for each one.

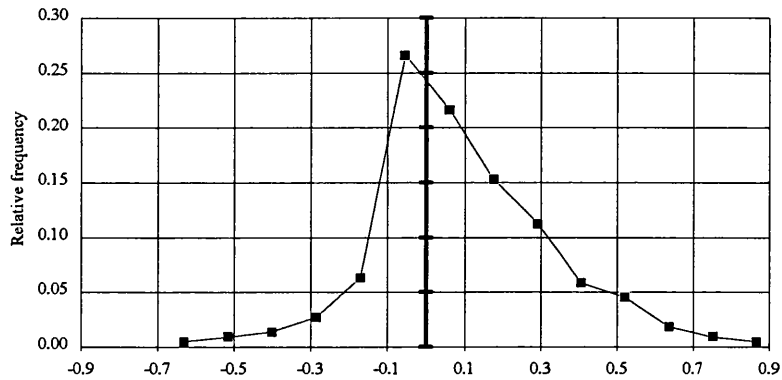


Figure 7.28 - Histogram of the slamming combination factor K ($H_s = 8$ m, $T_z = 8$ sec)

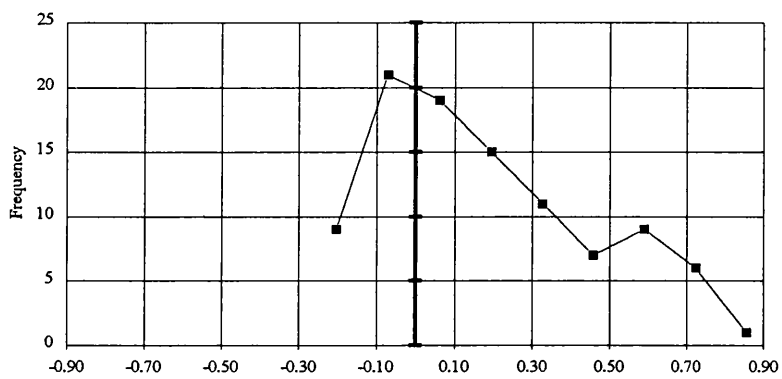


Figure 7.29 - Histogram of the slamming combination factor K ($H_s = 8$ m, $T_z = 10$ sec)

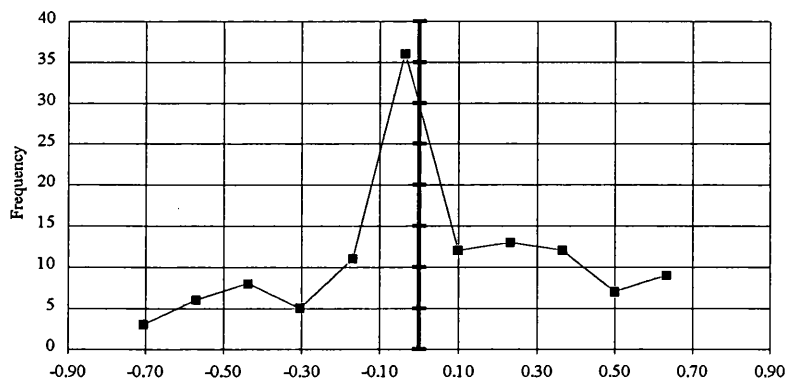


Figure 7.30 - Histogram of the slamming combination factor K ($H_s = 8$ m, $T_z = 13.2$ sec)

For the long term predictions the more important part of the distributions are the right tail of the probability functions. Using that statement, three Beta distributions truncated

between $[-1.0, 1.0]$ were fitted to the observed histograms of K_s . The parameters α , β of the proposed Beta density functions are represented in table 7.3 and the function is illustrated in Figs 7.30-7.31. This distribution was chosen because it can be easily truncated and fitted to the experimental observations by changing the two parameters.

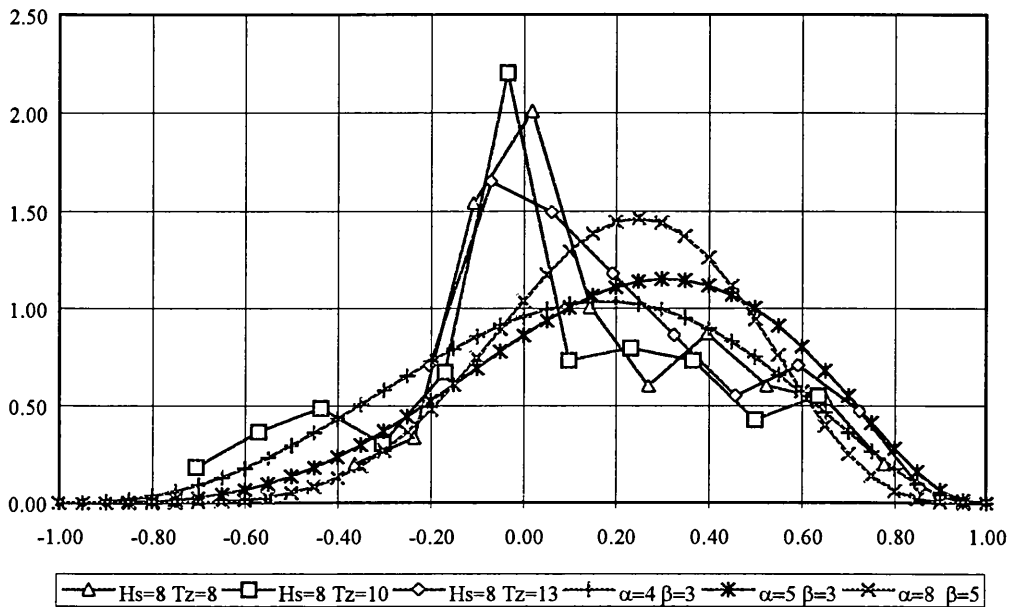


Figure 7.31 - Observed histograms and proposed distributions for K_s

α	4	5	8
β	3	3	5

Table 7.3 - Parameters proposed for the Beta function for the sagging condition

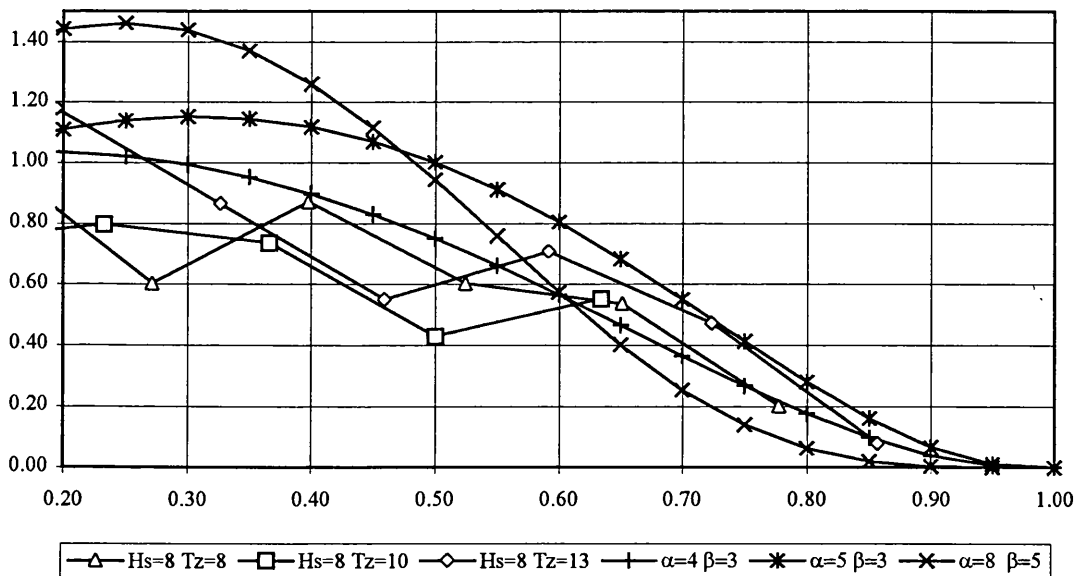


Figure 7.32 - Detail of the important region for the long term statistics of the observed histograms and proposed distribution for K_s

Another important aspect of the expression (7.63) is the correlation of the three distributions. The next two figures were obtained from the time domain simulation results for the sea spectra with a mean period of 10 seconds. The correlation coefficients are found to be very small, so the three distributions can be considered independent.

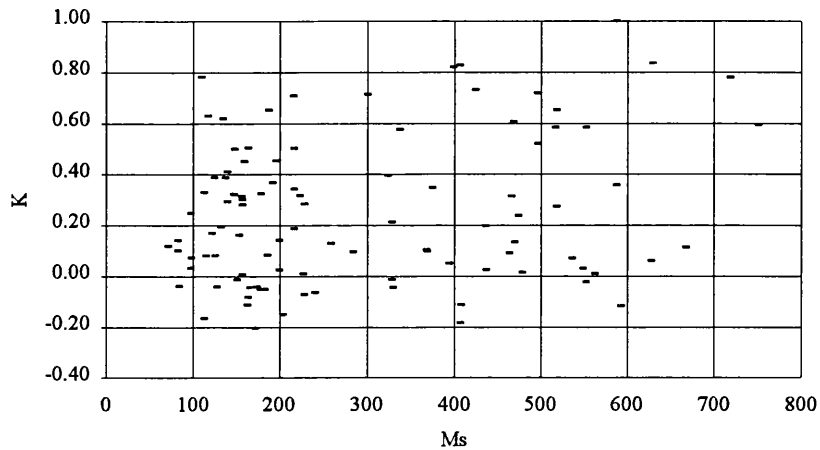


Figure 7.33 - Relation between the maximum whipping stresses and the slamming contribution factor

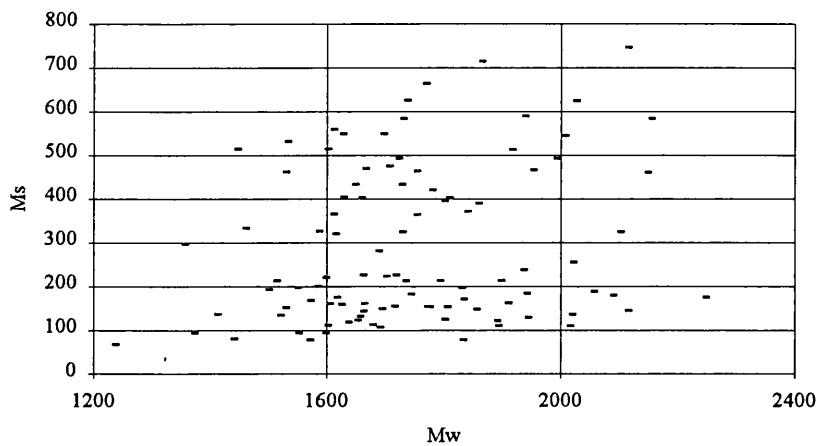


Figure 7.34 - Relation between the maximum whipping stresses and the maximum wave stresses
Assuming independence between the random variables M_s and K , and considering the following relation:

$$M_{sc} = K M_s \quad (7.64)$$

The density function of the new variable can be obtained by using the following expression:

$$p(m_{sc}) = \int_{-\infty}^{\infty} \frac{1}{k} p_{M_s} \left(\frac{m_{sc}}{k} \right) p_K(k) dk = \int_{-1}^1 \frac{1}{k} p_{M_s} \left(\frac{m_{sc}}{k} \right) p_K(k) dk \quad (7.65)$$

Figure 7.35 illustrates the distribution of M_s without the combination factor for the curve 1 and the several distributions M_{cs} obtained by using the three different proposed Beta functions to describe the slamming combination factor.

From the information contained in this figure it can be concluded that the distribution of k will reduce the contribution of the whipping stresses in the total bending moment on the order of 50% and also different distributions used to describe the K distribution will not produce significant deviations in M_{cs} . From fig. 7.35 one can conclude that using different parameters in the Beta function will not affect significantly the contribution of the whipping stresses to the total stresses.

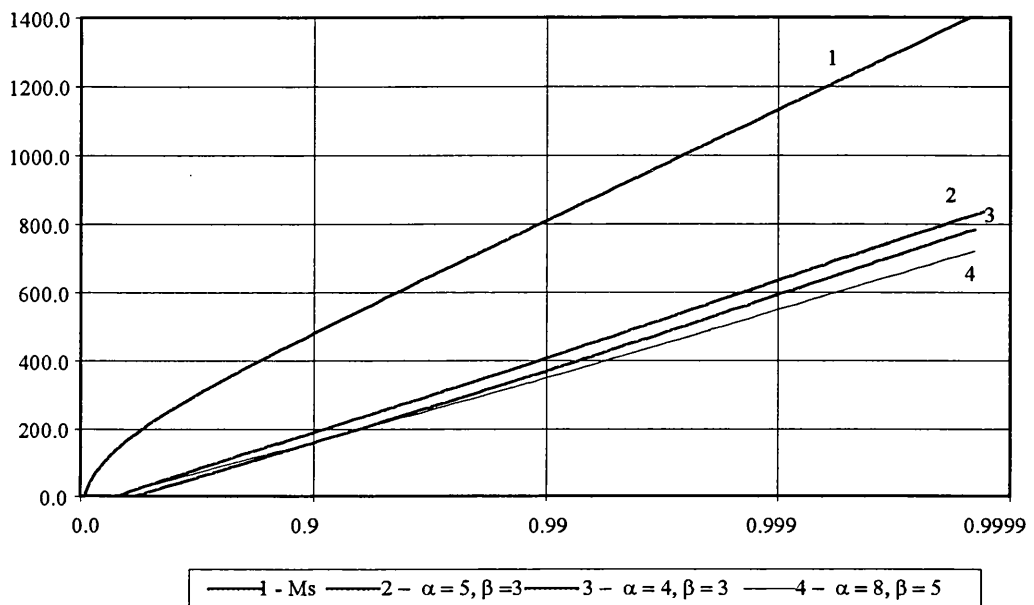


Figure 7.35 - Marginal functions for the slamming bending moment contribution (Sagging) amidships.

To see the relative contribution of the whipping stresses, equation (7.63) can be transformed into the following form using only two random variables:

$$M_c = M_w (1 + K') \quad (7.66)$$

where K' is the slamming component or the relative contribution of the whipping stresses in the combined bending moment. The figures 7.36 to 7.38 show this contribution using the same sea-states as used for the evaluation of the slamming component.

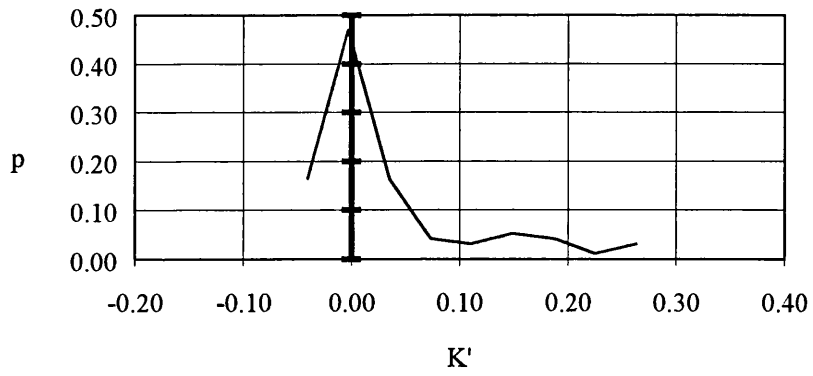


Figure 7.36 - Slamming component ($H_s = 8\text{ m}$, $T_z = 8\text{ s}$)

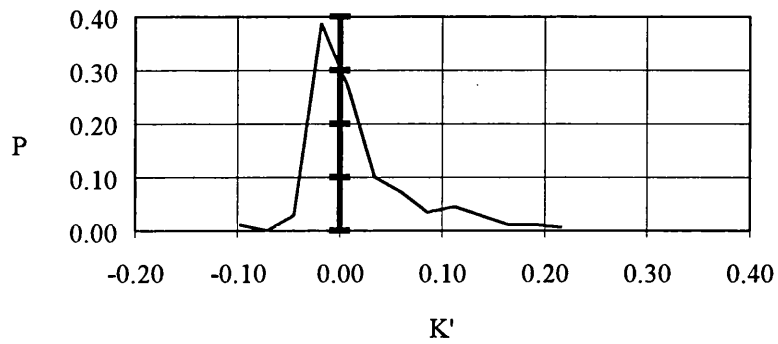


Figure 7.37 - Slamming component ($H_s = 8\text{ m}$, $T_z = 10\text{ s}$)

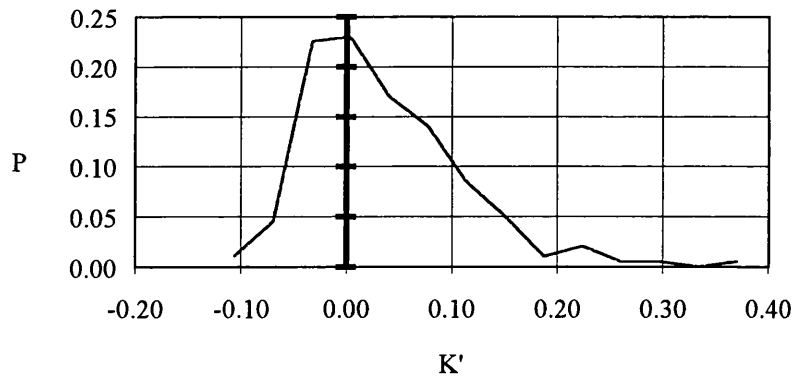


Figure 7.38 - Slamming component ($H_s = 8\text{ m}$, $T_z = 13\text{ s}$).

The K' distribution gave a more understandable information about the influence of the slamming stresses in the global stresses than the K distribution. However K is a more general distribution and it can be easily combined with other distributions for the low frequency stresses, as for example, with the one obtained from non-linear methods.

7.6 - CONCLUSIONS

In this chapter the important slamming parameters were studied for irregular seas, the whipping stresses were also combined with the low frequency stresses. Time and frequency analysis were performed for the calculation and prediction of the random variables associated with slamming. In this analysis the limitations of the methods based on the frequency domain were found and the problem of using time domain simulations were also stressed. Long term predictions based on time domain simulations were performed for the whipping bending moments.

The combined bending moment was also calculated in time domain and probabilistic distributions for the contribution of the slamming stresses in the total ones were proposed. From these results it was found that the whipping stresses can not simply added to the wave stresses.

From figures 7.36-7.38, which illustrate the final calculations, some conclusions can be drawn. The first one is that the mean period have small influence in the K' distribution, so the only dependence of this random variable is the significant wave height. The second one is the significant weight of the slamming stresses in the global stresses. The weight of this component will certainly increase with the significant wave height. Further investigations must be done in smaller vessels (between 100-150 m) where the slamming forces are even more dominant when compared with the wave and still water components. For this container ship with relative large length, the whipping stresses only have importance for high wave heights and for some cases the values are in the order of magnitude of 40% of the wave stresses.

CHAPTER 8

CONCLUSIONS

8.1 - GENERAL CONCLUSIONS

The principal aim of this research was the calculation of the global stresses induced by waves on ship hulls, and in particular the whipping stresses. To evaluate them several steps must be carried out, for which one, different approaches proposed by several authors can be used. Due to the significant differences given by the methods special attention was given to the comparison of the several theories with experimental results of a container ship in ballast condition.

One of the main assumptions of this work was to consider the total bending moment as a sum of the so called low frequency stresses calculated using linear strip theory methods with the high frequency or whipping stresses obtained from the hull structural response to slamming loads. From the comparisons with the experimental data one can conclude that, even for large wave amplitudes, this approach gives satisfactory results. It is also important to stress that from the observation of the experimental results the larger non-linear contribution in the stresses is given by the hull stresses, i.e. the whipping stresses. Good agreement was also found between the vertical motions given by the linear theory and the experiments for the different wave amplitudes.

Finally the global stresses were analysed in irregular seas based on time domain simulations and some probabilistic distributions of the global stresses were obtained. For this study the stresses were divided in two different components given by linear theory and by the whipping response and the maximum global stresses were assumed to be equal to the sum of the maximum given by low frequency and a percentage of the maximum whipping stresses modelled by a random variable. It was found that this variable can be described by a beta distribution which does not have significant variation with the sea state. From this distribution it was found that the relative contribution of the whipping stresses can be an important quantity and for some seastates about 50% of the whipping stresses should be added to the amplitude of the low frequency wave induced stresses.

8.1 - SPECIFIC CONCLUSIONS

In chapter 2 the important parameters involved with the determination of the added mass and damping coefficients were studied using the multipole expansion and mapping transformation of the section. These values were also compared with the results of the Frank close fit method. The conclusions collected from this study are:

- For the midship sections, small number of parameters are enough to obtain satisfactory results when compared with the Frank close fit method.
- For bow type sections with severe flare, great deviations in the hydrodynamic coefficients, and particularly for the damping coefficient, occurs using the Lewis transformation.
- The hydrodynamic coefficients obtained using the transformation method tend to approximate the Frank close fit method with the increase of the mapping parameters.
- The advantages of the transformation method when compared to the Frank method is the CPU time and the results confidence for high frequencies.
- Some correlation between the geometric errors and the hydrodynamic errors was found, especially for the added mass and using those results the hydrodynamic errors can be estimate by using the geometric errors.

In chapter 3 the vertical motions and loads were obtained using a linear strip theory and the hydrodynamic coefficients were obtained by using the formulation explained in chapter 2. The results for the vertical motions were obtained for a container ship and compared with experimental results. The conclusions obtained from this chapter are:

- For the heave and pitch motions, the predicted results are quite accurate when compared with experimental results.
- The variation in the number of mapping coefficients does not produce significant deviations in the transfer functions especially for the heave motion.

- Significant deviations were observed in the relative motion between the Lewis method the one that uses 9 parameters in the mapping transformation. This means that the relative motion transfer function is more sensitive to small variations in the hydrodynamic coefficients than the heave and pitch transfer functions, because to evaluate this function the phase between the motions and the wave is also taken into account.

In chapter 4 the important parameters related to the slamming pressures and loads were studied and the several formulations to predict them were compared. The maximum slamming pressure and force were compared for the several methods using wedge geometry with varying the deadrise angle. Two of the methods are empirical and based on experiments and the other formulations are analytical. The results for the maximum slamming pressure and force are the following ones:

- Large deviations exist between results of the methods and the higher results were obtained for analytical methods, particularly for small deadrise angles.
- Ochi method gives the lower results for the maximum slamming pressure for all deadrise angles.
- For the calculation of the maximum slamming force similar results were obtained for the Stavovy, momentum and Wagner methods.
- The Ochi's method, as for the maximum slamming pressure, produce the smaller results.

The impulse obtained by using the several methods were compared in three sections assuming constant impact velocity and in regular waves. Two different constant impact velocities were chosen for the first study and the following results were found:

- Different behaviour in the impulse functions were observed between the empirical and the analytical methods.
- The first group of methods assumed that the time history of the impact force depends on the Froude number and second one that the time history of the impact loads is dependent of the impact velocity and section shape.

- The impulse function for regular waves tends to give higher results than one which assume constant impact velocity.

In chapter 5 the finite element using Timoshenko's beam formulation, the modal analysis and direct integration methods to perform the structural response in time domain were described.

A small study to check the numerical methods when compared with the theoretical ones, were performed for a uniform Bernoulli's beam and the following conclusions were achieved:

- For the calculation of the natural frequencies and modes, the finite element method produces accurate results and this result doesn't depend on the number of elements used in the model.
- Different behaviour was found in the vertical shear forces and bending moments. For this quantities it was found that for the first 4 structural modes if the beam is divided using at least 20 elements quite satisfactory results were obtained.

Experimental work was carried out in the Hydrodynamics Laboratory of the University of Glasgow in a segmented model of a container ship and the summary of the measurement results is summarised in chapter 6. In this chapter the experimental results were also compared with the theoretical ones. The overall conclusions attained from this chapter are:

- The linear strip theory used for the determination of the ship motions agrees in a very satisfactory way with the experimental results for all the wave frequencies and for the different wave heights.
- Good agreement were also found for the vertical bending moment for small waves by using the linear theory.
- From the experimental results it can be concluded that the assumption that divided the total bending moment into two different components named as

linear and whipping, seems to be a reasonable approximation from the practical point of view.

- Good agreement was found between the experiments and the Stavovy and momentum theory for the coefficient K_s for the first two strain gages, but for the Ochi method some deviation appears and this method tend to produce lower values for the coefficient.
- For the last strain gage large deviations were observed between the experiments and the theories. Several factors, which are not related to the slamming loads can produce these deviations like the structural damping which was assumed constant, possible errors in the measurements and the interaction between the bars used in the forward part of the model which can induce extra loads and localised the bending moments in this strain gage due to the structural vibration of the model.

In chapter 7 the time and frequency domain analysis were performed in irregular seas for the wave, ship motions, slamming loads and whipping stresses and finally the combined bending moment. Some of the statistics for the slamming process were obtained and compared in time and frequency domain and good correlation were found for all of them.

The general conclusions obtained in this chapter are:

- Good correlation were found in the prediction of the statistics of slamming occurrence for time and frequency domain analyses.
- For the method used in the prediction in the slamming loads, these loads can be defined with a single impulse without significant deviations for the first structural modes and for the model used in chapter 6.
- The slamming stresses can have significant importance in the global primary stresses.
- The relative contribution of the whipping stresses in the global stresses is very important factor and the two magnitudes can not be simply added.

8.2 - RECOMMENDATIONS FOR FUTURE WORK

In the future work there several aspects that can be improved and developed. Some of those are:

- In the determination of the low frequency bending moments some other methods can be used in order to take into account the non-linearity of certain coefficients used in the linear theory.
- It is recommended to do more experimental work on the measurement of motions and stresses for severe regular and irregular waves in order to get more information for the validation of the theoretical methods.
- It is also important to do more research on the slamming in irregular seas in order to find new probabilistic methods based on the frequency domain calculations that can be taken into account the non-linear part of slamming and also the combination factors between low and high frequency stresses.

REFERENCES

Aertssen, G., (1968), "Laboring of Ships in Rough Seas with Special Emphasis on the Fast Ship", *SNAME Diamond Jubilee International Meeting*, June, pp. 18-21.

Aertssen, G., (1972), "Service Performance and Seakeeping Trials on a Large Container Ship", *Transactions RINA*, Vol. 108.

Aksu, S., Price, W.G., Temarel, P. (1991) "A Comparison of Two-Dimensional and Three Dimensional Hydroelasticity Theories Including the Effect of Slamming", *Proc. Instn. Mech. Engrs.*, Vol. 205, pp. 3-15.

Aksu, S., Price, W.G., Temarel, P. (1993) "A Comparative Study of the Dynamic Behaviour of a Fast Patrol Boat in Rough Seas", *Marine Structures*, Vol. 6, pp. 421-441.

Armand, J. L., Orsero, P., (1979), "A Method for Evaluating the Hydrodynamic Added Mass in Ship Hull Vibration", *Transactions SNAME*, Vol.87.

Belik, O., Bishop, R.E.D., Price, W.G. (1983), "A Simulation of Ship Responses due to slamming in irregular Head Waves", *Transactions RINA*, Vol. 125, pp. 237-253.

Belik, O., Bishop, R.E.D., Price, W.G. (1988), "Influence of Bottom and Flare Slamming on Structural Responses", *Transactions RINA*, Vol. 130, pp. 325-337.

Belik, O., Price, W.G., (1982), "Comparison of Slamming Theories in the Time Simulation of Ship Responses in Irregular Waves", *International Shipbuilding Progress*, Vol 29, pp. 173-187.

Bishop, R.E.D., Price, W.G. (1979), *Hydroelasticity of Ships*, Cambridge University Press.

Bishop, R.E.D., Price, W.G., Tam, P.K.Y. (1978), "Hydrodynamic Coefficients of Some Heaving Cylinders of Arbitrary Shape", *International Journal for Numerical Methods in Engineering*, Vol. 13, pp. 17-33.

Bishop, R.E.D., Price, W.G., Tam, P.K.Y. (1978), "The representation of Hull Sections and its Effects on Estimated Hydrodynamic Actions and Wave Responses", *Transactions RINA*, Vol. 121, pp. 115-126.

Bishop, R.E.D., Price, W.G., Tam, P.K.Y. (1980), "On the Dynamics of Slamming", *Transactions RINA*, Vol. 122, pp. 349-365.

Bishop, R.E.D., Price, W.G., Temarel, P. (1985), "A Hypothesis concerning the disastrous failure of the Onomichi-Maru", *Transactions RINA*, pp. 169-186.

Bishop, R.E.D., Price, W.G., Temarel, P. (1986), "On the Hydroelastic Response of a Swath to Regular Oblique Waves", *Advances in Marine Structures*, Elsevier Applied Science Publishers, pp. 89-110.

Chen, Y. H. (1980), "Ship Vibration in Random Seas", *Journal of Ship Research*, Vol. 24, pp. 156-169.

Chuang, S. L., (1966), "Slamming of Rigid Wedge-Shaped Bodies with Various Deadrise Angles", *DTMB Report 2268*.

Chuang, S. L., (1967), "Ship Slamming: Hydrodynamic Impact Between Waves and Ship Bottom Forward", *Fluid Solid Interaction Symposium, ASME*.

Chuang, S. L., (1973), "Slamming tests of Three-Dimensional Models in Calm Water and Waves", *NSRDC Report 4095*.

Daidola, C. (1984), "Natural Vibrations of Beams in a Fluid with Applications to Ships and Other Marine Structures", *Transactions SNAME*, Vol. 92, pp. 331-351.

Dobrovol'skaya, Z.N. (1969), "On Some Problems of Similarity Flow of Fluid with Free-Surface", *J. of Fluid Mech.*, Vol. 36, pp. 805-829.

Faltinsen, O.M. (1993), "On Seakeeping of conventional and High-Speed Vessels", *Journal of ship Research*, Vol. 37 No. 2, pp. 87-101.

Ferro, G., Mansour, A.E. (1985), "Probabilistic Analysis of the Combined Slamming and Wave-Induced Responses", *Journal of Ship Research*, Vol. 29 No. 2, pp. 170-188.

Folkstra, C. (1974), "Comparison of Ship Motions Theories with Experiments for a Container Ship", *International Shipbuilding Progress*, Vol. 21, pp. 168-189.

Frank, W., (1967), "Oscillation of Cylinders In or Below the Free Surface of Deep Fluids", *NRSDC*, Report No. 2357.

Gerritsma, J. (1960), "Ship Motions in Longitudinal Waves", *International Shipbuilding Progress*.

Gerritsma, J., Beukelman, W.(1967), "Analysis of the Modified Strip Theory for the calculation of Ship Motions and Wave Bending Moments", *NSRC, TNO Report*, No.96S.

Gerritsma, J., Beukelman, W. (1963), "Distribution of Damping and Added Mass along the Length of a Shipmodel", *NSRC, TNO Report*, No. 49 S.

Grim, O. (1959), "Oscillation of Buoyant two Dimensional Bodies and the Calculation of The Hydrodynamic Forms", *Hamburgische Schiffbau-Versuchsanstalt*, Report 1171.

Grim, O. (1960), "A Method for More Precise Computation of Heaving and Pitching Motions", *3rd Symposium on Naval Hydrodynamics*.

Guedes Soares, C., Nolasco, M. C. (1992), "Spectral Modeling of Sea States with Multiple Wave Systems", *Transactions of ASME*, Vol. 114, pp. 278-284.

Guedes Soares, C. (1989), "Transient Response of Ship Hulls to Wave Impact" *International Shipbuilding Progress*, Vol. 36, pp. 137-156.

Guedes Soares, C. (1990), "Comparison of measurements and Calculations of Wave Induced Vertical Bending moments in Ship models", *International Shipbuilding Progress*, Vol. 37, No 412, pp. 353-374.

Guedes Soares, C. (1990), "Effect of Transfer Function Uncertainty on Short Term Wave Induced ship Responses", *Applied Ocean Research*, Vol. 34, pp. 54-69.

Guedes Soares, C., Ferreira, A. M. (1995), "Analysis of the Seasonally in Non-Stationary Time Series of Significant Wave Height", *Proceedings II International Conference on Computational Stochastic Mechanics*, pp. 559-568.

Hagiwara, K., Yuhara, T. (1975), "Maximum Impact Pressures Acting on a Semi-Cylindrical Body Like Bow of a Large Ship", *J. Soc. Naval Arch. Japan*, Vol. 135, pp. 181-189.

Honkanen, M. (1976), "On the Wave Induced Motions of Ships", *Swedish Academy of Engineering Sciences in Finland*, Report No. 30.

Jensen, J.J., pedersen, T.P., (1978) "Wave Induced Bending Moment in Ships - A Quadratic Theory", *Transaction RINA*, Vol. 120, pp. 151-161.

Jong, B. (1973), "Computation of the Hydrodynamic Coefficients of Oscillating Cylinders", *Netherlands Research Centre*, TNO Report 145a.

Kaplan, P., Sargent, T.P. (1972), "Further Studies of Computer Simulation of Slamming and other Wave-Induced Vibratory Loadings on Ships in Waves", *Ship Structure Committee*, Report No. SSC-231.

Kawakami, M., Michimoto, J., Kobayashi, K. (1977), "Prediction of Long Term Whipping Vibration Stress Due to Slamming of Large Full Ships in Rough Seas", *International Shipbuilding Progress*, Vol. 24, pp. 83-110.

Korobkin, A. A. (1995), "Water Impact Problems in Ship Hydrodynamics", *Marine Hydrodynamics*, ed. M. Ohkusu.

Korobkin, A. A., Pukhnachov, V. V., (1988), "Initial Stage of Water Impact", *Ann. Rev. Fluid Mech.* pp.-159-185.

Korvin Kroukovsky, B.V., Jacobs, W.R. (1957), "Pitching and Heaving Motions of a Ship in Regular Waves", *Transactions SNAME*.

Krilov, A. A. (1896), "A New Theory of Pitching Motion of Ships in Waves", *Transactions INA*, Vol. 27, pp. 326-368.

Kumai, T., damping (1958), "Factors in the Higher Modes of Ship Vibrations", *European Shipbuilding*, Vol. 7, pp. 29-34.

Landweber, L., Macagno, M., (1967), "Added Masses of Two-Dimensional Forms by Conformal Mapping", *Journal of Ship Research*, June, pp. 109-116.

Landweber, L., Macagno, M.C., "Added Mass of Two Dimensional Forms Oscillating in a Free Surface", *Journal of Ship Research*, Vol. 1 , pp. 20-29.

Leibowitz, R. C. (1969), "A Method for Predicting Slamming Forces and Response of a Ship Hull", DTMB Report 1691.

Lewis, F.M. (1929), "The Inertia of Water Surrounding a Vibrating Ship", *Transactions SNAME*, Vol. 27, pp. 1-20.

Lin, Y. K. (1986), *Probabilistic Theory of Structural Dynamics*, Robert E. Krieger Publishing Company, Malabar, Florida.

Mansour, a., d'Oliveira J.M. (1975), "Hull Bending Moment Due to Ship Slamming in Regular Waves", *Journal of Ship Research*, Vol. 19 No. 2.

Mansour, A.E., Lozow, J. (1982), "Stochastic theory of the Slamming Response of Marine Vehicles in Random Seas", *Journal of Ship Research*, Vol. 26, No. 4 Dec., pp. 109-116.

Meyers, W.G., Sheridan, D.J., Salvensen, N. (1975), "Manual of NSRDC Ship-Motion and Sea-load computer program", *NRSDC*, Report No. 3376.

Newman, J.N. (1977), *Marine Hydrodynamics*, The MIT Press.

Newman, J.N. (1978), "Theory of Ship Motions", *Advances in Applied Mechanics*, Vol. 18.

Ochi, M.K., (1958), "Model Experiments on Ship Strength and Slamming in Regular Waves", *Transactions SNAME*, Vol. 66.

Ochi, M.K., (1964), "Extreme Behaviour of a Ship in Rough Seas, Slamming and Shipping of Green Water", *Transactions SNAME*, Vol. 72.

Ochi, M.K., Hubble, E.N. (1976), "On Six Parameter Wave Spectra", *Coastal Engineering*, Vol. 15, pp. 301-328.

Ochi, M.K., Motter, L.E., (1971), "A Method to Estimate the Slamming Characteristics for Ship Design", *Marine Technology*, Vol. 8, pp. 219-232.

Ochi, M.K., Motter, L.E., (1973), "Prediction of Slamming characteristics and Hull Responses for ship Design", *Transactions SNAME*, Vol. 81, pp. 144-190.

Ohtaka, K., Takaira, F., Hibino, F. (1966), "A Study of Vertical Vibration of Ships", *Journal of the Society of Naval Architectures of Japan*, Vol. 119 pp. 39-40.

Panel HS-2, (1993), "Notes on Ship Slamming", *Technical and Research Bulletin SNAME* 2-30.

Paulling, J.R., Richardson, R.K. (1962), "Measurement of Pressures, Forces and Radiating Waves for Cylinders Oscillating in a Free Surface", *University of California*, Series 82, Issue 23.

Petersen, J.B., (1992), "Non-Linear Strip Theories for Ship Response in Waves", *SHIPREL BRITE/EURAM Project 4554*.

Pierson, W.J., Moskowitz, L. (1963), "A Proposed Spectral form for Fully Developed Wind Seas Based on the Similarity Theory of S.A. Kitaigorodskii", *Tech. Report US Naval Oceanographical Office*, Contract 62306-1042.

Porter, W.R. (1960), "Pressure distribution, Added Mass and Damping Coefficients for Cylinders Oscillating in a Free Surface", *University of California, Institute of Engineering Research*, Series 82-16.

Radev, D., Beukelman, W. (1993), "Slamming on Forced Oscillating Wedges at Forward Speed", *International Shipbuilding Progress*, Vol. 40, pp. 71-92.

Salvinsen, N. Tuck E.O., Faltinsen, O. (1970), "Ship motions and Sea Loads", *Transaction SNAME*, Vol. 78, pp. 250-287.

St. Denis, M. Pierson, W.J. (1953), "On the Motions Of Ships in Confused Seas", *Transactions SNAME*, Vol. 61, pp. 280-354.

Stavovy, A.B., Chuang, S.L. (1976), "Analytical Determination of Slamming Pressures for high Speed vessels in Waves", *Journal of Ship Research*, Vol. 20, pp. 190-198.

Tasai, F. (1959), "On the Damping Force and Added Mass of Ships Heaving and Pitching", *Reports of Research Institute for Applied Mechanics*, Vol. 7 No. 26, pp. 131-153.

Tasai, F. (1960), "Formula for Calculating Hydrodynamic Force of a Cylinder Heaving on a Free Surface (N-Parameter family)", *Research Institute for Applied Mechanics*, Kyushu University, Report 31, pp. 71-74.

Tick, J.L. (1959), "Differential Equation with Frequency-Dependent Coefficients", *Journal of Ship Research*, Vol. 3, No. 3, pp. 45-46.

Townsin, R.L. (1969), "J Values for Ship Vibration Calculations Derived from Tests with Beams including Ellipsoids and Ship Models", *Transactions RINA*, Vol. 111, pp. 385-397.

Ursell, F., (1949), "On a Heaving Motion of a Circular Cylinder on the Surface of a Fluid", *Quarterly Journal Mech. and Applied Math.*, Vol. 2, pp. 218-231.

Von Kerczek, C., Stern, F. (1983), "The Representation of Ship Hulls by Conformal Mapping Functions: Fractional Maps", *Journal of Ship Research*, Vol. 27, No. 3 Sept, pp. 158-159.

Von Kerczek, C., Tuck, E.O. (1969), "The Representation of Ship Hulls by Conformal Mapping Functions", *Journal of Ship Research*, Vol. 13, No. 4 Dec., pp. 284-298.

Vugts, J. H. (1971), "Hydrodynamic Forces and Ship Motions in Oblique Waves", *NSRC*, Report No. 150S.

Vugts, J.H., (1968), "The Hydrodynamic Coefficients for Swaying, Heaving and Rolling Cylinders in a Free Surface", *Laboratorium Voor Scheepsbouwkunde, Technische Hogeschool Delft*, Report No. 194.

Weinblum, G. M., St Denis (1950), "On the Motions of Ships at Sea", *Transactions SNAME*, Vol. 58.

Yamamoto, Y., Sugai, K., Inoue, H., Yoshida, K., Fujino, M., Ohtsubo, H. (1986), "Wave Loads and Response of Ships and Offshore Structures From the Viewpoint of

Hydroelasticity ”, *Advances in Marine Structures*, Elsevier Applied Science Publishers, pp. 26-40.

Zhao, R., Faltinsen, O. (1993), “Water Entry of Two-Dimensional Bodies”, *J. of Fluid Mech.*, Vol. 246, pp. 593-612.

Stiansen, S. G., Mansour, A. E. (1976),), “Ship Primary Strength Based on Statistical Data Analysis”, *Transactions SNAME*, Vol. 84, pp. 214-243.

Wagner, V. H. (1932), “Uber Stoz und Gleitvorgange an der Oberflache von Flussigkeiten”, *Zeitschrift fur Angewandte Mathematik und Mechanik*, Vol. 12, No. 4, pp. 193-215.

